

WATER FLOW AND NUTRIENT TRANSPORT IN A LAYERED SILT LOAM SOIL

CENTRALE LANDBOUWCATALOGUS



0000 0795 4718

Promotoren: dr. ir. P.A.C. Raats
hoogleraar in de continuümmechanica

dr. ir. R.A. Feddes
hoogleraar in de bodemnatuurkunde,
agrohydrologie en grondwaterbeheer

NU08201, 2331

WATER FLOW AND NUTRIENT TRANSPORT IN A LAYERED SILT LOAM SOIL

J.A. de Vos

Proefschrift

ter verkrijging van de graad van doctor
op gezag van de rector magnificus
van de Landbouwuniversiteit Wageningen,
dr. C.M. KarsSEN,
in het openbaar te verdedigen
op vrijdag 17 oktober 1997
des namiddags te half twee in de Aula

van grijze

ACKNOWLEDGEMENT

The research presented in this thesis was embedded in different projects of the scientific programmes of the DLO Research Institute for Agrobiology and Soil Fertility (AB-DLO) at Haren, The Netherlands. These projects were part of Research Programme 223 "Physical soil quality in relation to soil function for agriculture and water, environmental and nature management" of the Netherlands Organisation for Agricultural Research (DLO) of the Netherlands Ministry of Agriculture, Nature Management and Fisheries (LNV).

As part of the Dutch Programme on Soil Ecology of Arable Farming Systems the work was in the first research period, 1986-1990, supported by the Netherlands Integrated Soil Research Programme (PCBB).

The later research, in the period 1994-1997, was part of the DGXII Environment Research Programme of the European Community, contract EV5V-CT94-0493, project PL93-1923: "Critical evaluation of selected models describing nitrate leaching and biological transformations. Quantification of the effect of various agricultural practices on nitrate pollution".

Cover:

Application of a tracer at the soil surface of the drainage experiment at the Lovinkhoeve. The white covers above the soil surface are on top of the hydrological instruments. Groups of these instruments are distributed over the field.

Nederlandse vertaling titel:

Waterstroming en nutriëntentransport in een gelaagde zavelgrond.

CIP-DATA KONINKLIJKE BIBLIOTHEEK, DEN HAAG

de Vos, J.A.

Water flow and nutrient transport in a layered silt loam soil. J.A. de Vos
PhD Thesis Wageningen Agricultural University.

- With ref. With summary in Dutch.

ISBN 90-5485-749-8

Stellingen

1. Het op vaste tijdstippen bemonsteren en analyseren van drainagewater of grondwater om de totale nitraatuitspoeling naar het oppervlaktewater te schatten kan leiden tot grote fouten.

Dit proefschrift

2. De beschrijving in numerieke waterstromingsmodellen van de intree weerstand van een drain door middel van een ideale drain met een zeer kleine equivalente diameter is onpraktisch.

Fipps, G., R.W. Skaggs and J.L. Nieber, 1986. Drains as a boundary condition in finite-elements. Water Resources Research 22: 1613-1621.

Dit proefschrift

3. Bij het meten van de waterdoorlatendheid bij verzagding van een bodemmonster dient de onderzijde van het monster volledig met water in contact te staan.

NEN-5789, 1991. Bodem. Bepaling van de verzagde waterdoorlatendheid. Nederlands Normalisatie Instituut, Delft.

Dit proefschrift

4. Pompen of verzuipen is het simpelste "poldermodel"; een tweedimensionaal waterstromingsmodel is een meer realistische variant.

Dit proefschrift

5. Processen die zich op overgangen afspelen zijn zeker geen randverschijnselen.

6. Het is overtuigender de beperkingen van een model te erkennen dan allerlei onbewezen mogelijke kwaliteiten te suggereren.

7. Boeren dienen een vergoeding te krijgen als op hun bedrijf de stikstofuitspoeling op jaarbasis lager is dan de atmosferische stikstofdepositie.

8. Het gebruik van winter- en zomertijd of van Juliaanse dagnummering leidt vaak tot misverstanden en fouten.
9. Wetenschappelijk onderzoek dat geen direct praktisch toepasbaar resultaat oplevert kan toch duidelijk maken wat zinnig, haalbaar of toelaatbaar is.
10. Het is geen taak voor de wetenschap om mystieke theorieën te weerleggen.
11. Veel managers moeten beter toneel leren spelen.
12. Personen die nergens aan twijfelen zijn gevaarlijk.
13. Zelf mondharmonica spelen is een hogere bezigheid dan luisteren naar Bach.
Godfried Bomans
14. Het is diepgaander iets grondig te onderzoeken dan iets tot op de bodem uit te zoeken.

Stellingen behorende bij het proefschrift *“Waterstroming en nutriëntentransport in een gelaagde zavelgrond”* van J.A. de Vos, Wageningen, 17 oktober 1997.

ABSTRACT

De Vos, J.A., 1997. Water flow and nutrient transport in a layered silt loam soil. Doctoral Thesis, Wageningen Agricultural University, Wageningen, The Netherlands, 287 p., 104 figures, 13 tables, 216 references, English and Dutch summaries.

Theory, numerical models, and field and laboratory measurements are used to describe and predict water flow and nutrient transport in a layered silt loam soil. One- and two-dimensional models based on the Darcy equation for water flow and the convection-dispersion equation for solute transport are evaluated. Pressure heads simulated with the one-dimensional water balance model SWATRE are too large. The two-dimensional SWMS_2D model simulates water flow well for the winter leaching periods. The layering of the soil profile and the height of the phreatic surface determine flow paths to the subsurface drain. The hydraulic conductivity at saturation ranged from 200 cm d^{-1} in the 0-25 cm depth topsoil to 10 cm d^{-1} in the 95-120 cm depth subsoil. Under wet conditions solutes are transported laterally from the 0-25 cm topsoil towards the drain. Under drier conditions drainage water originates mainly from the 75-120 cm depth soil layers. Water flow and solute transport through the larger pores and solute exchange between the soil and water in these pores appear to be important, which was confirmed by a bromide tracer experiment. The upward diffusion of $220 \text{ kg ha}^{-1} \text{ yr}^{-1}$ chloride (Cl) was a major term in the Cl mass balance. Estimates of yearly averaged nitrogen (N) losses for integrated and conventional arable farming plots were 45 and $72 \text{ kg N ha}^{-1} \text{ yr}^{-1}$, respectively. At an integrated plot measured N leaching ranged from 0 to $50 \text{ kg ha}^{-1} \text{ yr}^{-1}$. High nitrate (NO_3) concentrations in the drainage water were often measured during wet periods with shallow phreatic surfaces. Spatial differences in N content of 30 kg ha^{-1} were measured as a function of the distance from the drain, probably as a result of denitrification. Smaller drain spacing, precise application of fertilisers and irrigation water, and controlled drainage can reduce NO_3 leaching to groundwater and surface water.

Additional keywords: anisotropy, bromide tracer, chloride, dispersion, drainage, field measurements, finite difference model, finite element model, groundwater, nitrate leaching, nitrogen balance, polder, soil chemistry, soil ecosystem, soil physics, solute transport, TDR, two-dimensional model, water balance.

VOORWOORD

Het proefschrift is klaar! Het aantal pagina's groeide en groeide tijdens het afronden van het proefschrift. Het is dus een lijvig werk geworden, dat met hulp van vele anderen tot stand is gekomen.

Allereerst wil ik Pieter Raats noemen. Pieter, jouw enthousiasme voor het bodemfysisch onderzoek, al jouw internationale contacten waarvan ook ik profiteerde, onze discussies over het onderzoek en allerlei andere zaken, waren een grote stimulans voor het afronden van dit proefschrift. Keer op keer kwamen mijn manuscripten terug met gedetailleerd commentaar. Bedankt voor de goede begeleiding en ik waardeer het zeer dat onze samenwerking in een zo'n goede, vertrouwelijke sfeer plaatsvond. Ik beschouw je als mijn wetenschappelijke, bodemfysische mentor en het doet mij goed dat jij mijn promotor bent.

Pieter Raats was zo sterk bij het onderzoek betrokken, dat het goed was om ook een onafhankelijke deskundige als promotor te vinden. Reinder Feddes was bereid deze taak op zich te nemen. Reinder had een gezonde kritische houding ten opzichte van mijn werk en zorgde voor veel nuttige informatie op agrohydrologisch gebied. Aan het einde van de werkbesprekingen bood Reinder me meestal een grote stapel literatuur aan die ik maar eens moest doornemen. Ik bestudeerde doorgaans een selectie uit deze stapel. Reinder, bedankt voor alle hulp bij het totstandkomen van dit proefschrift.

Jan Zwiers is de man die veel van het echte werk uitvoerde. Met zijn karakteristieke Drentse stijl organiseerde en verrichte hij het veldwerk op de Lovinkhoeve. Daarnaast voerde hij veel van het laboratoriumwerk zelf uit. Jan, het was voor mij een plezier om zo lang en goed samen te werken in een groot onderling vertrouwen. Klaas Boersma kwam enige jaren geleden bij de sectie Bodemfysica. Klaas verzorgde de ontwerpen van de zelf gebouwde geautomatiseerde veldapparatuur en de uitwerking van een groot deel van de TDR meetgegevens en weersgegevens. Klaas, jij werkte altijd hard, leverde degelijk werk af en deed dit nog snel ook. Alleen begrijp je nog steeds niet dat sandalen niet de beste werkschoenen zijn op de Lovinkhoeve. Bedankt voor het vele werk dat jij voor mij hebt verzet. Ik heb het gevoel dat Jan Zwiers, Klaas Boersma en ik elkaar goed aanvullen en zo samen een team vormen dat goed werk verricht.

Op de Lovinkhoeve verzorgden Eduard Hummelink, Andries Siepel en vele (oud)-medewerkers de proefvelden, assisteerden bij het plaatsen van

apparatuur, en verrichtten metingen in het veld. Eduard, jij ontwikkelde je tot een zelfstandig technisch assistent die in weer en wind met de hand en met de computer gegevens voor mij verzamelde. Andries, jouw technisch inzicht en bereidheid om mee te denken en te werken bij het installeren van nieuwe apparatuur werd zeer gewaardeerd. Eduard, Andries en alle andere Lovinkhoevers bedankt voor de grote inzet.

Op het gebied van bodemfysica waren Marius Heinen en Kees Rappoldt mijn meest nabije collega's. Op wetenschappelijk en persoonlijk gebied kunnen wij het goed met elkaar vinden. Marius was, zoals voorspeld, eerder klaar met zijn proefschrift. Marius bedankt voor de milde competitie en de hulp bij het oplossen van allerlei probleempjes met computers en software. Kees Rappoldt en ik delen een natuurkundige achtergrond en wij geloven dat goed experimenteel werk noodzakelijk is in het landbouwkundig onderzoek. Kees overtuigde mij ervan een Apple Macintosh computer te kopen en leverde mij zijn zelfgemaakte software voor het produceren van mooie grafieken. Ons gezamenlijke werk op de Lovinkhoeve met betrekking tot de waterbalans, het zuurstoftransport en de denitrificatie heeft geleid tot sectie 6.6 van dit proefschrift. Kees bedankt voor de goede en prettige samenwerking.

Gerard Brouwer, Klaas Harmanny en Roel Vriesema voerden vele laboratoriumbepalingen uit. Mejid Lahmar en Klaas Boersma ontwierpen de specifieke elektronische apparatuur, die vervolgens met grote snelheid door Gerrit Bargerbos werd gebouwd. Samen met de technici in onze werkplaats, Eltje Groendijk, Jelles de Jong, John de Koning, Hobbe Pijpker, Rein Rieswijk, en Willem Smit, zijn mooie meetopstellingen gebouwd die door velen zijn bewonderd. Het is altijd een verademing om de werkplaats binnen te komen en weer eens te zien hoe een instrument wordt gebouwd. Alle algemene ondersteunende diensten in Haren zijn direct of indirect betrokken geweest bij het gereedkomen van dit proefschrift. De Proeftechnische Dienst nam vele grondmonsters. Het Centraal Laboratorium werd overspoeld met drainmonsters. De telefonistes waren mij 's ochtends vaak kwijt. Financiële Zaken begreep het samen met mij soms ook niet meer. Hendrik Terburg corrigeerde mijn Engels nog eens. De schoonmaakploeg kwam 's avonds gezellig even langs. Aaltje zorgde ervoor dat ik in de kantine niets tekort kwam. Aan alle collega's mijn dank voor de getoonde inzet en de plezierige samenwerking en verzorging.

Ik heb veel voldoening beleefd aan het begeleiden van stages en afstudeeronderzoeken, en een deel van dit werk is terug te vinden in dit

proefschrift. Ik bedank Sandra Boekhold, Madeleine Inckel, Tessa Slingerland, Emmy Theije, Melchior van den Broek en Falentijn Assinck voor hun bijdrage en de enthousiaste samenwerking.

It is very modern to plan and carry out interdisciplinary research. I was lucky that I had the opportunity to work with Dean Hesterberg on field solute transport at the Lovinkhoeve. He focused on the soil chemical aspects and I focused on the soil physical aspects. Dean did the main part of the work on solute transport and he is the first author of Chapter 7. But I considered it to be an indispensable part of the thesis to illustrate the complexity of the field-scale solute transport processes at the Lovinkhoeve. For me it was a pity that Dean decided to return to the USA, although the opportunity to visit him at the Department of Soil Science of the North Carolina State University was a nice side effect. Dean, thanks for the pleasant and stimulating cooperation. I hope to be able to visit you and your family again.

Vanaf 1986 werk ik op het DLO Instituut voor Agrobiologisch en Bodemvruchtbaarheidsonderzoek (AB-DLO), voorheen het DLO Instituut voor Bodemvruchtbaarheid (IB-DLO) te Haren. Dit proefschrift is gebaseerd op een gedeelte van het onderzoek dat ik in de afgelopen jaren in IB- en AB-projecten heb uitgevoerd. Vele keren veranderde ik van afdeling, veranderde de naam van de afdeling, kwam er een nieuw afdelingshoofd, werd mijn functiebeschrijving aangepast, maar steeds bleef ik werken aan de onderwerpen die in dit proefschrift staan beschreven. Ik dank alle afdelingshoofden en de directie van het AB en IB, die mij het vertrouwen en de mogelijkheden gaven om dit werk op deze wijze af te ronden.

Het getuigt van groot historisch besef als men juist in Groningen het bodemkundig en agrohydrologisch onderzoek naar de gevolgen van de waterhuishouding voor de landbouw hoog houdt. Uit de publicatie van P. Bruin en W.C. Visser "Het werk van Dr. S.B. Hooghoudt in dienst bij het landbouwkundig onderzoek" (Landbouwkundig Tijdschrift, 65e jaargang, no. 11, 1953: 650-657) blijkt dat S.B. Hooghoudt op het Bodemkundig Instituut in Groningen baanbrekend bodemfysisch en agrohydrologisch onderzoek heeft verricht. Hooghoudt combineerde theoretische kennis met zeer toegepast onderzoek en ontwikkelde zijn befaamde drainageformules. Ook beschreef hij reeds de tweedimensionale waterstroming naar drains. Met gepaste bescheidenheid zie ik een duidelijke overeenkomst tussen het werk van

Hooghoudt en het werk beschreven in dit proefschrift. Een bewijs dat dit type onderzoek in het noorden des lands goed uitgevoerd kon en kan worden.

De prettige atmosfeer op het AB-DLO in Haren heeft een belangrijke rol gespeeld bij het uitvoeren van het werk. Ondanks alle problemen met betrekking tot reorganisaties, vestigingsplaats, afslanking en dergelijke, bleven de persoonlijke verhoudingen goed. Voetbal, volleybal, muziek, dit alles veelal geactiveerd door Lucas Bouwman en de zijnen, en de wandelvakanties vormden belangrijke arbeidsvoorraarden die in geen enkel strategisch plan te vinden zijn, maar die voor mij en anderen van zeer grote betekenis zijn. De wat kleinere schaal heeft ook voordelen boven de grote gecentraliseerde structuren: "Small is beautiful".

Naast alle contacten binnen het AB-DLO waren er ook vele externe contacten. Binnen Nederland hebben de discussies binnen het groepje bodemfysici dat zich bezig hield met de normalisatie van meetmethoden (Nederlands Normalisatie-instituut (NNI), commissie Fysisch onderzoek van de onverzadigde zone) een belangrijke bijdrage geleverd aan mijn kennis. Ik heb zelf van onze aanbevelingen gebruik gemaakt en daarom ook aan de NNI-normen gerefereerd. In het bijzonder wil ik de goede en prettige samenwerking noemen met: Jûnt Halbertsma (DLO Winand Staring Centrum, Wageningen), Timo Heimovaara en Willem Bouter (Fysisch Geografisch en Bodemkundig Laboratorium, Universiteit van Amsterdam), en Chris Dirksen (vakgroep Waterhuishouding, Landbouwuniversiteit Wageningen). Het Koninklijk Nederlands Meteorologisch Instituut (KNMI) installeerde in 1986 een weerstation op de Lovinkhoeve. Sinds 1987 is dit geautomatiseerde weerstation "Marknesse" operationeel. De samenwerking met het KNMI is altijd plezierig verlopen en ik heb dankbaar gebruik gemaakt van de betrouwbare KNMI-weersgegevens.

Ook op internationaal gebied waren er vele contacten. Mijn eerste tropische ervaring was het uitvoeren en begeleiden van het bodemfysische veldwerk in het project Production Soudano-Sahélienne (PSS) in Mali. De warme persoonlijke banden die daarbij al snel ontstonden met verschillende personen blijven voor mij een belangrijke ervaring.

In February 1996 I felt it was necessary to accelerate my progress with two-

dimensional modelling of water flow and solute transport. I contacted the Soil Physics group of Rien van Genuchten at the USDA Salinity Laboratory at Riverside, California (USA). A few weeks later I was there and I had the opportunity to work with Jirka Simunek. Jirka, you helped me a lot in solving the practical problems with running a sophisticated model like SWMS_2D. You had just finished the HYDRUS-2D version of the model, including the user-friendly interface. Thanks a lot for your help and I hope you like the results presented in this thesis.

Naast bovengenoemde contacten had ik nog vele wetenschappelijke en zeer persoonlijke nationale en internationale contacten. Ik beschouw het als een voorrecht om als onderzoeker in deze situatie te kunnen verkeren.

Ik wil verder allen bedanken die het jarenlang volgehouden hebben om te vragen of het proefschrift al opschoot. De laatste tijd antwoordde ik dat ik nu al zolang bezig was dat het niet meer kon opschieten. White Flash, de bluesband uit Groningen, diende op donderdagavond en in vele weekends als swingende uitlaatklep. Want als ik mijn voorwoord nu zelf terug lees lijkt het er op dat het totstandkomen van dit proefschrift alleen maar een succesverhaal is. Dat is niet zo. Momenten van twijfel en zelfverzekerdheid, motivatie en demotivatie, concentratie en afwezigheid, waren mij niet vreemd. Deze stemmingen wisselden soms van dag tot dag. Uiteindelijk is het de vasthoudendheid en de wil, gestimuleerd door alle bovengenoemde positieve randvoorwaarden, die de voltooiing van dit proefschrift mogelijk maakten. U begrijpt dat iemand die zelfs voor zijn voorwoord al vijf pagina's nodig heeft, uitvoerig van stof is en er wel een tijdje over doet voor het proefschrift zelf af is. Toch is het nu zover!

Bram

CONTENTS

1. Introduction.....	1
1.1 Agriculture and environment.....	1
1.2 The water balance of the soil	2
1.3 Hypothesis and objectives of this study	3
1.4 Research approach.....	4
1.5 Outline of the thesis.....	5
2. Theory of water flow and solute transport in soil.....	9
2.1 Water flow	9
2.1.1 Unsaturated zone: the SWATRE water flow model.....	10
2.1.2 Saturated zone	13
2.1.3 The combined saturated-unsaturated zone: the SWMS_2D water flow model.....	15
2.1.4 Analytical expressions for the soil hydraulic characteristics	17
2.1.5 Time-depth curves of parcels of water.....	19
2.2 Solute transport: the SWMS_2D solute transport model.....	20
3. Field and laboratory methods.....	25
3.1 Field methods.....	25
3.1.1 General soil physical methods.....	26
3.1.2 Time Domain Reflectometry	30
3.1.3 Soil oxygen content measurements	38
3.1.4 Drain sampling device.....	40
3.1.5 Meteorological station Lovinkhoeve.....	42
3.2 Laboratory methods.....	45
3.2.1 Water retention characteristics.....	45
3.2.2 Hydraulic conductivity characteristics.....	46
3.2.3 Improved measurement of K_s	47
3.2.4 Calibration of the TDR water content measurements.....	50

4. The Lovinkhoeve experimental farm	51
4.1 General characteristics	52
4.1.1 Geological history	52
4.1.2 Soil profile and hydrological situation.....	53
4.1.3 Experimental plots and farm management	59
4.2 Soil physical characteristics.....	61
4.2.1 Water retention characteristics	61
4.2.2 Hydraulic conductivity characteristics	66
4.2.3 Analytical expressions for the hydraulic characteristics	67
4.2.4 Hydraulic conductivity at saturation.....	71
4.2.5 TDR calibration.....	73
5. Macroscopic soil physical processes considered within an agronomical and soil biological context.....	81
5.1 Interdependence of soil biological and soil physical processes.....	81
5.2 The Dutch Programme on Soil Ecology of Arable Farming Systems ..	82
5.3 Field measurements.....	83
5.4 Soil physical conditions during 1986-1990	86
5.5 Results of one-dimensional water balance simulations	98
5.6 Discussion	105
5.7 Evaluation of the soil ecology study of arable farming systems.....	108
5.7.1 Soil structure.....	108
5.7.2 Nitrogen mineralisation.....	111
5.7.3 Nitrogen balance.....	114
5.8 Conclusions	117
6. Field data on water flow, and on nitrate, chloride and bromide transport to a subsurface drain	121
6.1 Introduction.....	121
6.2 Description of the drainage experiments.....	122
6.3 Nitrate leaching 1991-1992	124
6.3.1 Drain discharge, and soil physical and soil chemical conditions	124
6.3.2 Interpretation of the field data	130

6.4 Long-term chloride mass balance and upward seepage	138
6.4.1 Situation after reclamation.....	139
6.4.2 Chloride mass balance	140
6.4.3 Discussion	145
6.5 Nitrogen balances and nitrate leaching 1991-1996.....	145
6.5.1 Field data 1991-1996	145
6.5.2 Discussion	150
6.6 Spatial patterns of hydrological conditions, soil oxygen contents and denitrification.....	161
6.6.1 Introduction.....	161
6.6.2 Hydrological conditions and soil oxygen contents.....	163
6.6.3 Discussion	167
6.7 Bromide tracer experiment 1994-1995	170
6.7.1 Bromide application, sampling and analysis	170
6.7.2 Bromide concentrations in the drainage water.....	171
6.7.3 Bromide concentrations in the soil water.....	174
6.7.4 Discussion	175
6.8 Conclusions.....	177
7. Multi-component solute transport to a subsurface drain	179
7.1 Introduction.....	179
7.2 Soil chemical methods.....	181
7.3 Composition of drainage water and soil chemical processes	184
7.4 Conclusions.....	197
8. Modelling two-dimensional water flow, and nitrate, chloride and bromide transport to a subsurface drain.....	199
8.1 Two-dimensional water flow and solute transport models	199
8.2 Modelling the Lovinkhoeve field.....	202
8.2.1 Flow domain and finite element grid.....	202
8.2.2 Hydraulic characteristics close to saturation.....	205
8.2.3 Calibration of the water flow part of the model.....	207
8.2.4 Calibration of the solute transport part of the model.....	214
8.3 Simulation of nitrate transport.....	216

8.4 Simulation of chloride leaching and the bromide tracer experiment	223
8.5 Discussion.....	227
8.6 Explorative two-dimensional simulations	233
8.6.1 Results of the simulations.....	234
8.6.2 Discussion.....	241
8.7 Conclusions	242
 Summary	245
 Samenvatting	253
 References	261
 List of main symbols	281
 Curriculum Vitae	285

1. INTRODUCTION

1.1 Agriculture and environment

Environmental problems are topical issues in society. Climatic change, erosion due to deforestation, and pollution of groundwater and surface waters are examples of processes that threaten the sustainability of the current world ecosystem in the long term and the quality of life in the short term. Parts of these problems are related to agriculture (Sposito and Reginato, 1992).

After 1945 yields increased as a result of the increased use of mineral fertilisers, the introduction of herbicides and pesticides, the improved plant varieties, and the growing scientific knowledge. Over the last two decades it became clear that these new farming practices caused negative side effects. Leaching of nutrients and pesticides to groundwater and surface waters, compaction of the topsoil, water and wind erosion, decreasing of organic matter contents and contamination of soils with heavy metals are world-wide examples of these negative effects. The development of new farming systems is enhanced by thinking in economical growth concepts and a growing demand by the increasing population (Meadows *et al.*, 1972; Van Dieren, 1995). In a historical overview of Dutch agriculture, Bieleman (1993) showed that also in the earlier periods of agriculture conflicts between agriculture and environment existed.

Nowadays, sustainable agriculture is an issue in public and scientific discussions (Spencer and Swift, 1992). Sustainable agriculture aims at a steady state for soil fertility, with all inputs balancing the outputs and a minimal (inevitable) loss of nutrients to the environment. Aspects like the integration of agriculture with nature (NLRO, 1990) and the role of soil ecosystems (Brussaard, 1994) are often included in studies of the potentials of sustainable agriculture.

In The Netherlands, agriculture is intensive with a high production per hectare on a limited area of land. Due to the application of large amounts of manure, parts of the sandy soils are saturated with phosphate (PO_4) (Oenema and Van Dijk, 1994). Phosphate and nitrate (NO_3) leach from soils, and pollute groundwater and surface waters. In surface waters the effect can be an excessive algal bloom, followed by anoxic conditions in the water when the algae die, which can have undesirable consequences for the aqueous ecosystem. High NO_3 concentrations in groundwater become a problem when this groundwater is

used for the production of drinking water. The national and international policy is to reduce the NO_3 and PO_4 load of groundwater and surface waters (Strelbel *et al.*, 1989; NLRO, 1994;). The actual EU-limit for NO_3 concentrations in groundwater is 50 mg l^{-1} (EU, 1991). However, the limits for NO_3 concentrations in groundwater and surface waters are still under discussion, but it is likely that they will become stricter. In The Netherlands a limit of 10 mg l^{-1} is advised for surface waters (Willems and Fraters, 1995).

Another nitrogen (N) loss from agriculture is denitrification of NO_3 present in the soil. Part of the NO_3 can be biologically transformed into dinitrous oxide (N_2O), which is a gas that might escape from the soil to the atmosphere. Scientific research is conducted to study the role of N_2O as a greenhouse gas and to understand and quantify the N_2O forming processes in soils (Groffman, 1991).

1.2 The water balance of the soil

The importance of the soil water balance

From an agricultural point of view, the challenge is to reduce the N losses to the environment and still supply the crops with a sufficient amount of N for crop growth. Insight in the regulating processes is needed to reach this goal. Although the N balance of the soil is strongly influenced by biological processes, the soil water balance is of major importance for the fate of N in the soil. In this doctoral thesis the water balance is studied to understand water flow and solute transport, especially NO_3 leaching. Soil water contents determine the possibilities for gas transport, with oxygen (O_2) and carbon dioxide (CO_2) as important gases being related to biological activity. Together with other conditions, like soil temperature, soil chemical status and the availability of organic matter, O_2 contents determine the denitrification rate. Also, N mineralisation strongly depends on the soil physical conditions. These biological N transformations illustrate the dependence of the dynamics of soil ecosystems on changing abiotic conditions. Soil chemical processes are also influenced by the soil physical processes. Convective solute transport is directly driven by water flow, and redox conditions are closely linked with the aeration status of the soil.

1. Introduction

Lovinkhoeve experimental site

Soil physical field experiments were performed at the experimental farm Dr. H.J. Lovinkhoeve from 1986 to 1990 as part of the Dutch Programme on Soil Ecology of Arable Farming Systems (Brussaard *et al.*, 1988; Brussaard, 1994). In that study a comparison was made between a conventional and an integrated arable farming system. The integrated system was a form of sustainable agriculture with reduced input of fertilisers, shallow soil tillage and a reduced use of herbicides as compared to the conventional system. After this study it was felt that a continuation of the soil physical research, with special emphasis on NO_3 leaching, was desirable (1991-1997). This new research has been continued over the period 1994-1997 in the European Community project: "Critical evaluation of selected models describing nitrate leaching and biological transformations. Quantification of the effect of various agricultural practices on nitrate pollution".

The Lovinkhoeve has a layered soil profile with a calcareous silt loam topsoil (0-25 cm depth) and a light loam subsoil (25-100 cm depth). Subsurface drains are located at a depth of about 1 m with a 12-m spacing. The soil of the Lovinkhoeve can be considered as representative for a large area in the Noordoostpolder.

1.3 Hypothesis and objectives of this study

This study explicitly approaches water flow using a Darcian formulation to evaluate how well the dominating patterns in macroscopic soil physical field conditions can be understood. This approach gives the possibility to characterise the flow properties using available methods at the same spatial scale. For the Lovinkhoeve fields it is expected that the relatively shallow, fluctuating phreatic surface has a dominant effect on the soil physical conditions. This specific phreatic surface behaviour, combined with the layered soil profile, could govern water flow and solute transport. The description of solute transport focuses on the behaviour of conservative solutes, which means that biological transformations and exchange processes with the solid phase and chemical reactions are not studied explicitly.

However, it has to be demonstrated that the Darcian approach is adequate for the Lovinkhoeve field situation. Field data of soil physical conditions, tracer

experiments, drain discharge, and the chemical composition of the drainage water will be used in combination with numerical models to evaluate this assumption.

The objective of this study is to quantify the flow and transport processes for the specific field location Lovinkhoeve and to evaluate the consequences for soil chemical and biological processes. Quantification of the drain discharge and corresponding leaching of nutrients, especially NO_3 , will give indications about the N budgets of the arable farming systems. Recommendations for appropriate measurement methods to quantify NO_3 leaching can be given. Based on this study, ideas for improved farm management systems and new strategies for environmental protection or regulations can be obtained.

1.4 Research approach

This study approaches the water balance within the soil-plant-atmosphere system from an agronomical point of view. The flow and transport processes are studied in a deterministic way, combining theory with field and laboratory experiments. Field experiments are conducted to quantify the different components of the soil water balance. It was decided not to measure a few components of the water balance on many plots followed by a statistical analysis. Instead, many instruments were installed at a few plots to obtain a detailed quantification and understanding of the flow and transport processes. The field scale is the relevant scale at which the processes take place, and where the effects of crops can be studied properly. The plant with its active root system plays a key role in such an agronomical approach. However, measuring in a field situation causes some problems. It is difficult to install and service instruments in a field where a crop is grown. No true repetitions in time are possible, and the time scale of the experiments is related to the agronomical time scale of the annual growing season or even a 4-year crop rotation period. The changing meteorological conditions present another uncertain factor, with a large influence on the experimental results. Models can be used as tools to evaluate the effects of changing soil characteristics, crop characteristics and meteorological conditions on transport processes and corresponding soil physical conditions. Field data have to be used to verify the model results.

1. Introduction

The continuity equation and Darcy's law are taken as starting points for the description of water flow in soil. This approach is applied to describe the water balance using existing numerical models. The one-dimensional SWATRE model (Belmans *et al.*, 1983) is used to describe the soil physical conditions in the unsaturated zone. To be able to extend the description to the saturated zone, including water flow to drains, the two-dimensional SWMS_2D model (Simunek *et al.*, 1994) is used.

Both models use the water retention and hydraulic conductivity characteristics as input. These characteristics are measured in the laboratory for the different soil horizons. The hydraulic conductivity at saturation (K_s) is measured in the vertical and horizontal direction for the different horizons to check whether anisotropy in K_s is present. The analytical functions of Van Genuchten (1980) and Mualem (1976) are used to describe the hydraulic characteristics.

A diversity of soil physical instruments were installed in the experimental fields, i.e. tensiometers, groundwater tubes, piezometers, Time Domain Reflectometry (TDR) sensors, soil temperature sensors, and oxygen chambers. To measure drain discharge rates and the chemical composition of the drainage water, a special drain sampling device was built and installed. An automated meteorological station became operational at the Lovinkhoeve in 1987, including a part which is operated by the Royal Netherlands Meteorological Institute (KNMI).

1.5 Outline of the thesis

This thesis describes the study of water flow and nutrient transport processes at the experimental fields of the Lovinkhoeve farm. Three coherent parts of the thesis can be distinguished. The introductory Chapters 1 to 4 present the general information, which constitutes the framework for the results discussed later. In Chapter 5, a one-dimensional description of water flow and solute transport is used to interpret the results of field experiments. Chapters 6 to 8 present a two-dimensional description of water flow and solute transport to describe the dynamics of water flow and solute transport to a subsurface drain.

Chapter 2 presents the theory for water flow and solute transport. The corresponding relevant characteristics of the SWATRE and SWMS_2D water flow and solute transport models are described. Attention is given to the concept of time-depth curves of parcels of water to visualise one-dimensional convective transport of a conservative solute. Drainage, especially water flow to subsurface drains, is considered as a special case of water flow in the saturated zone.

The methods used for the field and laboratory measurements are discussed in Chapter 3, including the description of the meteorological station. Special attention is given to a modified technique to measure the hydraulic conductivity at saturation and the calibration procedure for TDR water content measurements.

Chapter 4 gives a general overview of the experimental fields of the Lovinkhoeve, a description of soil genesis, soil characteristics, and the lay-out of the experimental plots. The hydraulic characteristics of the Lovinkhoeve soil are presented, including fits of the data to the analytical functions of Van Genuchten (1980) and Mualem (1976), and the TDR calibration curves.

Chapter 5 considers soil physical processes within an agronomical and soil-biological context. Measurement series of the soil physical conditions are presented, together with results of the one-dimensional SWATRE model. A general discussion is given on the soil biological results and the role of soil physics in the Dutch Programme on Soil Ecology of Arable Farming Systems.

The interpretation of experimental data on water flow and nutrient transport to a subsurface drain are described in Chapter 6. Time-series of NO_3 leaching data are presented and interpreted. The chloride mass balance is used to evaluate whether upward seepage occurs. A bromide tracer experiment is discussed to evaluate the nature of the field-scale solute transport. Consequences for drainage water sampling schemes are discussed.

Based on the field measurements, soil chemical aspects of the transport processes are presented in Chapter 7. The consequences for changing soil physical conditions on soil chemical processes and the resulting discharge of solutes through the drain are discussed.

1. Introduction

In Chapter 8 the SWMS_2D model is used to evaluate the two-dimensional characteristics of solute transport in a layered soil profile, especially NO_3 leaching to a subsurface drain. Attention is given to description of the hydraulic conductivity characteristic close to saturation. The model is used to simulate the effect of different meteorological conditions, smaller drain spacing, and N mineralisation on NO_3 leaching. Water management is discussed as a possible tool to reduce N losses to the environment.

2. THEORY OF WATER FLOW AND SOLUTE TRANSPORT IN SOIL

This chapter presents a general introduction to the theory of water flow and solute transport in soils. Numerical models that are used in this study are presented. The analytical functions describing the water retention and hydraulic conductivity characteristics are introduced. Time depth curves are presented as a tool to visualise one-dimensional water flow in the soil. Some relevant aspects of the drainage theory are discussed, also related to solute transport.

2.1 Water flow

Water flow in soil is described by the general flow equation, combining the equation for the conservation of mass and Darcy's law for the volumetric water flux. The mass conservation equation can be expressed as:

$$\frac{\partial \theta}{\partial t} = -\nabla \cdot \mathbf{q} - S, \quad (2.1)$$

where : θ = volumetric water content ($\text{m}^3 \text{ m}^{-3}$);
 \mathbf{q} = volumetric water flux density vector ($\text{m}^3 \text{ m}^{-2} \text{ d}^{-1}$);
 S = volumetric density of water uptake by plant roots ($\text{m}^3 \text{ m}^{-3} \text{ d}^{-1}$);
 t = time (d);
 ∇ = vector differential operator (m^{-1}).

The volumetric water flux density can be described by Darcy's law:

$$\mathbf{q} = -K \nabla H, \quad (2.2)$$

with: $H = h + z, \quad (2.3)$

where : K = hydraulic conductivity (m d^{-1});
 H = hydraulic head (m);
 h = pressure head (m);
 z = gravitational head (m); also vertical coordinate, with the origin at the soil surface, directed positively upwards (m).

Combining Eqs. 2.1, 2.2 and 2.3 gives the general flow equation:

$$\frac{\partial \theta}{\partial t} = \nabla \cdot (K \nabla h + K \nabla z) - S. \quad (2.4)$$

In this equation K and S can be functions of position, θ or h , and t . Generally, K may have an anisotropic character.

However, in this study it is implicitly assumed that K is isotropic, unless stated otherwise. It is also assumed that all transport processes take place in a rigid soil, under isothermal conditions, and that the soil physical characteristics do not change as a function of time. The effects of gradients in osmotic potential and vapour pressure are also ignored.

It is practical to distinguish between the unsaturated and saturated zones in the soil because the nature of the partial differential equation 2.4 is rather different for each of these zones.

2.1.1 Unsaturated zone: the SWATRE water flow model

For water flow in the unsaturated zone of the soil, Eq. 2.4 can be expressed as a function of h :

$$C \frac{\partial h}{\partial t} = \nabla \cdot (K \nabla h + K \nabla z) - S, \quad (2.5)$$

with:
$$C = \frac{d\theta}{dh}. \quad (2.6)$$

The differential water capacity term C (m^{-1}) corresponds to the slope of the water retention characteristic. Although the water retention characteristic generally has a hysteretic character (e.g., Otten, 1994; Heinen, 1997), this aspect is not taken into account in the models being discussed later on. Because of the non-linear nature of K and C as functions of h , the possible time dependence of boundary conditions and the spatial distribution of S (Hillel, 1980) Eq. 2.5 is difficult to solve analytically. Therefore, numerical methods are most frequently used to solve Eq. 2.5.

2. Theory

SWATRE model

The SWATRE model simulates water flow in the unsaturated zone of the soil. The model was originally developed for agricultural applications (Feddes *et al.*, 1978) and includes the effects of uptake of water by plant roots. A detailed description of the model is given by Belmans *et al.* (1983). Here, only a brief summary of the essential characteristics of the model is given.

Equation 2.5 is simplified to a one-dimensional form for the vertical direction:

$$\frac{\partial h}{\partial t} = \frac{1}{C} \frac{\partial}{\partial z} \left[K \left(\frac{\partial h}{\partial z} + 1 \right) \right] - \frac{S}{C}. \quad (2.7)$$

Water uptake by plant roots is described as:

$$S = \gamma(h) S_{max}, \quad (2.8)$$

where: $\gamma(h)$ = prescribed function of h (see Fig. 2.1) (-);
 S_{max} = maximum possible extraction rate ($m^3 m^{-3} d^{-1}$).

with: $S_{max} = \frac{T}{|z_r|}, \quad (2.9)$

where: T = potential transpiration rate ($m d^{-1}$);
 z_r = bottom of the root zone (m).

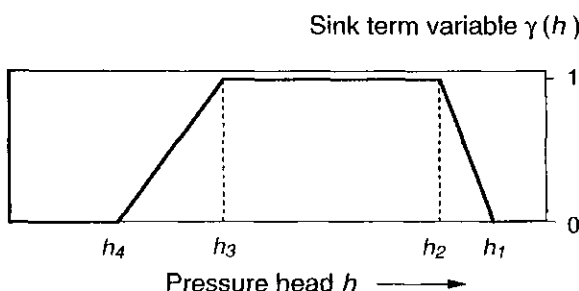


Figure 2.1 General shape of the dimensionless sink term variable as a function of pressure head (after Feddes *et al.*, 1978).

Figure 2.1 shows that water uptake by roots is assumed to be zero above h_1 ("anaerobiosis point") and below h_4 ("wilting point"), maximally between h_2 and h_3 , and to vary linearly from h_1 to h_2 and from h_3 to h_4 .

The potential evapotranspiration rate E_p (m d^{-1}) of a cropped surface is calculated from:

$$E_p = f E_{ref}, \quad (2.10)$$

where: f = crop factor (-) (Feddes, 1987);

E_{ref} = maximum possible evapotranspiration rate
of a reference crop (m d^{-1}).

For grassland in the Dutch climate E_{ref} is given according to Makkink (1957) as:

$$E_{ref} = c_{cv} \left[0.65 \frac{s}{\lambda(s+g)} G \right], \quad (2.11)$$

where: λ = latent heat of vaporisation of water (J kg^{-1});

G = global radiation flux density (W m^{-2});

s = rate of change of the saturation water vapour pressure with
temperature at air temperature (Pa K^{-1});

g = psychrometer constant (Pa K^{-1});

$c_{cv} = 864$ ($\text{m}^3 \text{kg}^{-1}$) = conversion factor from ($\text{kg m}^{-2} \text{s}^{-1}$) to (m d^{-1}).

In SWATRE, Eq. 2.7 is solved by using a finite-difference scheme which is implicit and applies an explicit linearisation. In this study the soil profile is divided into compartments of variable thickness with a maximum of 10 cm. The time steps for the calculations are variable and are estimated from the change in water content in the previous time step. Generally, the time steps for the numerical calculations are smaller than 0.1 d.

2. Theory

2.1.2 Saturated zone

In the saturated zone $\theta = \theta_s$ is constant; θ_s is the volumetric water content at saturation ($\text{m}^3 \text{ m}^{-3}$). At saturation $S = 0$, according to Fig. 2.1. Flow equation 2.7 can thus be simplified to:

$$\nabla \cdot (K_s \nabla h + K_s \nabla z) = 0, \quad (2.12)$$

where : K_s = hydraulic conductivity at saturation (m d^{-1}).

Equation 2.12 is a linear partial differential equation describing groundwater flow (Bear and Verruijt, 1992). It should be noted that a capillary fringe can extend the saturated zone above the phreatic surface. Equation 2.12 is relatively easy to solve, and analytical solutions are available for special cases. However, for practical transport problems with time-dependent boundary conditions and spatially distributed soil physical properties, numerical models have to be used (Zaradny, 1993).

Drainage equations

In agro-hydrological literature much emphasis is given to water flow in the saturated zone to describe the performance of drains (Van Schilfgaarde, 1974). The Dupuit-Forchheimer approach is often used, which assumes horizontal water flow in the soil towards a ditch or drain. For subsurface water flow to a drain this simplified approach can be used to describe the relationship between the elevation of the phreatic surface and the drain discharge rate. Hooghoudt (1940) considered steady water flow to parallel ditches or drains with an impermeable layer at the bottom of the flow domain, and derived (Fig. 2.2):

$$q = \frac{8 K_{s,b} d m_0 + 4 K_{s,a} m_0^2}{L^2}, \quad (2.13)$$

where : q = drain discharge rate (m d^{-1});

m_0 = elevation of the phreatic surface midway between the drains relative to the drain level (m);

L = drain spacing (m);

$K_{s,a}$ = hydraulic conductivity at saturation above the drain (m d^{-1});

$K_{s,b}$ = hydraulic conductivity at saturation below the drain (m d^{-1});
 d = depth interval of the soil layer between drain and impermeable layer (m).

To account for the extra head losses due to radial flow close to the drain, Hooghoudt introduced an equivalent depth $d_{eq} < d$:

$$q = \frac{8 K_{s,b} d_{eq} m_0 + 4 K_{s,a} m_0^2}{L^2}. \quad (2.14)$$

For a given drain radius r , drain spacing L and depth d , the equivalent depth d_{eq} can be found in tables (Hooghoudt, 1940). The Hooghoudt equation 2.14 can be used when the drain is located on an impermeable layer or at the interface of two soil layers (Ritzema, 1994).

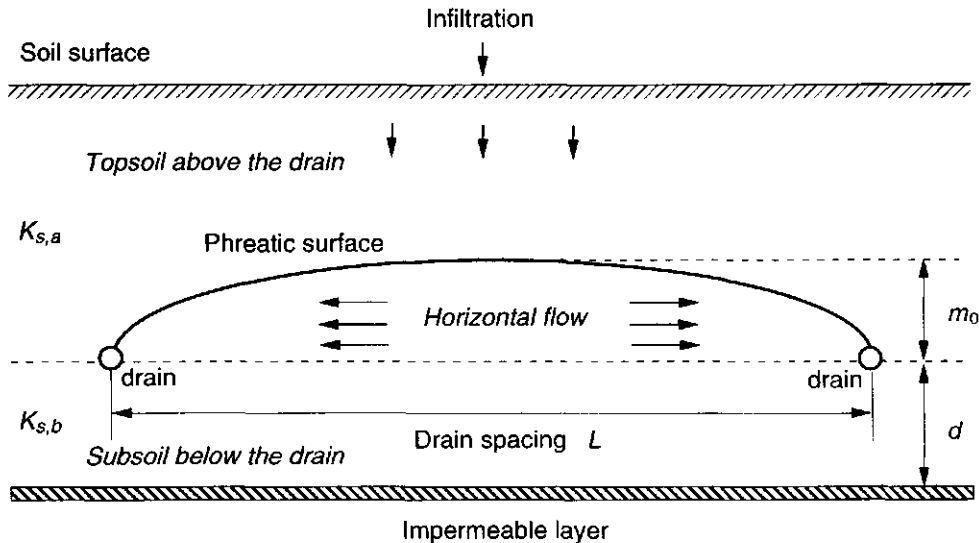


Figure 2.2 Steady water flow to a subsurface drain with horizontal Dupuit-Forchheimer flow below the phreatic surface. The characteristic quantities for the Hooghoudt equation 2.14 are indicated.

2. Theory

Ernst (1956, 1962) derived an equation for a two-layered soil profile with the drain located at any position within the soil profile. Ernst assumed that water flow from the phreatic surface to the drain could be split into a vertical, a horizontal and a radial component. By summing all hydraulic head gradients, the elevation of the phreatic surface above the drains can be calculated. Ritzema (1994) points out that the application of the Ernst equation is especially useful for soil profiles where the hydraulic conductivity in the topsoil is smaller than in the subsoil, with the drain located in the subsoil.

For transient groundwater flow to subsurface drains the concept of drainable pore space can be used, which reflects the change in water storage in the unsaturated zone when the position of the phreatic surface changes. The Glover-Dumm equation (Dumm, 1954) can be used for a falling phreatic surface and the De Zeeuw-Hellinga equation (De Zeeuw and Hellinga, 1958) for a fluctuating phreatic surface. Ritzema (1994) concludes that the applicability of these type of equations is limited, because only homogeneous soil profiles can be considered, the water flow in the zone above the drain depth is not taken into account, and the drainable pore space is not a constant but varies as a function of the distance from the drain.

Anisotropy in the soil profile, for example due to the layering of the soil, can be taken into account, leading to more complex drainage equations (Maasland, 1957). All these approaches mainly focus on the water balance of the soil under steady conditions. To describe solute transport to a drain, the overall water balance of the soil is not of major importance, but the description of the flow paths and corresponding residence time distributions of solutes.

2.1.3 The combined saturated-unsaturated zone: the SWMS_2D water flow model

The model SWMS_2D (Simunek *et al.*, 1994) simulates simultaneously Darcian water flow in a two-dimensional flow domain in the unsaturated-saturated zone. SWMS_2D numerically solves flow equation 2.4. In the present study SWMS_2D is applied for a fall-winter-spring leaching period only, when there is no water uptake by plants ($S = 0$). Under these conditions, Eq. 2.4 becomes:

$$\frac{\partial \theta}{\partial t} = \nabla \cdot (K \nabla h + K \nabla z) . \quad (2.15)$$

As initial condition, $h(x,z)$ has to be given for the whole flow domain. Different types of boundary conditions can be implemented, such as specified fluxes ("Neumann condition") or specified pressure heads ("Dirichlet condition"). The interaction between the soil surface and the atmosphere, like evaporation and infiltration, is treated similarly as in SWATRE (Feddes *et al.*, 1978). Ponding is not simulated in SWMS_2D; all ponded water is immediately removed (run-off). A special boundary condition is used at the subsurface drain, which will be discussed in detail when the model is applied to the specific field situation. The soil hydraulic characteristics have to be described by analytical functions.

The Galerkin finite element method with linear basis functions (Zienkiewicz, 1977) is used to solve the flow equation with the corresponding initial and boundary conditions. The flow domain is subdivided into a network of triangular elements, with nodes at the corners of the elements. An implicit finite difference scheme is used to derive the matrix equations, representing the discretised partial differential equations. The linearised system of equations is solved iteratively, using Gaussian elimination or a conjugated gradient method, considering the values of the coefficients in the matrix equations at the former iteration step. Mass balance is satisfied, using the method proposed by Celia *et al.* (1990). Numerical time steps in the model are related to the spatial discretisation of the flow domain, the time course of the boundary conditions, and the desired output intervals. When solute transport is taken into account, the time step is also subject to accuracy and stability criteria for calculating solute transport.

Construction of the finite element grid

The flow domain has to be divided into triangular elements, and the nodes and elements have to be numbered. In zones where large H gradients or changing directions of the H gradients are expected, the density of the grid must be higher, e.g., close to the soil surface or near a drain. Triangular finite element grids can follow irregular geometrical boundaries and allow for local changes in grid densities. The HYDRUS-2D grid generator (Simunek *et al.*, 1996) was used to create the triangular grids automatically. A triangular grid is generated and an output file is made with the nodes and elements. The details of a specific finite

2. Theory

element grid are given in Chapter 8 (Fig. 8.1).

Darcian fluxes in finite elements

The Darcian fluxes are implied in the flow equation, but they are not calculated separately during the computations of h . Fluxes of water are important when solute transport has to be calculated and when fluxes are given or must be calculated at the boundaries of the flow domain. When the Darcian fluxes are calculated using ∇H between the nodes, assuming a constant ∇H and an average K for each element, discontinuities in the fluxes will occur at the nodal points and at the element boundaries. These discontinuities are physically impossible and lead to local and overall mass balance errors (Yeh, 1981). This problem can be solved by using a dense grid and checking whether the mass balance errors are acceptable for the specific flow problem.

SWMS_2D uses the arithmetically averaged K 's of the elements to solve the discretised flow equation. However, the Darcian fluxes are calculated for each node, by taking the arithmetical average of the ∇H contributions of the surrounding elements, multiplied by the local K at the node. This approach does not correspond with the use of the element-averaged K in the discretised flow equation, and results in local discontinuities in the calculated fluxes. Although the water balance errors remain small, for solute transport this approach can result in substantial mass balance errors. This problem is solved by using a dense grid and checking whether the solute mass balance errors are acceptable for the specific transport problem.

Triangular elements having nodes with different soil physical characteristics at their corners, will have averaged soil physical characteristics implied by the nature of the finite element algorithm. This averaging smoothes sharp changes between distinct soil layers. When the differences in soil physical characteristics are large between two adjacent zones, this procedure can have substantial consequences for the calculated fluxes. A denser grid in this zone can solve this problem.

2.1.4 Analytical expressions for the soil hydraulic characteristics

The water retention and hydraulic conductivity characteristics are needed as input data to solve Eqs. 2.5 and 2.7. Tabulated data based on laboratory

measurements can be used in numerical water flow models, but interpolation techniques have to be used to obtain a complete table in small steps of volumetric water contents. Therefor, there are a number of advantages in using analytical expressions to describe the soil hydraulic characteristics. It is easier to have an input of a few parameters rather than handling large tables of data. This simplifies varying the soil hydraulic characteristics for the purpose of sensitivity analysis of the model, thus making use of, e.g., Monte-Carlo simulations easier. Hopmans (1987) used this technique for calculating the effects of spatial variability of hydraulic characteristics on the soil physical processes. The use of analytical expressions can also be seen as an averaging and interpolation technique for the measured points of the soil hydraulic characteristics.

In this study the analytical expressions of Van Genuchten (1978, 1980) and Mualem (1976) will be used. Van Genuchten's expression for the water retention characteristic is:

$$S_e = \frac{(\theta - \theta_r)}{(\theta_s - \theta_r)} = \left[1 + (\alpha|h|)^n \right]^{-m}, \quad (2.16)$$

where: S_e = degree of saturation (-);
 θ_r = residual volumetric water content ($m^3 m^{-3}$);
 α = empirical parameter (m^{-1});
 n and m are empirical parameters (-).

Mualem's expression for the hydraulic conductivity characteristic is:

$$K = K_s S_e^L \left(\frac{\int_0^1 \frac{1}{h(x)} dx}{\int_0^1 \frac{1}{h(x)} dx} \right)^2, \quad (2.17)$$

where: L = empirical constant (-);
 x = dummy variable (-).

2. Theory

Solving Eq. 2.16 for h and substituting this expression in Eq. 2.17 gives an expression for K in terms of S_e . Closed forms of the integrals can be obtained for integer values of $m - 1 + (1/n)$ (Van Genuchten, 1980; Raats, 1992).

Van Genuchten (1986) developed a non-linear least-square fitting procedure (RETC) to estimate the parameters α , n (and m), θ_r and θ_s from measured water retention data. A later version of this procedure is used here (Leij *et al.*, 1992), which allows a simultaneous fit to measured water retention and hydraulic conductivity data, including estimates of K_s and L .

For the soil of the Lovinkhoeve De Vos *et al.* (1992) evaluated twelve options for the fitting program RETC. The conclusions of this study were that:

1. Both water retention and hydraulic conductivity characteristics are measured, and hence a simultaneous fit was possible.
2. The precision of the hydraulic conductivity data is assumed to be an order of magnitude less than that of the water retention data. For this reason we assigned a value of 0.1 to the weighing factor W_1 for the hydraulic conductivity data in the fitting procedure. This is consistent with the studies of Wösten and Van Genuchten (1988) and Sisson and Van Genuchten (1991), who successfully used values between 0.1 and 1.0 for W_1 .
3. The measured hydraulic conductivity at saturation can be greatly influenced by a few cracks and macro-pores, especially in the silt loam topsoil of the Lovinkhoeve and may thus not represent the bulk soil. Therefore K_s is omitted from the fitting procedure.
4. The method yields a simple closed-form relationship for the hydraulic conductivity characteristic, by assuming $m = 1 - (1/n)$.
5. A high R^2 and a visually reasonable fit are judged to be important. R^2 is an average measure for the similarity between the measured and the fitted data for the water retention and hydraulic conductivity fits.

2.1.5 Time-depth curves of parcels of water

Usually, the results of the one-dimensional numerical water balance calculations are presented in the form of volumetric water content profiles. These profiles give only a small part of the desired information. Especially if the behaviour of solutes is of interest, flow paths and residence times are important features. Duynisveld (1984) introduced time-depth curves of parcels of water as a

tool to present the results of numerical water balance models. Earlier analytical solutions of flow problems were visualised as time-depth curves by Raats (1975). Time-depth curves are graphical representations of the kinematics of water in the unsaturated zone of the soil (see Fig. 5.16). Using a one-dimensional piston-flow approach, the locations of parcels of water in the course of time can be calculated. The calculations are based on daily water balance data obtained from water balance models or field measurements. A detailed description of the method and a FORTRAN program is given by De Vos (1991).

2.2 Solute transport: the SWMS_2D solute transport model

The solute mass conservation equation can be described as:

$$\frac{\partial(\theta c)}{\partial t} = -\nabla \cdot \mathbf{F}_s - S_c, \quad (2.18)$$

where : c = solute concentration (mg m^{-3});

\mathbf{F}_s = solute flux density vector ($\text{mg m}^{-2} \text{d}^{-1}$);

S_c = solute uptake by plant roots ($\text{mg m}^{-3} \text{d}^{-1}$).

Adsorption, exchange and chemical reactions are not taken into account in Eq. 2.18. This study concentrates on the effect of the transient water flow on solute transport. The solute transport module of SWMS_2D (Simunek *et al.*, 1994) is used to solve Eq. 2.18 numerically.

Drainage water is a mixture of water from different stream tubes. The contribution of each stream tube can only be quantified when the details of water flow in the whole flow domain are known. For steady flow patterns, De Valk and Raats (1995) developed a theory based on the concept of following parcels of water along a stream tube and taking into account adsorption and exchange of solutes by the solid phase. For conservative solutes, the steady multidimensional transport to a ditch or drain can be described by the travel time density distribution. For steady groundwater flow with a uniform step input at the top of a rectangular aquifer at initial concentration $c = 0$, with drains or ditches at the sides, the travel time density distribution can be approximated by (Raats, 1981b):

2. Theory

$$\frac{c_{out}}{c_{in}} = 1 - \exp\left(-\frac{t}{\tau_{aq}}\right), \quad (2.19)$$

where : c_{out} = solute concentration in the outlet (mg m^{-3});

c_{in} = step input solute concentration (mg m^{-3});

τ_{aq} = turnover time of the system (d).

The turnover time τ_{aq} of the system is equal to the volume of the water in the aquifer divided by the total flux through the aquifer. Equation 2.19 also describes a solute leaving a well-mixed vessel after a step input. This simple example stresses the fact that the water quality reaction time of an aquifer is totally different from the water quantity reaction time. In general, water quality reaction times are much longer. When the exchange of solutes with the solid phase is also considered, an extra retardation will result for many solutes. Diffusion and hydrodynamic dispersion will result in a broadening of solute peaks, and leading to shorter travel times for a fraction of the solutes (Van Kooten, 1996). Under certain conditions preferential flow through cracks or macro-pores, or preferential flow induced by unstable flow can occur. Such phenomena are not explicitly considered in this study. For field situations with a strongly fluctuating phreatic surface, it is much more difficult to describe the transport of solutes to a drain. In the course of time, water can flow via different pathways to the drain, which can have substantial consequences for solute transport.

SWMS_2D solute transport model

The SWMS_2D model (Simunek *et al.*, 1994) simulates solute transport in a two-dimensional flow domain in the saturated-unsaturated zone. SWMS_2D solves solute transport equation 2.18 numerically, assuming that \mathbf{F}_s is composed of a convective and a dispersive component:

$$\mathbf{F}_s = \mathbf{q} c - \theta \mathbf{D} \nabla c, \quad (2.20)$$

where : \mathbf{D} = dispersion tensor ($\text{m}^2 \text{d}^{-1}$).

The components of \mathbf{D} are given by Bear (1972):

$$\theta D = \theta D_{ij} = a_T |\mathbf{q}| \delta_{ij} + (a_L - a_T) \frac{q_i q_j}{|\mathbf{q}|} + \theta D_d \tau \delta_{ij}, \quad (2.21)$$

where : D_{ij} = components of the dispersion tensor ($\text{m}^2 \text{d}^{-1}$);
 a_L = longitudinal dispersivity (m);
 a_T = transversal dispersivity (m);
 D_d = molecular diffusion coefficient in free water ($\text{m}^2 \text{d}^{-1}$);
 q_i = i -component of \mathbf{q} ($\text{m}^3 \text{m}^{-2} \text{d}^{-1}$);
 $|\mathbf{q}|$ = absolute value of the water flux density ($\text{m}^3 \text{m}^{-2} \text{d}^{-1}$);
 τ = tortuosity factor (-);
 δ_{ij} = Kronecker delta function ($\delta_{ij} = 1$ if $i=j$, and $\delta_{ij} = 0$ if $i \neq j$).

The tortuosity factor is calculated according to Millington and Quirk (1961):

$$\tau = \frac{\theta^{7/3}}{\theta_s^2}. \quad (2.22)$$

To solve Eqs. 2.18, and 2.20 to 2.22, the solution of the water flow section of SWMS_2D is used to obtain \mathbf{q} and θ . The same grid is used as in the water flow section for the division of the flow domain into triangular elements. As initial condition, $c(x,z)$ for the whole flow domain has to be given. Prescribed concentrations ("Dirichlet condition") or prescribed solute fluxes ("Neumann condition") can be given as boundary conditions.

The solution procedure for the solute transport equation is largely similar to the solution procedure for the water flow equation. For each numerical time step the flow equation is solved first. Then, the coefficients of the discretised solute transport matrix equations can be calculated using an explicit, a Crank-Nicholson or a fully implicit scheme. These schemes represent the way of time weighing of the coefficients during the time step. An upstream weighing procedure can be used to minimise numerical oscillations for simulations with steep concentration gradients. Other measures to reduce oscillations are related to the combination of space and time discretisations. The Peclet number represents the ratio between convective and dispersive transport terms:

2. Theory

$$Pe_i^e = \frac{q_i \Delta x_i}{\theta D_{ii}}, \quad (2.23)$$

where : Pe_i^e = grid Peclet number of finite element e in the i -direction (-);
 q_i = i -component of q ($m^3 m^{-2} d^{-1}$);
 Δx_i = characteristic length of finite element e in the i -direction (m).

It is recommended to fulfil the condition:

$$Pe_i^e < 10. \quad (2.24)$$

The grid Courant number is defined as:

$$Cr_i^e = \frac{q_i \Delta t}{\theta \Delta x_i}. \quad (2.25)$$

To prevent oscillations it is advised to fulfil the condition:

$$Cr_i^e \leq 1. \quad (2.26)$$

A combined criterion to minimise oscillations is:

$$Pe_i^e \cdot Cr_i^e \leq 2. \quad (2.27)$$

The maximum permitted time step is calculated using all three criteria 2.24, 2.26 and 2.27.

3. FIELD AND LABORATORY METHODS

The field and laboratory methods used in this thesis are presented in this chapter. The field methods served to monitor the soil physical and meteorological conditions as a function of position and time. One of the laboratory methods described is the calibration of a field method. Methods and procedures which are specific for this study receive most attention. The more standard methods are only mentioned briefly.

3.1 Field methods

The instruments, installation and measurement procedures of the field methods are described. For all methods an indication is given of the measurement accuracy. This accuracy is related to the instrument characteristics and response times of the system. The interpretation of spatial variability and spatial patterns in the field is discussed later. However, the fact that in a field large spatial differences in the soil physical conditions can occur, resulted in a preference for repeating measurements throughout the field instead of increasing the accuracy of individual measurements.

The vertical positions of the probes were measured using water-levelling equipment. All readings were converted to values relative to the average level of the soil surface ($z = 0$). Horizontal positions relative to fixed known points in the field were measured using tapes.

Groups of instruments were installed in the field and had to be read and serviced, so that a person had to walk in the field. It was attempted to prevent local soil compaction and damage to the crop, especially near the instruments. Under wet conditions boards on blocks were temporarily placed in the field to be able to approach the instruments without disturbing the soil surface.

3.1.1 General soil physical methods

Pressure head

In 1986 mercury-filled tensiometers (Klute, 1986) were used to measure pressure heads (reading accuracy: ± 100 Pa; i.e. $\Delta h = \pm 10$ cm). From 1987 onward tensiometers were used in which the pressure head was measured with a mobile pressure transducer (Soil Measurement Systems, Las Cruces, USA; model: Tensiometer) (Marthaler *et al.*, 1987). An air gap of 1.5-2.0 cm³ was maintained above the water level in the tensiometer, which was closed with a septum stopper (Fig. 3.1). The mobile pressure transducer (accuracy: ± 10 Pa; i.e. $\Delta h = \pm 1$ cm) was connected with the air in the tensiometer by injecting a needle through the septum stopper. Normally, 30 s after injection a reading is made, and equilibrium between the energy status of the soil water and the air in the pressure transducer is assumed. Because the air in the pressure transducer and in the needle are both at atmospheric pressure, a change of the air pressure in the air gap (h_{air}) will occur when the needle is injected. This change is a systematic measurement error, which is ± 50 cm at $h_{air} = -800$ cm, 6 cm at $h_{air} = -100$ cm and -1 cm at $h_{air} = -10$ cm (Marthaler *et al.*, 1987), where h_{air} is expressed as a head relative to the atmospheric pressure. Due to water flow through the ceramic cup during the injection of the needle and the equilibration time, the errors will become smaller.

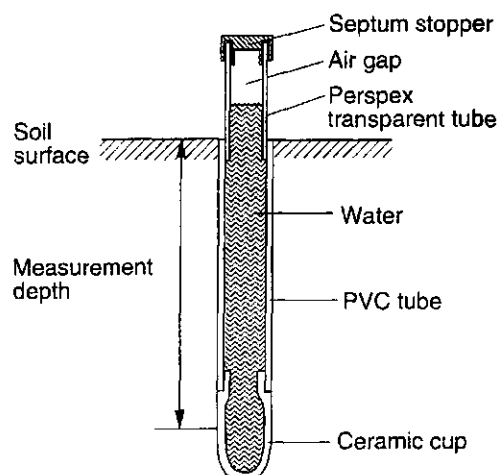


Figure 3.1 Tensiometer with an air gap above the water column. A septum stopper closes the air gap, in which the pressure can be measured by injecting a needle connected to a mobile pressure transducer (Marthaler *et al.*, 1987).

3. Field and laboratory methods

The transparent upper tube of the tensiometers was covered with a white PVC cover to prevent heating and expansion of the air gap. To further reduce temperature effects, pressure head readings were made during the morning, when the sun radiation is not intense. During the growing season the water extraction by the crop is not yet at a maximum in the morning, which means that the tensiometer readings will not represent the driest soil conditions during the day, but the wetter soil conditions during the night and morning period (Towner, 1980; Towner, 1984).

Groups of tensiometers were installed vertically at a minimum horizontal distance of 20 cm, with increasing measurement depths (Fig. 3.2), and a parallel orientation to the drains. When row crops were grown, tensiometers were placed midway between the rows. For all tensiometers, ceramic cups (Soil Moisture Equipment Corp., Santa Barbara, USA.; model 653X05-B1M3) with a diameter of 1.8 cm and a length of 5 cm were used. The length of the cup is an indication for the depth interval over which the pressure head is averaged.

The tensiometer readings are converted to pressure heads at the measurement depth (NEN-5783, 1991; NEN-5785, 1991). When $h < -800$ cm the values are rejected, because close to $h = -800$ cm air bubbles may form in the tensiometers and no reliable measurements can be no longer be made. During winter, tensiometers were filled with a mix of 40% ethanol and 60% water (v/v) to prevent freezing of the upper parts. No corrections are made for the different fluid characteristics, because there is only a small difference between the specific densities of 1000 kg m^{-3} for water and 790 kg m^{-3} for ethanol. It is assumed that most of the fluid remains within the tensiometer, which means that the higher viscosity of the ethanol-water mixture will not lead to lower hydraulic conductivities in the soil as compared to normal soil water. So, no effect is expected on the reaction time of the tensiometer.

Groundwater level

Groundwater levels were measured with PVC tubes which were perforated over the whole length of the tube (Fig. 3.2), except the top 10 cm to prevent infiltration of water into the tubes during short periods with saturated conditions in the topsoil. A tube diameter of 2 cm was used with perforations every 3 cm and holes of 0.5 cm. The tube was covered with a nylon filter cloth (0.1 mm) to prevent penetration of soil. Tube lengths of 1.5 and 2.0 m were chosen and the tubes were installed directly in a bore-hole without extra filter material. The tubes were

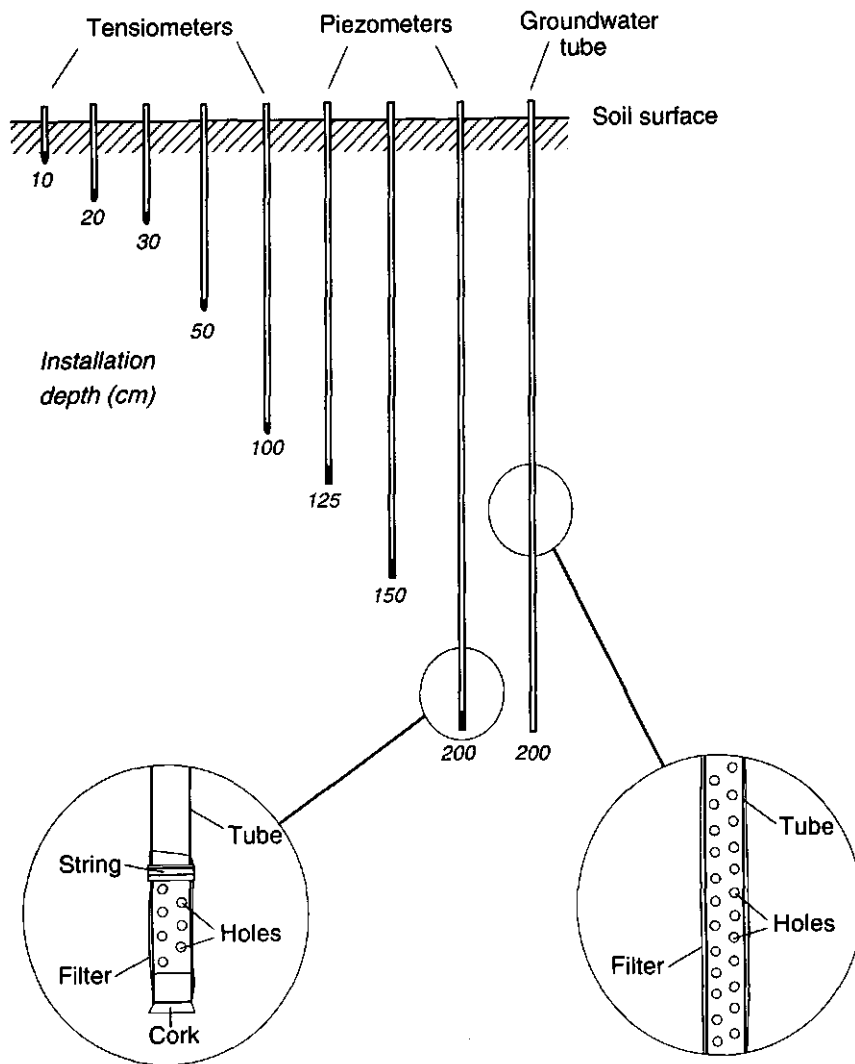


Figure 3.2 Outlay of a group of tensiometers, piezometers and a groundwater tube, installed at different depths in the soil, and some details of a piezometer (perforated over 5 cm length close to the bottom) and a groundwater tube (perforated over the entire length).

3. Field and laboratory methods

often installed in the same row as the tensiometers (Fig. 3.2). Readings were made using an electronic device which detected the water level and a ruler which indicated the depth (accuracy: ± 0.5 cm).

One groundwater level was measured every 15 minutes using a pressure transducer (Keller, Winterthur, Switzerland; model RN19, accuracy: ± 10 Pa; i.e. $\Delta z = \pm 1$ cm). The dimensions of this pressure transducer made it necessary to use a larger tube of 4 cm diameter. Coarse sand was used as extra filter material, because the bore hole had to be made wider than the tube. The pressure transducer was calibrated in the laboratory, and field measurements of the water level in the tube were used to check the proper functioning of the pressure transducer.

Hydraulic head

In the saturated zone, the soil hydraulic heads were measured by means of piezometers. Similar PVC tubes were used as for the groundwater tubes, but they were only perforated over 5 cm length to the bottom of the tubes (Fig. 3.2). The piezometers were installed at measurement depths of 1.0, 1.5 and 2.0 m. Measurement procedures were similar to those for the groundwater levels. In August 1993 two extra piezometers with a diameter of 4 cm were installed at 3 and 4 m depth to measure whether downward or upward seepage occurred.

Soil temperature

Soil temperatures were measured with thermistors (Fenwal, USA; Uni-Curve, model: UUA33J1) which were incorporated in stainless steel probes. These thermistors are electronic components with a non-linear temperature-dependent resistance, ranging from 30000Ω at -20°C to 1600Ω at 40°C . A mobile electronic device was built which measured the resistance and converted the readings to temperatures (accuracy $\Delta T = \pm 0.2^\circ\text{C}$).

Close to the soil surface, steep vertical temperature gradients can occur. When temperatures at a specified depth have to be measured, it is necessary to install the soil temperature probes horizontally to prevent vertical heat conduction through the stainless steel. Deeper than about 50 cm, the vertical gradients are much smaller and temperatures can be measured by installing the probes vertically from a soil pit at 50 cm depth, with the thermistor located close to the front end of the probe. Depths of the soil temperature probes are given relative to the level of the local soil surface.

At the meteorological station, Pt-100 platinum resistors incorporated in stainless steel probes were used. Pt-100 sensors are known to be extremely stable (Fritschen and Gay, 1979), which makes them suitable for long-term measurements. However, special measurement techniques have to be used to measure the small change in resistance ($40 \text{ m}\Omega \text{ }^{\circ}\text{C}^{-1}$) relative to the nominal resistance of 100Ω (at $0 \text{ }^{\circ}\text{C}$). An accuracy of $\Delta T = \pm 0.1 \text{ }^{\circ}\text{C}$ was achieved for the temperature measurements at the meteorological station.

Volumetric water content and bulk density

Volumetric water content θ and (dry) bulk density ρ_b were measured by taking 100 cm^3 (height = 5.0 cm , diameter = 5.05 cm) undisturbed soil samples and using the procedures described in NEN-5781 (1992). Accuracies of $\pm 0.01 \text{ m}^3 \text{ m}^{-3}$ for volumetric water content and $\pm 10 \text{ kg m}^{-3}$ for the bulk density could be obtained. In this thesis only dry bulk densities are considered, referred to as bulk density.

3.1.2 Time Domain Reflectometry

Time Domain Reflectometry (TDR) soil water content measurements are based on travel time measurements of electromagnetic (EM) waves in TDR probes installed in soil (Topp *et al.*, 1980). The relative dielectric permittivity (ϵ_r) of the soil, which is strongly related to the volumetric water content θ , determines the velocity v (m s^{-1}) of the EM waves:

$$v = \frac{c_{\text{light}}}{\sqrt{\epsilon_r}}. \quad (3.1)$$

with: c_{light} = speed of light = $3 \cdot 10^8 \text{ (m s}^{-1}\text{)}$.

The decrease in amplitude of a reflected EM wave can be used to calculate the electrical conductivity of the medium (Dalton and Van Genuchten, 1986). A cable-tester can be used to measure the (one-way) travel time Δt of the EM wave in the TDR probe. Because the length L_{probe} (m) of the TDR probe is known, the velocity of the wave can be calculated:

3. Field and laboratory methods

$$v = \frac{L_{probe}}{\Delta t}. \quad (3.2)$$

The apparent relative permittivity ϵ_a is defined as the relative permittivity which is measured without corrections for dielectric losses and without an exact specification of the measurement frequencies. It can be calculated by combining Eqs. 3.1 and 3.2 and setting $\epsilon_r = \epsilon_a$:

$$\epsilon_a = \left(\frac{c_{light} \Delta t}{L_{probe}} \right)^2. \quad (3.3)$$

When a Tektronix (Tektronix, Beaverton, Oregon, USA) cable-tester is used as TDR instrument, a step pulse is generated as a wave form. Heimovaara (1993) analysed the frequency spectrum of this step pulse and concluded that frequencies from 20 kHz to 1 GHz were present in the pulse. The high frequencies have a dominant effect on the measured travel times in soil.

Topp-curve

Topp *et al.* (1980) showed that for mineral soils a general calibration curve between ϵ_a and θ could be used:

$$\theta = -0.53 \cdot 10^{-1} + 0.292 \cdot 10^{-1} \epsilon_a + 0.55 \cdot 10^{-3} \epsilon_a^2 + 0.43 \cdot 10^{-5} \epsilon_a^3. \quad (3.4)$$

However, under field conditions there are a few complicating factors. The bulk density of the soil has an effect on ϵ_a and will affect the calibration curve.

De Loor-curve

Dirksen and Dasberg (1993) showed that for many clay soils the TDR calibration curves can be predicted by applying a theoretical mixing model based on the Maxwell equation. In this model, components with a different ϵ are thought to be randomly distributed in a homogeneous mixture (De Loor, 1966, 1990). Dirksen and Dasberg (1993) distinguished four components: solids, air, free water, and bound water. They assumed that in a clay soil a mono-molecular water layer ($3 \cdot 10^{-10}$ m thick) covered the mineral surfaces of the solids, which results in a lower $\epsilon_{bw} = 3.2$ for this layer of bound water as compared to $\epsilon_w = 80.4$ ($T = 20^\circ\text{C}$) for free water. For solids $\epsilon_s = 5$, and for air $\epsilon_{air} = 1$ were used.

Dirksen and Dasberg (1993) used the equation for the De Loor model given by Dobson *et al.* (1985):

$$\varepsilon = \frac{3\varepsilon_s + 2(\theta - \theta_{bw})(\varepsilon_w - \varepsilon_s) + 2\theta_{bw}(\varepsilon_{bw} - \varepsilon_s) + 2(\phi - \theta)(\varepsilon_{air} - \varepsilon_s)}{3 + (\theta - \theta_{bw})\left(\frac{\varepsilon_s}{\varepsilon_w} - 1\right) + \theta_{bw}\left(\frac{\varepsilon_s}{\varepsilon_{bw}} - 1\right) + (\phi - \theta)\left(\frac{\varepsilon_s}{\varepsilon_{air}} - 1\right)}, \quad (3.5)$$

where: ε = relative dielectric permittivity of the mixture;

θ_{bw} = volume fraction of bound water ($\text{m}^3 \text{ m}^{-3}$);

ϕ = porosity ($\text{m}^3 \text{ m}^{-3}$).

Equation 3.5 accounts for the effect of changes in bulk density and the amount of bound water on the ε - θ relation, and implies the assumption that $\theta < 0.33 \text{ m}^3 \text{ m}^{-3}$. The volume fraction of bound water θ_{bw} can be estimated from the specific surface S of the clay minerals. For many clay soils the hygroscopic water content gives a reliable estimate of θ_{bw} .

Refractive index

The apparent refractive index n_a measured with TDR is defined as (Heimovaara, 1993):

$$n_a = \frac{c_{light}}{v} = \sqrt{\varepsilon_a}, \quad (3.6)$$

where: c_{light} = speed of light (m s^{-1});

v = velocity of the EM wave measured by TDR (m s^{-1}).

Ledieu *et al.* (1986) and Herkelrath *et al.* (1991) showed that the volumetric water content is linearly related to the refractive index. Heimovaara (1995) fitted a linear relationship for the Topp-curve:

$$\theta = 0.103 n_a - 0.135, \quad R^2 = 0.993. \quad (3.7)$$

For a silt loam soil, with a high bulk density $\rho_b = 1562 \text{ kg m}^{-3}$, Heimovaara (1995) also fitted a linear relationship:

3. Field and laboratory methods

$$\theta = 0.124 n_a - 0.133 , \quad R^2 = 0.998. \quad (3.8)$$

TDR measurement volume and soil temperature effects

In this study, an individual calibration line was constructed for each depth interval, using the average bulk density of that depth interval. However, the spatial variability of the bulk density and the composition of the soil will affect the local dielectric properties around the TDR probe, and will influence the TDR signal. The actual measurement volume depends on the dimensions of the TDR probe and to a much lesser extent on the water content of the soil. In this study, 3-rod TDR probes were used, which have a good signal quality (Zegelin *et al.*, 1989). The measurement volume of these probes can be approximated by a cylinder of soil around the centre rod. The diameter of this cylinder is about twice the distance between the outer rods, and the length corresponds with the length of the rods. Knight (1992) showed that positions just around the inner rod are the most sensitive positions within the measurement volume. The diameter of the rods has to be chosen large enough to prevent the concentration of the electric field just around the centre rod. The installation of the TDR probes must be carried out very carefully, without compaction and without creating air gaps between the centre rod and the soil. Compaction of the soil cannot be prevented, but will stay within reasonable limits by choosing small-diameter rods. The dimensions of the TDR probes described in the next paragraph are a compromise between the conflicting demands described above. It remains difficult to detect whether the installation of TDR probes was done properly or not, which leads to another source of uncertainty in TDR measurements.

The relative dielectric permittivity of water ε_w depends on temperature T ($^{\circ}\text{C}$) (Wobschall, 1977):

$$\varepsilon_w = 87.8 - 0.37 T. \quad (3.9)$$

Especially in the 0-30 cm depth topsoil, the daily and seasonal variations in soil temperature can be substantial and corrections for the effect of these changes on the calculation of θ have to be made.

Field setup

An automated TDR system with 34 probes was installed in the drainage experiment to obtain measurement series of θ at different depths and at various distances from a drain (Fig. 3.3). Every hour the wave forms of all probes were measured, using a Tektronix 1502B cable tester and a multiplexing and control system developed by Heimovaara and Bouting (1990). The wave forms were stored in a personal computer. The hourly measurement and storage of 34 wave forms took about 25 minutes in the period between November 1991 and September 1993. Due to a faster communication protocol this time was reduced to 10 minutes from September 1993 onwards. The collected data were transferred on floppy-discs to the laboratory and they were analysed, using the procedures and programs of Heimovaara and Bouting (1990).

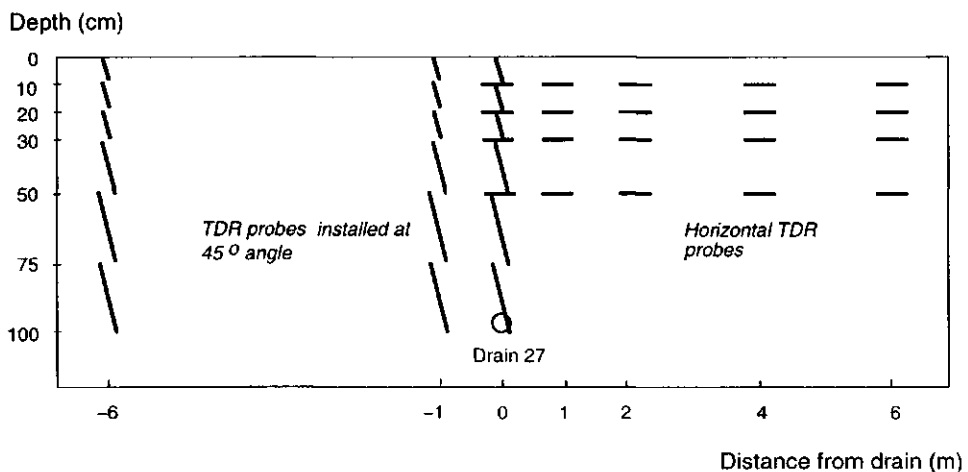


Figure 3.3 Overview of 34 TDR probes installed at various depths at different distances from drain 27. Probes at a distance from the drain ≤ 0 are installed under a 45° angle; probes at a distance from the drain ≥ 0 are horizontally installed with all rods in the same horizontal plane.

3. Field and laboratory methods

TDR probes

Two types of TDR probes were used (Fig. 3.4). Twelve 30 cm long TDR probes (Fig. 3.4a) were installed horizontally at 10, 20, 30 and 50 cm depth at different distances from drain 27 (Fig. 3.3). The impedance of these probes in air is approximately $Z_p = 152 \Omega$. The probes were inserted from a small pit, and were meant to measure θ at specific depths. TDR probes with three rods at the bottom of a PVC tube were developed (Fig. 3.4b) to measure θ at various depth intervals. The impedance of these probes in air is approximately $Z_p = 121 \Omega$. The probes were installed directly from the soil surface. At three distances from the drain a vertical array of six of these probes were installed. The three shallowest probes had a rod length of 14.2 cm and were inserted under an angle of 45°, which means that the measured θ 's are averages for the 0-10, 10-20 and 20-30 cm depth intervals. The installation under an angle has the advantage of creating a longer probe length for a fixed depth interval, making travel times longer and thus allowing more accurate measurement. The installation under a slope also reduces the chance of preferential flow along the walls of the PVC tubes to the rods. However, the installation costs much more time and requires more skill compared to vertical installation. For the deeper layers, probes with lengths of 28.3 and 35.4 cm were installed under an angle of 45°, resulting in the 30-50, 50-75 and 75-100 cm measurement depth intervals. The measurements of the six integral volumetric water contents at successive vertical depth intervals makes it possible to calculate the total water content of the 0-100 cm depth interval.

For all 34 probes, the electric probe length and the travel time of the EM wave in the epoxy material were determined, using the field TDR system, including the field cables, by performing calibration measurements in water and air in the laboratory (Heimovaara and Bouting, 1990). The travel time in the epoxy material was typically 20-80 ps, and the electrical length of a TDR probe was typically 2-5 mm longer than the normal length.

TDR wave forms

Figure 3.5a shows a TDR wave form of a 30 cm long horizontal probe. Tangent lines are drawn along the wave form according to the procedures of Heimovaara and Bouting (1990). The intersections of these tangent lines result in the reflection times of the start of the probe and the end of the probe. After the corrections for the travel time in the epoxy material, the travel time of the wave in

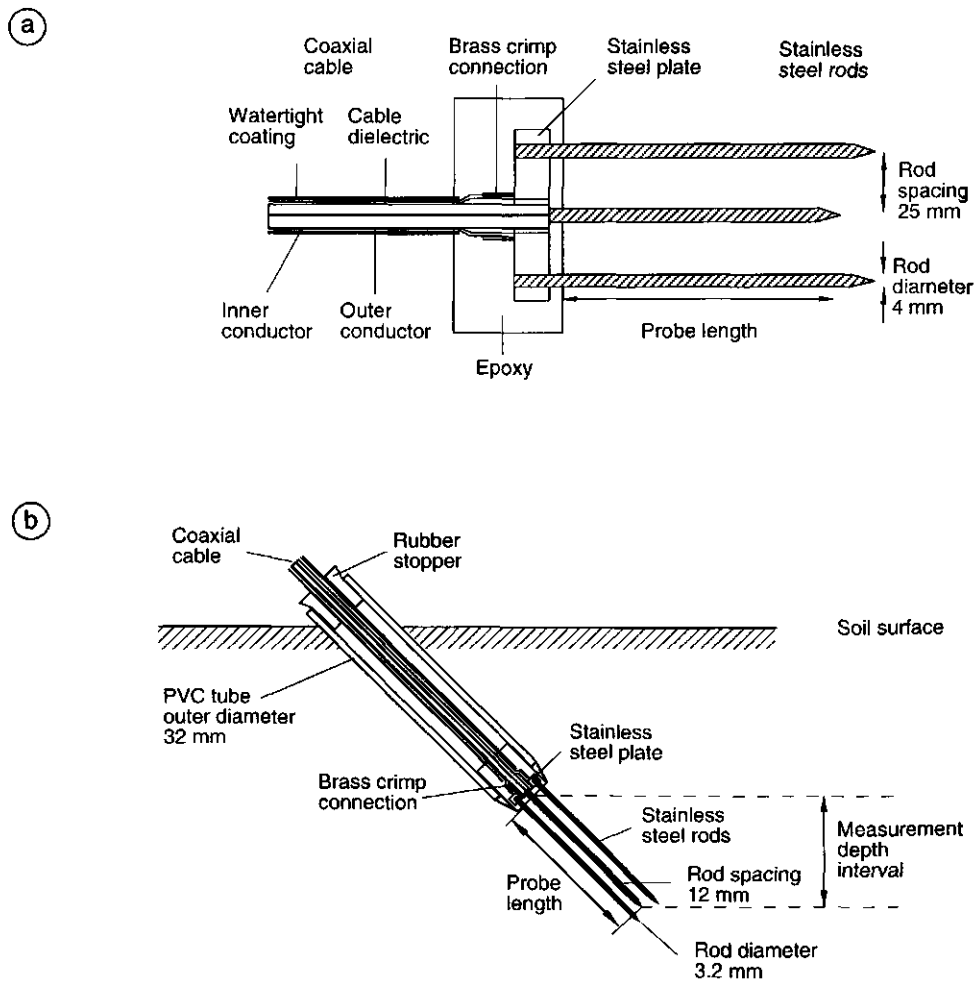


Figure 3.4 **a.** A 3-rod TDR probe to be installed horizontally. **b.** A 3-rod TDR probe integrated in a PVC tube installed from the soil surface at a 45° angle.

3. Field and laboratory methods

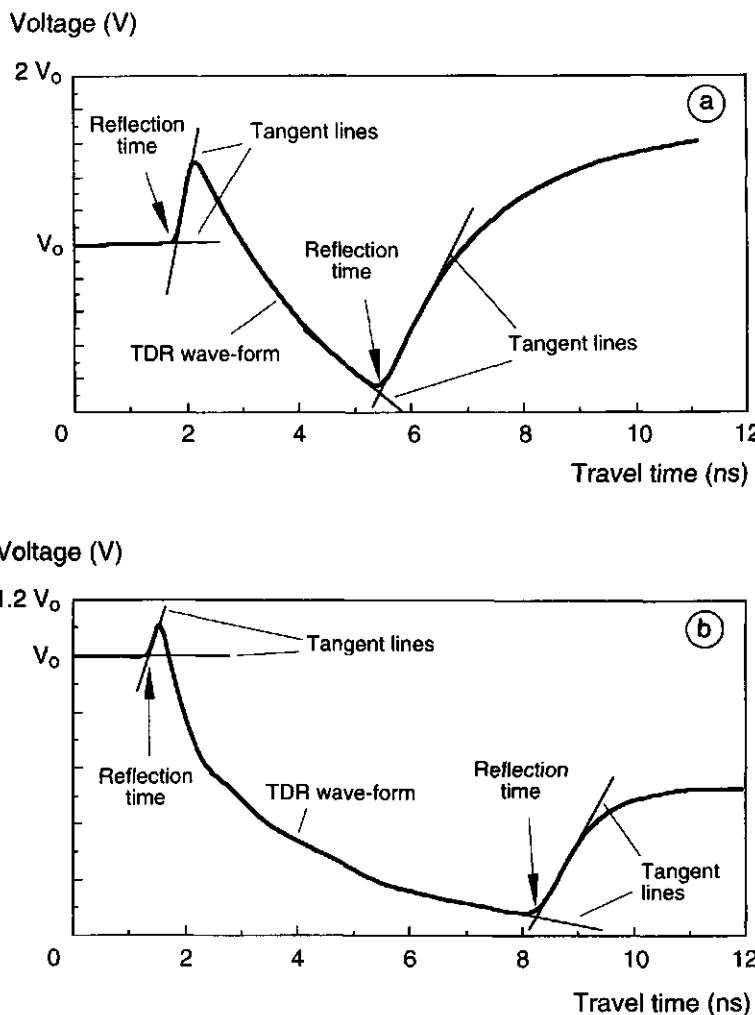


Figure 3.5 a. TDR wave form on 26 January 1994, 4.00 h, measured with a 30 cm long horizontal TDR probe at 30 cm depth. The intersections of the tangent lines are the reflection times, resulting in a $\Delta t = 3.56$ ns, corresponding to $\epsilon_a = 11.85$ and $\theta = 0.223$. b. TDR wave form, measured with a 35.4 cm long TDR probe installed at 45° angle at a depth of 75-100 cm, on 26 January 1994, 4.00 h. The intersections of the tangent lines are the reflection times, resulting in a $\Delta t = 6.93$ ns, corresponding to $\epsilon_a = 33.58$ and $\theta = 0.470$. The amplitude of the TDR wave form is presented as a voltage relative to the voltage V_0 of the step pulse reaching the TDR probe.

the soil and the corresponding ε_a can be calculated using Eq. 3.3. Using a calibration curve and a temperature correction, θ can be found. Figure 3.5b shows a TDR wave form of a 35.4 cm long probe installed at 45°.

However, sometimes the automatic analysis of wave forms can give problems and wave forms have to be judged individually. Over the 3-year permanent installation period, various technical problems arose: hares eating the coaxial cables, failure of the coaxial multiplexers, mistakes in the communication protocol between cable-tester and personal computer, and inexplicable wave forms. However, with the growing experience and the help of colleagues, most of the problems were solved and valuable measurement series were obtained.

It is difficult to give an estimate of the accuracy of the water content measurement with TDR. The local effects of the soil around the TDR probe and the sensitivity of proper installation, especially in a silt loam soil, makes the calculation of absolute volumetric water contents uncertain. However, changes in the volumetric water content can be determined accurately ($\pm 0.001 \text{ m}^3 \text{ m}^{-3}$), which is already very useful to understand the dynamics of the water balance.

3.1.3 Soil oxygen content measurements

Rappoldt and Corré (1997) used a method to measure macroscopic soil oxygen contents in the field, which will be outlined briefly (Fig. 3.6). Cylindrical chambers are installed in the soil at various depths. The walls of the chambers are perforated and covered with a gas-permeable cloth to prevent soil entering the chambers. The perforated oxygen chambers had a length of 5 cm for the chambers installed at 10 and 20 cm depth, and a length of 10 cm for the chambers installed at 30, 50 and 70 cm depth, corresponding to chamber volumes of 14 and 28 cm³, respectively. Two metal capillary tubes, with a 1 mm internal diameter, connected to the chamber provide an inlet and an outlet at the soil surface. The inlet and outlet are usually closed with a stopper and periodically connected to a mobile field oxygen analyser. At the moment of a measurement, the gas in the chamber is assumed to be in equilibrium with the air in the surrounding soil. The oxygen analyser pumps the gas around in a closed circuit with an oxygen electrode measuring the oxygen content. After about 20 s of pumping, a stationary oxygen concentration is measured. However, this measured concentration represents the concentration of a mixture of the oxygen

3. Field and laboratory methods

initially present in the chamber, and the oxygen initially present in the 8.3 cm³ volume of the tubes and in the analyser itself. To compensate for the latter, corrections are made by measuring the chambers in an order of expected decreasing oxygen contents; the corrections are normally < 10% of the measured oxygen content. Before and after a series of measurements, the oxygen electrode is calibrated using atmospheric air (21% O₂) and pure nitrogen (0% O₂). Also, temperature corrections are made for the sensitivity of the electrode. Leakage of oxygen during the measurements can be ignored.

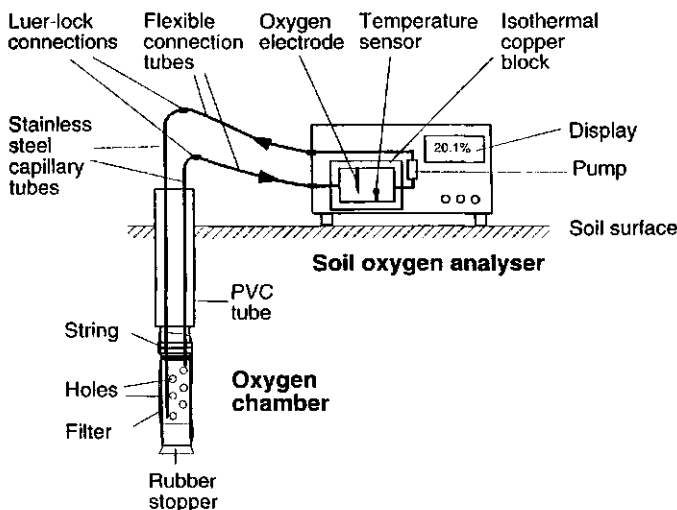


Figure 3.6 Oxygen measurement system (after Rappoldt and Corré, 1997).

Forty oxygen chambers were installed at 10, 20, 30, 50 and 70 cm depth in November 1993 in the integrated arable farming plot at various distances from drain 27 (Fig. 3.7). Detailed measurements of the dynamics of the water were performed simultaneously in this plot. Oxygen measurements were made at time intervals of about 2-3 weeks to monitor characteristic oxygen conditions over the year. The oxygen contents in the soil are expressed as percentages of the gas-filled pore volume (% v/v).

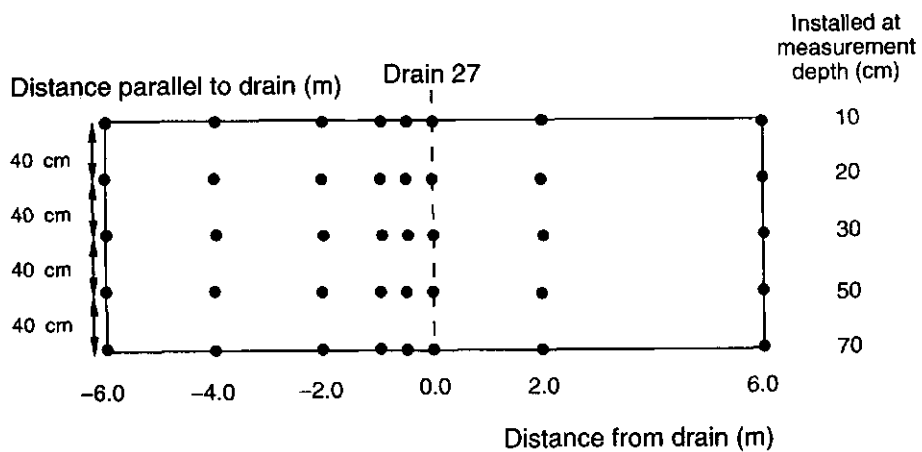


Figure 3.7 Outlay of oxygen chambers (●) installed at the integrated arable farming plot at various distances from drain 27.

3.1.4 Drain sampling device

The drain sampling device used in this study monitored the drain discharge rate and took flow-proportional sub-samples of the drainage water. Inspired by the design of Van Ommen *et al.* (1989), a modified sampling system was developed which collected the drainage water in a main reservoir (Fig. 3.8). Whenever this main reservoir was filled, a sample of this volume of water (V_{res}) was taken and the reservoir was emptied. The times at which the main reservoir was completely filled were recorded, so the average drain discharge rate over each time interval could be calculated.

At the ditch, the drain outlet was connected to a flexible plastic tube with a larger inner diameter ($d = 7.5$ cm) than the drain tube. In the middle of the ditch this tube was connected with a float, which kept the bottom of the tube at the water level of the ditch (Fig. 3.8 - "Float"). In this way, the drainage water always had the same hydraulic head as drainage water discharging directly into the ditch. On the float, part of the plastic tubing was transparent to be able to monitor the proper functioning of the system. A small vertical tube was placed on this plastic tube to let air enter the system to prevent the siphon effect. This small

3. Field and laboratory methods

vertical tube can also function as an overflow when the system behind this tube would be blocked by a technical failure. In such situations, the soil physical conditions in the field will then not be disturbed. The float was installed in such a way that it could not fall below the depth of the outlet of the drain. In situations with a low ditch water level, a horizontal connection between the drain outlet and the small reservoir was established. The float in the ditch was protected against extreme external influences, like wind, precipitation, waves, and frost by installing watertight wooden barriers in the ditch with a water inlet below the drain level. This provision prevented the float level from fluctuating too strongly. The whole setup was covered by a plastic screen.

The flexible tube was connected to a small reservoir to collect the drainage water (Fig. 3.8). From this small reservoir, which was located below the depth of the drain outlet, the drainage water was pumped continuously via the intermediate reservoir to the main reservoir. These reservoirs were located above the soil surface and were placed in a shelter, which was kept at a temperature above 3 °C to prevent freezing. The drainage water entered the intermediate reservoir and flowed to the main reservoir. The flow was controlled

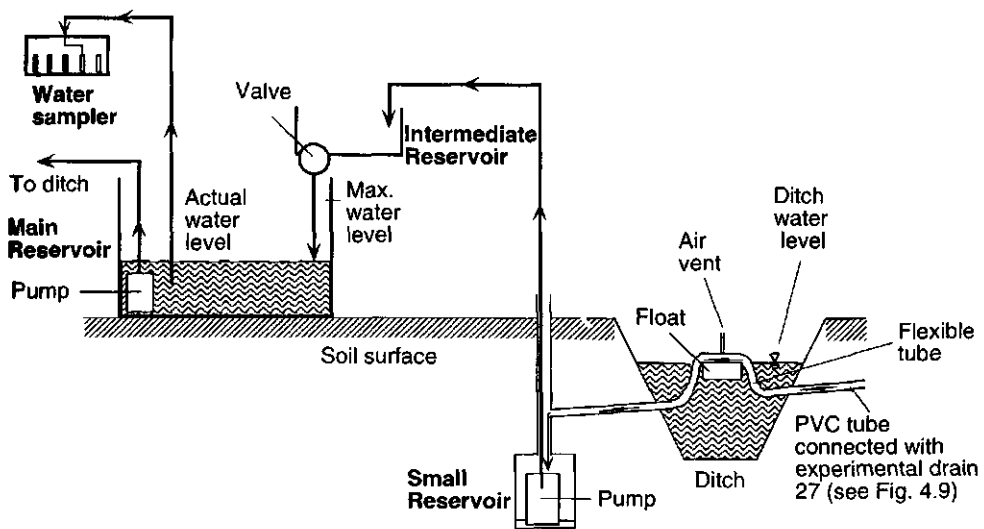


Figure 3.8 Schematic illustration of the drain sampling process. The arrows indicate the direction of the water flow.

by an electrical valve. Each time the water level in the main reservoir reached a pre-set level ($V_{res} = 365$ l), the electrical valve was shut and the time recorded by a data logger (Datataker DT-100, Data Electronics Ltd., Australia). At the same time, a 500 ml sample of the water in the main reservoir was collected in polyethylene sample bottles, by an automated water sampler (ISCO model 2900, ISCO Inc., Nebraska, USA). The main reservoir was then emptied by a pump, and the valve to the intermediate reservoir was opened again. While the main reservoir was being sampled (duration about 90 s), any incoming drainage water was stored in the intermediate reservoir without influencing the discharge rate or sampling process. The bottled water samples were used for chemical analyses. The discharge rate over each discrete time interval was calculated from the times recorded by the data logger and the known volume V_{res} . One volume V_{res} corresponded with a cumulative discharge of 0.49 mm of the experimental field.

3.1.5 Meteorological station Lovinkhoeve

An automated meteorological station (Fritsch and Gay, 1979; WMO, 1983) was established at the Lovinkhoeve (Fig. 3.9). Meteorological data are necessary to interpret the experimental results of the agricultural field trials and they can be used as boundary conditions in simulation models, especially in water balance models. The automated meteorological station was operationalised in 1987. At the time, a broad discussion started on the need of an integrated agricultural meteorological network, which could be operated and serviced by a central organisation. This good idea was never realised, but the philosophy presented in the final report (AMWO, 1988) was incorporated in the later innovations of the AB-DLO meteorological station.

In 1986, the Royal Netherlands Meteorological Institute (KNMI) became interested in establishing a KNMI synoptical station at the Lovinkhoeve, and since 1987 an automated KNMI station has also been operational. The AB-DLO and KNMI stations are supplementary: the AB-DLO station performs additional radiation and soil physical measurements, while the great advantage of the KNMI station is the reliability of the data due to the professional technical service and the strict calibration and quality procedures.

3. Field and laboratory methods

The meteorological stations are located at parcel S37 (see Fig. 4.7), and grass at the field is kept short. At the KNMI station the following quantities are measured at the given heights:

- wind speed (10 m);
- wind direction (10 m);
- relative air humidity (1.5 m);
- air temperature (1.5 m);
- precipitation (0.4 m);
- soil temperatures (5, 10, 20, 50 and 100 cm depth).

All quantities are averaged or summed over 10 minutes and sent to the central KNMI computer in De Bilt. These data are checked and the hourly averages or sums are, as ASCII-files, sent to AB-DLO.

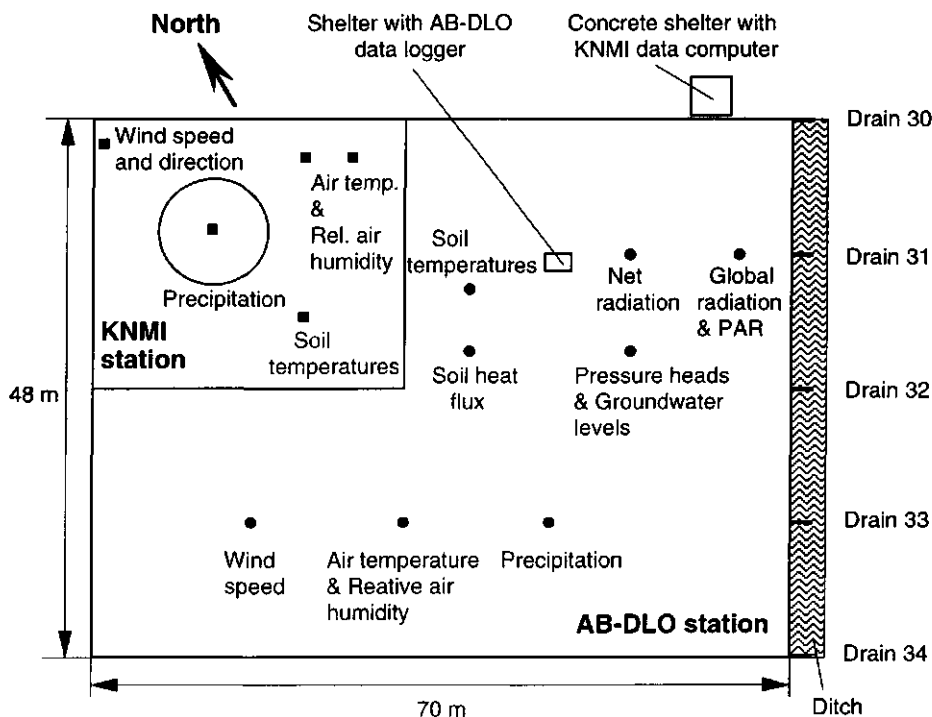


Figure 3.9 Locations where the quantities were measured at the KNMI and AB-DLO meteorological station.

At the AB-DLO station the following quantities are measured at the given heights:

- wind speed (2 m);
- relative air humidity (2 m);
- air temperature (2 m);
- precipitation (0.4 m);
- global incoming radiation (1 m);
- global reflected radiation (1 m);
- net radiation (1 m);
- photo-synthetic active radiation (1m);
- soil temperatures (2, 5, 10, 20, 30, 50, 100 and 200 cm depth);
- soil heat flux (10 cm depth);
- pressure heads (10, 20, 30, 50, 100 cm depth);
- groundwater levels.

The specifications of the AB-DLO instruments are given by Zandt (1995). Of all quantities, 10-minute averages or sums are calculated with a local data logger (Datataker DT-200, Data Electronics Ltd., Australia) in the field. Special measures are taken to prevent the loss of data, like a battery back-up for the data logger. The data are transferred to a computer at the farmhouse. A database programme on a weekly basis (Zandt, 1995) on a personal computer is used to check the proper functioning of the probes and to be able to present the recent data on site. The 10-minute averaged data are imported into an ORACLE (Oracle, 1990) database at the main computer at AB-DLO Haren. Long-term overviews and different types of output files can be generated with this database. For precipitation, also an ASCII-file is generated with data on a 1-minute basis. It is time-consuming to keep a meteorological station operational. However, also due to the cooperation with the KNMI, a good meteorological data set is available.

3. Field and laboratory methods

3.2 Laboratory methods

A brief description of the methods used to characterise the water retention and hydraulic conductivity characteristics is given in Pars. 3.2.1 and 3.2.2. The measurements were carried out by E.C. Vos of the DLO Winand Staring Centre in the period 1985-1989 and are presented in a joint publication (De Vos *et al.*, 1994). It is realised that nowadays (1997) better methods for the determination of the soil hydraulic characteristics (Dirksen, 1991; Stolte *et al.*, 1994; NVN-5791, 1995; NVN-5790, 1996). It was decided not to repeat these measurements, but to focus on the field-scale water flow and solute transport processes. However, in the course of the study it became necessary to measure the hydraulic conductivity at saturation K_s in more detail, including measurements in the horizontal direction. The improved method to measure K_s and the calibration procedure for TDR water content measurements are described in more detail, because they were specific for this study.

3.2.1 Water retention characteristics

The filter-funnel suction method was used for measuring the water retention characteristics in the pressure head range $-300 < h < 0$ cm (Klute, 1986; NEN-5786, 1991). Undisturbed soil samples (10 cm diameter, 10 cm height) were placed on a porous plate and then saturated with water. By changing the height of a water column under the porous plate, different suctions were applied to the samples. The outflowing water was collected in a burette via a watertight flexible tube. After reaching equilibrium, the extracted amount of water was read off the burette directly. By drying the sample after the last measurement, the corresponding volumetric water contents of the soil sample can be calculated for each established pressure head.

A method based on pressure heads measured with tensiometers was used in the range $-800 < h < -300$ cm (Boels *et al.*, 1978; NEN-5785, 1991). Tensiometers were installed in an undisturbed soil column (12 cm diameter, 15 cm height) at different depths. From an initially wet condition, the soil was dried by natural evaporation from the top surface. At measured pressure heads of $h = -500$ cm and $h = -800$ cm, undisturbed soil samples were taken from the column at the depths of the tensiometers. The corresponding volumetric water contents

of the samples were measured by standard oven drying procedures.

For the range $h < -800$ cm of the water retention characteristics, disturbed soil samples were placed on pressure extractors and the water extraction was measured on a mass basis (Klute, 1986; NEN-5788, 1994). The corresponding volumetric water contents were calculated using the simultaneously measured bulk densities of the original soil samples.

3.2.2 Hydraulic conductivity characteristics

The hydraulic conductivity at saturation K_s was measured by applying a constant water level at the top of an undisturbed soil sample of 12 cm diameter and 15 cm height. The soil sample was placed on a funnel, allowing free drainage at the bottom of the sample. By measuring the amount of outflow of the sample under steady conditions over a known period of time, K_s was calculated (Klute, 1986; NEN-5789, 1991).

The same samples were used to measure the hydraulic conductivity K for unsaturated conditions. An artificial crust was placed on the soil surface and a constant water level was maintained on top of the crust. As before, the soil sample was placed on a funnel under free drainage at the bottom of the soil sample. At various depths, tensiometers were installed in the soil sample. By measuring the outflow of the sample under steady conditions over a known period of time, the water flux through the soil could be calculated. The hydraulic conductivity K was calculated as the ratio between the volumetric flux density q and the gradient of the hydraulic head. This method could be used in the pressure head range $-15 < h < 0$ cm (Hillel and Gardner, 1970). The same method was used for pressure heads in the range $-70 < h < -15$ cm by placing the soil column on a layer of sand in which the pressure head was controlled (Wösten, 1990).

For the range $h < -70$ cm, the hot air evaporation method was used (Arya et al., 1975). Moist, undisturbed soil samples of 5 cm diameter and 10 cm height were exposed to a jet of hot air to force evaporation from the soil surface. After an exposure of 10 to 15 minutes, the soil sample was quickly cut to slices of 5 mm, of which the volumetric water contents were measured. The diffusivity of the soil was calculated from these data. The hydraulic conductivity was calculated by combining the data of the water retention characteristic and the diffusivity.

3. Field and laboratory methods

3.2.3 Improved measurement of K_s

The later measurements of K_s were based on the method described in NEN-5789 (1991), extended with a few innovations. Soil samples were taken from the field in 10 cm high PVC cylinders with a 19.1 cm inner diameter and a 4 mm wall thickness. These PVC cylinders, provided with a cutting attachment, were smoothly pushed into the soil using the hydraulic system of a tractor. The samples were taken both in the vertical and horizontal directions. The horizontal samples were taken in the direction perpendicular to the drains, because this direction corresponds to the principal lateral flow direction of the groundwater to the drains. The soil samples were transported to the laboratory and a fine nylon filter (0.1 mm) was placed at the bottom of the samples to keep the soil in the PVC cylinders. At least for two days, the samples were saturated by placing the samples in the K_s apparatus (Fig. 3.10) and fixing the PVC cylinder watertight between rubber rings using clamps. The water level was maintained at 2 cm below the top of the samples. Then, the water level was raised and a constant water level was maintained on top of the soil sample, and the outlet was placed at a position close to this water level to obtain a small hydraulic head gradient within the sample (Fig. 3.11). Air was removed from the reservoir under the nylon filter by flushing.

Preliminary experiments with Lovinkhoeve soil samples showed that the measured K_s was sometimes a factor 2-3 larger when the bottom reservoir was filled with water, as compared to a free drainage situation, when the bottom reservoir was filled with air and the outlet was positioned underneath the soil sample. This free drainage situation is described in NEN-5789 (1991). With air under the soil sample, unsaturated zones can develop at the bottom of the soil sample between the points where water drops are formed. Water flow has to converge to the dripping points, and a higher flow resistance can result compared to a situation with a more uniform outflow at the bottom of the soil sample. K_s was measured with the bottom reservoir filled with water. This method also gave the possibility of manipulating the hydraulic head gradient by varying the position of the outlet.

A standard procedure was developed to measure K_s of Lovinkhoeve soil. For each sample a measurement series was started at a small hydraulic head gradient $|\nabla H| = 5.3$. The total volume of water (V) which flowed through the sample over a time interval (Δt) of about 5 minutes was measured in a burette. K_s

can be calculated from:

$$K_s = \frac{V}{|\nabla H| \Delta t A}, \quad (3.10)$$

with: $\nabla H = \frac{z_{ref} - z_{out}}{L}, \quad (3.11)$

where: L = height of the soil sample (m);
 A = cross section of the soil sample (m^2);
 $|\nabla H|$ = absolute hydraulic head gradient;
 z_{ref} = position of water level at the top of the soil sample (m);
 z_{out} = position of outlet (m).

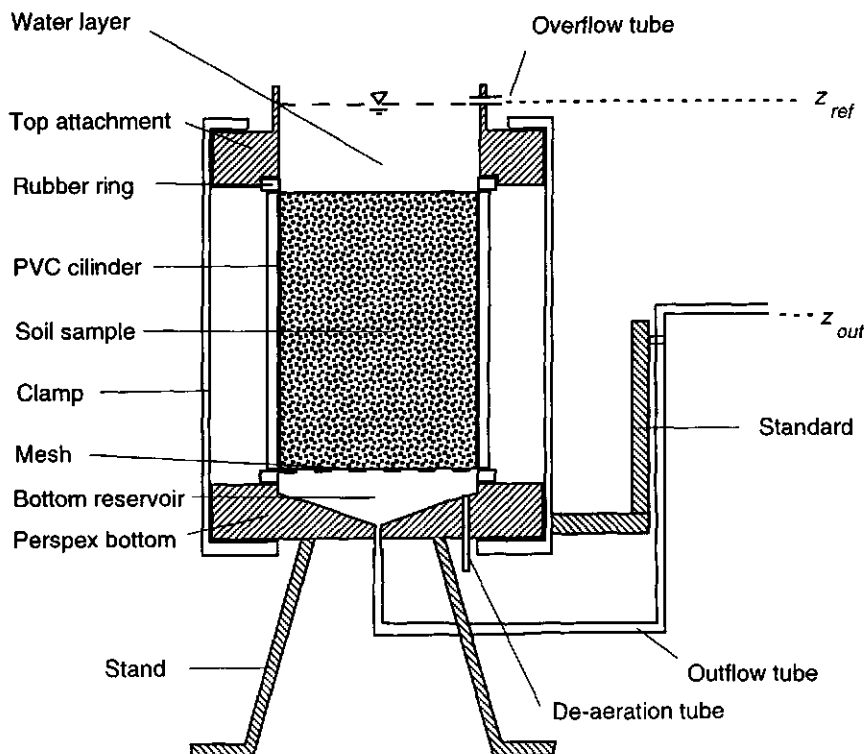


Figure 3.10 Schematic representation of the improved apparatus to determine the hydraulic conductivity at saturation K_s , based on NEN-5789 (1991).

3. Field and laboratory methods

This measurement was repeated three times. When the variation between the three measurements was smaller than 10%, the average K_s was calculated. The measurements were repeated at higher hydraulic head gradients of $|\nabla H| = 17.6$ and $|\nabla H| = 21$. In general, higher values of K_s were found at higher hydraulic head gradients. It was concluded that $|\nabla H| = 5.3$ was more representative for field conditions, and it was the lowest practical $|\nabla H|$ to carry out the measurements. Finally, saffranine, a red dye, was added to the water above the soil sample at $|\nabla H| = 21$, and after the discharged water turned red, the soil sample was taken out of the K_s apparatus. The soil sample was cut into slices and the location of the saffranine was visualised by pressing a filter paper against the soil. This procedure was used to check whether preferential water flow occurred along the walls of the PVC cylinder and whether the functioning of macro-pores had a substantial contribution to K_s . When no flow along the walls occurred, the average K_s measured at $|\nabla H| = 5.3$ was taken as the representative value of K_s .

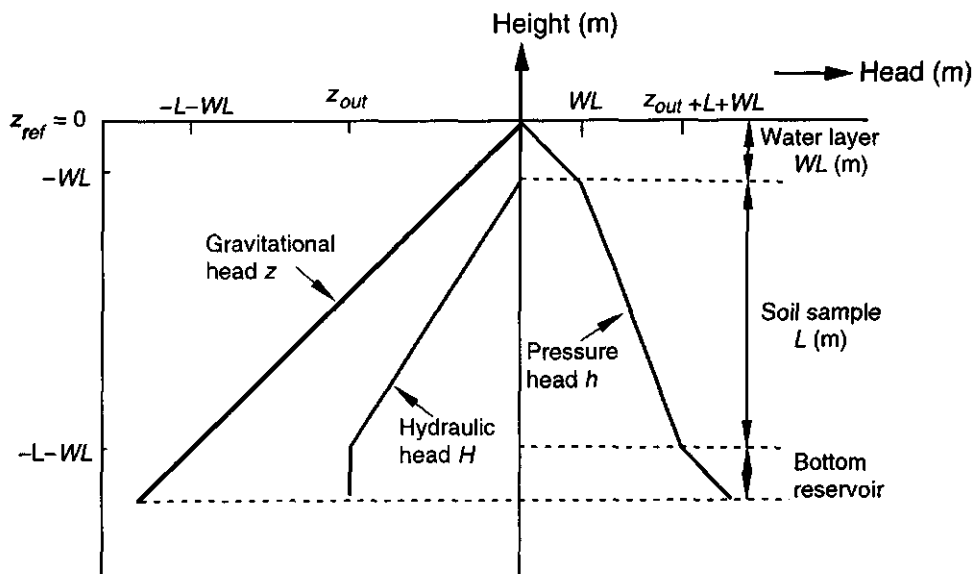


Figure 3.11 The distribution of the hydraulic head H , pressure head h and gravitational head z in the water of the K_s apparatus of Fig. 3.10.

3.2.4 Calibration of the TDR water content measurements

The relation between θ and ε_a was determined for the different soil layers of the Lovinkhoeve by using a modified version of the procedure described by Dirksen and Dasberg (1993). The soil profile was subdivided into five soil horizons, similar as outlined in Table 7.1, in which the TDR probes were installed: 0-36, 36-46, 46-64, 64-83 and 83-100 cm depth. Per soil horizon, soil was collected, air-dried, and homogenised. PVC cylinders, with a closed bottom, with a 19.1 cm inner diameter and a 20 cm height, were filled with a known mass of soil. By compacting the soil with a special tool, bulk densities (ρ_b) comparable with the average field bulk densities could be obtained. A 15 cm long 3-rod TDR probe, with 3 mm diameter rods and a 12.5 mm rod spacing, was installed close to the centre of the cylinder. The apparent relative dielectric permittivity ε_a of the soil was measured using the TDR procedures described earlier, choosing the most precise settings of the cable tester manually. This TDR measurement was repeated five times and the average travel time was used as a final result. Two soil samples were taken from the soil with a 1 cm diameter auger and the gravimetric water content was measured (NEN-5781, 1992), and θ was calculated using the average ρ_b of the column. All soil was removed from the cylinder and an amount of new soil was added and mixed to replace the amount of soil which had been sampled. With a fine water spray the water content of the soil was increased and the cylinder was filled again. The TDR probe was installed and ε_a was measured. This procedure was repeated until the water content became too high to refill the cylinders, typically at $\theta > 0.30 \text{ m}^3 \text{ m}^{-3}$. Cylinders with an open bottom were used for the higher water contents. These cylinders were filled at a relatively low water content and placed on a water retention sand bath. By manipulating the pressure head, different higher water contents could be obtained. Under these wet conditions, a gradient in h and θ within the cylinders is inevitable. To obtain water contents at saturation, the open cylinders with soil were placed in a reservoir and the water level was raised to the top of the cylinder. This condition was maintained for at least 48 hours, before a TDR measurement was carried out. For the five different soil layers, the clay, silt, sand and organic matter contents were measured, to be able to compare the results with the theory and results of Dirksen and Dasberg (1993).

4. THE LOVINKHOEVE EXPERIMENTAL FARM

The Dr. H.J. Lovinkhoeve is an experimental farm of the DLO Research Institute for Agrobiology and Soil Fertility (AB-DLO), located in the Noordoostpolder near Marknesse, The Netherlands (Fig. 4.1). The Noordoostpolder was reclaimed from the IJsselmeer in 1942 and the experimental farm was founded in 1943 by the Directorate Wieringermeer. In 1953 the farm was taken over by the Agricultural Research Station and Soil Science Institute TNO at Groningen, the later (1957) Institute for Soil Fertility at Groningen and at Haren from 1968 onward, which in 1993 merged with the former Centre for Agrobiological Research at Wageningen to form AB-DLO, with locations at Wageningen and Haren. The agricultural history of all plots of the Lovinkhoeve is well known since the foundation of the farm, including some long-term experiments running since 1943. This chapter gives a summary of the geological history, the characterisation of the soil profile, the hydrological situation, an overview of the Lovinkhoeve and its management, and the locations and histories of the relevant plots for this study. Finally, the soil physical characteristics for these plots are presented.



Figure 4.1 The AB-DLO experimental farm Dr. H.J. Lovinkhoeve is located at Marknesse in the Noordoostpolder, The Netherlands.

4.1 General characteristics

The general characteristics of the Lovinkhoeve are summarised in this section. Later sections and chapters will focus on the characteristics of individual plots, which can differ from these general characteristics as a result of the agricultural treatments.

4.1.1 Geological history

The formation of the soil of the Noordoostpolder is described in detail by Zuur (1951) and Wiggers (1955) and information about the Lovinkhoeve is given by Kooistra *et al.* (1989). Diluvial sediments form the basement of the soil. The soil developed in sediments which were deposited under water. In the period before 1300 AD the sea level and the groundwater level in the region rose and marshes with peat growth developed. Due to the changing hydrological conditions, part of this peat was abraded and redeposited. Finally, a lake was formed, the Flevomeer. Until about 1600 AD the influence of the sea was not very strong and the water of the lake remained fresh to slightly brackish due to the influence of the fresh water of the river IJssel, which had a large discharge in that period. Around 1600 AD the influence of the sea increased and the Zuyderzee, a lagoon, was formed and marine sedimentation took place. In 1932 a dam, the Afsluitdijk, closed off the Zuyderzee from the sea and the lake became rapidly fresh again. This lake was named IJsselmeer. The Noordoostpolder was reclaimed from the IJsselmeer in 1942.

In general, a distinction in clay content can be found between fresh water and marine deposits. In fresh water sediments the ratio of clay (< 2 μm) to silt (2-16 μm) particles is much lower than in marine sediments. The clay fraction determines to a large extent the chemical and physical behaviour of the soil. Because the clay to silt ratio in the marine deposits of the Noordoostpolder is often lower than the general ratio of 1:2 for most Dutch marine deposits, it is important to use the clay fraction as an indicator and not the sum of the clay and silt fraction, i.e., all particles < 16 μm . Figure 4.2 shows an overview of the deposits in the Noordoostpolder.

4. Lovinkhoeve experimental farm

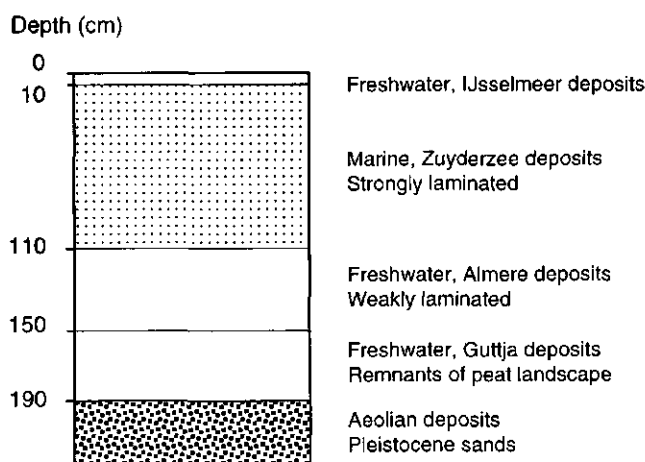


Figure 4.2 Schematic cross-section of Holocene deposits near Marknesse (after Kooistra *et al.*, 1989).

4.1.2 Soil profile and hydrological situation

Soil profile

The Lovinkhoeve soil profile after reclamation (Fig. 4.3) consisted of a loamy topsoil (0-30 cm), an intermediate clay layer (30-39 cm), a very thin fine sand layer (39-42 cm), a subsoil consisting of a heavy loam layer (42-46 cm), and a light loam layer (46-100 cm). The topsoil was formed as a freshwater deposit when the local water velocities were very low because dikes were constructed to reclaim the polder. These circumstances explain the higher clay content of the topsoil as compared to the deeper layers. The sand layer must have been formed in a period with high local water velocities, resulting in the sedimentation of mainly the larger sand particles. Deeper layers to a depth of about 70 cm developed as marine deposits with a lower clay content than the topsoil. The light loam subsoil was deposited in freshwater again, but due to the origin of the water and the higher local water velocities, the clay content is lower than in the fresh water deposits in the topsoil. The peat layer (120-200 cm depth) has a variable thickness and was formed in the period that marshes were present.

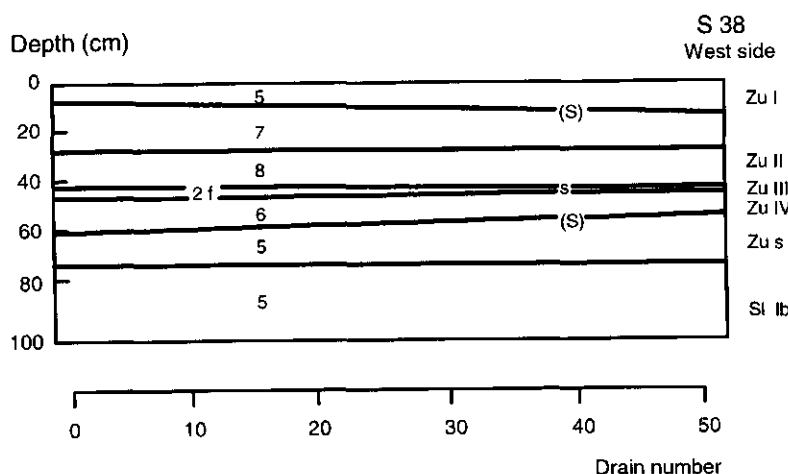


Figure 4.3 Soil profile of the Lovinkhoeve just after reclamation (1942). 5 Zu = light loam, 8-12% clay; 7 Zu I = heavy loam, 17-25% clay; 8 Zu II = clay, 25-35% clay; 2f Zu III = very fine sandy layer; 6 Zu IV = heavy loam, 12-17% clay; 5 Zu s = light loam, 8-12% clay; 5 Si lb = light loam, 8-12% clay; s = change in deposition from salt water (marine) to fresh water; Si = deposition in fresh water; S = layer of shells. Particles with an effective diameter between 0 and 2 μm are defined as clay ("Iltum" in Dutch).

Processes like evaporation, freezing, and drainage caused an irreversible formation of soil structure (Domingo, 1951; Smits *et al.*, 1962). When it became possible to till the land and grow crops, the ripening process proceeded faster. The physical ripening of the soil became visible by the formation of bio-pores and cracks, especially in the topsoil. Quantitatively, the decrease in porosity is a measure of the stage of the ripening process. As a result of the ripening process and soil tillage, the loamy topsoil became thinner and was mixed with part of the intermediate clay layer. Owing to soil tillage, the texture of the 0-25 cm topsoil is now homogeneous. The thin, very fine sand layer is still largely intact and is now located around the depth interval 30-35 cm. The effect of the soil ripening process is illustrated in Fig. 4.4, showing the change in bulk density for the period 1960-1981, and Fig. 4.5, showing the change of the gravimetric water content of the topsoil at $h = -100$ cm, for the period 1941-1981.

The soil classification of the Lovinkhoeve is given by Kooistra *et al.* (1989). The soils have AC-profiles and are classified as Typic Fluvaquents (Soil Survey Staff, 1975) or as Calcaric Fluvisols (FAO-UNESCO, 1974). In the Dutch classification they are calcareous polder vague soils with a loamy surface layer,

4. Lovinkhoeve experimental farm

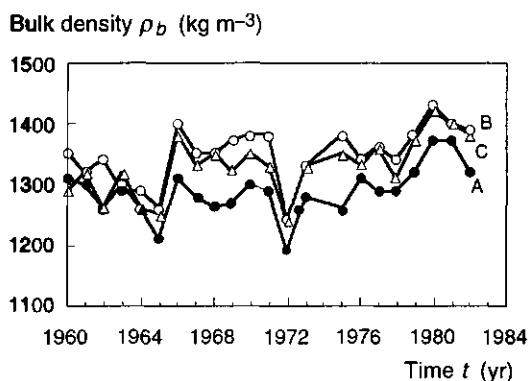


Figure 4.4 Bulk density ρ_b of the topsoil of different systems of organic manuring at the Lovinkhoeve. According to Boekel (1985):
 A = clover, green manuring in addition to chemical fertiliser;
 B = fertiliser, six year rotation without ley; chemical fertiliser additions only;
 C = ley, eight-year rotation including two-year ley.

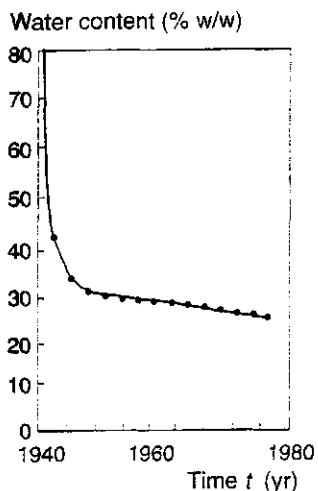


Figure 4.5 Water content (% w/w) at $h = -100$ cm of the topsoil of the Lovinkhoeve during the years after reclamation: 1942-1980 (after Boekel, 1985).

mapping unit Mn25A (De Bakker and Schelling, 1966; De Bakker, 1979). The soil of the Lovinkhoeve is young and the soil ripening process is still continuing. Differences in soil structure and organic matter content between different arable farming systems exist especially in the topsoil (Brussaard *et al.*, 1988). Some characteristics of the soil profile for a conventional plot are given in Table 4.1 and Fig. 4.6. The small differences between the data in Table 4.1 and Fig. 4.6 are related to measurements carried out on different fields at different times by different laboratories, and they can be interpreted as an indication of the uncertainty in the soil profile data. The calcareous silt loam soil with the relatively high organic matter content is considered as a very fertile soil with respect to nutrient availability.

Water flow and nutrient transport in a layered silt loam soil

Table 4.1 Particle size distribution, CaCO_3 content, pH and organic matter content (OM) for different soil horizons of a field under conventional management at the Lovinkhoeve (after Kooistra *et al.*, 1989).

Soil horizon	Depth (cm)	Particle size distribution (%v/v)					CaCO_3 (%w/w)	pH (kCl)	OM (%w/w)
		< 2 μm	2-16 μm	16-50 μm	50-150 μm	> 150 μm			
Ap	0-28	20.4	15.1	52.8	10.5	1.2	9.3	7.3	2.2
C21g	28-36	9.2	7.3	53.3	29.5	0.7	8.1	7.5	1.6
C22g	36-58	16.7	20.8	58.4	3.3	0.8	9.8	7.6	2.7
C23g	58-96	14.2	29.3	52.6	3.0	0.9	12.5	7.7	2.9
CG	> 96	10.2	23.6	64.9	0.8	0.5	14.0	7.7	2.6

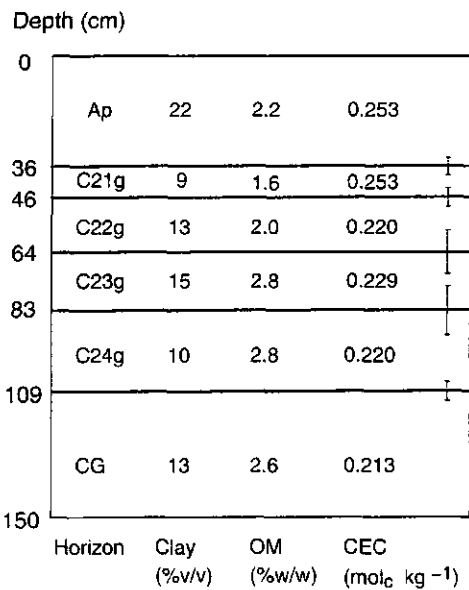


Figure 4.6 The soil profile of the field plot of the drainage experiment at the Lovinkhoeve (1991). For each horizon the clay content (measured in 1991) the organic matter content (OM), and the cation exchange capacity (CEC) are indicated. The error bars give the standard deviation of the horizon depths.

4. Lovinkhoeve experimental farm

Hydrological situation

The design of the drainage system in the Noordoostpolder was based on the clay content in the topsoil (0-25 cm) and the subsoil (25-100 cm) (Sieben, 1951; Zuur, 1952; Fokkens, 1966). The Lovinkhoeve had a clay content of 20.4% in the topsoil and of about 15.0% in the subsoil (Table 4.1). The heavy loam topsoil overlying a light loam subsoil resulted in a drain spacing of 12 m (Sieben, 1951; Table 12). The design criterion for the drainage system was that the phreatic surface will not rise above 40 cm depth at a steady precipitation rate of 10 mm d⁻¹.

The subsurface tile drains were laid by hand in the drain trench (width = 20 cm). An individual tile drain is 30 cm long and has a 7.5 cm outer diameter. The pipes were connected head to tail, and a small amount of peat was put around the pipes as a filter. Water enters the drain through the gap in between the tiles. The drain depth ranges from about 85 cm depth in the middle of the field to a depth of 115 cm at the ditches, which means a slope of 0.002 over 150 m length.

The average yearly precipitation at the Lovinkhoeve is 745 mm for the years 1943-1996. The annual actual evapotranspiration for arable land can be estimated to be about 445 mm (Klein Tank, 1996). So, a yearly precipitation excess of about 300 mm has to be removed.

Van der Molen (1958) gives a detailed overview of the salt balance of the Noordoostpolder. The salt concentrations in the soil profile after reclamation were a result of the salinisation period from 1600 till 1931. During this period salt of the sea water of the Zuyderzee could diffuse into the soil to about 10 m depth. In the period 1932-1941 salt from the 0-100 cm soil layer diffused in the opposite direction to the relatively fresh water of lake IJsselmeer. After the digging of trenches and the installation of drains, the desalination of the 0-100 cm depth soil layer in the Noordoostpolder proceeded rapidly. Van der Molen (1958) presents measurements showing that at the Lovinkhoeve the salt content in the 0-80 cm depth layer dropped rapidly. Because the salt concentrations in the deeper layers (> 100 cm depth) were high, a possible upward seepage could lead to salt problems related to crop growth. Van der Molen and Sieben (1955) made an overview of the occurrence of upward and downward seepage in the Noordoostpolder by analysing groundwater levels, salt concentrations and the quality of the ice in the ditches in winter. Based on these results, a small (< 0.2 mm d⁻¹) or no upward seepage is expected at the Lovinkhoeve.

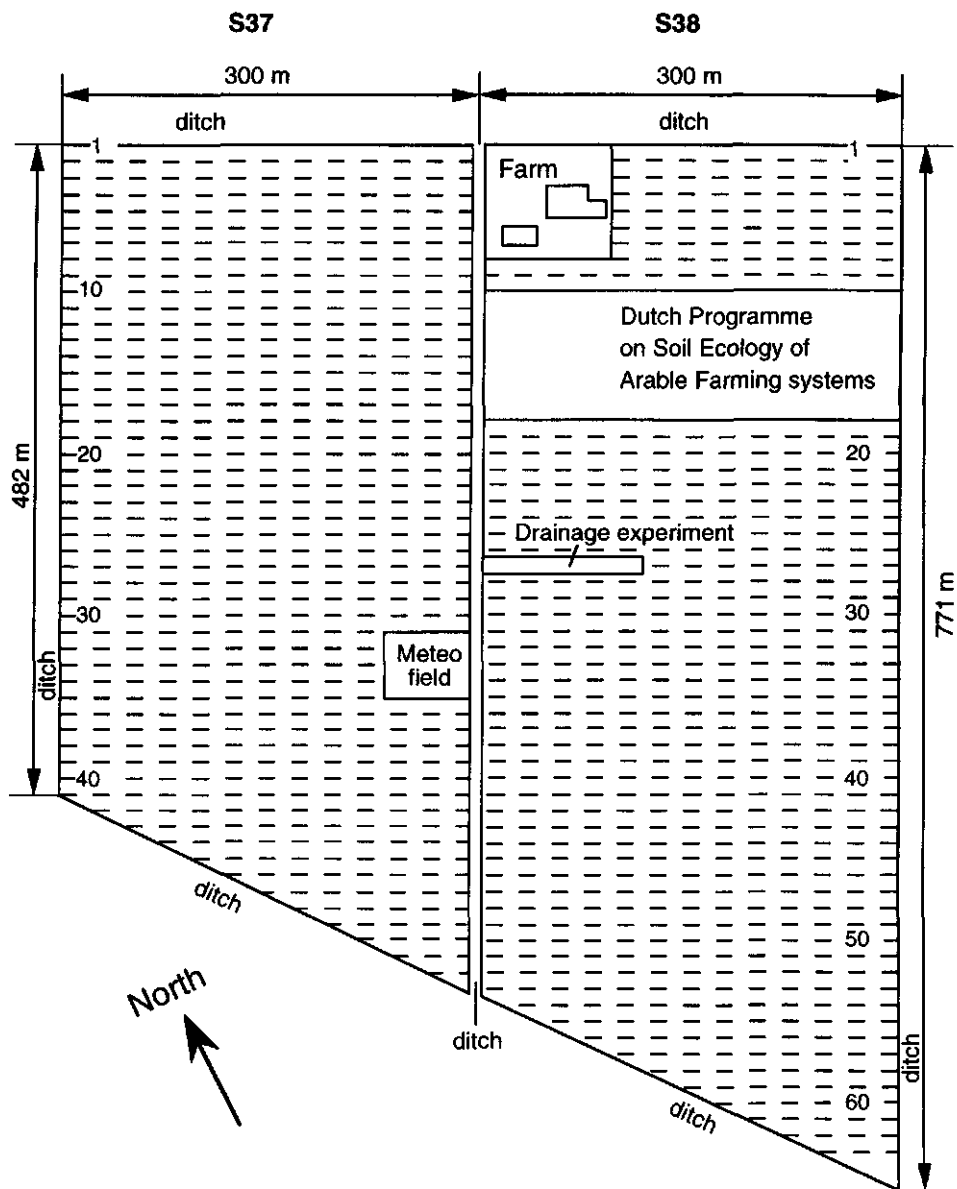


Figure 4.7 Outlay of the parcels S37 and S38 of the Lovinkhoeve farm of the DLO Research Institute for Agrobiology and Soil Fertility. The experimental fields have a width of 12 m and are separated by the subsurface drains, except for the drainage experiment which will be described in detail later.

4. Lovinkhoeve experimental farm

4.1.3 Experimental plots and farm management

Experimental plots

Figure 4.7 presents an outlay of the Lovinkhoeve. The area of 38 hectares is divided into two parcels, S37 and S38, both surrounded by ditches. The experimental plots are located between the adjoining subsurface drains and are numbered accordingly, except for the drainage experiment which will be described in detail later (see Fig. 4.9). The locations of the experimental plots and the meteorological station are indicated in Fig. 4.7.

The experimental plots of the Dutch Programme on Soil Ecology of Arable Farming Systems (1985-1990) were located at fields 10-17 of parcel S38. Figure 4.8 shows three blocks with different histories of soil and crop management in the previous 30 years (1955-1985). The "ley" field (A-block) had two extra years of ley in a six-year rotation. The "fertiliser" field (B-block) had no external input of organic matter, only inorganic fertiliser was applied. At the "clover" field (C-block) clover was one of the crops in the rotation, serving as an organic fertiliser. These treatments resulted in different organic matter contents in the topsoils of the fields: 2.8% for "ley", 2.2% for "fertiliser", and 2.3% for "clover". These different

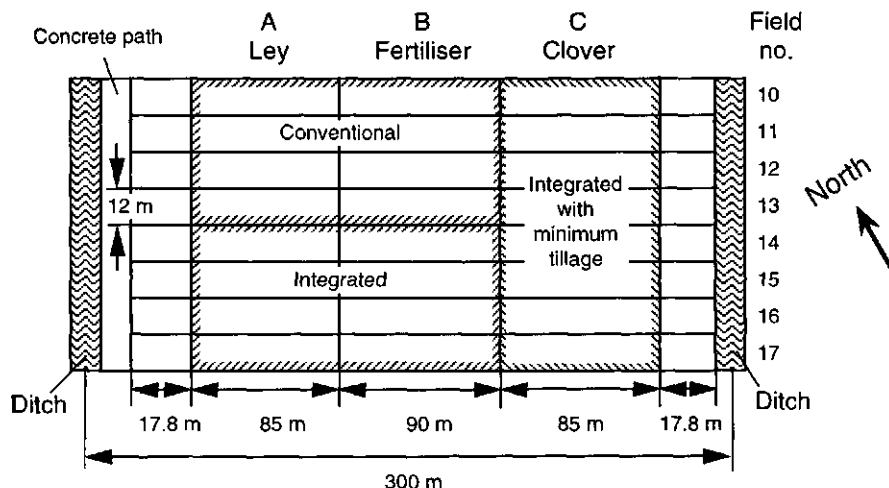


Figure 4.8 Outlay of the Lovinkhoeve field plots of the Dutch Programme on Soil Ecology of Arable Farming Systems, with the positions of the new variants laid on the Ley, Fertiliser and Clover blocks of the previous long-term experiment (after Van Faassen and Lebbink, 1990).

histories provided the point of departure in 1985 for the Dutch Programme on Soil Ecology of Arable Farming Systems.

The drainage experiment was located at parcel S38 in the A-block on fields 27 and 28 (Fig. 4.9). It was necessary to isolate experimental drain 27 from the other parts of the field, because these parts had different fertilisation and soil tillage treatments. The part of drain 27 lying outside the net experimental plot was short-circuited to drains 26 and 28 by excavating a trench between the drains and connecting them using PVC tubing (Fig. 4.9). To reduce boundary effects close to the ditch, a 20 m long trench was dug and a PVC tube was inserted between the drain and the sampling device. Overall, a net experimental field of 62.5×12 m was created, assuming that the water divide will be exactly in the middle of two adjacent drains. The depth of the experimental drain ranged from about 91 cm in the middle of the field (Fig. 4.9, location M) to about 104 cm close to the ditch (Fig. 4.9, location D).

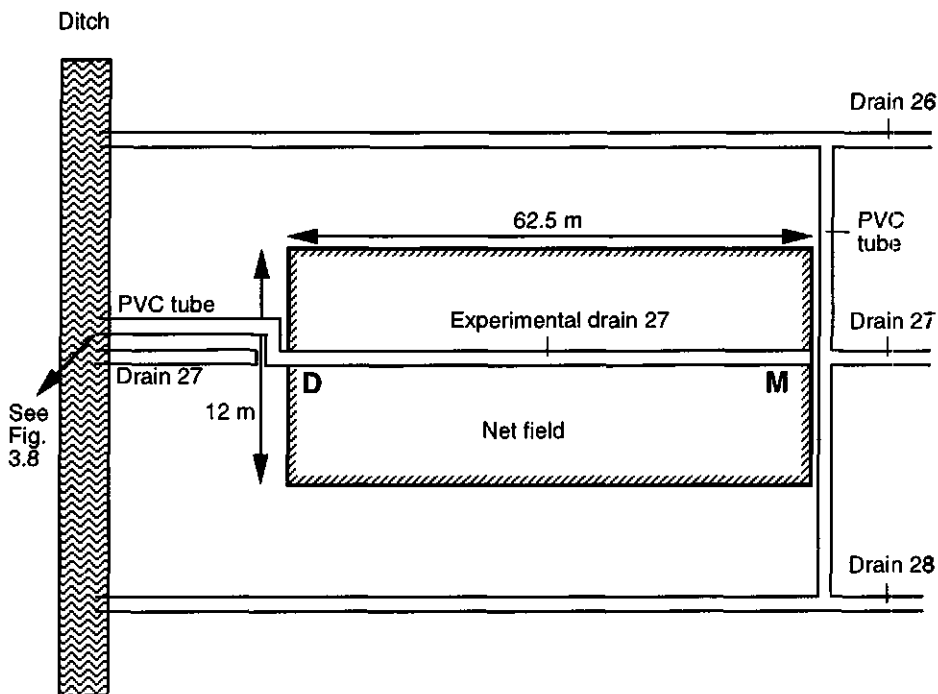


Figure 4.9 Outlay of drain 27 and the connections of this drain with drains 26 and 28 by PVC tubing designed to create a net experimental field. The positions indicated by M and D are referring to the corresponding positions in Fig. 6.1.

4. Lovinkhoeve experimental farm

Farm management

A conventional 4-year crop rotation in the Noordoostpolder is potatoes-winter wheat-sugar beet and spring barley. At the Lovinkhoeve, applications of nitrogen (N), phosphorous (P) and potassium (K) were based on the recommendations of the Extension Service of the Dutch Ministry of Agriculture, Nature Management and Fisheries. Average annual values for the conventional 4-year crop rotation were about 200 kg ha⁻¹ nitrogen (N), 50 kg ha⁻¹ phosphorous (P) and 125 kg ha⁻¹ potassium (K). Nowadays, N-fertilisation is often based on the amount of mineral N found in the soil in spring (Van Faassen and Lebbink, 1990). Every autumn the soil is ploughed to a depth of 25 cm; in spring a seedbed or ridges for potatoes are prepared. Soil tillage has a substantial effect on soil structure (Kooistra *et al.*, 1989). Surface slaking and internal slaking can occur (Boersma and Kooistra, 1994).

The Lovinkhoeve has some fields with an integrated arable farming system, where N fertilisation, the depth of ploughing and the use of herbicides are reduced as compared to a conventional system. Details of the management practices will be discussed when the specific field experiments are described.

4.2 Soil physical characteristics

The water retention and hydraulic conductivity characteristics were measured in the period 1985-1989, using samples from the plots of Dutch Programme on Soil Ecology of Arable Farming Systems (Fig. 4.8). In 1994, extra data on the hydraulic conductivity at saturation and TDR calibration data were collected using samples from the plots of the drainage experiment (Fig. 4.9).

4.2.1 Water retention characteristics

Laboratory water retention characteristics

Based on the description of the soil profile presented in Par. 4.1.2, the soil profile was divided into three depth layers: the topsoil (0-25 cm), the intermediate layer (25-40 cm), and the subsoil (40-100 cm). The laboratory water retention characteristics (lwrcs) were obtained by taking soil samples in the field in spring

and determining the desorption curves, using the methods described in Par. 3.2.1. All data of the different years of a specific plot are combined to one geometrically averaged Iwrc (Vos and Kooistra, 1988), because the data showed a log-normal distribution (see also Wosten *et al.*, 1987). Figure 4.10 illustrates the large variation in Iwrc data on which the geometrical means are based. Comparing the results for each of the three layers of the different plots, Vos and Kooistra (1994) concluded that the Iwrcs are distinguishable only for the topsoil. Figure 4.11 gives a summary of the data. The topsoil of plot 16A has a larger volumetric water content than the topsoil of plot 12B at all pressure heads. This difference is related to the higher organic matter content (2.8%) in plot 16A than in plot 12B (2.2%). The curves for the topsoils of plots 12C and 16B occupy intermediate positions. The Iwrcs of the intermediate layer and the bottom layer differ from those of the topsoil and from each other. The soil at those depths still has a somewhat unripened character, resulting in high volumetric water contents at saturation, especially in the bottom layer. A major part of the soil water is released in the interval $-1000 < h < -100$ cm.

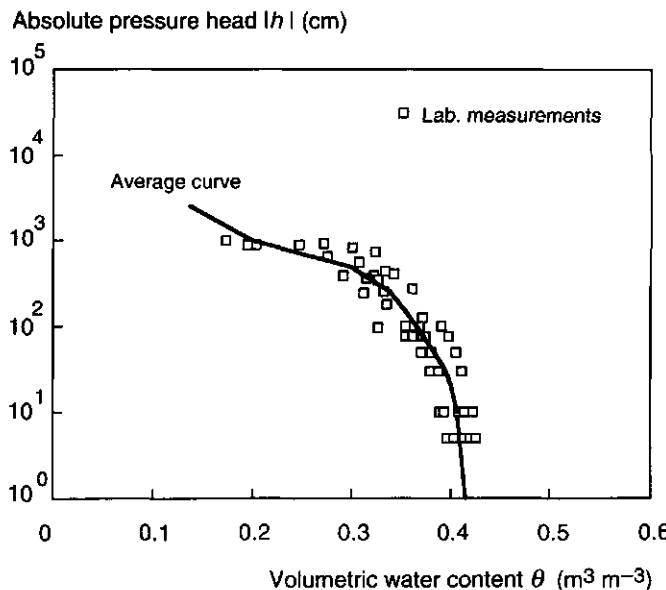


Figure 4.10 The laboratory water retention characteristic (Iwrc) for the topsoil (0-25 cm depth) of plot 12B. The individual measurements are given by the symbols, the curve is the geometrically averaged Iwrc. The pressure head (negative) is expressed by its absolute value $|h|$.

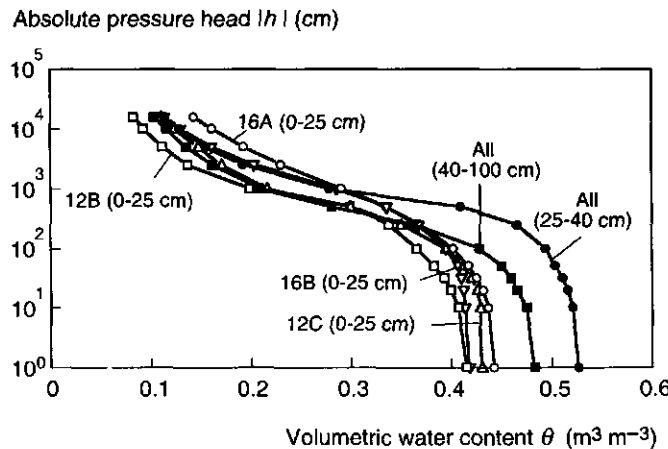


Figure 4.11 The laboratory water retention characteristics (lwrcs) of the topsoils (0-25 cm depth) of the different plots, and the general characteristics of the intermediate layer (25-40 cm depth) and the subsoil (40-100 cm depth). The symbols indicate the geometrically averaged measured values. The pressure head (negative) is expressed by its absolute value $|h|$.

Field water retention characteristics

The field water retention characteristics (fwrcs) were obtained from measured volumetric water contents of soil samples and tensiometer readings. Undisturbed soil samples were taken at the depth of the tensiometer within a distance of 1 m from the tensiometer. Data points of the fwrcs of the topsoil are shown in Fig. 4.12a, together with the corresponding lwrcs. For $h > -100$ cm, the field volumetric water contents are much smaller than the laboratory volumetric water contents at the same pressure head. Hence, the pressure heads corresponding to particular water contents measured in the field are nearly always larger than would be expected on the basis of the lwrcs. Possible causes for this difference are air entrapment and hysteresis occurring in the field. For $h < -100$ cm, the differences between fwrcs and lwrcs were smaller. The general form of the curves tend to be similar. Field data of plot 16A always showed larger volumetric water contents than on plot 12B. This is in line with the lwrcs for these plots.

For the intermediate layer (Fig. 4.12b), when the field data at 30 cm depth

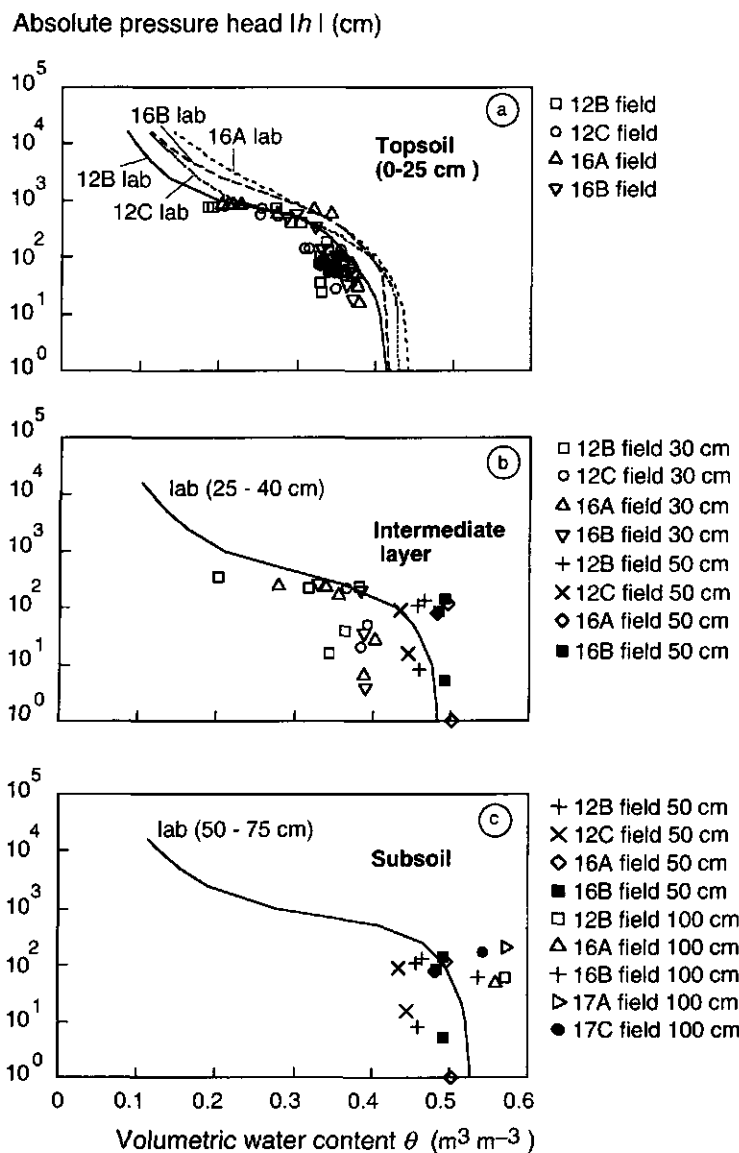


Figure 4.12 Individual measurements of the field water retention characteristics (fwrcs) and the geometrically averaged laboratory water retention characteristics (lwrcs) for the different plots. The plot and depth of measurement are indicated for the fwrc data, for **a**, the topsoil, **b**, the intermediate layer, and **c**, the subsoil. The pressure head (negative) is expressed by its absolute value $|h|$.

4. Lovinkhoeve experimental farm

are considered, the field volumetric water contents were also always much smaller than the laboratory volumetric water contents at the same pressure head for $h > -100$ cm. The field data at 50 cm depth showed much higher volumetric water contents than those at 30 cm depth. For $h < -100$ cm, the field data are again closer to the Iwrcs. Differences between the plots are less pronounced than in the topsoil.

In the subsoil (Fig. 4.12c), differences between the field data at 50 cm and 100 cm depth were observed. Compared with the layer at 50 cm depth, the soil layer at 100 cm depth was less ripened and sometimes had a high organic matter content, due to a large fraction of peat, resulting in higher volumetric water contents at the same pressure head.

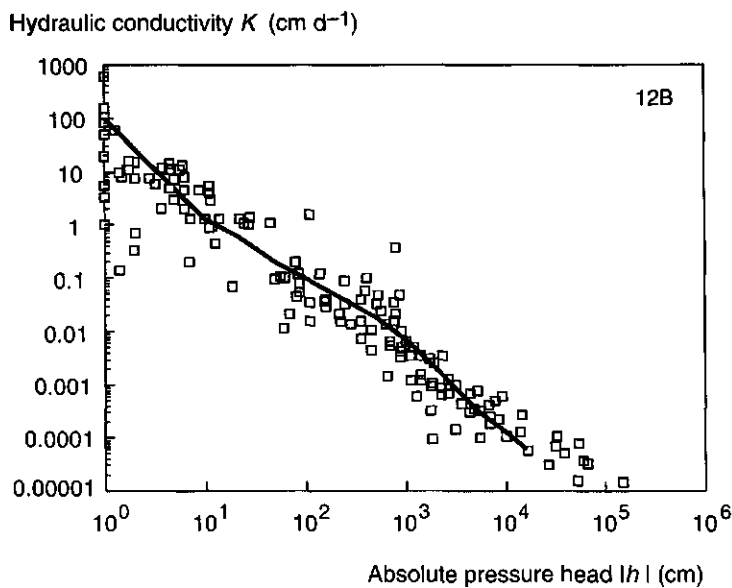


Figure 4.13 The laboratory hydraulic conductivity characteristic for the topsoil (0-25 cm depth) of plot 12B. The individual measurements are given by the symbols, the curve is the geometrically averaged Iwcc. The pressure head (negative) is expressed by its absolute value $|h|$

4.2.2 Hydraulic conductivity characteristics

The laboratory hydraulic conductivity characteristics (lhccs) were obtained by taking undisturbed soil samples in spring and using the various measurement methods described in Par. 3.2.2. The samples were taken at the same depths as the samples used for the Iwrc. There was a large variation between the individual measurements of each plot (Fig. 4.13). All lhcc data of the different years of an individual plot are combined to a geometrically averaged lhcc (Fig. 4.14). The hydraulic conductivity at saturation is an order of magnitude higher than the hydraulic conductivities close to saturation. At lower water contents ($\theta < 0.4 \text{ m}^3 \text{ m}^{-3}$), the hydraulic conductivity decreases nearly exponentially as a function of the (decreasing) volumetric water content. The higher volumetric water contents of the intermediate layer and the subsoil did not result in higher hydraulic conductivities.

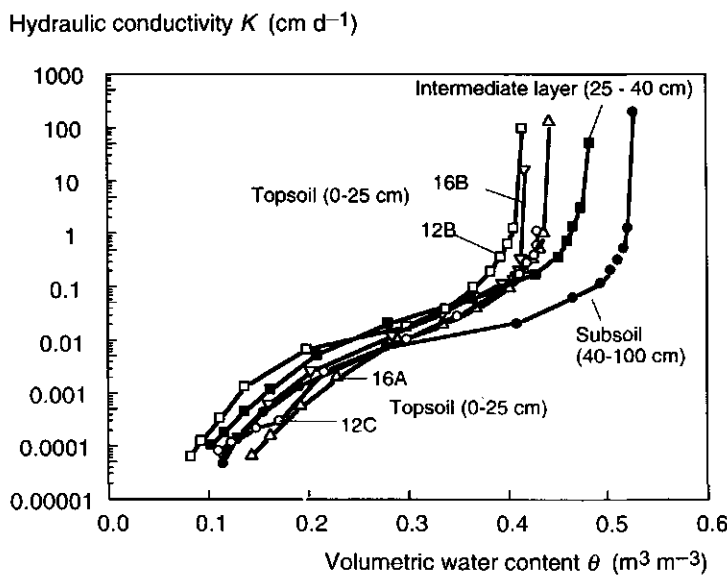


Figure 4.14 The laboratory hydraulic conductivity characteristics for the topsoils (0-25 cm depth) of the different plots, and the general characteristics of the intermediate layer (25-40 cm depth) and the subsoil (40-100 cm depth). The symbols indicate the geometrically averaged measured values.

4.2.3 Analytical expressions for the hydraulic characteristics

The fitted parameters of the Van Genuchten (Eq. 2.16) and Mualem (Eq. 2.17) expressions for the geometrically averaged laboratory hydraulic properties are given in Table 4.2. The results and the measured data are presented graphically in Figs. 4.15 a, b and c. The hydraulic properties of the different plots are distinguished for the topsoil, but not for the intermediate layer and the subsoil. The Iwrcs are well described by the analytical expressions: the form of the curves follows the measured data and differences between measured and fitted data are small. For the Ihccs the analytical expressions are more problematic. The form of the curves seems reasonable, but differences between measured and fitted data are large, especially at water contents close to saturation. Of course, this is a result of the choice of the weighing coefficient $W_1 = 0.1$, and the choice to omit the hydraulic conductivity at saturation from the fitting procedures (Par. 2.14). Only for the topsoil of plot 16B the Iwrc and the Ihcc are both satisfactory. For the other plots the fits of the Ihccs in the volumetric water content range $0.20 < \theta < 0.40 \text{ m}^3 \text{ m}^{-3}$ are usually too large compared to the Ihcc data. This is an important range for water flow in the field. Considering the pressure heads measured in the field in all soil layers and plots, it was found that the main part of the flow occurred in the range $-1000 < h < 0 \text{ cm}$, corresponding with a range of about $0.20 < \theta < 0.55 \text{ m}^3 \text{ m}^{-3}$.

Table 4.2 Optimised parameters of the analytical expressions of Van Genuchten (Eq. 2.16) and Mualem (Eq. 2.17) for describing the hydraulic characteristics of the different layers of the Lovinkhoeve soil; θ_r = residual volumetric water content ($\text{m}^3 \text{ m}^{-3}$), θ_s = volumetric water content at saturation ($\text{m}^3 \text{ m}^{-3}$), K_s = hydraulic conductivity at saturation (cm d^{-1}), α (cm^{-1}), n and L are empirical parameters .

Plot-layer	θ_r ($\text{m}^3 \text{ m}^{-3}$)	θ_s ($\text{m}^3 \text{ m}^{-3}$)	K_s (cm d^{-1})	α (cm^{-1})	n	L
12B top	0.05523	0.39921	0.514	0.00293	1.67828	-2.01297
12C top	0.08444	0.42630	0.506	0.00400	1.59343	-1.61168
16A top	0.04040	0.43709	2.038	0.00436	1.30740	-2.02754
16B top	0.02725	0.41407	0.544	0.00232	1.42167	-2.58159
Int. layer	0.08165	0.47303	1.624	0.00525	1.62422	-1.84898
Subsoil	0.10060	0.51506	0.373	0.00207	1.91432	-1.46461

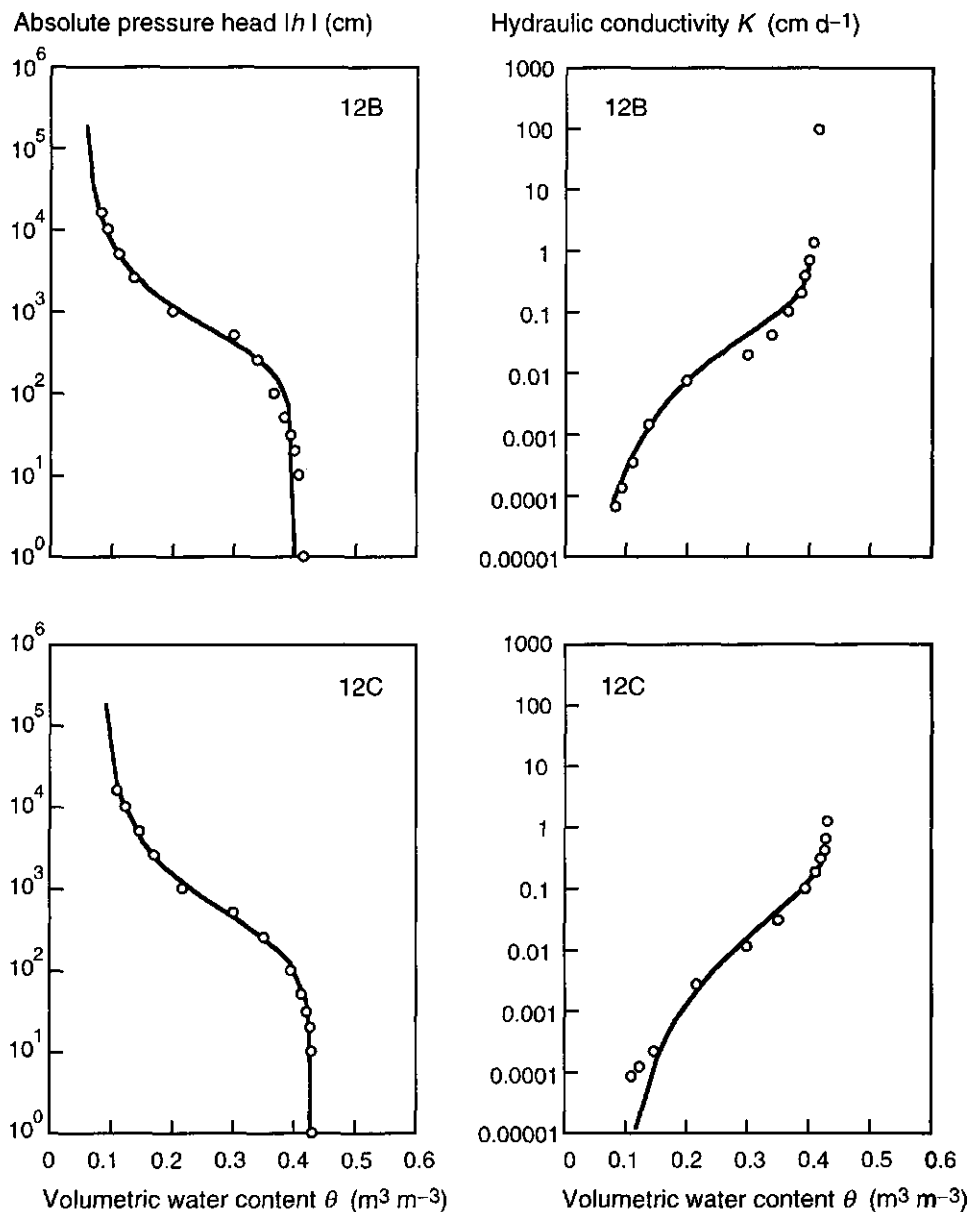


Figure 4.15a Analytical description (fits) of the water retention and hydraulic conductivity characteristics for the topsoils (0-25 cm depth) of plots 12B and 12C. The symbols indicate the measured values. The pressure head (negative) is expressed by its absolute value $|h|$.

4. Lovinkhoeve experimental farm

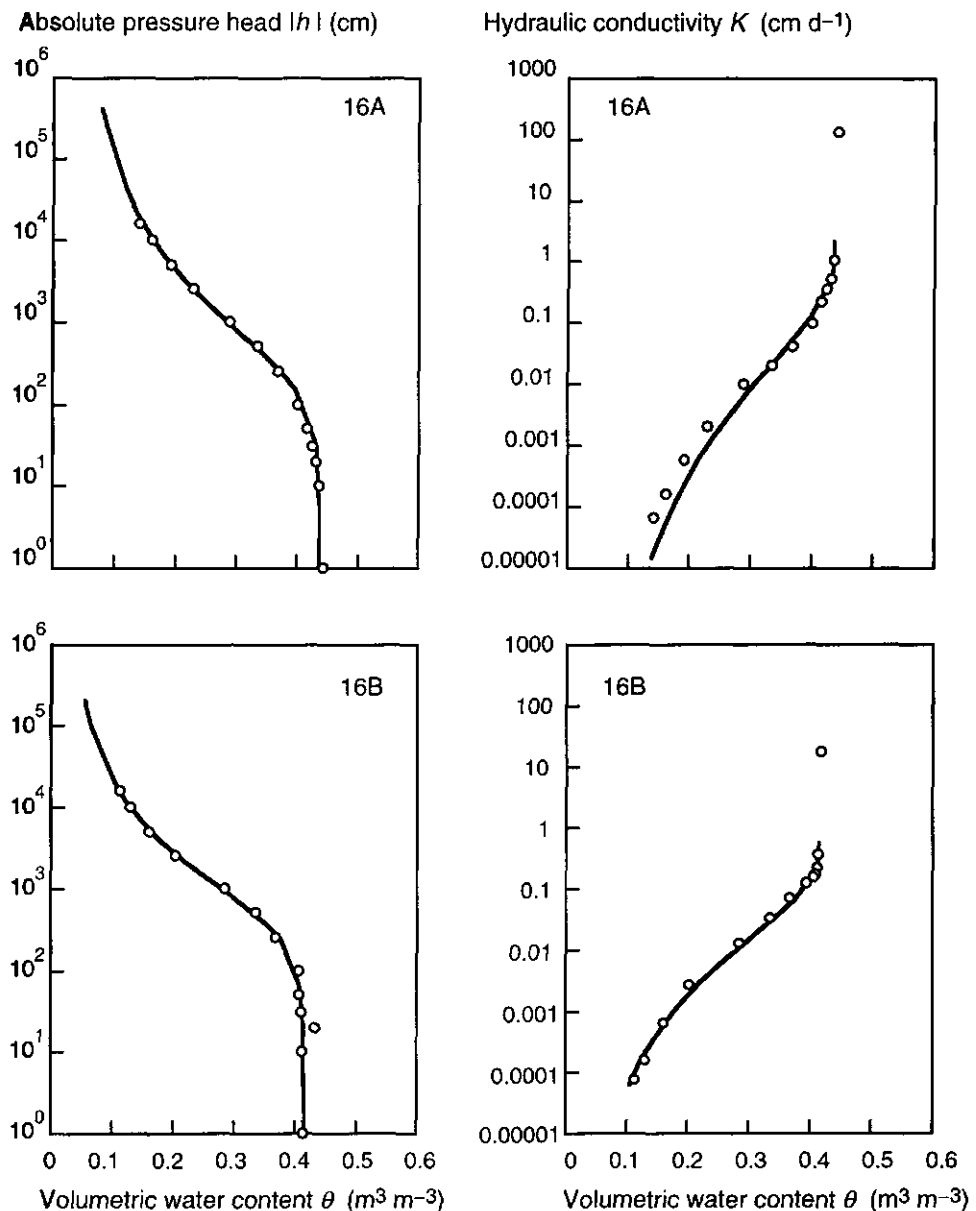


Figure 4.15b Analytical description (fits) of the water retention and hydraulic conductivity characteristics for the topsoils (0-25 cm depth) of plots 16A and 16B. The symbols indicate the measured values. The pressure head (negative) is expressed by its absolute value $|h|$.

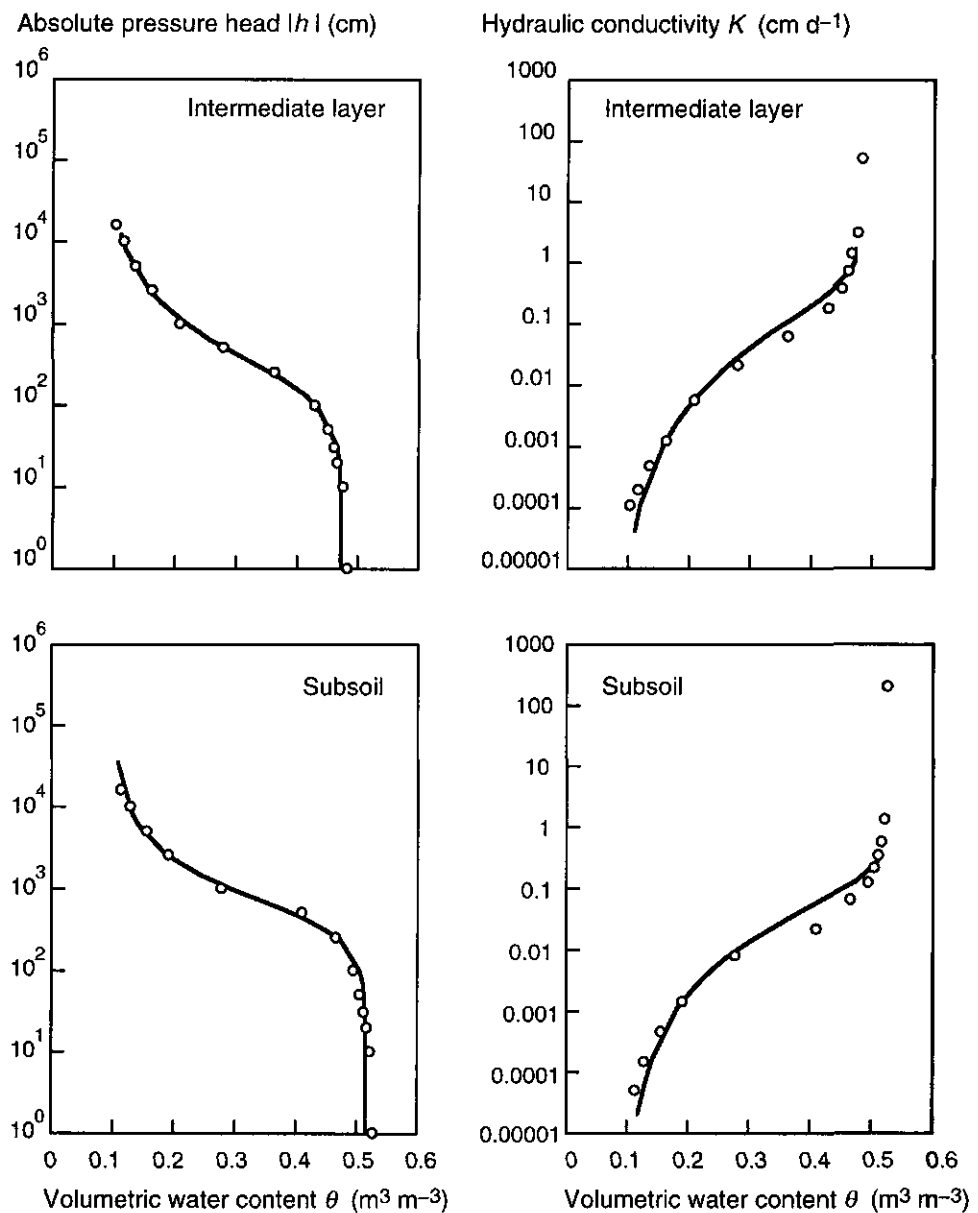


Figure 4.15c Analytical description (fits) of the water retention and hydraulic conductivity characteristics for the intermediate layer (25-40 cm depth) and subsoil (40-100 cm depth) for all plots. The symbols indicate the measured values. The pressure head (negative) is expressed by its absolute value $|h|$.

4.2.4 Hydraulic conductivity at saturation

The hydraulic conductivity at saturation K_s was measured in 1994 in samples from the net experimental field around drain 27 (Fig. 4.9), using the improved method to measure K_s , described in Par. 3.2.3. The K_s data are shown in Fig. 4.16 for measurements in the vertical and horizontal directions. For both directions, the variation in K_s at each depth is large, varying 1 to 2 orders of magnitude. However, a decreasing trend in K_s can be observed for the soil layers below 75 cm depth. At 120 cm depth, the soil samples contained pure peat, which had a distinctly lower K_s than all other layers. For the soil layers above 75 cm depth, K_s was generally found to be in the range $10 < K_s < 100 \text{ cm d}^{-1}$, both in the horizontal and vertical directions. The data indicate that the layering of the soil profile has an effect on K_s . Within each soil layer, no differences of K_s for the vertical and horizontal directions due to a possible micro-layering could be found, except for the soil layer at 38-58 cm depth. For the horizontal direction, K_s in this layer was substantially higher than for the vertical direction, K_s in this layer and also higher than K_s at all other depths. This large K_s for the horizontal direction is attributed to the presence of the sand layer, of about 3-5 cm thickness, in this plot found between 36-46 cm depth. The K_s in the vertical direction in the drain trench was larger than in the other parts of the field.

The addition of saffranine to the water on top of the soil samples in the K_s apparatus was a useful tool to check the proper functioning of the method. Flow along the wall of the PVC cylinders was rarely observed, which was probably due to a minimal swelling of the soil after saturation. Values of $K_s > 100 \text{ cm d}^{-1}$ always corresponded to one or more functioning macro-pores, which caused non-uniform water flow through the soil. For the soil samples with $K_s < 1 \text{ cm d}^{-1}$, no saffranine was found in the discharged water. In one sample, an active earthworm appeared at the surface of the soil sample, resulting in an increase in K_s . This measurement was not taken into account.

The averaged K_s data of the plots of the Dutch Programme on Soil Ecology of Arable Farming Systems (Fig. 4.8) fall all within the measurement range of the K_s data measured later with the improved K_s apparatus. The large difference between K_s and $K(h)$ close to saturation indicates once again the contribution of macro-pores to K_s , which is also reported by Bouma (1982).

Since values of $K_s > 100 \text{ cm d}^{-1}$ are due to the functioning of macro-pores,

the length, direction and continuity of those macro-pores at the field scale will define the impact on water flow and solute transport under saturated conditions. The size of the soil samples (height = 10 cm, diameter = 19.1 cm) corresponds to the grid size used in the numerical transport models. For the horizontal samples this procedure resulted in average K_s data for a depth interval of 19.1 cm. The relatively small height of the samples can result in overestimation of the effect of macro-pores, because the possibility of measuring a functioning macro-pore increases with a decreasing height of the soil sample. For the description of water flow and solute transport at the field scale, data have to be used which represent the behaviour at this scale. Field data of drain discharge and groundwater levels can be used to infer average K_s data at the field scale and these results can be compared with the K_s laboratory data. Field data of tracer experiments can be used to get an indication of the dispersion of solutes at the field scale. Dispersion can be considered as a macroscopic effect, as a result of the variation in K_s and $K(h)$ at the smaller length scales, causing variations in the water velocities (Dagan, 1989).

Depth (cm)

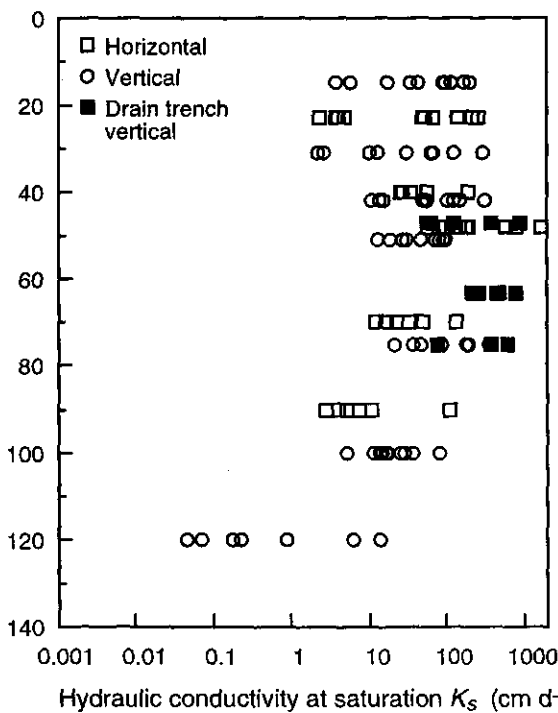


Figure 4.16 The hydraulic conductivity at saturation measured in the vertical and horizontal directions at different depths in the soil profile and in the drain trench.

4. Lovinkhoeve experimental farm

4.2.5 TDR calibration

Topp-curve

The data of the TDR calibration for all soil horizons are given in Fig. 4.17, together with the Topp-curve (Eq. 3.4). The trend in the experimental data corresponds well with this curve, although the data have generally a smaller apparent relative dielectric permittivity ϵ_a at a fixed θ . For $\theta > 0.40 \text{ m}^3 \text{ m}^{-3}$, the measured ϵ_a are substantially lower than the Topp-curve.

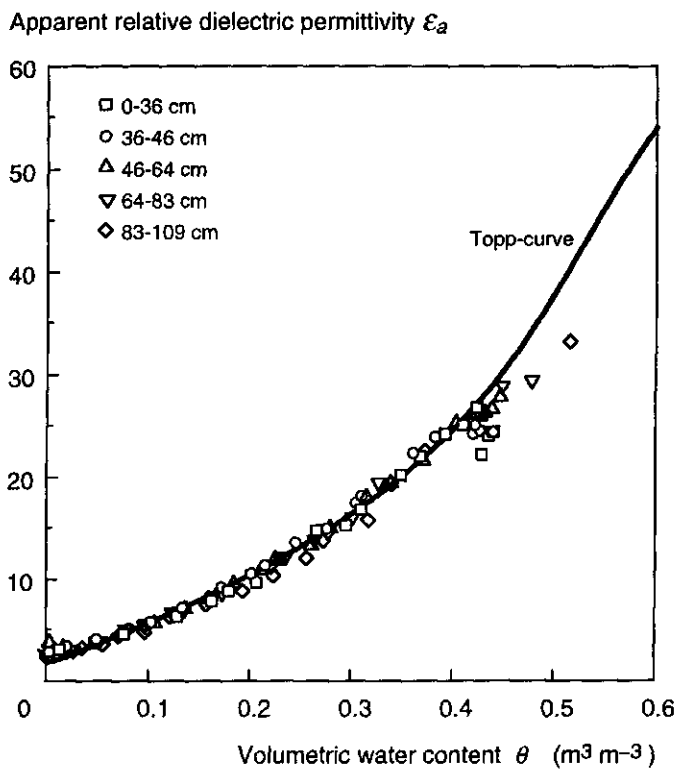


Figure 4.17 The relationship between the apparent relative dielectric permittivity and the volumetric water content for the TDR calibration data of the different soil horizons, and the Topp-curve (Eq. 3.4).

De Loor-curves

The TDR calibration results of the individual soil horizons are also compared with the De Loor model (Eq. 3.5) (Fig. 4.18). Table 4.3 shows the characteristics of the five soil horizons. The data concerning the different types of clay minerals are taken from Chapter 7. The bulk densities are the average bulk densities that were realised in the calibration experiments, and which correspond to the average field bulk densities. The hygroscopic water content θ_{hygr} was measured by drying disturbed soil samples at an air temperature of 25 °C and a relative humidity of 82%, which corresponds with a pressure head $h = -2.8 \cdot 10^5$ cm.

Apparent relative dielectric permittivity ϵ_a

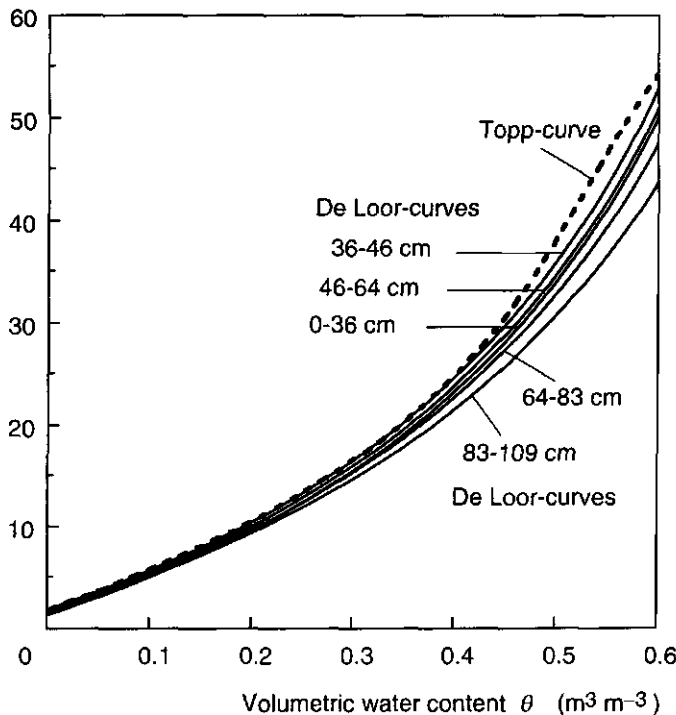


Figure 4.18 The relationship between the apparent relative dielectric permittivity and the volumetric water content for the De Loor-curves (Eq. 3.5) calculated for each soil horizon, and the Topp-curve (Eq. 3.4).

4. Lovinkhoeve experimental farm

Table 4.3 Characteristics for the different soil horizons. The different clay minerals and organic matter contents are expressed as % (w/w). Clay content, organic matter content, bulk density ρ_b , porosity ϕ , specific surface S , bound water fraction θ_{bw} and hygroscopic water content θ_{hygr} are given for the soil used in the TDR calibration experiments.

Depth (cm)	Clay (%w/w)	Smectite (%w/w)	Vermiculite (%w/w)	Hilite (%w/w)	Kaolinite (%w/w)	Organic matter (%w/w)	ρ_b (kg m ⁻³)	ϕ (m ³ m ⁻³)	S (m ² g ⁻¹)	θ_{bw} (m ³ m ⁻³)	θ_{hygr}
0-36	22	40	20	30	10	2.2	1340	0.493	73	0.029	0.036
36-46	9	50	10	30	10	1.6	1370	0.483	31	0.013	0.023
46-64	13	50	10	30	10	2.0	1330	0.497	44	0.018	0.027
64-83	15	50	0	40	10	2.8	1230	0.533	47	0.017	0.021
83-109	10	40	10	30	20	2.6	1090	0.587	30	0.010	0.018

Average values were used for the specific surfaces of the clay minerals: smectite, $S = 500 \text{ m}^2 \text{ g}^{-1}$; vermiculite, $S = 400 \text{ m}^2 \text{ g}^{-1}$; illite, $S = 150 \text{ m}^2 \text{ g}^{-1}$; and kaolinite, $S = 50 \text{ m}^2 \text{ g}^{-1}$. The measured hygroscopic water content θ_{hygr} was larger than the estimated bound water fraction θ_{bw} but the trends in differences between the soil horizons were similar (Table 4.3). For the calculation of the De Loor-curves θ_{bw} was used. The bulk densities at all realised water contents remained constant and the soils were kept at room temperature of $T = 20 \pm 2 \text{ }^{\circ}\text{C}$. The low organic matter fraction is not explicitly taken into account in the De Loor-model, which means that the $\varepsilon_s = 5$ is assumed to be the average value for solids, i.e., the combination of minerals and organic matter. Figure 4.18 shows the De Loor-

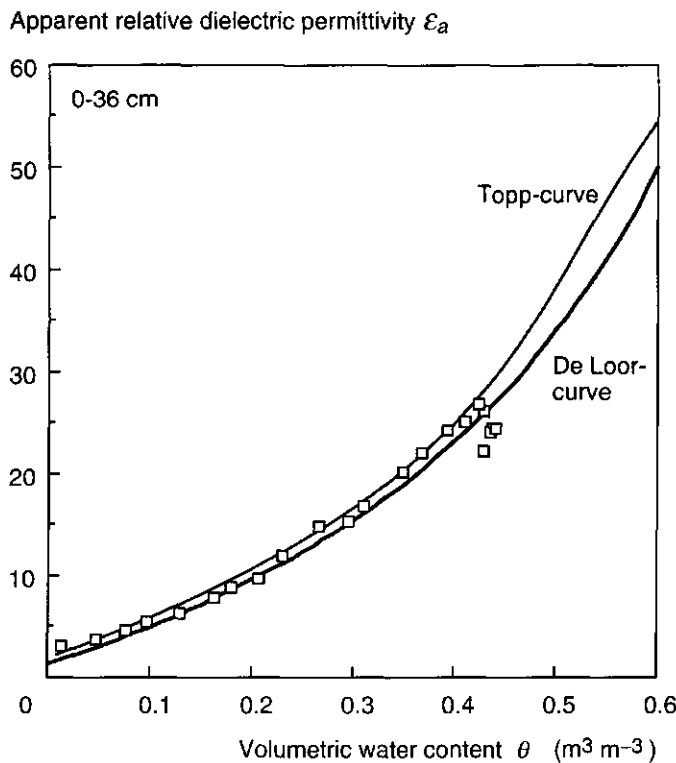


Figure 4.19 The relationship between the apparent relative dielectric permittivity and the volumetric water content for the TDR calibration data for the topsoil (0-36 cm), the De Loor-curve (Eq. 3.5) and the Topp-curve (Eq. 3.4).

4. Lovinkhoeve experimental farm

curves (Eq. 3.5) for the five soil horizons. The De Loor-curve of the 36-46 cm horizon is very close to the Topp-curve. The De Loor-curve of the 89-109 cm horizon shows lower ε_a values than the Topp-curve due to the lower bulk density in this soil horizon. The other soil horizons show an intermediate behaviour when the calibration data are compared with both the De Loor and the Topp-curve for each soil horizon. In the range $0 < \theta < 0.33 \text{ m}^3 \text{ m}^{-3}$, where the assumptions of the De Loor-model are valid, the De Loor-curves are closer to the data than the Topp-curve for all soil horizons, which is illustrated for the 0-36 cm horizon in Fig. 4.19.

However, in this study higher water contents are important too. For $\theta > 0.40 \text{ m}^3 \text{ m}^{-3}$, a deviation of the data from the curves can be observed for all soil horizons. These data were obtained using the saturation procedure described

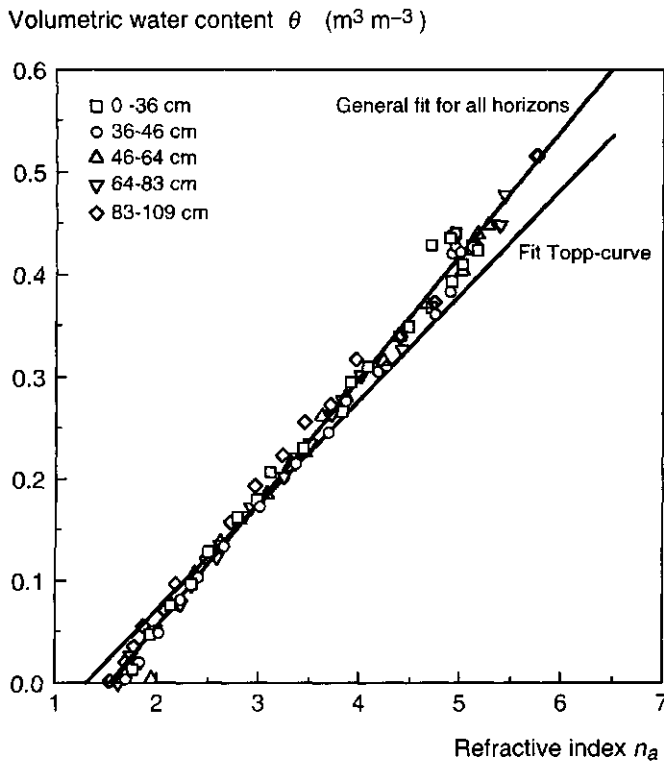


Figure 4.20 The relationship between volumetric water content and the refractive index for the TDR calibration data, the fit of the linear relationship for the combined data of all horizons, and the fit for the Topp-curve of Heimovaara (1993).

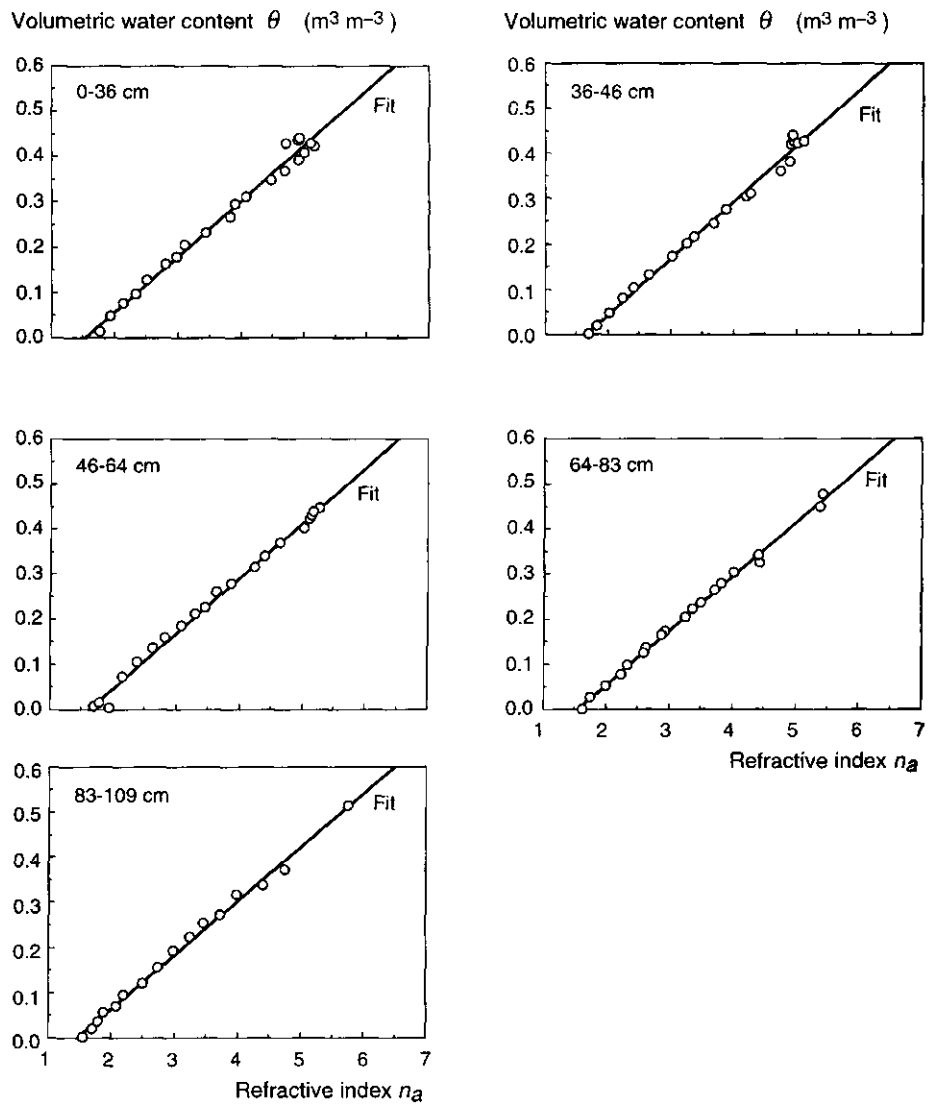


Figure 4.21 Relationship between volumetric water content and the refractive index for the TDR calibration data for each horizon, the linear fit for the corresponding soil horizon, and the general linear fit for the combined data of all horizons.

4. Lovinkhoeve experimental farm

earlier. Variations in volumetric water contents were found between the soil samples of the 0-7.5 cm and the 7.5-15 cm depth layers. Especially for the 0-36 cm and the 36-46 cm soil horizons, it seems that the measured water contents for $\theta > 0.40 \text{ m}^3 \text{ m}^{-3}$ are too high or that the measured ε_a are too low. Although the soil samples were saturated for at least two days, the highest measured volumetric water contents were 0.042 to $0.072 \text{ m}^3 \text{ m}^{-3}$ lower than the porosity.

For the Lovinkhoeve, Figs. 4.20 and 4.21 show the linear relationships between the refractive index n_a and the volumetric water content θ for the combined data of all soil horizons and the five separate soil horizons, respectively. The results of the linear regression analysis are given in Table 4.4. This fitting procedure, using a linear functional dependence between θ and n_a , results in a suppression of the weight of the data close to saturation as compared to fitting procedures using a functional dependence between θ and ε_a . This weighing can be considered as a positive side effect because of the uncertainty in the data close to saturation. The individual linear relationships for each soil horizon (Table 4.4) will be used as TDR calibration lines. The differences in the slopes between the lines for the soil horizons were judged to be substantial. Some TDR probes were installed in two soil horizons; for these probes a calibration line is calculated, weighted for the length fraction of the rods in each soil horizon.

Table 4.4 Results of the regression analysis for the linear relationship $\theta = a + b n_a$ between the volumetric water content θ and the refractive index n_a for the different soil horizons and for the combined data of all horizons.

Depth cm	a	b	R ²
0-36	-0.187	0.1223	0.986
36-46	-0.206	0.1252	0.992
46-64	-0.197	0.1223	0.995
64-83	-0.184	0.1198	0.997
83-109	-0.172	0.1192	0.996
0-109 (All)	-0.188	0.1215	0.992

5. MACROSCOPIC SOIL PHYSICAL PROCESSES CONSIDERED WITHIN AN AGRONOMICAL AND A SOIL BIOLOGICAL CONTEXT

5.1 Interdependence of soil biological and soil physical processes

Lately, much attention is being paid to the study of biological processes in the soil. Complex processes such as the functioning of soil communities are studied, often related to agricultural sustainability problems, and sometimes mainly to gain fundamental scientific insight. In the soil, these biological processes occur simultaneously with physical and chemical processes. These processes are interrelated and for this study it is relevant how soil physical conditions and processes influence the course of soil biological processes.

Soil biological and physical processes may occur at different spatial and temporal scales. The soil physical conditions can be defined for different spatial scales, from a single pore to an entire field. In principle, soil physical processes can be described at these different scales. A practical problem arises when, e.g., water flow has to be described at a micro-scale (< 1 cm), while hydraulic properties are generally measured at a macroscopic scale (1-10 cm).

Soil structure, especially the connectivity of pore space, affects the biological activity, for example by influencing the availability of food for organisms (Postma, 1989; Kuikman, 1990). It is difficult to characterise this aspect of soil structure in order to relate it to the functioning of soil organisms. Possibilities are the deduction of pore diameters from wetting and drying curves of the water retention characteristic, resulting in a rough idea of accessibility of pore space for organisms (Heil, 1988), or the way soil structure affects denitrification (Leffelaar, 1987). The processes of wetting and drying of aggregates determine under which conditions denitrification may occur. Even for such a micro-scale approach, macroscopic soil physical phenomena play an important role: water flow and transport of solutes and oxygen to an aggregate have to be described at the macroscopic scale. Smiles (1988) gave an overview of the relationships between the soil physical conditions at the macroscopic scale and at smaller scales.

5.2 The Dutch Programme on Soil Ecology of Arable Farming Systems

The Dutch Programme on Soil Ecology of Arable Farming Systems (Brussaard *et al.*, 1988) was set up to study the soil ecosystem under different types of arable farming practices. The programme was focused on possibilities to manipulate the soil processes in desirable directions. The goal was a more sustainable form of arable cropping with reduced nutrient inputs, minimum soil tillage, and restricted use of biocides. The programme had an agricultural background, the sustainable development of healthy crops being the ultimate goal. Therefore, the mechanisms that regulate the nutrient supply to the crop received much attention, especially the pools and flows of nitrogen and carbon in the soil-crop system.

In this programme the soil biological and soil physical processes were studied primarily under field conditions. When necessary, laboratory experiments were carried out. A four-year rotation of potatoes - winter wheat - sugar beet - spring barley was studied with one "conventional" and two "integrated" variants. In the "integrated" variants the mineral nitrogen inputs were about 60% of the conventional inputs. In the integrated variants organic matter was applied in the form of compost and processed animal manure (Van Faassen and Lebbink, 1994). This organic matter input, together with the mineral N input, resulted in a total N input in the integrated plots of about 90% of the conventional N inputs. Further details on field site and crop management are given by Brussaard *et al.* (1988), Kooistra *et al.* (1989), and Lebbink *et al.* (1994).

Soil tillage has direct effect on the soil physical properties and an indirect effect on soil biological processes. The depth of soil tillage was 25 cm in the "conventional" plots, 15 cm in the "integrated" plots, and 5 cm in the "integrated with minimum tillage" plots (Fig. 4.8). It was hypothesised that a reduction in soil tillage depth may change the detrital pathway from bacterial-dominated to fungal-dominated as a result of the changed spatial distribution of decomposing organic matter from residues incorporated into the topsoil. This would be a rather direct effect of soil physical changes. It was also expected that a reduced soil tillage and application of organic matter would change the soil hydraulic properties.

In the soil physical part of the project, a combined approach of monitoring and modelling was chosen. Field measurements of pressure heads, groundwater

5. *Macroscopic soil physical processes*

levels, and soil temperatures were performed at 2-3 day intervals in the different plots (Fig. 4.8) and meteorological conditions were measured continuously at a grass field (Fig. 3.9). The hydraulic characteristics of the soil of the different plots have already been presented in Chapter 4. The differences between plots were evaluated in relation to the arable farming systems. Model calculations were performed to evaluate the various components of the water balance. Water fluxes, which determine the convective component of the flux of solutes, were calculated. The Dutch Programme on Soil Ecology of Arable Farming Systems will be evaluated, focusing on soil structure, N mineralisation and the N balance in relation to soil physical processes and conditions. Finally, specific soil physical and general conclusions will be drawn, and ideas for future research will be formulated.

5.3 Field measurements

Field measurements were performed in the years 1986 to 1990 on different plots. Special attention was given to the growing seasons, because the largest differences in soil physical conditions and biological activity were expected in these periods. Bulk densities, pressure heads, groundwater levels and soil temperatures were measured. The pressure heads and groundwater levels were measured at 2-3 day intervals during the growing season. The tensiometers and groundwater tubes were located in between the crop rows, at a distance of 3 m from a drain, except in the year 1988 when the tensiometers were distributed over the field with a variable distance to the drains. Pressure heads smaller than -800 cm (see Par. 3.1.1) and groundwater levels below the depth of the groundwater tubes (\approx 175 cm) are not plotted in Figs. 5.3 - 5.7. In order to compare the results of the different years, it was decided to present only the average pressure heads of the topsoil (20 cm depth) and the subsoil (50 or 60 cm depth), together with the precipitation rate and the groundwater levels (Figs. 5.3 - 5.7).

The dates of sowing, emergence, harvest and the crop yield for the relevant plots are given in Table 5.1. Data on the time course of dry matter production are given by Lebbink *et al.* (1994). Root depth and root length densities were measured on several plots (Van Noordwijk *et al.*, 1994).

Some extra soil physical measurements were performed on the

meteorological grass field (Figs. 3.9 and 4.7). This plot was accessible even under very wet conditions. At different distances from the drain in this plot, groundwater levels were measured. Drain depth and hydraulic characteristics of the subsoil for the grass field and the other field plots were similar.

Table 5.1 Crop and yield data for the plots where soil physical measurements were performed in the years 1986-1990.

Year	Plot	Crop	Sowing date	Emergence date	Yield (t ha ⁻¹)
1986	12B	Winter wheat	1-11-1985	18-11-1985	7.5 ^a
	16A	Winter wheat	1-11-1985	18-11-1985	6.8 ^a
1987	12B	Sugar beet	24-4-1987	11-5-1987	9.3 ^b
	12C	Sugar beet	24-4-1987	11-5-1987	9.3 ^b
	16A	Sugar beet	24-4-1987	6-5-1987	8.6 ^b
1988	16B	Sugar beet	24-4-1987	6-5-1987	7.3 ^b
	12B	Spring barley	7-4-1988	20-4-1988	4.6 ^a
	12C	Spring barley	7-4-1988	20-4-1988	3.4 ^a
1989	16A	Spring barley	7-4-1988	20-4-1988	4.1 ^a
	16B	Spring barley	7-4-1988	20-4-1988	4.2 ^a
	17A	Sugar beet	10-4-1989	27-4-1989	12.0 ^b
1990	17C	Sugar beet	10-4-1989	27-4-1989	12.7 ^b
	12B	Winter wheat	26-10-1989	15-11-1989	7.4 ^a
	16A	Winter wheat	26-10-1989	15-11-1989	5.7 ^a

^a grain dry weight

^b sugar

5. Macroscopic soil physical processes

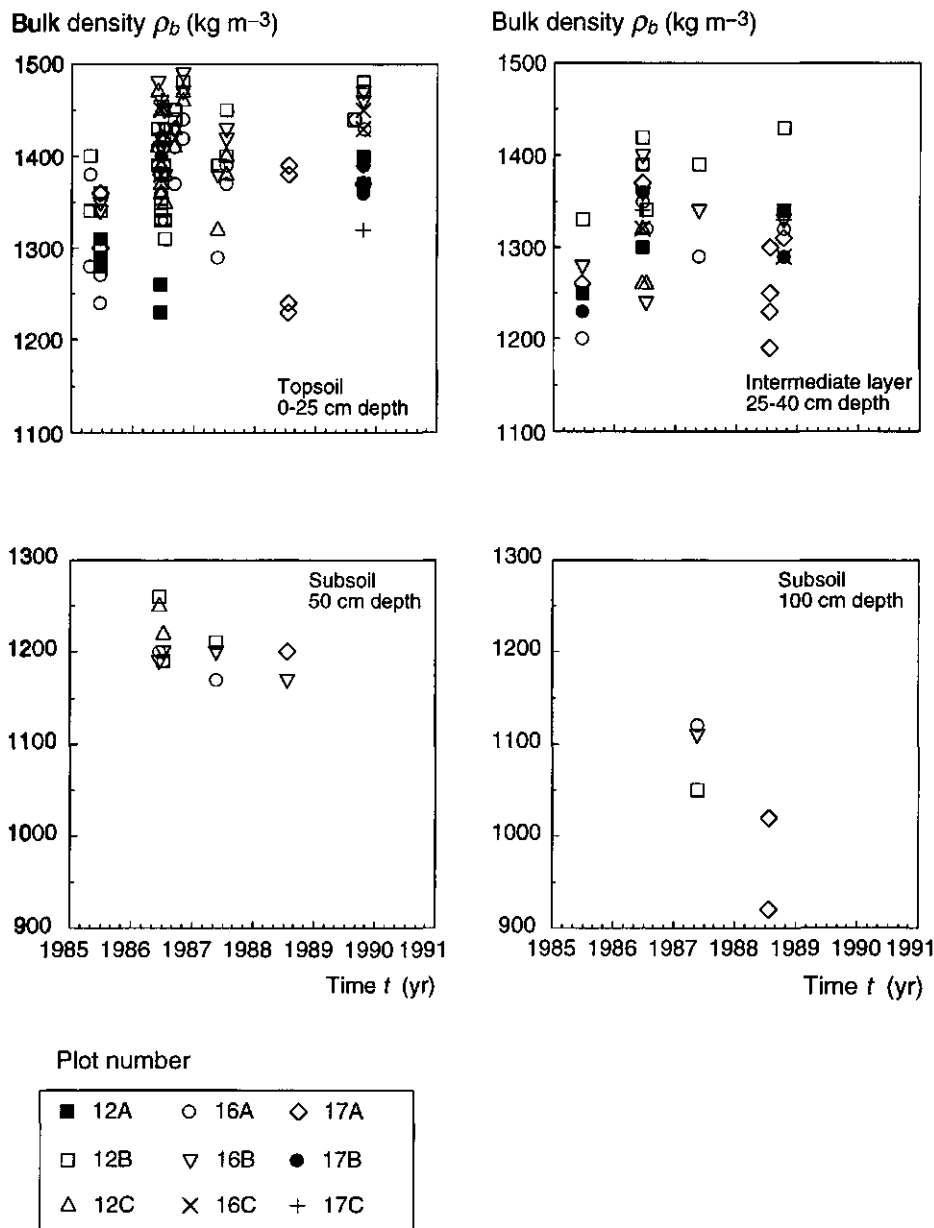


Figure 5.1 Bulk densities in the different years of the research period, for the topsoil (0-25 cm depth), the intermediate layer (25-40 cm depth), the subsoil at 50 cm depth and the subsoil at 100 cm depth of different plots. Note the differences in the scale of the bulk densities between the top and bottom figures.

5.4 Soil physical conditions during 1986-1990

Bulk densities

The bulk density ρ_b of the soil was measured several times during the research period (Fig. 5.1). The bulk density in the topsoil changed during this period due to soil tillage, soil traffic, and repacking. Normally, bulk densities were determined in spring, when a stable situation had been reached following the soil tillage during the preceding autumn and winter. The 100 ml samples were taken from the undisturbed soil, outside the tracks of the farm machinery. There was a large variation in bulk density within the plots. The bulk density in the topsoil (0-25 cm depth) of all plots ranged between 1200 and 1500 kg m⁻³, and in the intermediate layer (25-40 cm depth) between 1175 and 1450 kg m⁻³. The average bulk density of the subsoil at 50 cm depth was close to 1200, and that of the subsoil at 100 cm depth close to 1000 kg m⁻³.

The yearly averages of the bulk density ρ_b for the topsoil (0-25 cm depth) of the historical treatments (Fig. 4.8) "ley (A-block)", "fertiliser (B-block)" and "clover (C-block)" in Fig. 5.2 show the same trend as the results in Fig. 4.4. The "ley" had lower bulk densities than the other treatments. Boekel (1985) already concluded that this difference is caused by the larger organic matter content of the "ley" (2.8%) compared to "clover" (2.3%) and "fertiliser" (2.2%) plot. The bulk density is directly related to the porosity of the soil. Lower bulk densities correspond with larger porosities, due to a larger number pores with an equivalent diameter > 20 μm (Boersma and Kooistra, 1994; Heil, 1988).

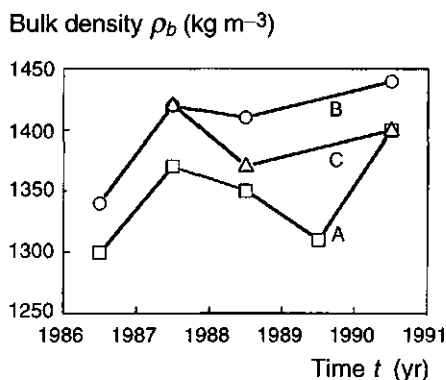


Figure 5.2 Averaged bulk densities of the topsoil per historical treatment as used by Boekel (1985, see Fig. 4.4):
 A = clover, green manuring in addition to chemical fertiliser;
 B = fertiliser, six year rotation without ley; chemical fertiliser additions only;
 C = ley, eight-year rotation including two-year ley.

5. Macroscopic soil physical processes

Soil physical conditions during the 1986 growing season

During the 1986 growing season, pressure heads were measured at n different positions at depths of 10 ($n = 5$), 20 ($n = 5$), 40 ($n = 4$) and 60 cm ($n = 4$) in plots 12B and 16A, where winter wheat was grown. In 1986 the reaction of the average pressure heads at 20 cm depth to precipitation in the period $t = 155-160$ d was evident (Fig. 5.3). The pressure head at 20 cm depth gave a fast response, while at 60 cm depth there was no response to the precipitation. Water uptake by the roots counteracted the increase of the pressure heads, thus contributing to the observed damping of the increase of the pressure heads with depth.

A dry period started at $t = 160$ d, and the pressure heads in the topsoil decreased rapidly for $t > 160$ d. For $t > 170$ d the tensiometers in the topsoil fell dry and thus no longer functioned. The averaged pressure heads at 60 cm depth in plots 12B and 16A differed during the course of the growing season. The values of plot 12B were lower, indicating a larger water extraction by the roots in plot 12B than in plot 16A. This difference corresponds with a difference in yield of winter wheat: 7.5 t ha^{-1} for the conventional plot 12B and 6.8 t ha^{-1} for the integrated plot 16A.

Throughout the full measurement period, the gradient in hydraulic head between 40 and 60 cm depth (data not shown) always indicated capillary rise between those depths. This corresponds with the falling groundwater level for $t > 170$ d. A small upward seepage or horizontal infiltration of water from the ditch could explain the small rise in groundwater level in this period.

Soil physical conditions during the 1987 growing season

During the 1987 growing season, pressure heads were measured at 5 positions ($n = 5$) at depths of 10, 20, 30, 50, and 100 cm in plots 12B, 12C, 16A and 16B, where sugar beet were grown. In the wet period $155 < t < 180$ d the averaged pressure heads at 20 cm depth were similar for all plots, except for plot 12C where lower pressure heads were observed (Fig. 5.4). At $t = 161$ d and $t = 180$ d pressure heads were very high in all plots, indicating that the groundwater level was close to the soil surface, and that the soil profile was very wet. In the dry period $180 < t < 197$ d the pressure heads of all plots decreased. For $200 < t < 295$ d the soil was very wet again; the pressure heads at 20 cm depth were always larger than -200 cm. These pressure heads became positive several times, indicating that the groundwater level came close to the soil surface or that stagnant water was present. At $t = 162$ d and $t = 208$ d there were very high

groundwater levels in all plots, except plot 12C. The slower and less pronounced reaction of the groundwater level in plot 12C is observed throughout the total measurement period. The extreme fluctuations of the groundwater level in plot 12B and 16A indicate that the soil profile was close to saturation, and that the resistance to flow to the drain was high. The pressure heads in the topsoil of plot 12C were more negative, resulting in a larger capacity for the storage of infiltrating water. This effect cannot be explained by the differences in water retention characteristics (Figs. 4.11 and 4.12), but must be related to differences in water extraction by the crop. Nevertheless, the yield of plot 12C is comparable with the yields on plots 12B and 16A (Table 5.1).

Soil physical conditions during the 1988 growing season

During the 1988 growing season, pressure heads were measured at 5 positions ($n = 5$) at depths of 10, 20, 30, 50 and 100 cm in plots 12B, 12C, 16A and 16B where spring barley was grown. The locations of the tensiometers were distributed over the field with a variable distance to the drains. During the growing season the periods $130 < t < 150$ d and $162 < t < 182$ d were dry and the period $t > 182$ d was wet (Fig. 5.5). The differences in pressure head between the plots were small, except for plot 12C which had lower pressure heads in the period $182 < t < 221$ d. The pressure heads at 100 cm depth confirmed the differences between plot 12C and the other plots. However, the pressure head was larger at this depth in plot 12C. The differences could be a result of the root distributions in the soil profile. A main difference between plot 12C and the other plots was the poor development of the spring barley on plot 12C, which resulted in an accelerated development of a grass undercrop. A major portion of the grass roots was present at 0-30 cm depth in the topsoil of plot 12C, and water was extracted preferentially from the topsoil. At larger depth, the roots extracted less water in plot 12C, due to the relatively poor development of the main crop. The groundwater level of plot 12C, like in 1987, was reacting more slowly to precipitation than the other plots.

Soil physical conditions during the 1989 growing season

During the 1989 growing season, pressure heads were measured at 5 positions ($n = 5$) at depths of 10, 20, 30, 50 and 100 cm in plots 17A and 17C where sugar beet were grown. It was a relatively dry growing season; the tensiometers in the topsoil fell dry around $t = 170$ d, and did not function again

5. Macroscopic soil physical processes

until $t = 250$ d, due to the high water extraction rate of the sugar beet (Fig. 5.6). The pressure heads at 20 cm depth in plot 17C decreased faster than in plot 17A, indicating a larger relative water extraction in the topsoil. At a depth of 50 cm, the pressure heads of both plots were similar. At 100 cm depth the pressure head in plot 17A is more negative during the total growing season (data not shown), caused by a larger water extraction from the entire soil profile. This observation was in line with the sugar beet yield of 88 t ha^{-1} for plot 17A and 81 t ha^{-1} for plot 17C (Table 5.1). The soil profile became extremely dry for $t > 200$ d, the pressure heads at 100 cm depth became < -200 cm (data not shown).

Soil physical conditions during the 1990 growing season

From winter 1989 until summer 1990 pressure heads were measured at 5 positions ($n = 5$) at depths of 10, 20, 30, 50 and 100 cm in plots 12B and 16A where winter wheat was grown. Time t^* is the time (d) after 30 November 1989. In the wet winter period ($0 < t^* < 120$ d) the differences in pressure head in the topsoil of the plots are small (Fig. 5.7). For $t^* > 120$ d dry and wet periods occurred, with precipitation rather evenly distributed throughout the season. Plot 12B had more negative pressure heads in the topsoil in the drier periods compared to plot 16A. The groundwater level is decreasing for $t^* > 100$ d, first by the effect of drainage by the tile drain at 97.5 cm depth, later ($t^* > 150$ d) by capillary rise. The average groundwater level of plot 16A was somewhat lower than of plot 12B.

Water flow and nutrient transport in a layered silt loam soil

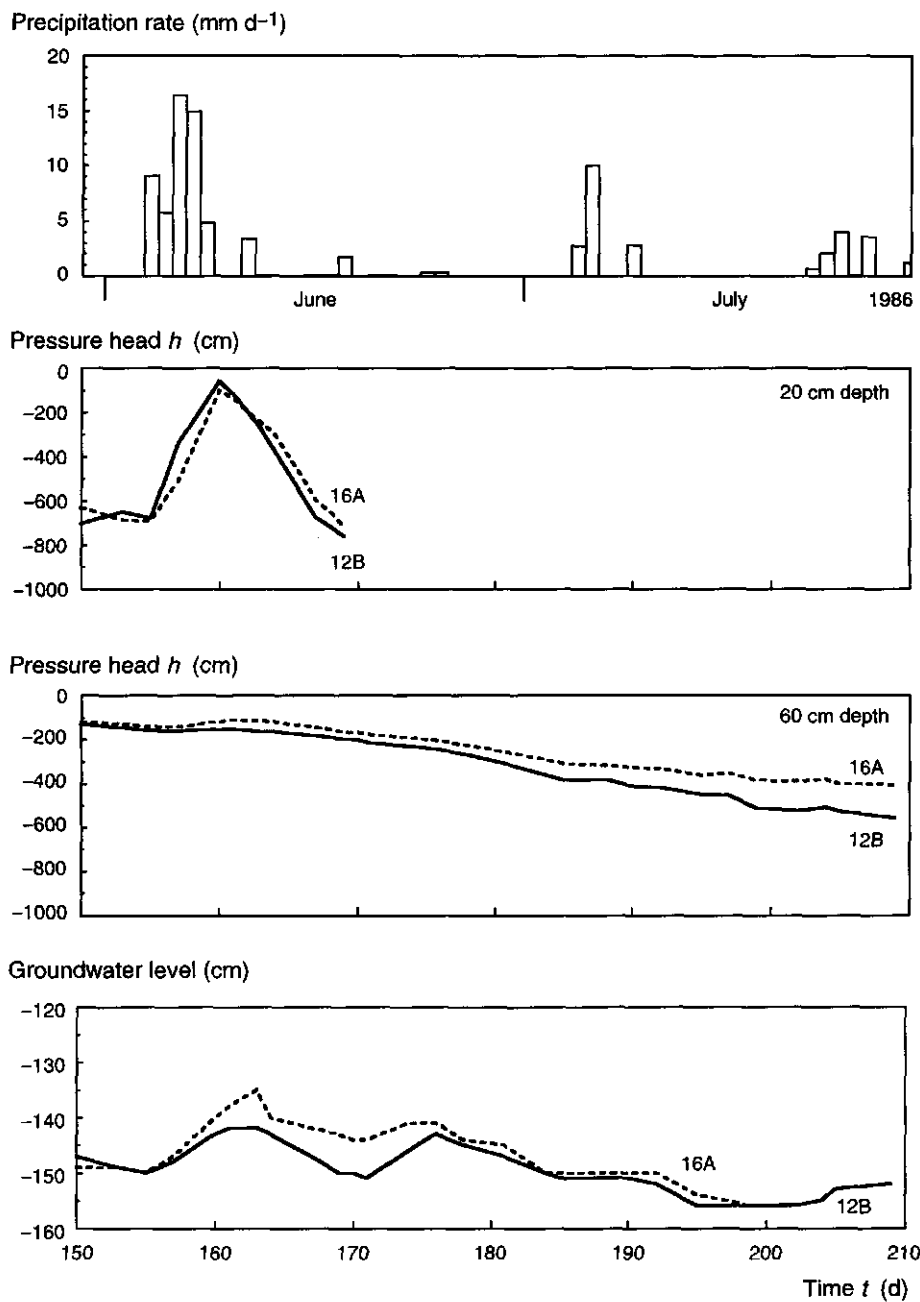


Figure 5.3 Field measurements in 1986: precipitation rate; pressure heads at 20 cm depth; pressure heads at 60 cm depth; and groundwater levels at plots 12B and 16A. Time t is the Julian day (bottom); the corresponding months are indicated also (top).

5. Macroscopic soil physical processes

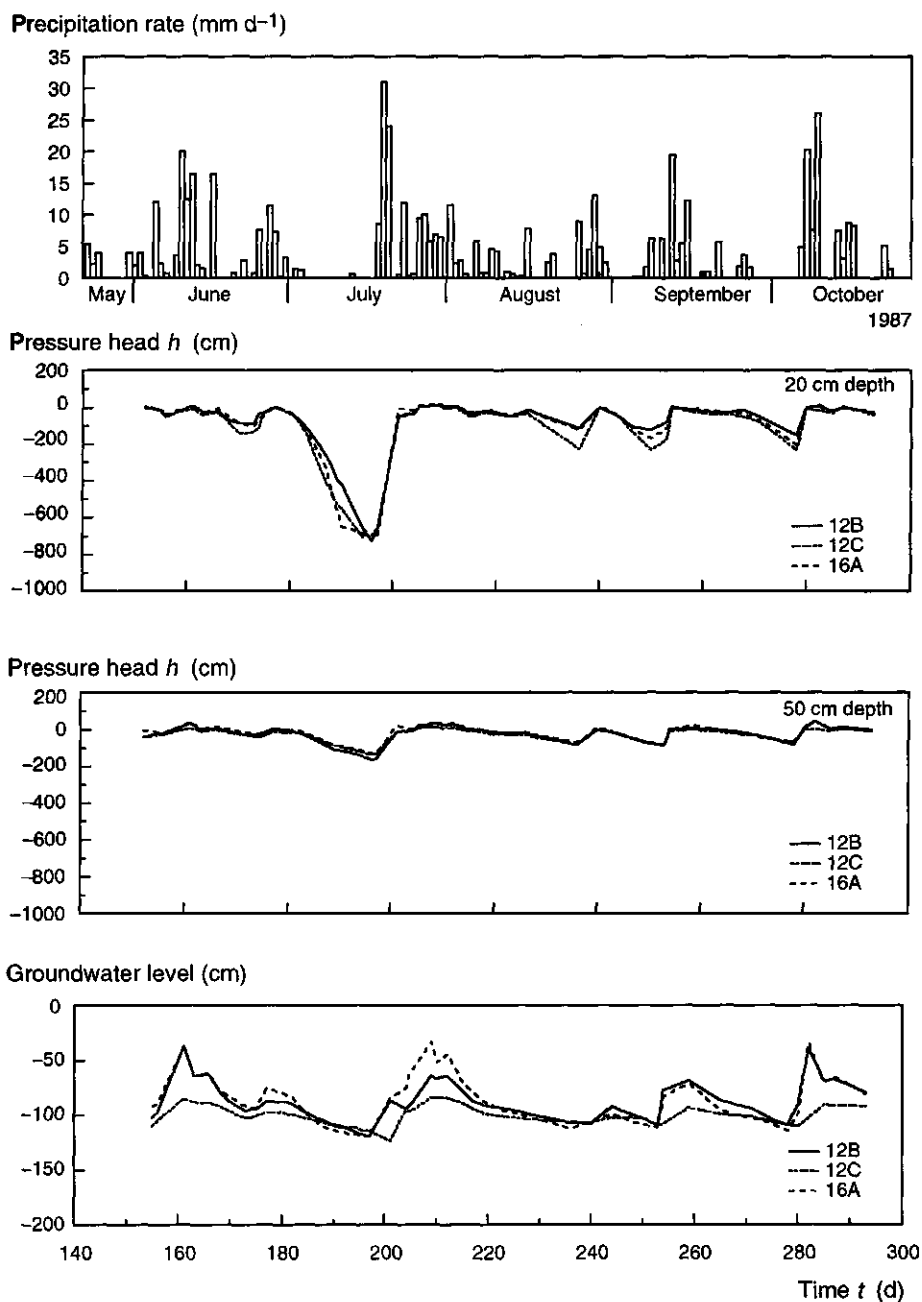


Figure 5.4 Field measurements in 1987: precipitation rate; pressure heads at 20 cm depth; pressure heads at 50 cm depth; and groundwater levels at plots 12B, 12C and 16A. Time t is the Julian day (bottom); the corresponding months are indicated also (top).

Water flow and nutrient transport in a layered silt loam soil

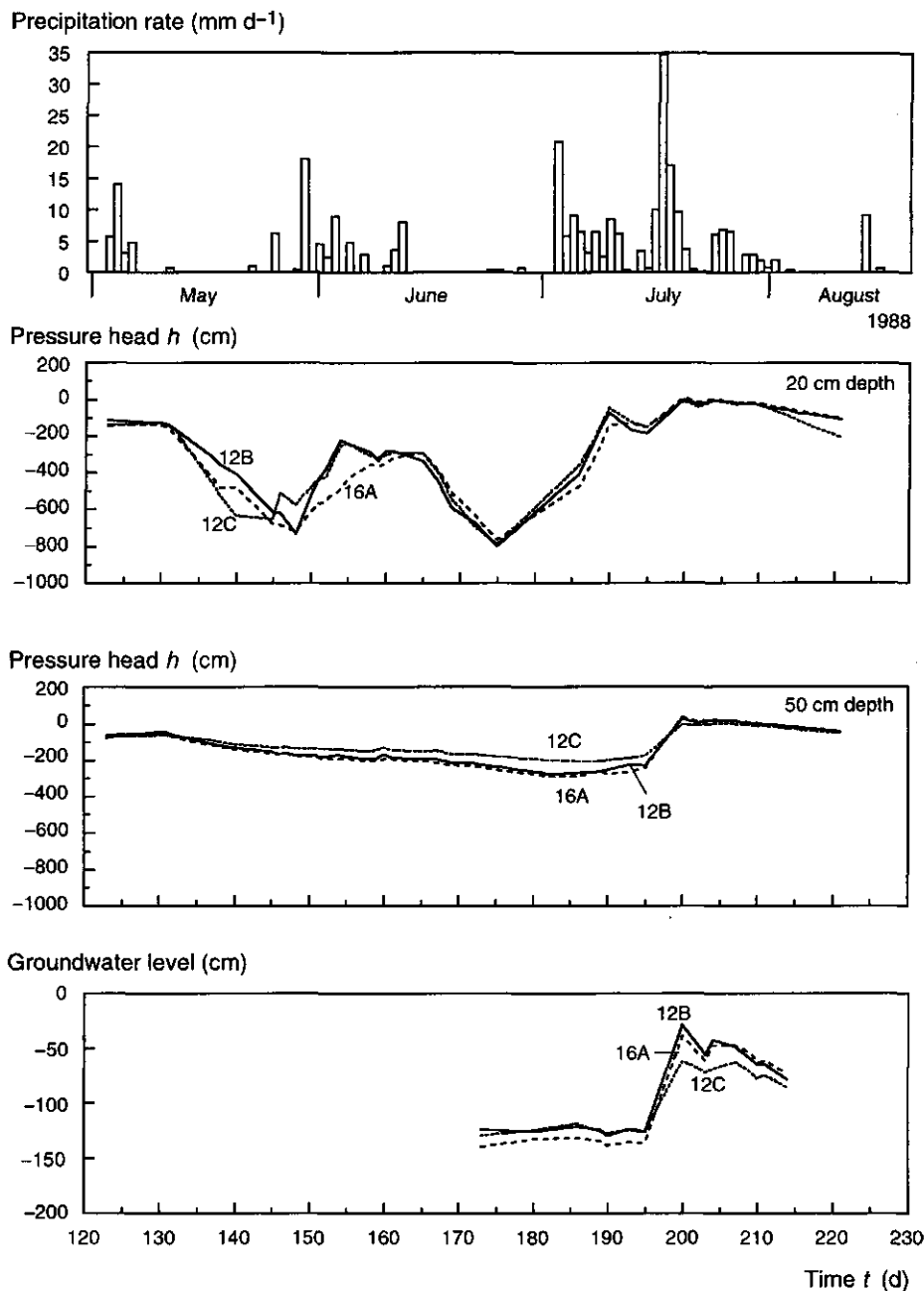


Figure 5.5 Field measurements in 1988: precipitation rate; pressure heads at 20 cm depth; pressure heads at 50 cm depth; and groundwater levels at plots 12B, 12C and 16A. Time t is the Julian day (bottom); the corresponding months are indicated also (top).

5. Macroscopic soil physical processes

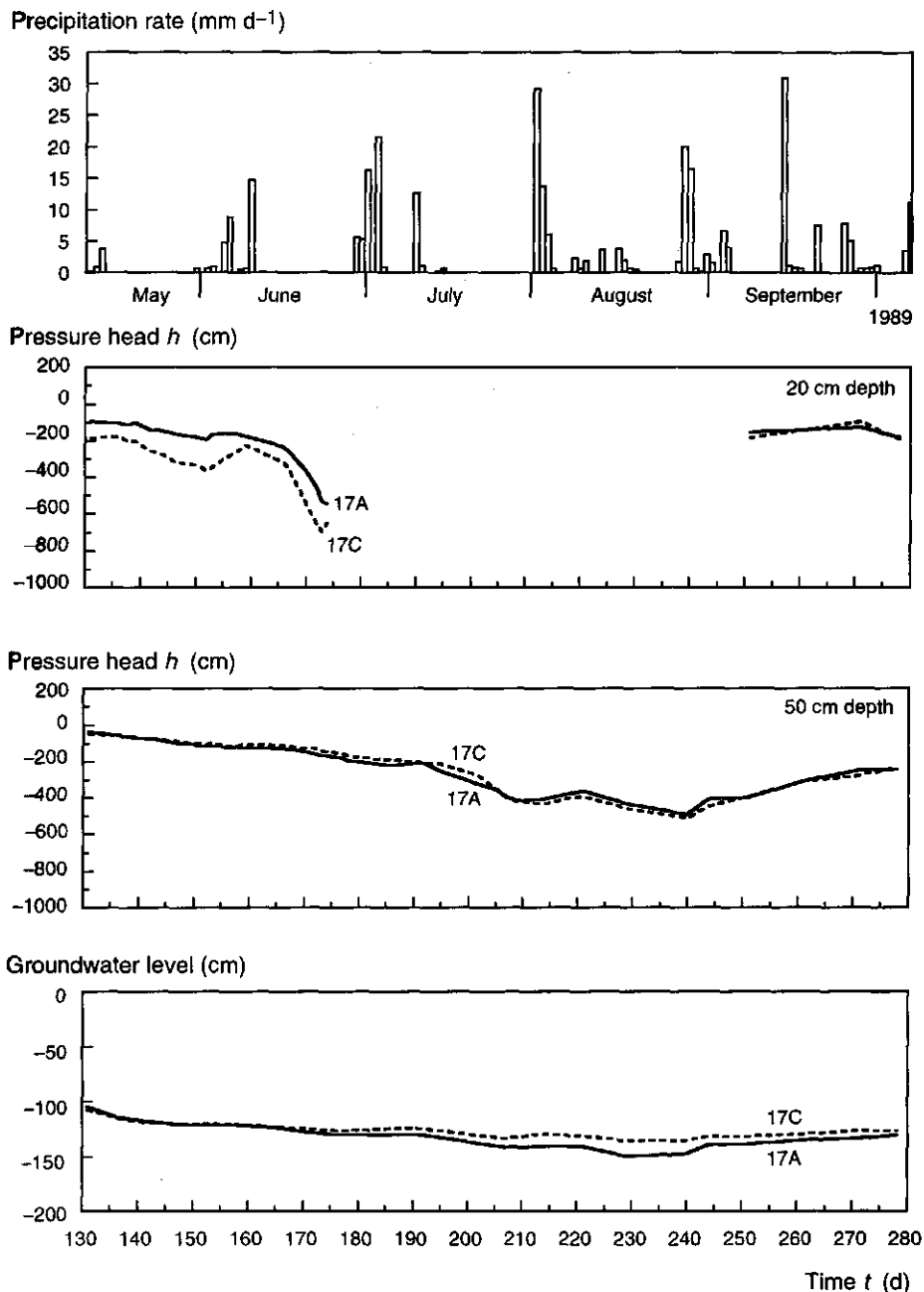


Figure 5.6 Field measurements in 1989: precipitation rate; pressure heads at 20 cm depth; pressure heads at 50 cm depth; and groundwater levels at plots 17A and 17C. Time t the Julian day (bottom); the corresponding months are indicated also (top).

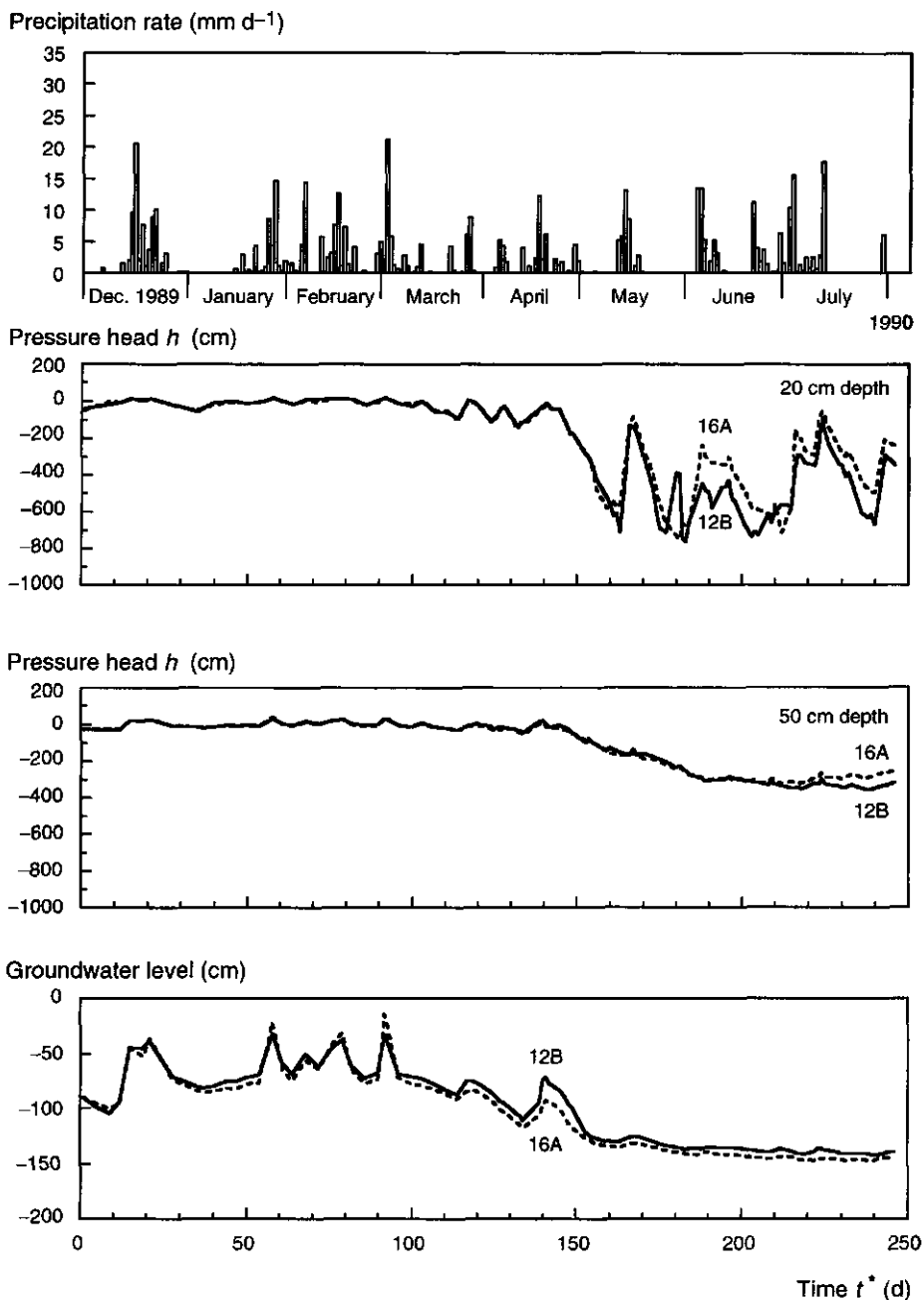


Figure 5.7 Field measurements in 1989-1990: precipitation rate; pressure heads at 20 cm depth; pressure heads at 50 cm depth; and groundwater levels at plot 12B and 16A. Time t^* is the time (d) after 30 November 1989; the corresponding months are indicated also (top).

5. Macroscopic soil physical processes

Soil physical conditions as a function of distance from the drain

Most of the field data were collected at 3 m distance from a drain. During the research period it was decided to install a line of groundwater tubes in between two drains at the grass field of the meteorological station (Fig. 3.9). The measured groundwater levels for 1989 are presented in Fig. 5.8. Under wet conditions ($0 < t < 120$ d and $t > 270$ d) the differences in groundwater levels for different positions were large. At $t = 62$ d the groundwater level above the drain (0 m) was -68 cm, while in the middle between the drains (6 m) the groundwater level rose to -8 cm. The falling of the phreatic surface is presented in Fig. 5.9. Also during this period, the groundwater level in between the drains was the highest, until the phreatic surface drops below the drain depth of 100 cm. The large fluctuations in groundwater level are partly a consequence of the steep slope of the water retention characteristic close to saturation. A small change in water volume results in a large change in pressure head. For all plots, except plot 12C, the fluctuations in groundwater level were large under wet conditions. The measured pressure heads showed that no stagnation of water in the soil profile occurred. The relatively high drainage resistance of the subsoil must be the reason for the large fluctuations, and for the slow falling of the groundwater level.

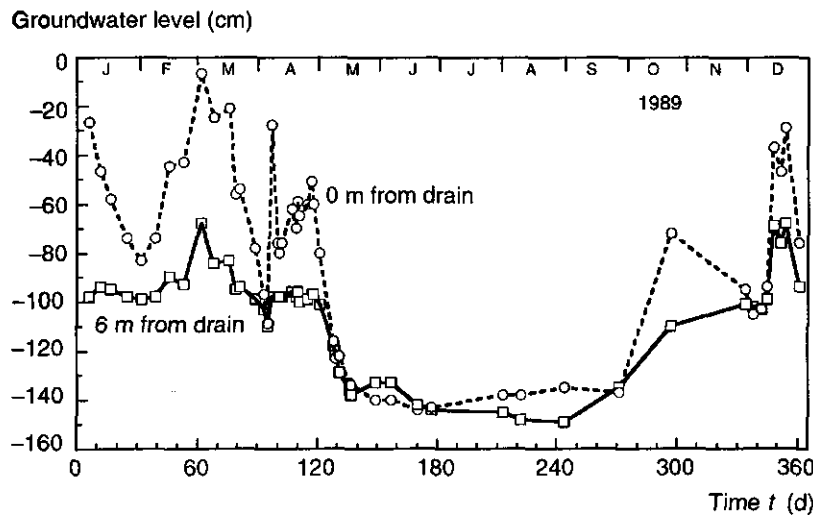


Figure 5.8 Time course of the groundwater levels at the grass field of the meteorological station at distances of 0 and 6 m from the drain during 1989. Time t is the Julian day; the corresponding months are indicated also (top).

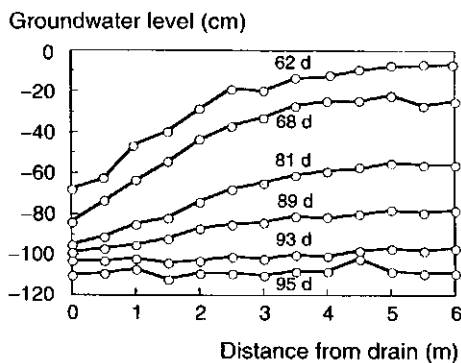


Figure 5.9 The phreatic surface at the grass field of the meteorological station on different days in 1989 for half the drain spacing. The distance between the drains is 12 m.

The average pressure heads give only part of the information on the soil water status in the field. The differences in measured pressure heads give an indication of the spatial variability of the pressure heads within a plot. Figure 5.10 shows that the variation in the pressure heads at 10 cm depth was larger under dry conditions than under wet conditions. This was also true at a depth of 100 cm. The effect of different distances from the drain have not yet been discussed; this will be analysed in the next chapter.

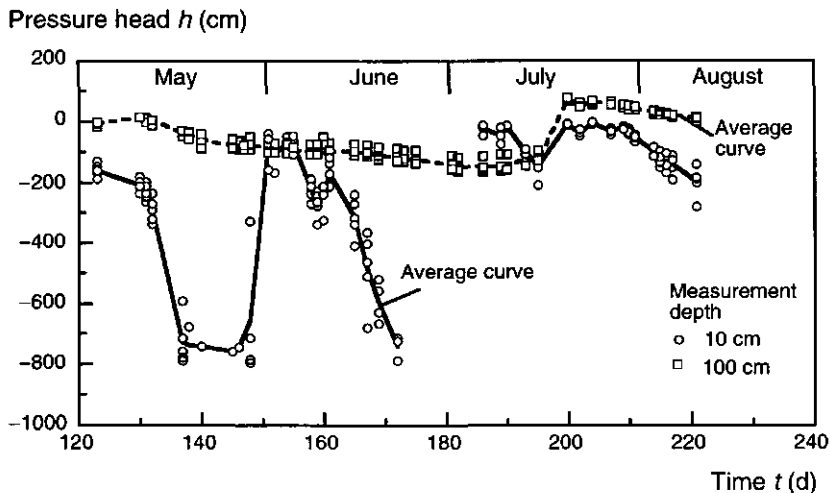


Figure 5.10 Averaged pressure heads and individual measurements at plot 12B in 1988 at 10 cm and 100 cm depth. Time t is the Julian day, the corresponding months are indicated also.

Some aspects of the spatial and temporal distributions of soil temperatures

The theory of heat transport in soils is described in detail by Van Wijk (1963). Two illustrative examples of measured soil temperatures at the Lovinkhoeve are presented in this paragraph.

The soil temperature of plot 12B under a winter wheat crop is presented in Fig. 5.11 for a 24 hour period from 7.00 h on 10 August ($t = 7$ h) to 7.00 h on 11 August 1986 ($t = 31$ h). The soil temperature at 5 cm depth rose to 18.5 °C in the afternoon ($t = 17$ h) and dropped to 13 °C in the early morning ($t = 4$ h), and showed a sinusoidal fluctuation. At 20 cm depth, the peak in temperature arrived at midnight ($t = 24$ h) and the amplitude was lower. At 100 cm depth, no diurnal variations were observed.

The daily averaged soil temperatures under the grass field of the meteorological station for 1990 are presented in Fig. 5.12. The daily fluctuations corresponding to weather patterns over several days are seen at 5 and 20 cm depth; at 100 cm depth the daily fluctuations are damped out and mainly the yearly temperature fluctuations can be seen. At all depths, the yearly averaged soil temperature was close to 10 °C.

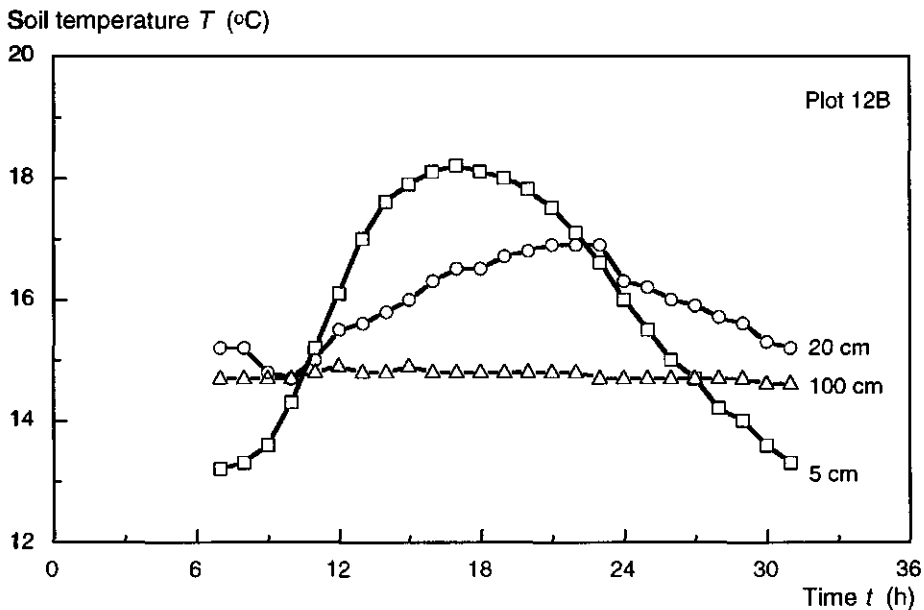


Figure 5.11 Diurnal variations in soil temperature under winter wheat on plot 12B from 7.00 h at 10 August ($t = 7$ h) till 7.00 h at 11 August 1986 ($t = 31$ h) at different depths.

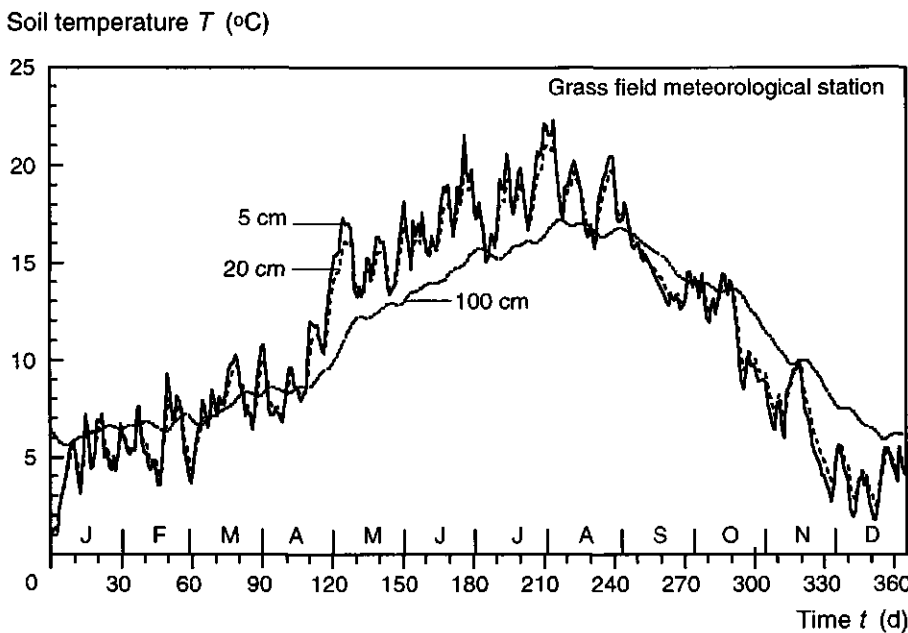


Figure 5.12 Daily averaged soil temperatures of the grass field of the meteorological station in 1990. Time t is the Julian day number; the corresponding months are indicated also.

5.5 Results of one-dimensional water balance simulations

Water balance

The water balance model SWATRE was used to simulate the field water balance of the Lovinkhoeve. The results for plot 17A in 1989 are shown as an example. In the first approach the analytical expressions of the soil hydraulic characteristics were used as input, and the measured groundwater level, the locally measured precipitation, and the potential evaporation data of the KNMI station Leeuwarden were used as boundary conditions. The development of the sugar beet is described by analogy with Feyen and Van Aelst (1983), using leaf area index (LAI) and root depth as parameters for the crop development. In the calculations a maximal root depth of 100 cm is used, after a period of 90 days of linear root growth following emergence.

Under wet conditions, when the groundwater level rises close to the soil surface, the execution of SWATRE failed due to the steepness of the water

5. Macroscopic soil physical processes

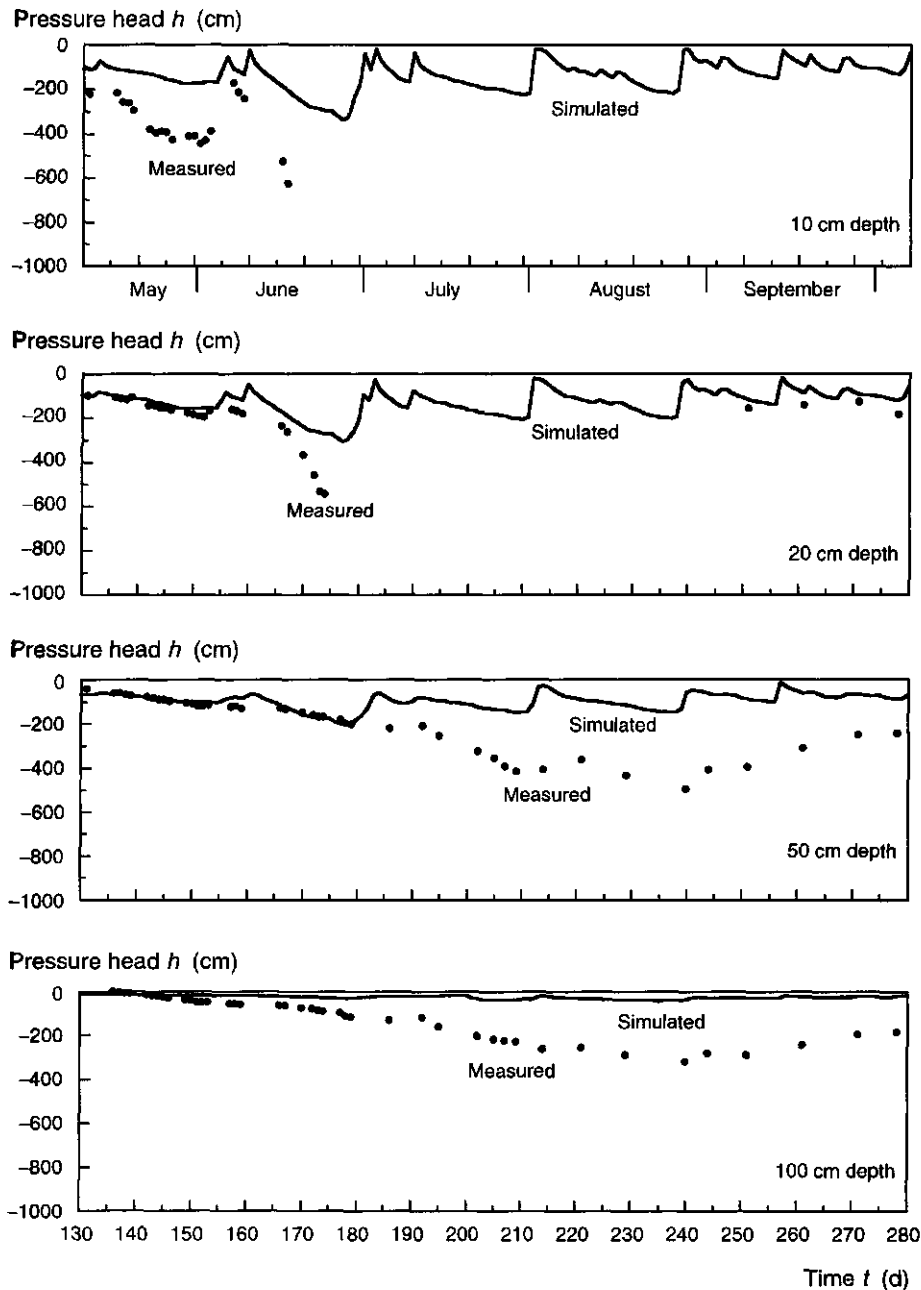


Figure 5.13 Initial results of the simulated pressure heads at four depths for plot 17A, compared with the measured pressure heads for a relevant period of the 1989 growing season. Time t is the Julian day number; the corresponding months are indicated also (top).

retention curve of the topsoil close to saturation, when using the analytical expressions. This phenomenon is also described by Vogel and Cislerova (1988). The problem was resolved by repeating the calculations using the tabulated analytical expressions. By using tabulated data, the water retention characteristic close to saturation became less steep than the analytical expressions. The differential water capacity remained at a value just above zero, which resulted in less severe numerical problems.

The simulated pressure heads were much larger than the measured pressure heads for all depths (Fig. 5.13). Especially the very high pressure heads that were simulated at 100 cm depth indicate that capillary rise in the subsoil is so large that the total soil profile is easily wetted. The simulated pressure heads showed near hydrostatic equilibrium with the groundwater level. Field measurements indicate that, e.g., in the period $150 < t < 157$ d, the pressure heads at 100 cm depth were much lower. The hydraulic head gradient between 50 and 100 cm depth in the field was $dH/dz = -0.26$ in this period. The measured pressure heads at 50 cm depth were $-122 < h < -108$ cm and at 100 cm depth $-60 < h < -44$ cm. The laboratory hydraulic conductivity characteristic is presented as a function of h in Fig. 5.14. If the lowest $h = -122$ cm at 50 cm depth is

Hydraulic conductivity K (cm d⁻¹)

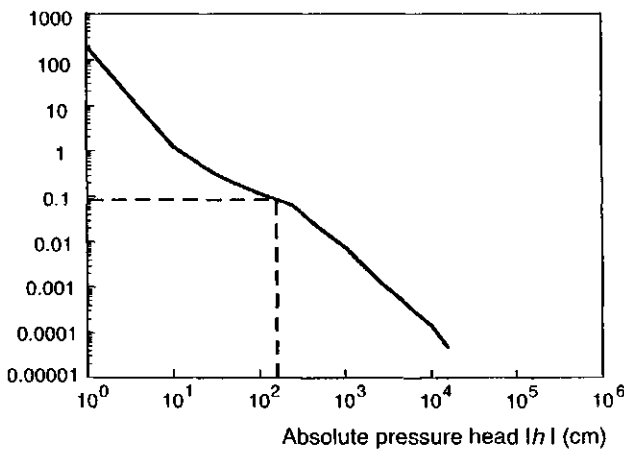


Figure 5.14 The laboratory hydraulic conductivity characteristic of the subsoil with dashed lines indicating values mentioned in the text. The pressure head (negative) is expressed by its absolute value $|h|$.

5. Macroscopic soil physical processes

Together with the observed hydraulic head gradient, this gives an upward flux of 0.23 mm d^{-1} in the subsoil. With actual evapotranspiration rates of $3-4 \text{ mm d}^{-1}$ assumed to correspond with the (minimal) relevant hydraulic conductivity between 50 and 100 cm depth, a hydraulic conductivity $K = 0.09 \text{ cm d}^{-1}$ is found. This results in drying out of the soil profile. This analysis indicates that the simulated pressure heads in the subsoil were too high, resulting in a too large capillary rise. The water holding capacity of the soil under field conditions can be smaller than the measured capacity after saturation under laboratory conditions. Under equal water extraction amounts, this will lead to lower water contents, and due to the smaller hydraulic conductivity, also to a lower capillary rise. The hydraulic conductivity of the subsoil was not measured at depths larger than 75 cm. Due to the unripened character of the soil at these depths the hydraulic conductivity may be smaller than the measured hydraulic characteristics for the subsoil. This could result in an even smaller upward flow at the measured hydraulic head gradient.

Reducing the water holding capacity of the soil by reducing the volumetric water content at saturation in the analytic expressions for the hydraulic characteristics, did not have a very positive effect on the simulation results. The capillary rise still kept the calculated pressure heads at 100 cm depth much too high. Only by reducing the hydraulic conductivity in the subsoil by a factor 10 and using the field water retention characteristic for the topsoil, the differences between simulated and measured pressure heads became much smaller (Fig. 5.15).

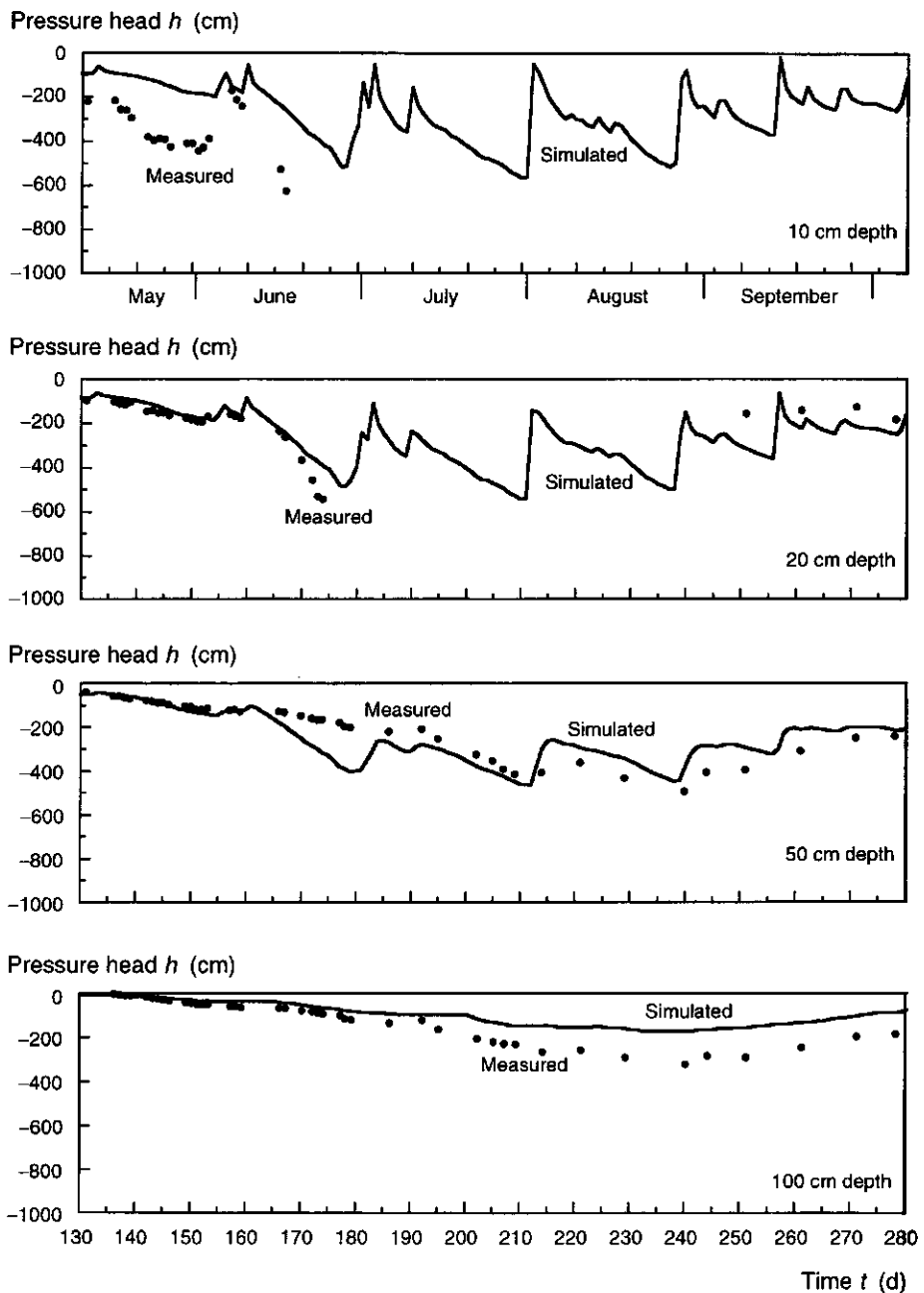


Figure 5.15 Final results of the simulated pressure heads at four depths for plot 17A, compared with the measured pressure heads for a relevant period of the 1989 growing season. Time t is the Julian day number; the corresponding months are indicated also (top).

Time-depth curves 1989

The time-depth curves of parcels of water (see Par. 2.1.5) presented in Fig. 5.16 are based on the simulations of the water balance using SWATRE for plot 17A for the entire year 1989. At $t = 0$ d, the starting positions of the time-depth curves are calculated as a function of depth. In between two time-depth curves, a parcel of water is located with an initial total water content of 7.5 cm. The positions of the parcels of water can be followed in the course of time. In the wet period $0 < t < 100$ d all parcels move downwards as a result of the precipitation excess. High precipitation rates caused the occasional rise of the groundwater level. At $t = 114$ d the sugar beet crop emerged, and for $t > 114$ d water extraction in the root zone took place. The uptake can be noticed in Fig. 5.16; the depletion of the parcels of water caused the time-depth curves to come closer together in the root zone. For $137 < t < 230$ d the parcels move upwards from the subsoil. Capillary rise occurred in this period, accompanied by a slow drop of the groundwater level. For $t > 270$ d the infiltration at the soil surface caused the parcels to move downwards again.

The time-depth curves represent the flow of water or the transport of solutes by convection without dispersion. For example, the parcel of water which was at $t = 0$ d located just below the soil surface moved down to 50 cm depth. Then the roots reached that depth and started extracting water from that parcel. Finally at $t = 365$ d the parcel reached 70 cm depth. So, over one year the displacement of the parcel was 70 cm downwards. If for example nitrate was applied at the soil surface at $t = 0$ d, the nitrate was available for the crop in the period $150 < t < 290$ d. Even a parcel that was located at a depth of 90 cm at $t = 0$ d, reached the root zone after a period of capillary rise. Due to the larger volumetric water contents associated with the larger porosity, yearly net downward movement of the parcels of water in the subsoil is much less than that in the topsoil.

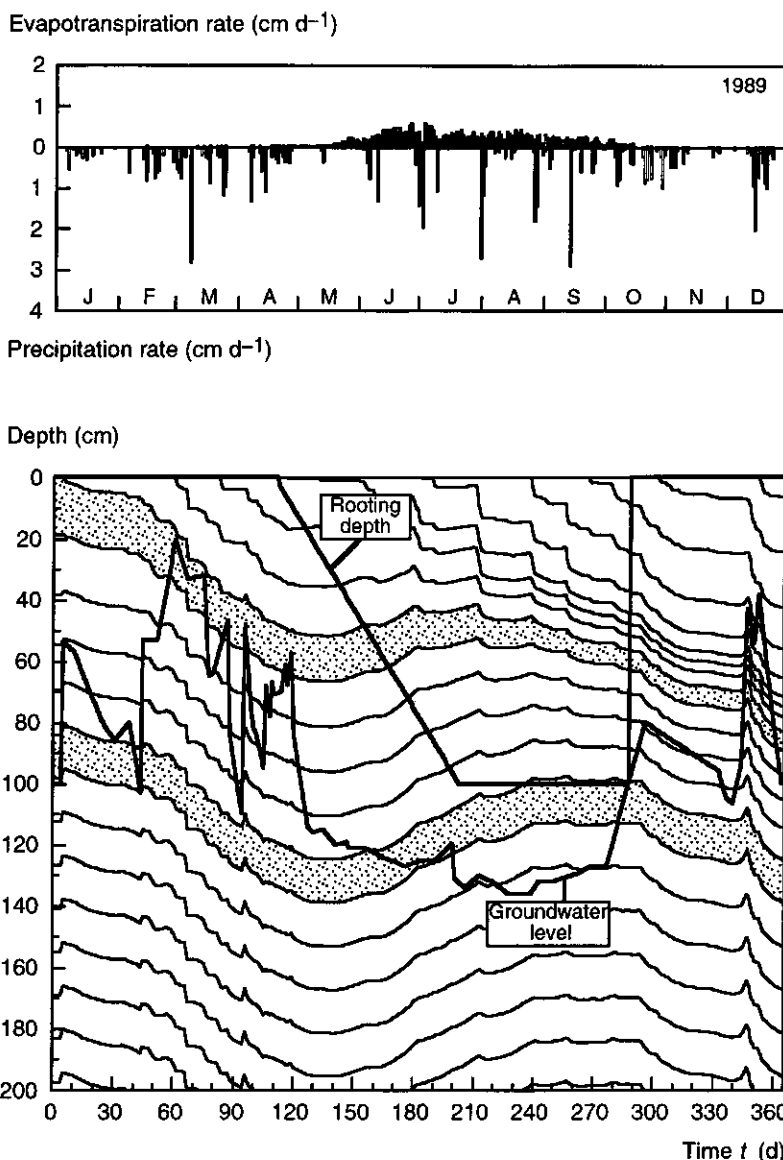


Figure 5.16 Time-depth curves (bottom) based on water balance simulations by SWATRE for the year 1989, representing the movement of parcels of water in the course of time. The dashed areas between two lines represent specific parcels of water. Rooting depth and groundwater level are indicated. The actual evapotranspiration rate and precipitation rate are given in the top figure. Time t is the Julian day number; the corresponding months are indicated also (top).

5.6 Discussion

Soil physical characteristics

The topsoil has the most ripened character, and shows the annual effects of soil tillage. The topsoil has the highest bulk density, which is reflected in the relatively low porosity. The deeper soil layers have lower bulk densities, and associated larger porosities. There is a large variability in the bulk density data.

The largest differences in hydraulic characteristics do not occur among the different plots, but among the different soil layers in the same plot (Chapter 4). Comparison of the different plots shows that only the topsoil of the "ley" plot stands out as a result of its higher organic matter content. This plot has a lower bulk density and a larger water holding capacity. However, the quantification and evaluation of the effects of the differences in hydraulic properties requires computations based on a water balance model.

The order of magnitude of the difference between the hydraulic conductivity at saturation compared to the hydraulic conductivity at slightly lower pressure heads is caused by the different pores that are involved in the flow of water. At saturation, the hydraulic conductivity is determined mainly by flow in a few macro-pores, in the form of cracks, worm holes or channels left behind by decayed roots, through which the main part of the flow occurs. Above the phreatic surface, such macro-pores will contribute only after heavy rainfall, when free water is present at the soil surface.

The differences between the laboratory water retention characteristics and field water retention characteristics may have important implications for the air contents, especially in the topsoil under wet conditions. At the same pressure head, the field water retention characteristic indicates lower volumetric water contents and thus larger volumetric air contents, as compared to the laboratory water retention characteristic. Fig. 5.17 shows the difference by indicating the volumetric water contents corresponding to the laboratory water retention characteristics and the field water retention characteristics. The volumetric air contents can be inferred from the difference between the porosity (≈ 0.445 in Fig. 5.17) and the actual water content at a given pressure head. Clearly, for the interpretation of field conditions the field water retention characteristic should be used. This conclusion is consistent with the study of Diels (1994), who concluded that field water retention characteristics should be used to model water flow for a field.

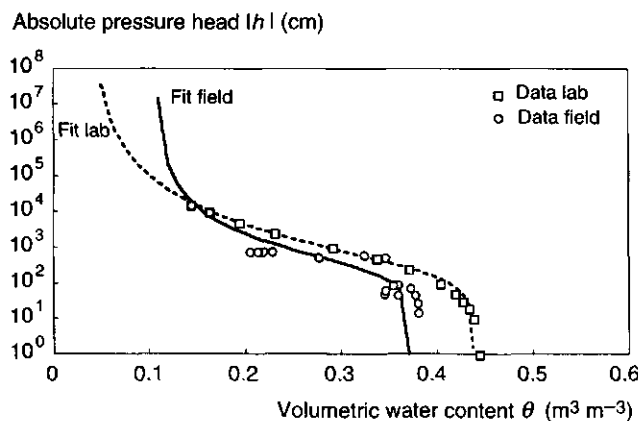


Figure 5.17 Analytical description of the field water retention curve and the laboratory water retention curve. The symbols indicate the measured values. The pressure head (negative) is expressed by its absolute value $|h|$.

Soil physical conditions

The measured pressure heads give direct information on the soil water status of the different plots over the different years. This information is of direct relevance to soil ecologists. The effects of precipitation and water extraction by the crops can be easily identified. The space-time pattern of the pressure head was comparable for all plots, except for the plots with an integrated treatment with minimum tillage. The pressure heads were more negative in the topsoil of these plots than on the other plots. In the minimum tillage plots, the dense soil might impair penetration of plant roots, resulting in a large fraction of the roots being present in the topsoil (0-25 cm depth) and fewer roots penetrating the deeper layers. Together with the better development of undercrops and weeds on these plots, this may explain the rapid drying of the topsoil. Comparing the results for different plots, it appears that the differences in crop development are more important than the differences in soil hydraulic properties.

Variability in water uptake by plant roots, in soil hydraulic properties, and in infiltration and evaporation may cause variability in pressure heads. Under wet conditions relatively larger hydraulic conductivities favour smaller differences in pressure head than under drier conditions. This holds also for the topsoil, without the direct influence of the groundwater level.

During wet periods, soil physical conditions vary systematically and widely

5. Macroscopic soil physical processes

within plots. If the groundwater level rises above the drain depth, lateral flow of groundwater to the drains will occur and a curved phreatic surface will be present, resulting in differences in the corresponding pressure heads close to the groundwater level. The flow of water in the saturated and unsaturated zones is then no longer one-dimensional. Positions in the middle between two drains then become wettest, and positions close to the drain remain relatively dry. These differences are likely to be critical for the probability of occurrence of denitrification.

Water balance simulations

The water balance model SWATRE did not simulate the field water balance accurately. In particular, a discrepancy between measured and simulated pressure heads was found. Even after reducing the hydraulic conductivity for the subsoil by a factor ten, thus reducing the capillary rise, the measured pressure heads still remained more negative than simulated pressure heads.

The calculations were based on the average hydraulic characteristics. A large variation in those characteristics was observed (Par. 4.2). A sensitivity analysis of the model could delineate the effect of this variation on the calculated pressure heads. However, it is not likely that a general sensitivity analysis is useful, because the high capillary rise is too dominant. A more precise determination of the soil hydraulic characteristics for the different soil layers of the subsoil (> 50 cm depth), especially in the important pressure head range $-200 < h < 0$ cm, could help to quantify the capillary rise more precisely.

The root distribution was measured by Van Noordwijk *et al.* (1994). A high root length density in the topsoil was observed, and at larger depths the densities decreased. In principle it is possible to use these densities in a water balance model, and to distribute the water uptake over the root zone, depending on spatial distributions of root length densities and pressure heads (De Willigen, 1990; Heinen, 1997). It is likely that a better description of the water uptake by the roots is as important as an appropriate description of the soil physical characteristics for accurate dynamical water flow simulations.

Time-depth curves

The time-depth curves are based on the final simulations of the water balance model. These simulations were not yet accurate. This of course influences the reliability of the time-depth curves. However, the time-depth curves

are mainly influenced by the water retention characteristic of the soil, and less by the hydraulic conductivity characteristic. It has been pointed out earlier that the measurements of the water retention characteristics are much more reliable than those of the hydraulic conductivity characteristics. Although the details of the water balance were not simulated accurately, the water balance considered over longer periods can be expected to be more accurate. At least qualitatively the time-depth curves give a good impression of the flow of water and the convective transport of solutes. Under conditions with a shallow phreatic surface, a two-dimensional flow pattern to a drain will occur. Then the one-dimensional piston flow used in calculating the time-depth curves is no longer realistic.

5.7 Evaluation of the soil ecology study of arable farming systems

The role of soil physical processes in relation to the soil biological results of the Dutch Programme on Soil Ecology of Arable Farming Systems (Brussaard *et al.*, 1994) is discussed in this section. For the soil at the Lovinkhoeve, an overview is given of the most important biological processes, and measured field N balances are summarised. The soil biological studies focused on the top 25 cm of the soil, because this is the zone with the highest biological activity. Inputs of organic matter occur mainly in this part of the soil. During the growing season, the abiotic conditions in the topsoil, like soil temperature and aeration, are generally favourable for most soil organisms. The habitat of the soil organisms is determined by the soil structure and the physical, chemical and biochemical processes within this structure. Some characteristic results of studies on soil structure will be discussed first.

5.7.1 Soil structure

Soil structure formation processes

Soil structure can be defined as the size and spatial distribution of particles in the soil. Soil structure changes in the course of time. Root growth and activity of soil organisms affect soil structure. Soil tillage and soil traffic are human activities which can change the soil structure drastically. After soil tillage, which is

5. Macroscopic soil physical processes

meant to create a favourable soil structure for crop growth, the change in soil structure continues due to the consolidation of the soil driven by atmospheric conditions and due to biological activity. Boersma and Kooistra (1994) measured and described the soil structure resulting from various agricultural management practices. Their results were mainly based on measurements in spring in different years. The larger biological activity in integrated plots compared to conventional plots corresponded to a larger percentage of the soil structure which was formed by soil organisms, with primary biological voids forming about 5% of the total macro-porosity ($> 20 \mu\text{m}$). Although the influence of soil organisms on soil structure could be detected, no interpretation of the impact of groups of organisms on soil structure could be given yet. Schoonderbeek and Schouthe (1994) found the loosest soil structure in the 10-20 cm depth layer. In the conventional system this layer had horizontal cracks, indicating compaction of the soil during harvest and tillage traffic, while for the integrated system the 18-26 cm depth layer had high numbers of vughs (cavities), probably due to biological activity.

Marinissen (1994) showed that earthworm activity increased the stability of soil aggregates in the 0-5 cm depth layer. Smaller aggregates (0.3-1 mm) were more stable than larger aggregates (4.8-8 mm). Earthworm populations ranged between 0-650 individuals per m^2 , with peaks occurring in spring and autumn. Earthworms are only present at a part of the Lovinkhoeve due to the colonisation pattern in this young soil. Effects of soil tillage, especially the inversion of the topsoil, work out differently for various earthworm species. When root crops are grown, such as potato and sugar beet requiring heavy traffic often under wet conditions, soil tillage remains necessary to manage the soil structure.

Soil structure and land qualities

Boersma and Kooistra (1994) qualified the soil structure as "good" in an old minimum tillage system, and the soil structure in the integrated system was "better" than in the conventional system. These qualitative interpretations are believed to say something about the agronomical experience with soil structure in relation to crop production. However, trying to relate soil structure to soil processes remains a difficult task.

Water retention and hydraulic conductivity characteristics were determined (De Vos *et al.*, 1994; Vos and Kooistra, 1994; Pars. 4.2.1 and 4.2.2, this thesis) and for the topsoil differences could be measured between the integrated field

with a high organic matter content (plot 16A), the conventional field with a low organic matter content (plot 12B), an old pasture (plot 20A), and a new and old minimum tillage system. Vos and Kooistra (1994) compared land qualities for the different systems, based on water balance and crop growth simulations for a 30 year period with varying meteorological conditions. The land qualities considered were the number of workable days in spring and autumn, the air-filled porosity in the 0-10 cm depth layer and crop production (Van Lanen *et al.*, 1987). Old pasture land and the old minimum tillage system had the most favourable soil physical properties for growing crops, and the conventional and integrated systems had the least favourable properties.

Discussion

Soil structure, the habitat of soil organisms, has been described in great detail (Boersma and Kooistra, 1994) and the influence of different soil organisms could be distinguished. Although the land qualities approach is a tool to interpret differences in soil structure, expressing the probabilities of occurrence of soil conditions, some critical remarks should be made. The soil physical characteristics for each system exhibit a large variation, especially the hydraulic conductivity characteristics. These characteristics were determined on samples taken in spring from undisturbed soil. For the 0-5 cm depth layer it is impossible to measure the macroscopic soil physical characteristics, because the soil is too loose to take samples. In the simulations for the number of workable days, pressure heads in the 0-10 cm depth layer were used. The conditions in the topsoil are important for the defined land qualities, especially the conditions in wet situations. Comparison of measured pressure heads and simulations with SWATRE (De Vos *et al.*, 1994; Par. 5.5, this thesis), showed that the simulated pressure heads were too high, which corresponds with too high water contents. Under wet conditions, the two-dimensional water flow in soil has a great impact on the distribution of water in the topsoil as a function of the distance to the drain. So, use of the one-dimensional SWATRE model is not justified for estimating land qualities. The role of nitrogen and the actual root distribution are not discussed by Vos and Kooistra (1994), and probably they assumed a sufficient nitrogen supply for the crop, and ignored the consequences of the water balance for denitrification. Due to all uncertainties, especially under wet conditions in the topsoil, the results concerning land qualities must be interpreted as an exercise

indicating the importance of the soil physical characteristics for conditions in the soil, rather than a simulation of the potential field conditions.

The role of soil structure becomes even more important when the N balance is studied. After ploughing, organic matter is distributed in the topsoil and due to biological activity, redistribution and decomposition of organic matter can take place. Hassink (1992) and Matus (1994) argue that the location of organic matter within aggregates results in a physical protection of the organic matter against biological transformations, and thus affects the mineralisation rate. Nitrate present in the soil can be denitrified under anoxic conditions when enough organic food is available for the micro-organisms. These types of processes occur at the aggregate scale (mm-cm). Rappoldt (1992) showed that in a structured soil the occurrence of anoxic conditions in the soil matrix depends on the distance from cracks or channels, which are assumed to have atmospheric oxygen (O_2) contents, O_2 diffusion in the soil matrix, and the location and activity of soil organisms. The water balance of the soil will have a great impact on O_2 transport because macroscopic water contents determine the O_2 diffusion coefficient in the soil matrix. The link between the input of organic matter and the effect of soil structure on water and O_2 transport processes has to be studied in more detail. Single values of 12% gas-filled pore space at $h = -100$ cm (Lebbink *et al.*, 1994) or 9% air content (Vos and Kooistra, 1994) as threshold values are too much a simplification of the soil physical processes influencing N dynamics.

5.7.2 Nitrogen mineralisation

The role of micro-organisms and microbivores

Bloem *et al.* (1994) studied the dynamics of micro-organisms and microbivores and its effect on N mineralisation in a winter wheat field (1989-1990) under a conventional and under an integrated management system. The bacterial biomass was about 100 times larger than the fungal biomass in both systems. So, the decomposition of organic matter is dominated by bacteria. The decomposed organic matter is partly used for the production of microbial biomass (growth) and the rest is mineralised to CO_2 , H_2O , mineral N and other nutrients. Depending on the C/N ratio of the decomposing organic matter and the C/N ratio of the bacteria, N mineralisation or N immobilisation can occur when the bacteria population grows; but when the C/N ratio of the decomposing

organic matter is larger than 15 it is assumed that N immobilisation occurs. The bacteria can be grazed upon by bacterivores, predominantly nematodes and protozoans at the Lovinkhoeve. Their C/N ratio is similar to that of the bacteria, but due to a growth efficiency of about 50%, a substantial part of the predated bacteria is excreted, leading to an excess of NH_4 , which will be rapidly biologically transformed to NO_3 (De Ruiter *et al.*, 1993). Bloem *et al.* (1994) measured the biomass of the bacterivores and the activity of bacteria in the field plots at time intervals, ranging from 1 week to 6 weeks, and performed multiple regression analysis to distinguish between different factors influencing N mineralisation, including the effect of soil temperatures and volumetric water contents in the two layers, 0-10 cm and 10-25 cm depth.

Although the bacterial biomasses were similar in the conventional and integrated plots, the biomasses of other organisms were larger in the integrated system. Also the biological activity seemed to be higher, as was indicated by the larger potential O_2 consumption rates measured in laboratory incubation of the soil from the plots. Also the net mineralisation in the topsoil (0-25 cm depth) over the growing season was 30% larger in the integrated plot (101 kg N ha^{-1}) than in the conventional plot (78 kg N ha^{-1}). This difference must be due to the 30% higher organic matter content, but also to more favourable soil physical conditions. The 0-10 cm depth layer had a larger biomass and activity than the 10-25 cm depth layer in the integrated plot. This might also have been due to the higher organic matter content. Although soil temperature and soil water content are important abiotic conditions influencing microbial activity, in this study it was found that these conditions did not influence bacterial growth significantly.

The role of bacterivorous protozoans and nematodes

Bouwman and Zwart (1994) studied the role of bacterivorous protozoans and nematodes, considering the soil water content as an important factor. For the 0-25 cm depth layer the biomasses of bacteria, protozoans and bacterivorous nematodes averaged over the years 1986-1990 and the management systems were 236, 11 and 0.6 kg C ha^{-1} , respectively. For the year 1990, the annual productions in the same layer calculated for the conventional and integrated system were 660 and $930 \text{ kg C ha}^{-1} \text{ yr}^{-1}$ for bacteria, 73 and $142 \text{ kg C ha}^{-1} \text{ yr}^{-1}$ for protozoans and 11.5 and $11.8 \text{ kg C ha}^{-1} \text{ yr}^{-1}$ for nematodes, respectively. These results show the high turnover rates of the protozoans and bacterivorous

5. Macroscopic soil physical processes

nematodes, which are responsible for about 30% of the N mineralisation in these soils.

Protozoans and nematodes are aquatic animals. They move and feed in the waterfilm around soil particles. Depending on the species, different modes of movement and feeding are distinguished. Nematodes start to loose water at relative air humidities below 99.7%, which corresponds to a pressure head of $h < -4000$ cm. Under slowly developing dry conditions protozoans and nematodes can survive by transition into a survival stage, encysting or becoming dormant. The effect of water contents on the growth of protozoans and nematodes was studied in laboratory experiments by Bouwman and Zwart (1994). In these experiments with undisturbed Lovinkhoeve soil, different nematode species reacted differently to pressure heads of -31, -100 and -310 cm. The numbers of some species were reduced at a pressure head of -310 cm, which was qualified as "dry", while the numbers of other species showed no significant change.

Lovinkhoeve food web model

De Ruiter *et al.* (1994) used a food web model to describe the interrelations of soil organisms. The food web is based on population size and C dynamics, which can be expressed in terms of $\text{kg C ha}^{-1} \text{ yr}^{-1}$. Within taxonomic units, species were aggregated into functional groups, which were defined according to their principal food source (De Ruiter *et al.*, 1993). Using C/N ratios, energy conversion efficiencies and specific death rates for the different functional groups, N dynamics can be inferred. Inputs for the food web model are the measured biomasses of functional groups and experimental and literature data on their energy conversion efficiencies and specific death rates. Detritus with a constant C/N ratio of 10 or 12 was chosen as substrate. This C/N ratio is the most critical input parameter, together with the C/N ratios and specific death rates of the bacteria and protozoans. The high sensitivity of the model results to those values appeared from a sensitivity analysis, indicating that the fauna mineralised 90% of the nitrogen when the C/N ratios are 12 and 4 for detritus and bacteria, respectively, and 30% when the C/N ratios are 10 and 4 for detritus and bacteria (De Ruiter *et al.*, 1993). The fit between simulated and observed annual averaged N mineralisation rate was best for C/N ratios of 10 and 5 for detritus and bacteria, respectively. The dynamics was best simulated with C/N ratios of 12 and 4 for detritus and bacteria, respectively.

Discussion

Soil physical and meteorological conditions were monitored and used for the interpretation of soil biological results. The statistical analysis of Bloem *et al.* (1994) used average soil temperatures for 6-week periods and volumetric water contents measured at the sampling dates. The use of these water contents is problematic. During a 6-week period extreme changes in volumetric water contents can occur, which can be inferred from the measured pressured heads in Fig. 5.7. Reaction times of soil organisms related to these changes will be in the order of days. The changes in water content could dominate the behaviour of soil organisms in the 6-week period, but they are missed by using only water contents at the sampling times.

The food web model predicted trends in mineralisation well, based on the biomass measurements of functional groups. In the model, soil temperature influenced the specific death rates, but soil water content was not taken into account. All information about the porous soil structure in which the soil biological interactions occur, are indirectly incorporated into the different coefficients for the functional groups. Soil is not explicitly taken into account as a spatial continuum.

Soil biological models and organic matter models often use time steps of weeks. With these large time steps it is difficult to take the dynamic soil physical processes into account. The spatial scale of processes can differ from the field scale for a process such as leaching to the pore scale for biological processes. In the Dutch Programme on Soil Ecology of Arable Farming Systems not much attention is given to theoretical problems arising from considering processes at different scales (Moene, 1992; Hofstee, 1993). In some models the spatial scale is not evident at all because the influence of the scale is hidden in specific rate coefficients.

5.7.3 Nitrogen balance

Van Faassen and Lebbink (1994) studied the organic matter and N dynamics in the conventional and integrated systems at the Lovinkhoeve. In the comparison between the conventional (CONV) and integrated (INT) system the organic matter content in the 0-25 cm depth layer played an important role. Plots

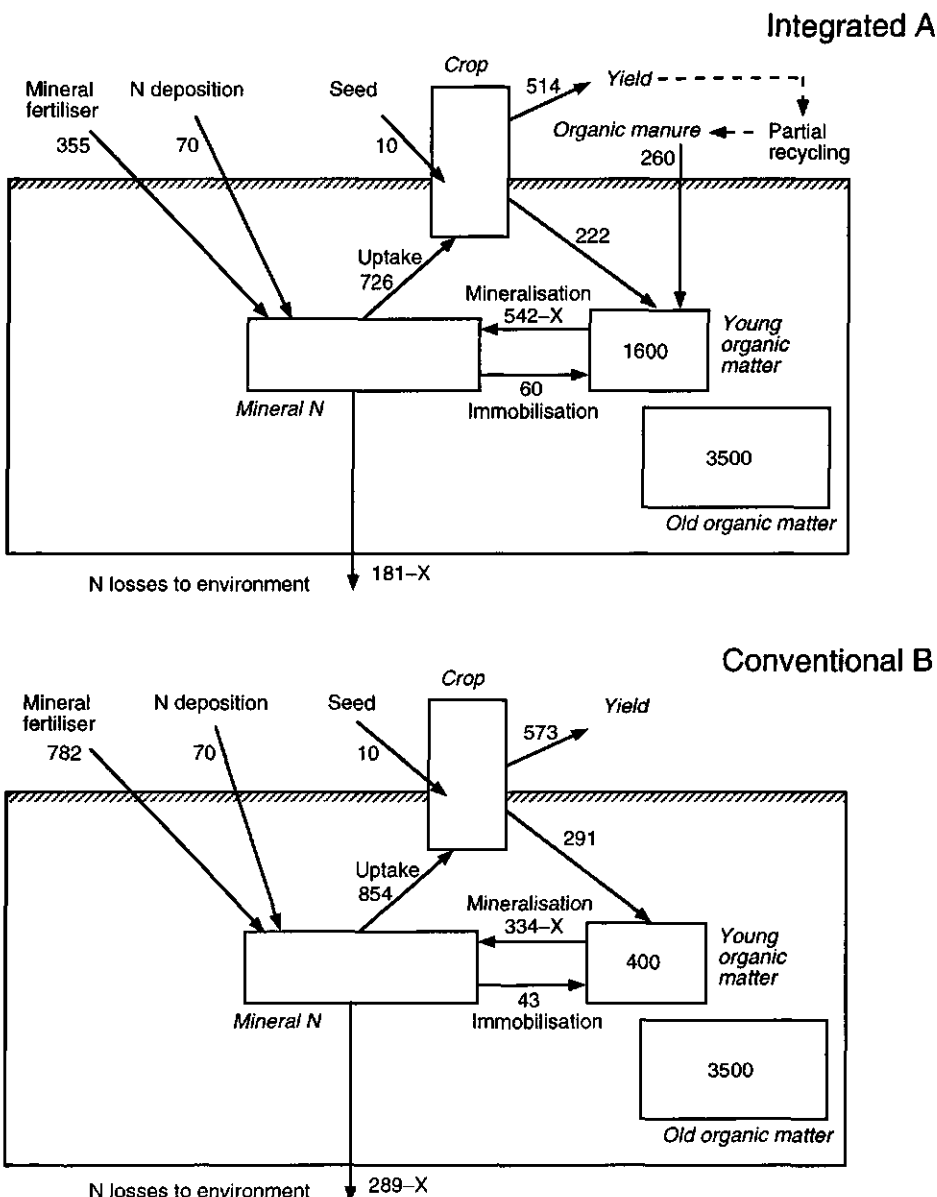


Figure 5.18 The N balance for a 4-year crop rotation (1988-1991) for a conventional (Conventional B) and an integrated (Integrated A) arable farming system for the 0-60 cm soil layer (after Van Faassen and Lebbink, 1994). The young and old organic matter pools are given for the 0-25 cm soil layer. The factor X indicates an uncertainty term in mineralisation from the young organic matter pool, which results in an uncertainty in the estimated N losses.

at block A (Fig. 4.8) had initially (1985) a high organic matter content of 2.8% (CONVA and INTA), and block B had a lower organic matter content of 2.2% (CONVB and INTB). Because the organic matter input in the integrated system was larger, due to the application of compost and processed animal manure, at INTA the high organic matter content was maintained, while it increased on INTB. Only mineral fertiliser was applied on the conventional plots and consequently the initially high organic matter content decreased on CONVA and the low organic matter content was conserved on CONVB. It is difficult to calculate accurate N balances for the plots with a changing organic matter pool containing large amounts of organic N, for example about $3500 \text{ kg N ha}^{-1}$ in old organic matter in the 0-25 cm depth layer. Because the changes in organic matter were small in CONVB and INTA, their N balances can be considered to get an idea of the magnitude of the various components of the N balance. The N balance is made over the 0-60 cm depth soil layer (Fig. 5.18), assuming that the N content in the young organic matter pool is constant ($X = 0$ in Fig. 5.18). For a 4-year crop period CONVB had an input of 792 kg N ha^{-1} of mineral fertiliser, 70 kg N ha^{-1} atmospheric deposition, and an output of 573 kg N ha^{-1} in harvested products, resulting in a loss of 289 kg N ha^{-1} . INTA had an input of 465 kg N ha^{-1} of mineral fertiliser, 260 kg N ha^{-1} organic fertiliser, 70 kg N ha^{-1} atmospheric deposition, and an output of 514 kg N ha^{-1} in harvested products, resulting in a loss of 181 kg N ha^{-1} . At INTA part of the harvested products were returned to the soil and this amount is included in the 260 kg N ha^{-1} organic fertiliser.

Model calculations of C and N dynamics (Van Faassen and Lebbink, 1994) are based on a subdivision of organic matter into pools with different C/N ratios, using first-order, temperature-dependent rate constants for the biological transformations. Soil water contents are not taken into account. Simulation results were used to understand the C and N dynamics and to calculate the size of the different pools (Fig. 5.18), using field data as inputs.

Integrated crop yield was on average 90% of the conventional crop yield. The lowest N losses are expected in the integrated system, especially for winter wheat and spring barley. The highest risks of N losses are expected from potato and sugar beet, due to high soil NO_3^- contents that are present in spring, and denitrification can easily occur because soil temperatures are high enough and there may be wet situations. After the harvest of potatoes, there is a high risk of leaching in the following winter period. The presence of a green manure crop or stimulation of N immobilisation by the incorporation of decomposable organic

5. Macroscopic soil physical processes

matter with a high C/N ratio could reduce NO_3 leaching.

Discussion

The N balance simulations give a good overview of the different pools and flows of N, and indicate high N losses to the atmosphere and to the groundwater. Nitrate leaching and denitrification are important terms in the N balance, and these losses were not quantified directly in the field in the Dutch Programme on Soil Ecology of Arable Farming Systems, whereas these losses are crucial in comparing a conventional and integrated system.

5.8 Conclusions

Soil physical research

Soil physical research in The Dutch Programme on Soil Ecology of Arable Farming Systems focused on the characterisation of the soil physical environment with respect to soil biological processes in conventional and integrated arable farming systems. A hypothesis was that arable farming systems with a different organic matter input and soil tillage depth, would result in different soil physical characteristics in the topsoil of the corresponding fields. It was difficult to find substantial differences between the soil hydraulic characteristics of the fields. The uncertainty and variability in the results were large. Differences in the hydraulic characteristics of the different soil layers were more pronounced than between the topsoils of the different fields. A direct measurement of the soil physical field conditions in the course of time was a more successful approach to detect differences between fields.

The average bulk densities over the 1986-1990 period for different plots were 1345, 1395, 1400 kg m^{-3} , as a result of the historical differences in organic matter contents of 2.8, 2.3 and 2.2%, respectively.

The time-scale of the fluctuations in pressure heads was in the order of days in all growing seasons, except after heavy rainfall when the pressure heads in the topsoil reacted more quickly. Especially the plot with minimum tillage showed lower pressure heads in the topsoil and larger pressure heads in the subsoil than the other plots. Crop development and the water uptake pattern by the roots dominated the differences in pressure heads between the fields.

Measurements of soil temperature showed the diurnal fluctuation in temperature in the topsoil (0-30 cm depth) and the yearly fluctuations at all depths around an average soil temperature of about 10 °C.

The curved phreatic surface caused spatial patterns in pressure heads, water contents and air contents in the unsaturated zone, which can have consequences for the spatial pattern of denitrification. The field water retention characteristic has to be used when field air contents have to be inferred from measured pressure heads.

An attempt to simulate the Lovinkhoeve field water balance using a one-dimensional model resulted in too large simulated pressure heads. The hydraulic conductivity characteristic of the subsoil had a substantial impact on the water balance and strongly influenced the soil physical conditions in the topsoil. Using the field water retention characteristic for the topsoil improved the simulations, but even then large differences between simulations and measurements remained.

The Dutch Programme on Soil Ecology of Arable Farming Systems

The description of soil structure and soil structure formation processes indicated differences between the arable farming systems, due to biological activity and soil tillage. However, it remained hard to relate the measured quantities to field-scale processes like water flow and oxygen transport. Especially in a biologically oriented project more emphasis on oxygen transport related to biological activity might have been expected.

N mineralisation is dominated by bacteria decomposing organic matter and bacterivorous protozoans and nematodes predating the bacteria. Bacterial growth was never limited by low soil water contents. However, the number of some nematode species decreased at a pressure head $h = -300$ cm.

Net mineralisation in the topsoil (0-25 cm depth) was estimated to be 101 kg N $ha^{-1} yr^{-1}$ in an integrated plot and 78 kg N $ha^{-1} yr^{-1}$ in a conventional plot. The larger mineralisation in the integrated plot than in the conventional plot is a result of the higher organic matter input and the higher biological activity.

The Lovinkhoeve food web model interrelates different functional groups of soil organisms. Simulated N mineralisation for an integrated and a conventional plot compared well with the field measurements. However, soil structure and changing soil physical conditions were not yet explicitly taken into account.

The N balances for an integrated and conventional plots indicated yearly

5. Macroscopic soil physical processes

averaged N losses of 45 and 72 kg N ha⁻¹ yr⁻¹, respectively. However, these estimates based on the calculation of N losses as the rest term of the overall field N mass balance, and are not accurate because a small change in the organic matter pool of the soil has a major impact on the estimated N losses. No discrimination is made between nitrate leaching and denitrification.

In the Dutch Programme on Soil Ecology of Arable Farming Systems much emphasis was placed on soil biological research, resulting in a relatively limited soil physical research effort. Although the monitoring of the water balance was detailed, water balance simulations were not yet accurate. More attention should have been given to processes like solute transport, in particular NO₃ leaching, and O₂ transport related to denitrification. It is necessary to quantify NO₃ leaching by direct measurements, because the calculation of NO₃ leaching as the rest term of the overall field N mass balance is not accurate and does not yield information on the dynamics of the leaching process. A two-dimensional model for water flow and nutrient transport has to be used to describe the field scale transport processes at the Lovinkhoeve. These conclusions are the starting point for the research focusing on NO₃ leaching and denitrification presented in the following chapters.

6. FIELD DATA ON WATER FLOW AND ON NITRATE, CHLORIDE AND BROMIDE TRANSPORT TO A SUBSURFACE DRAIN

6.1 Introduction

Leaching of NO_3 from the root zone to the subsoil, groundwater, or surface water is a problem in high-input agriculture (Strebel *et al.*, 1989). Nitrate concentrations in these environmental compartments often exceed criteria set by the European Union (EU, 1991). The nitrogen cycle in general and NO_3 leaching in particular have been studied frequently in past years, using both field experiments and numerical models (e.g., Cannell *et al.*, 1984, Harris *et al.*, 1984; Addiscott and Powlson, 1992). In many field experiments it was difficult to quantify NO_3 leaching. One problem was the large spatial variability of NO_3 concentrations measured in soil, soil solution, or groundwater samples (Addiscott *et al.*, 1991). This variability made it difficult to draw conclusions for an entire field (Roth *et al.*, 1990).

In a recent project, carbon and nitrogen transformations were studied in arable farming systems at the Lovinkhoeve (Brussaard *et al.*, 1988; Brussaard, 1994; Chapter 5 of this thesis). An integrated system with a reduced mineral N fertiliser input appeared to be a farming system with relatively low NO_3 losses to the environment (Van Faassen and Lebbink, 1994). Nitrate leaching was, however, not measured.

This earlier research yielded indications that the peat layer at about 120 cm depth at the Lovinkhoeve (Fig. 4.2), with a low hydraulic conductivity (Fig. 4.16), could result in a small water flow as well as solute transport to and from the deeper subsoil. Most water and solutes discharging from a drain then originate from the 0-120 cm depth soil layer of the catchment area of a drain. This circumstance will be used to estimate N leaching by measuring N discharge from a drain. Thus, a spatially integrated value for a catchment can be found, which circumvents the problem of spatial variability encountered by other techniques to quantify N leaching from a field.

Field data on water flow and on solute transport are presented and discussed in this chapter. After a general introduction and a description of the field experiment, field data on nitrate and chloride transport over the leaching period 1991-1992 are presented and analysed in detail. Data on chloride

concentrations in the drainage water and in the soil profile are presented and compared with the data on NO_3 . The chloride mass balance is made for the period 1942-1991. The interpretation of the different terms of this mass balance will be used to evaluate whether upward seepage occurred. Next, an overview is given for the entire field monitoring period 1991-1996, with emphasis on the overall N balance and NO_3 leaching. Simultaneous measurements of hydrological conditions and soil oxygen contents were carried out in 1994. The consequences of spatial patterns in these conditions for denitrification are evaluated, and possibilities of water and nutrient management strategies based on this information will be discussed. Finally, the results of a bromide tracer experiment, conducted in the period 1994-1995, will be discussed.

6.2 Description of the drainage experiments

Experimental plots

An integrated arable farming plot (Fig. 4.8) with reduced mineral N inputs was monitored from December 1991 onwards. The layout of the experimental plot has already been given in Par. 4.1.3 and the functioning of the drain sampling device in Par. 3.1.3.

Soil physical field measurements

For monitoring the soil physical conditions, tensiometers, groundwater tubes, and piezometers were installed in the field (see Par. 3.1.1). The locations in the field were chosen on the basis of variations in soil physical conditions as a function of the distance from the drain and the change in drain depth over the length of the field. These considerations resulted in a subdivision of the field into blocks with different distances to the drain (Fig. 6.1). To check whether there was a symmetric flow field around the drain, instruments were placed at both sides of the drain. Pressure heads, groundwater levels and hydraulic heads were measured twice a week at location II and once a week at locations I and III (Fig. 6.1). The groundwater level was also measured automatically every 15 minutes midway between the experimental drain and the adjacent drain (Fig. 6.1).

6. Field data on water flow and solute transport

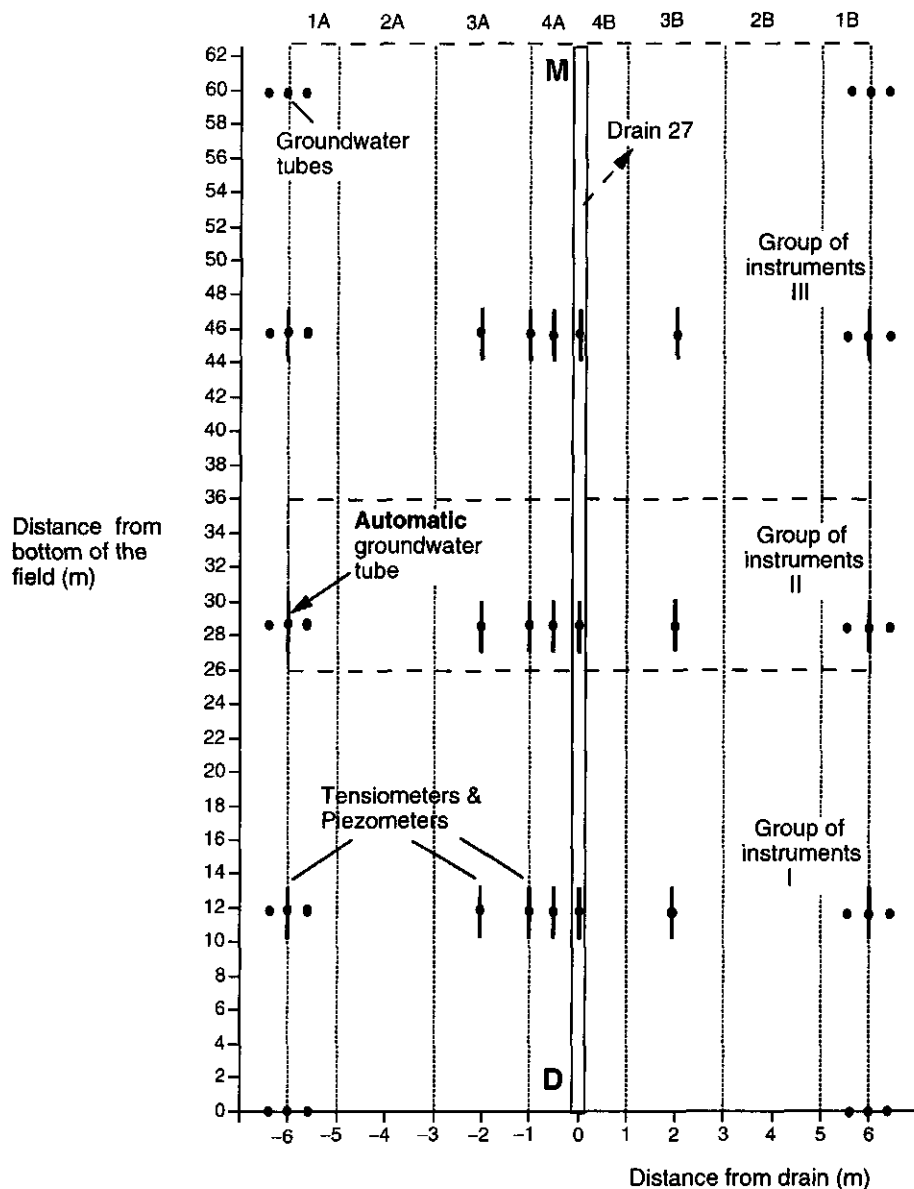


Figure 6.1 Overview of the experimental field in the catchment area of drain 27 at the Lovinkhoeve. The thick lines indicate a combined series of tensiometers and piezometers, the thick dots represent groundwater tubes. The position of the automated groundwater tube is shown. The numbers at the top indicate the blocks at different distances from the drain. The roman numerals at the right hand side indicate the different groups of instruments. The positions indicated by **M** and **D** referring to similar positions in Fig. 4.9.

6.3 Nitrate leaching 1991-1992

6.3.1 Drain discharge, and soil physical and soil chemical conditions

Precipitation and drainage

The drain discharge measurement period reported on here ran from 17 December 1991 ($t = 0$) to 8 April 1992 ($t = 114$ d), corresponding to the period from the first post-summer drainage to the time of spring barley sowing. Figure 6.2 shows the precipitation rate, groundwater level, drain discharge rate, and the NO_3 concentration in the drainage water as functions of time. During the measurement period the soil surface was bare. Drain discharge started on 19 December ($t = 2$ d). Other drains at the Lovinkhoeve experimental farm were discharging already a few weeks before $t = 0$. Large extraction of soil water by the preceding sugar beet crop explains the delayed drainage from the experimental field.

Precipitation had a strong effect the groundwater level. In the period $0 < t < 2$ d the subsoil became saturated and the groundwater level rose quickly. Later, high precipitation rates also caused peak groundwater levels, which resulted in corresponding peaks in discharge rates. Groundwater levels sometimes rose to near the soil surface; e.g., the maximum level of -18 cm at $t = 21$ d resulted in a peak discharge rate of 23 mm d^{-1} . During certain periods, e.g., $40 < t < 45$ d, the groundwater levels were below the 97.5 cm drain depth.

Groundwater levels

The behaviour of the groundwater levels was different for the different lateral distances from the drain. Large fluctuations were measured at the positions midway between the drains at -6 and 6 m, there were nearly no fluctuations at the position just above the drain at 0 m, and fluctuations were intermediate at 2 m from the drain. During the wet periods, $20 < t < 35$ d and $90 < t < 100$ d, the groundwater level at -6 m came close to the soil surface (Fig. 6.2b).

6. Field data on water flow and solute transport

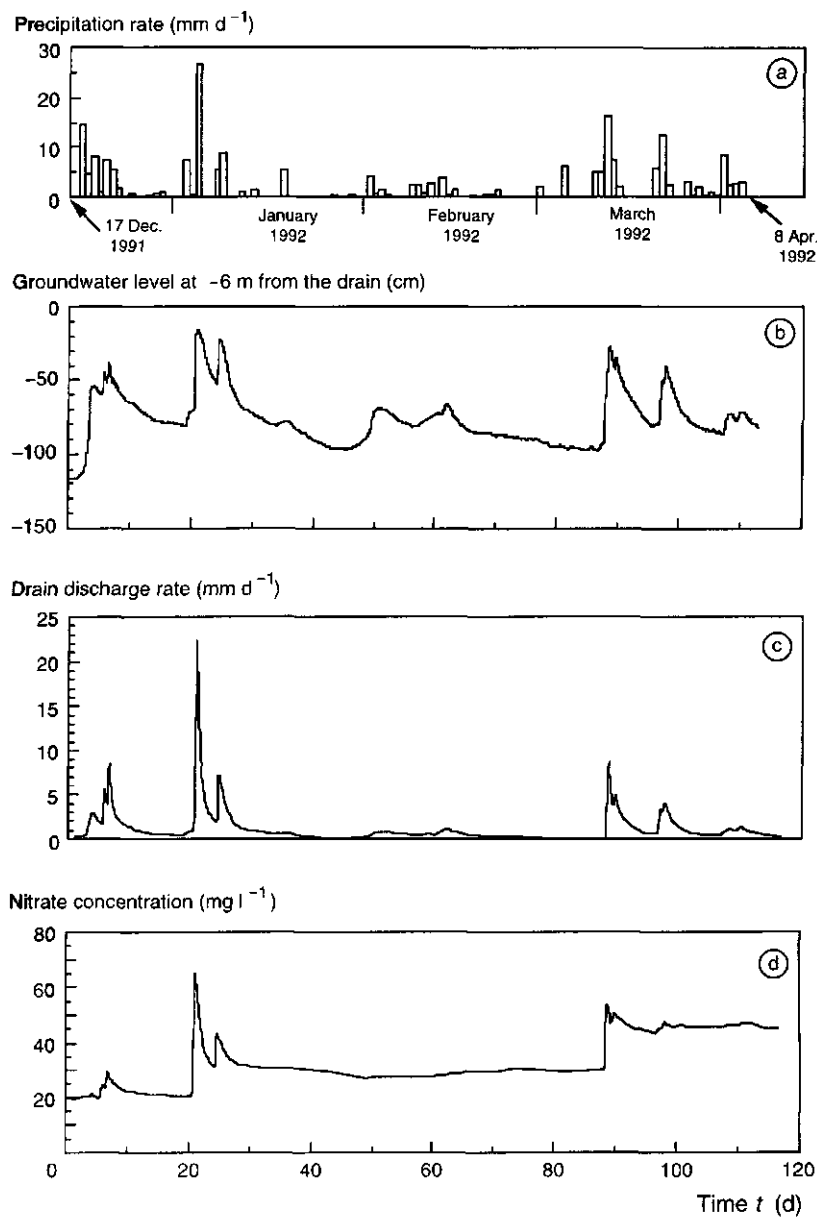


Figure 6.2 Precipitation rate (a), groundwater level at -6 m from drain 27 (b), drain discharge rate (c), and nitrate concentration in the drainage water (d) during the leaching period from 17 December 1991 ($t = 0$) to 8 April 1992 ($t = 114 \text{ d}$).

This resulted in a curved phreatic surface between the drains (Fig. 6.3), which lasted until the phreatic surface dropped below the drain depth at $t = 42$ d. The three groundwater levels measured close to the borders of the experimental plot (-6 m and 6 m) showed that at one side of the drain the maximum of the phreatic surface was reached at -5.5 m most of the time (Fig. 6.3). At the other side of the drain this maximum was reached at 6.0 m. These maxima indicate that the catchment boundary of the experimental plot was close to these positions. This means that the experimental plot has a net drain spacing of 11.5 m, which reduces the net surface by 4%, compared to the 12 m distance.

Nitrate concentration in the drainage water

The fluctuations of the NO_3 concentration in the drainage water corresponded with those of the groundwater levels and drain discharge rates (Fig. 6.2d). For $0 < t < 20$ d the NO_3 concentrations were at a moderate level close to 20 mg l^{-1} . At $t = 21$ d there was a NO_3 concentration peak of 65 mg l^{-1} . Under the relatively steady discharge conditions for $30 < t < 90$ d the NO_3 concentration was about 30 mg l^{-1} . For $t > 90$ d the NO_3 concentration increased to about 50 mg l^{-1} , the EU limit for groundwater.

In some drainage water samples the ammonium (NH_4) concentration was measured. Because the NH_4 concentration was nearly constant at 0.2 mg l^{-1} , the contribution of NH_4 to the nitrogen balance was neglected.

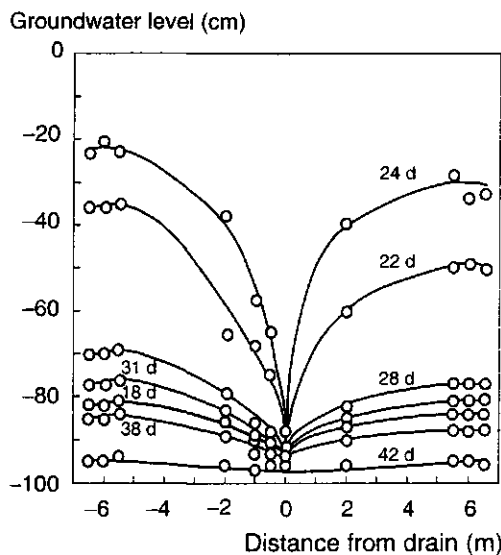


Figure 6.3 Groundwater levels at different distances from drain 27 for some characteristic days during the period from 8 January 1992 ($t = 22$ d) to 28 January 1992 ($t = 42$ d).

Hydraulic heads

The definition of the hydraulic head H is given in Eq. 2.3, in which the average level of the soil surface of the experimental plot is defined as $z = 0$. The levels of H increased quickly when the profile was filled with water in the period $0 < t < 10$ d (Fig. 6.4). After this period the behaviour of H at different positions from the drain was similar to the groundwater level at that position (data not shown). At all positions there was a H gradient for $t > 12$ d indicating downward flow in between the three depths.

In the periods $42 < t < 50$ d and $80 < t < 87$ d, the phreatic surface dropped below the drain depth. Visual observations of the drain showed that the discharge ceased, which was not reflected in the measured discharge because this is calculated between two discrete times. Also, H at the drain depth and at the different positions from the drain (see Fig. 6.9) dropped below $H = -97.5$ cm, corresponding to the H of free water at the depth of the drain.

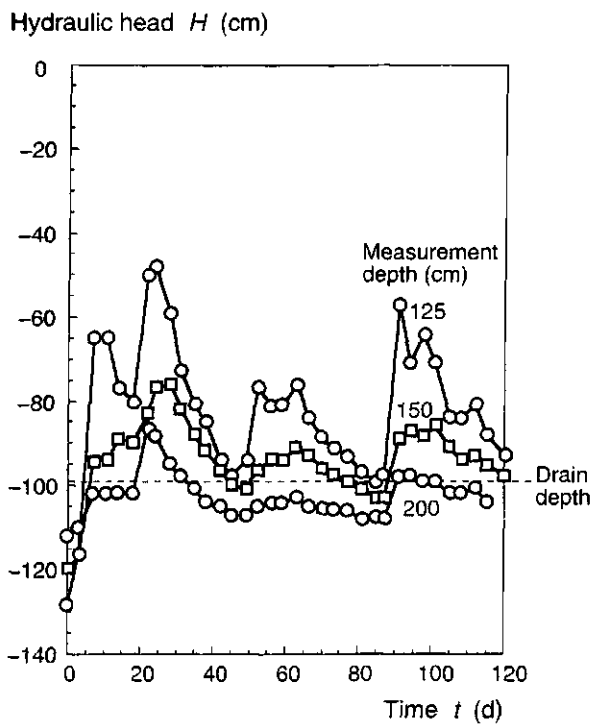


Figure 6.4 Hydraulic heads at three soil depths at a distance of -6 m from drain 27, measured at 29 m distance from the bottom of the catchment area (Group of instruments II in Fig. 6.1) in the leaching period from 17 December 1991 ($t = 0$) to 14 April 1992 ($t = 120$ d).

Nitrate concentration profiles

On 17 December 1991 ($t = 0$), five weeks after the sugar beet crop was harvested, NO_3^- concentrations and volumetric water contents were measured in the soil profile at 10-cm intervals between 0 and 150 cm depth. In each block of the net experimental field (Fig. 6.1) with a different distance from the drain, five soil samples of each depth interval were taken randomly at both sides of the drain. It was assumed that all NO_3^- was dissolved in the soil water. Figure 6.5 shows that on 17 December 1991 the NO_3^- concentrations were higher for the block at a distance of 0.1 m from the drain than for the other blocks. The highest NO_3^- concentrations occurred in the 0-50 cm soil depth interval. For depths larger than 100 cm, the NO_3^- concentrations were low. The 0-150 cm depth soil profile shows a statistically significant ($P = 0.05$) difference in the total N content of the block at a distance of 0.1 m from the drain of 93 kg ha^{-1} , and the average of the other blocks of 64 kg ha^{-1} .

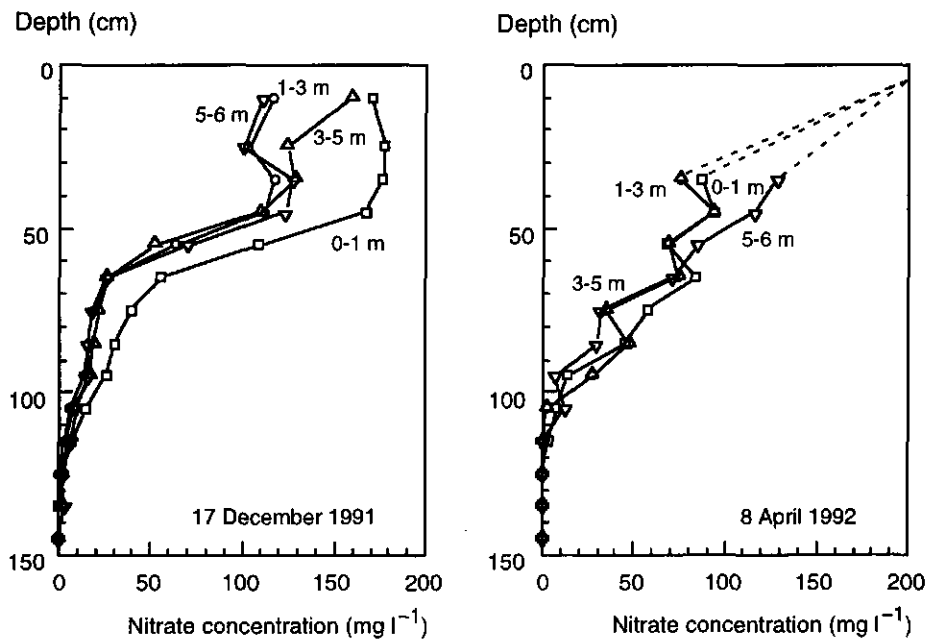


Figure 6.5 Nitrate concentrations in the soil water for the blocks at different distances from drain 27, measured by soil sampling on 17 December 1991 ($t = 0$) and 8 April 1992 ($t = 114$ d), assuming all nitrate was dissolved in the soil water. On 8 April 1992 the data of the topsoil are dubious due to the interference of fertiliser granules in the samples (see text).

6. Field data on water flow and solute transport

The mineral nitrogen content on 8 April 1992 (Fig. 6.5) was measured just after the application of N fertiliser, which resulted in very high NO_3 concentrations in the topsoil. The NO_3 concentrations for the 0-30 cm depth layer are corrected for this N application, but remain rather dubious due to the large variation in N content in the soil samples due to the fertiliser granules. At depths larger than 30 cm, no substantial differences were found in total N content as a function of the distance from the drain.

Chloride concentrations in the drainage water

Figure 6.6 shows Cl concentrations in the drainage water and the drain discharge rate. The data show a remarkably consistent opposite relationship between dissolved Cl concentration and drain discharge rate. At each peak in drain discharge rate, there was a depression in Cl concentration. Even peak drain discharge rates that appear as local maxima on larger peaks (e.g., $5 < t < 8$ d in Fig. 6.6) corresponded to local minima in the Cl concentration data. During the highest drain discharge period around $t = 21$ d, the Cl concentration varied from about 180 to 90 mg l^{-1} . The pattern of dissolved Cl over time contrasted with dissolved NO_3 , which showed peak concentrations at peak drain discharge rates (Fig. 6.2d).

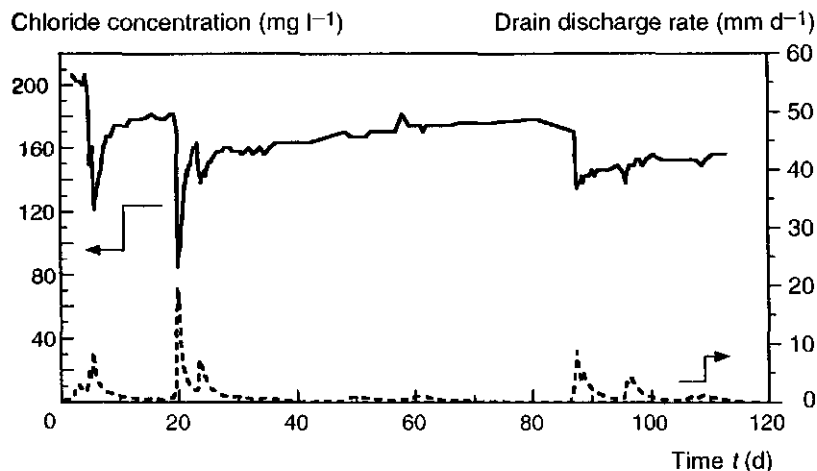


Figure 6.6 Chloride concentrations in the drainage water and corresponding drainage flow rates as a function of time in the leaching period from 17 December 1991 ($t = 0$) to 14 April 1992 ($t = 120$ d).

Soil extractable Cl and soil water contents were measured at soil depths from 0-150 cm in blocks at different distances from the drain (Fig. 6.1). The Cl concentrations were calculated, assuming all Cl was dissolved in the soil water. No substantial differences in Cl concentrations were found as a function of the distance from the drain. The trend in Cl concentrations with depth (Fig. 6.7) was opposite to the NO_3 concentrations, and unlike NO_3 , Cl showed no obvious peak concentrations in the profile above the drain. The history of the Noordoostpolder explains the high Cl concentrations in the subsoil (Pars. 4.1.1 and 4.1.2)

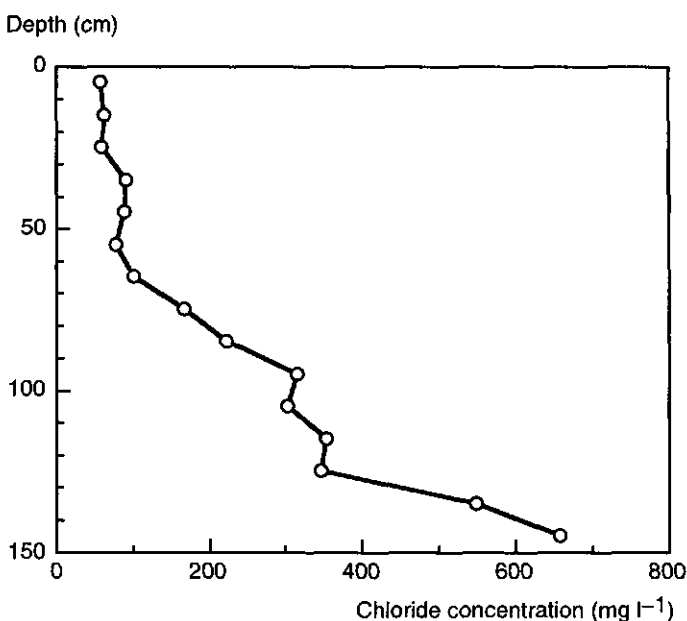


Figure 6.7 Chloride concentrations in the soil water at different depths on 17 December 1991 ($t = 0$).

6.3.2 Interpretation of the field data

Water balance

The soil water balance of the experimental field can be calculated for a well-defined volume of soil (V_s) for a unit surface area over the total measurement period:

6. Field data on water flow and solute transport

$$\Delta W = Q_{in} - Q_{out}, \quad (6.1)$$

where: ΔW = increase in water storage in V_s (mm);
 Q_{in} = cumulative amount of water entering V_s (mm);
 Q_{out} = cumulative amount of water leaving V_s (mm).

The net experimental field to a depth of 120 cm was in this case chosen as basis for calculating V_s . Assuming that no water flowed through the plane of symmetry midway between two drains, i.e., water can leave or enter the system only via the top or bottom surface and via the drain, then

$$Q_{in} = P + Q_{up}, \quad (6.2)$$

$$Q_{out} = E + Q_{down} + Q_{drain}, \quad (6.3)$$

where: P = precipitation (mm);
 E = soil evaporation (mm);
 Q_{up} = upward flux from the subsoil (mm);
 Q_{down} = downward flux to the subsoil (mm);
 Q_{drain} = drain discharge (mm).

Over the total period ($0 < t < 114$ d) 8688 l water was discharged, corresponding to $Q_{drain} = 120$ mm. Precipitation P was 213 mm in this period. The potential Makkink evapotranspiration, as given by the Royal Netherlands Meteorological Institute (KNMI) based on a reference grass field (Makkink, 1957; De Bruin, 1987), was 70 mm for this period. The evaporation for a bare soil surface is difficult to quantify on the basis of meteorological data alone. However, evaporation is often a small component in the long-term water balance. Because the soil surface of our experimental field was wet during the period, a reduction factor in the range of 0.7 to 1.0 can be used for the bare soil, resulting in an actual cumulative soil evaporation $E = 49$ to 70 mm. The 19 mm precipitation up to $t = 2$ d was still necessary to fill the soil profile until equilibrium with the phreatic surface at 97.5 cm depth was established. At $t = 114$ d the soil profile was considered to be in equilibrium with the phreatic surface at a similar groundwater depth as at $t = 2$ d (Fig. 6.2b), resulting in $\Delta W = 19$ mm.

Using $E = 49$ mm, from Eqs. 6.1, 6.2 and 6.3 it follows that $Q_{down} - Q_{up} = -\Delta W + P - E - Q_{drain} = -19 + 213 - 49 - 120 = 25$ mm water disappeared as net downward seepage. Using the maximum $E = 70$ mm results in $Q_{down} = 4$ mm.

Because the net field was located far from the ditch, there was no horizontal flow component towards the ditch. Water flow can be considered in the two-dimensional vertical plane perpendicular to the drains. During the leaching period the measured H gradient (Fig. 6.4) indicated downward seepage. However, the phreatic surface never fell far below the drain depth during relatively dry periods (Fig. 6.2b). This indicates a small vertical hydraulic conductivity in the subsoil.

Nitrate and chloride data

The peaks in NO_3 concentrations correspond to the peaks in groundwater levels and drain discharge rates (Fig. 6.2). The variations of the water flow pattern to the drain must be the explanation for the fluctuations in NO_3 concentrations. Under discharge conditions with a phreatic surface close to the drain depth, like in the period $30 < t < 90$ d, the origin of the discharged water was mainly from depths below the drain. The NO_3 concentrations in the soil water were relatively low in that zone (Fig. 6.5). When the phreatic surface rose in a short period to a shallow depth (0-50 cm), like in the periods $20 < t < 25$ d and $90 < t < 100$ d, a substantial part of the discharged water originated from the zone where NO_3 concentrations were higher. The discharged water is always a mixture of water from different origins, but the sharp changes in the measured NO_3 concentrations indicate an abrupt shift of the stream tubes and a contribution to drainage and leaching from correspondingly different zones in the soil. This conclusion is supported by the Cl data, which show opposite trends to NO_3 , both in soil profile distribution and drainage water concentration.

To monitor such a dynamic behaviour of the drain discharge, a high frequency or flow-proportional sampling of drainage water is necessary to accurately determine solute discharge. Measuring NO_3 concentrations only a few times during a leaching period can lead to substantial errors. Two illustrative examples are given of sampling schemes at 30-day intervals (Fig. 6.8). Sampling scheme A just samples the maximum NO_3 concentration at $t = 21$ d. Sampling scheme B misses this maximum concentration. The exact drain discharge data are used to calculate the cumulative drain discharge corresponding with the time interval around the sampled NO_3 concentration (Fig. 6.8). The NO_3 leaching was

6. Field data on water flow and solute transport

estimated as the product of the cumulative discharge and the measured NO_3 concentration. For the 114-day leaching period, sampling scheme A resulted in $13.7 \text{ kg ha}^{-1} \text{ N}$ leaching, which is 30% larger than the actual 10.6 kg ha^{-1} . Sampling scheme B resulted in $8.6 \text{ kg ha}^{-1} \text{ N}$ leaching, which is 20% lower than the actual N leaching. In this example the cumulative drain discharge rate is exactly known. However, when no drain discharge data are available, the drain discharge has to be estimated from the precipitation excess, introducing further errors. A less fluctuating NO_3 concentration and a higher sampling frequency will result in more accurate estimates of the cumulative NO_3 leaching using fixed time interval sampling schemes. However, without prior knowledge of the NO_3 concentration distribution in the soil and the transport processes in the soil, a

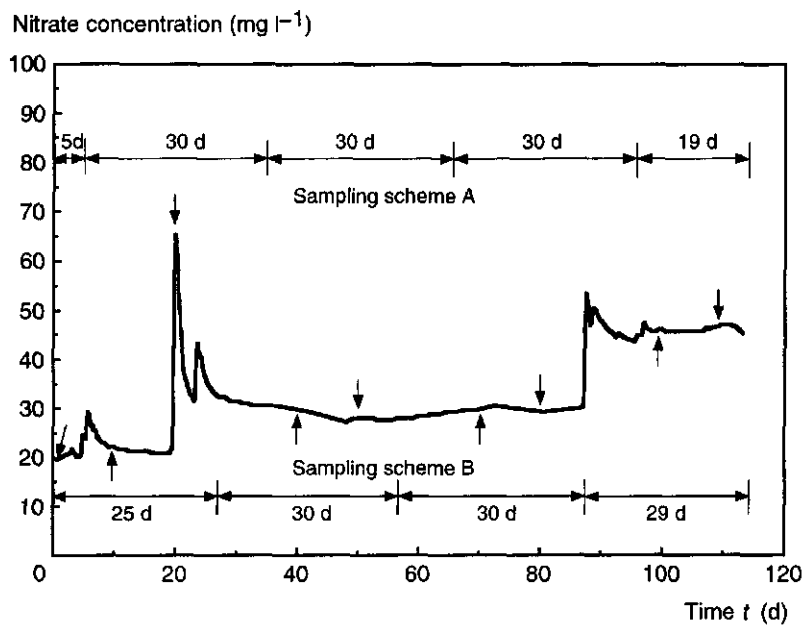


Figure 6.8 Examples of two 30-day interval sampling schemes, A and B, to measure NO_3 concentrations in the drainage water for N leaching estimations for the leaching period from 17 December 1991 ($t = 0$) to 8 April 1992 ($t = 114 \text{ d}$). The time of sampling (individual arrows) and the representative time interval corresponding to a sample are indicated for both sampling schemes.

flow-proportional sampling scheme has to be used. In this experiment, a flow-proportional sampling device measuring the average solute concentration in every 0.5 mm discharge was adequate to measure the dynamics of the NO_3 leaching process.

During periods of intense precipitation, peak NO_3 concentrations in drainage water (30 to 70 mg l^{-1} - Fig. 6.2d) were larger than the NO_3 concentrations in the saturated zone below the drain depth (< 20 mg l^{-1} - Fig. 6.5). So, NO_3 losses through a drain cannot be estimated by measurements of NO_3 concentrations in the groundwater. For example, 39% of cumulative NO_3 discharge over the total measurement period occurred during the peak discharge rate over the period $20 < t < 30$ d (Fig. 6.9), and a substantial part of the NO_3 originated directly from the topsoil. In view of the initial NO_3 contents presented in Fig. 6.5, NO_3 concentrations in the drainage water close to 70 mg l^{-1} can only originate from depths smaller than 50 cm.

The total amount of N leached was 10.6 kg ha^{-1} in the 114-d monitoring period (Fig. 6.9). This loss is a small amount relative to the total N amount of about 90 kg ha^{-1} in the soil profile (0-150 cm depth) and the N fertiliser application of 120 kg ha^{-1} for the sugar beet crop. However, even under this integrated arable farming system, the EU limits for the NO_3 concentration in groundwater of 50 mg l^{-1} were exceeded at times, but, over the total period the average NO_3 concentration was below the groundwater quality criterion.

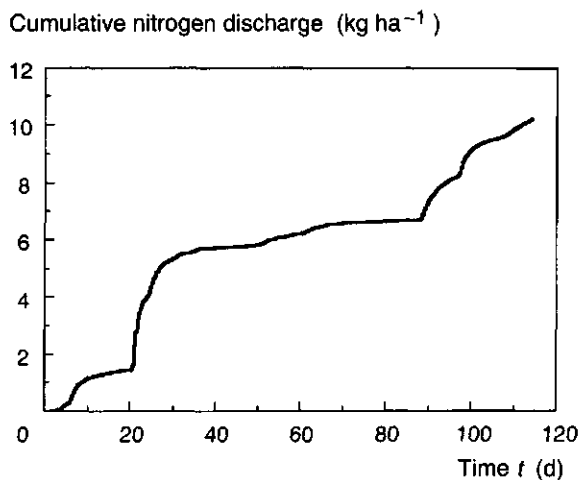


Figure 6.9 Cumulative amount of N discharged through the drain in the leaching from 17 December 1991 ($t = 0$) to 8 April 1992 ($t = 114$ d).

6. Field data on water flow and solute transport

Spatial nitrogen patterns related to distance from the drain

The spatial differences in N content in the soil profile on 17 December 1991 were 29 kg ha⁻¹. The area within 0-1 m from the drain represents only 17% of the total field, which limits the quantitative importance of the extra N amount of 29 kg ha⁻¹ in this area. It appears that differences in soil water content in the topsoil had created differences in anoxic conditions in the topsoil, such that the highest rates of denitrification might be expected at positions midway between the drains, where the soil is wetter. The phreatic surface in Fig. 6.3 shows that the gradient in groundwater levels was large in the zone -1 to 1 m from the drain. All positions further from the drain had somewhat similar groundwater levels. The main differences in soil NO₃ contents were also found between those zones (Fig. 6.5). The profile distribution of NO₃ suggests also that a fraction of NO₃ reaching the saturated zone is lost by denitrification.

Gradients in hydraulic conditions related to the distance from the ditch

Figure 6.10 shows field data of tensiometers, piezometers and groundwater tubes at different distances from the ditch. The instruments were installed at a distance of -6 m from the experimental drain (Fig. 6.1). All data are converted to hydraulic heads *H*. The drain depth is increasing towards the ditch, with an average slope of 0.002. So, the drain depth is 94.1, 97.5 and 100.9 cm at 66, 49 and 32 m distance from the ditch, respectively. Figure 6.10a shows no systematic trends in *H* as a function of the distance from the ditch. At *t* = 21 d, two positive *H* values were measured, suggesting that the soil was saturated and ponding occurred. However, the corresponding groundwater levels show indeed shallow groundwater levels, but no ponding. Perhaps these tensiometers were affected by compression of entrapped air. The piezometers at 125 cm depth show large dynamic variations, but differences as a function of the distance from the ditch are small. The piezometer at 200 cm depth shows slow fluctuations in hydraulic heads around *H* = -100 cm. This piezometer is located in the relatively impermeable peat layer, which apparently damped out the hydraulic head variations. Figure 6.10d shows that an automated groundwater tube with a measurement frequency of at least 15 minutes is necessary to monitor the dynamics of the groundwater level. Differences in groundwater level as a function of the distance from the ditch are small. The data of the automated groundwater tube are close to the data of the discrete measurements. So, for later leaching periods, only the data of the automated groundwater tube will be

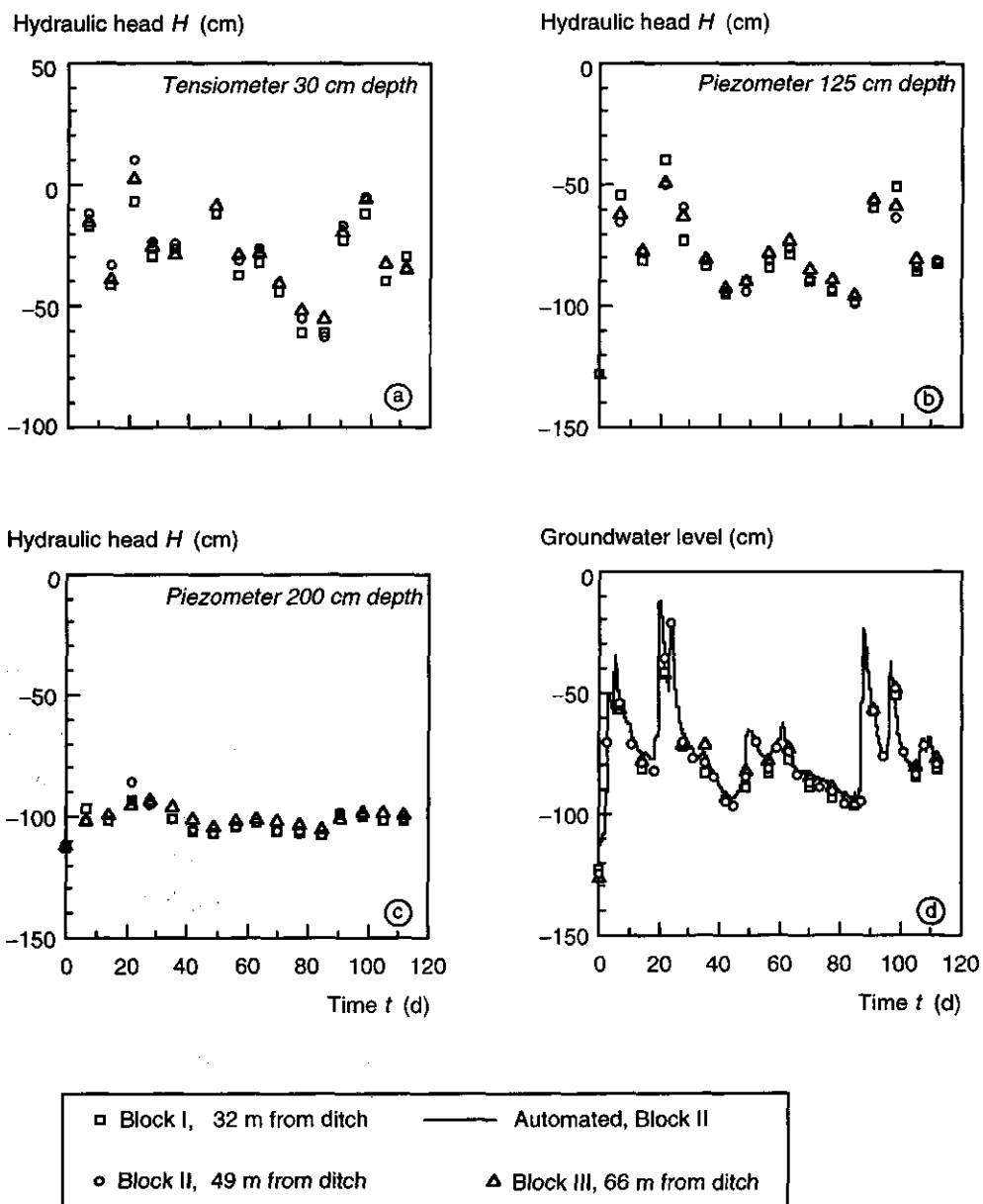


Figure 6.10 Hydraulic heads and groundwater levels as a function of time, measured at various distances from the ditch at -6 m from experimental drain 27 in the period from 17 December 1991 ($t = 0$) to 8 April 1992 ($t = 114$ d). Note that the scale of the hydraulic head of figure a differs from b and c.

6. Field data on water flow and solute transport

presented. However, data of the other groundwater tubes were used to check, and if necessary to correct, the data of the automated groundwater tube.

The small difference of 6.8 cm in drain depth over the experimental field did not result in substantial differences in hydrological conditions as a function of the distance from the ditch. This conclusion justifies the later use of a two-dimensional approach, taking into account only the depth and the distance from the drain to model water flow and solute transport processes of this experimental field.

Patterns of flow to the drain

There was a net infiltration $P - E = 16.4$ cm during the 114-day monitoring period. This infiltration corresponded with 36.4 cm vertical displacement, using an average $\theta = 0.45$ in the soil profile between 0-100 cm depth. Assuming vertical piston flow without dispersion, the front of the peak in NO_3 concentration, initially present at 50 cm depth (Fig. 6.5), would not have reached the 97.5 cm drain depth. However, for $t > 88$ d the measured NO_3 concentrations in the drainage water remain close to 50 mg l^{-1} , also under conditions with a deep phreatic surface. This result indicates that the NO_3 peak was close to the drain depth, resulting in less variation in NO_3 contents as drain discharge rates varied.

A one-dimensional description of the water flow to the drain is not appropriate. The NO_3 concentrations in the drainage water indicate two-dimensional flow patterns. Figure 6.11 shows a sharp increase in drain discharge rate when the groundwater level midway between the drains is above -30 cm. Assuming horizontal "Dupuit-Forchheimer" flow in a homogeneous, isotropic soil in the zone above the drain, an increase of the drain discharge rate proportional to the square of the groundwater level height above the drain is expected (Eq. 2.14). Indeed the layered soil profile (Fig. 4.6) has a relatively high hydraulic conductivity at saturation (K_s) in the topsoil (Fig. 4.16). Under conditions with a shallow phreatic surface this part of the soil will substantially contribute to the lateral water flow and enhance fast lateral transport of solutes. The drain trench (width = 20 cm) above the drain has a relatively high K_s also (Fig. 4.16), leading to a rapid vertical water flow to the drain. A similar phenomenon was reported by Martinez Beltran (1988).

The field measurements showed that the changes in the hydrological processes largely govern the solute transport and the corresponding NO_3 and Cl concentrations in the drainage water.

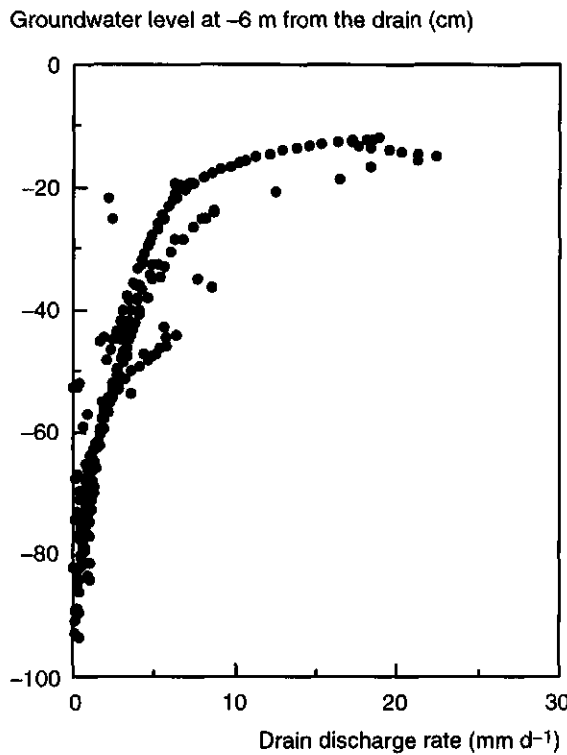


Figure 6.11 Drain discharge rates as a function of the groundwater level midway between the drains for the period from 17 December 1991 ($t = 0$) to 8 April 1992 ($t = 114$ d). The points indicate the measured data.

6.4 Long-term chloride mass balance and upward seepage

High Cl concentrations were still measured in the drainage water 49 years after reclamation of the lake bottom soil! By making a Cl mass balance for the period after reclamation, it may be possible to infer whether Cl is transported from deeper soil layers by upward seepage to the drains.

6.4.1 Situation after reclamation

The soil of the Lovinkhoeve was reclaimed from Lake IJsselmeer as described in Chapter 4. The salt content of the lake water decreased after the completion of the "Afsluiddijk" in 1932, so that before the reclamation in 1942 the lake water became relatively fresh. However, the soil of the polder still showed high salt contents, with NaCl as the major salt. Smits *et al.* (1962) report salt concentrations of 5.5 g l^{-1} in the lake water above the soil surface just before reclamation. The same authors also measured salt contents in the soil profile just after reclamation and five years later at a location in the centre of the Noordoostpolder (Table 6.1). These data are in line with the results of Van der Molen (1958) as discussed in Par. 4.1.2. In these first five years after reclamation large amounts of salt were leached, corresponding with estimated Cl amounts of 8645 kg ha^{-1} .

The following analysis considers the Lovinkhoeve soil profile to 120 cm depth, because at that depth the relatively impermeable peat layer starts. The Cl concentration at 120 cm depth in 1942 and 1947 is estimated at 3.3 g l^{-1} , based on the data of Smits *et al.* (1962). As a first approach, the 0-120 cm soil layer is considered to discharge water and Cl only through the subsurface drain. The possible exchange with the subsoil is evaluated later.

Table 6.1 Chloride concentrations in the soil water and Cl contents in the soil profile for different soil layers for different years. The data of 1942 and 1947 are taken from Smits *et al.* (1962) for the 0-20, 20-50 and 50-80 cm depth intervals; in the deeper layers extrapolation is used to estimate Cl concentrations in the 80-120 cm depth interval. An average volumetric water content $\theta = 0.5 \text{ m}^3 \text{ m}^{-3}$ is assumed to estimate the Cl contents in the soil layers. The data of 1991 were measured at the Lovinkhoeve, and field water contents were used to calculate the Cl contents in the soil layers.

Depth interval (cm)	Year					
	1942		1947		1991	
Depth interval (cm)	Cl conc. (mg l^{-1})	Cl content (kg ha^{-1})	Cl conc. (mg l^{-1})	Cl content (kg ha^{-1})	Cl conc. (mg l^{-1})	Cl content (kg ha^{-1})
0-20	970	970	60	60	100	60
20-50	1335	2000	120	180	150	180
50-80	1760	2640	245	365	200	240
80-120	2425	4850	610	1210	400	800
0-120		10460		1815		1280

6.4.2 Chloride mass balance

The 1942-1991 archives of the experimental farm Lovinkhoeve were studied to estimate the amount of Cl applied to the experimental field where the drainage experiment was carried out. Potassium chloride (KCl) was applied as potassium (K) mineral fertiliser. Normally KCl was applied before a potato or sugar beet crop. Before 1964 no KCl fertiliser was applied because the natural soil fertility with respect to K was adequate. Over the entire period 1964-1977 a total Cl amount of 120 kg ha^{-1} was applied. Later, the amounts of KCl fertiliser were drastically increased, resulting in a total Cl amount of 1450 kg ha^{-1} in the period 1977-1991. Mushroom compost was applied as organic manure in the years 1975-1991, which resulted in a total Cl application of 440 kg ha^{-1} . The average Cl concentration in the precipitation water in the Noordoostpolder is 5 mg l^{-1} (Ridder, 1978). Taking the average annual 745 mm precipitation at the Lovinkhoeve results in a Cl deposition of $37 \text{ kg ha}^{-1} \text{ yr}^{-1}$. The Cl uptake by the crop was relatively small. For the 4-year rotation potato - winter wheat - sugar beet - spring barley, taking average Cl contents in the crops according to Houba and Uittenbogaard (1994), the average Cl amount removed by the harvested crop parts was $10 \text{ kg ha}^{-1} \text{ yr}^{-1}$. Table 6.1 shows the total Cl concentrations and amounts in the soil profile down to 120 cm depth in 1942, 1947 and 1991. For the calculations of the total Cl amounts an average volumetric water content $\theta = 0.5 \text{ m}^3 \text{ m}^{-3}$ was used, while for 1991 the measured volumetric water contents were used.

A Cl mass balance (kg ha^{-1}) has been made for the period 1942-1991:

$$M_{1942} - M_{1991} + M_{fert} + M_{man} + M_{dep} = M_{disch} + M_{uptake}, \quad (6.4)$$

where: M_{1942} = Cl in the soil profile in 1942 (kg ha^{-1});

M_{1991} = Cl in the soil profile in 1991 (kg ha^{-1});

M_{fert} = Cl applied as KCl fertiliser between 1942 and 1991 (kg ha^{-1});

M_{man} = Cl applied as manure between 1942 and 1991 (kg ha^{-1});

M_{dep} = Cl deposited in precipitation water between 1942 and 1991 (kg ha^{-1});

M_{disch} = Cl discharged between 1942 and 1991 (kg ha^{-1});

6. Field data on water flow and solute transport

M_{uptake} = Cl taken up by the crop between 1942 and 1991 (kg ha^{-1}).

Over the period 1942-1991, a Cl amount of $M_{disch} = M_{1942} - M_{1991} + M_{fert} + M_{man} + M_{dep} - M_{uptake} = 10460 - 1280 + 1570 + 440 + 1810 - 490 = 12510 \text{ kg ha}^{-1}$ was discharged by the subsurface drain.

The annual precipitation excess of approximately 300 mm over 49 years corresponds with a total water column of 14.7 m. Using the average volumetric water content $\theta = 0.5 \text{ m}^3 \text{ m}^{-3}$, this results in a 29.4 m displacement of the soil water. In case of one-dimensional piston flow, this would mean that the water in the soil profile had been refreshed 24.5 times. The travel time density distribution approach equivalent to Eq. 2.19, with a characteristic residence time $\tau_{aq} = 2 \text{ yr}$, would also result in a nearly complete depletion of the Cl originally present in the 0-120 cm soil layer. However, the Cl contents in the soil profile are still high, especially at larger depths. This cannot be explained by the inputs at the soil surface only.

The average Cl concentration in the drainage water was 150 mg l^{-1} in the leaching period 1991-1992 (Fig. 6.6). The total Cl amount discharged in this period was 182 kg ha^{-1} . The leaching period 1991-1992 was dry, resulting in relatively high Cl concentrations in the drainage water because a substantial part of the water is originating from the deeper zones. The entire year 1991, including the growing season, was relatively dry with a total precipitation of 658 mm. This resulted in the relatively high Cl concentrations in the soil profile (Fig. 6.7). In a normal hydrological year the precipitation excess and corresponding cumulative drain discharge is about 300 mm. When the average Cl concentration in the drainage water is 150 mg l^{-1} this corresponds with a Cl discharge of $450 \text{ kg ha}^{-1} \text{ yr}^{-1}$. However, under wetter conditions the Cl concentrations in the topsoil will become lower and a larger part of the drainage water will originate from the topsoil. So, the yearly Cl discharge will be considerably smaller than $450 \text{ kg ha}^{-1} \text{ yr}^{-1}$.

In the period 1981-1991 an average Cl amount of $90 \text{ kg ha}^{-1} \text{ yr}^{-1}$ was applied as KCl fertiliser, $28 \text{ kg ha}^{-1} \text{ yr}^{-1}$ was applied as mushroom compost, the natural deposition was $37 \text{ kg ha}^{-1} \text{ yr}^{-1}$, and $10 \text{ kg ha}^{-1} \text{ yr}^{-1}$ was removed by the crop. This results in a total net Cl input of $145 \text{ kg ha}^{-1} \text{ yr}^{-1}$ at the soil surface, which corresponds with a Cl concentration of 48 mg l^{-1} in the soil water, when all Cl is dissolved in the 300 mm precipitation excess. However, the Cl concentrations in the soil profile on 17 December 1991 were at least a factor 2

higher (Fig. 6.7), and the concentrations in the drainage water in 1991-1992 were a factor 3 higher (Fig. 6.6). The high Cl concentrations in the topsoil can be explained by the relatively dry conditions before the sampling date and the dry leaching period as discussed above. However, the high Cl concentrations in the drainage water and in the subsoil (80-150 cm depth), and the imbalance between Cl input and discharge suggest another Cl source which increased the Cl concentrations in the soil profile.

Upward seepage and capillary rise

The Cl data might suggest upward seepage of water and Cl to explain the prevailing high Cl concentrations. However, it is questionable whether upward seepage occurs. Figure 6.12 shows that the hydraulic heads measured at 3 and 4 m depth were always smaller than the hydraulic heads at shallower depths. Most of the time, the hydraulic head at 150 cm depth is smaller than the hydraulic head at 125 cm depth, indicating downward flow. However, the hydraulic conductivity in the peat layer at these depths is very small (Chapter 4), so the downward flow is small too.

Usually, the hydraulic heads at 3 and 4 m depth are practically the same (Fig. 6.12), but in drier periods, i.e. $1300 < t < 1500$ d, a small H gradient is present, indicating upward seepage in the 3 to 4 m depth interval. In case the hydraulic head in the ditch is smaller than the hydraulic head at 3 m depth, water flow at this depth below the impermeable peat layer is ditch-oriented. Flow velocities can be large in this zone due to the large hydraulic conductivity at saturation in these sandy layers. A direct connection of these layers with the bottom of the ditch might exist, which facilitates the rapid transport of water and solutes to the ditch. This possibility is also mentioned by Van der Molen (1958).

Capillary rise may occur in summer periods. The water flux density may potentially reach 3 mm d^{-1} at depths between 50 and 100 cm (Chapter 5). This means a redistribution of water and Cl, resulting in an upward movement of Cl in the 0-120 cm soil layer. However, on a yearly basis no extra Cl is entering the soil profile at 120 cm depth, because the hydraulic head gradients at larger depths indicate there is no upward seepage.

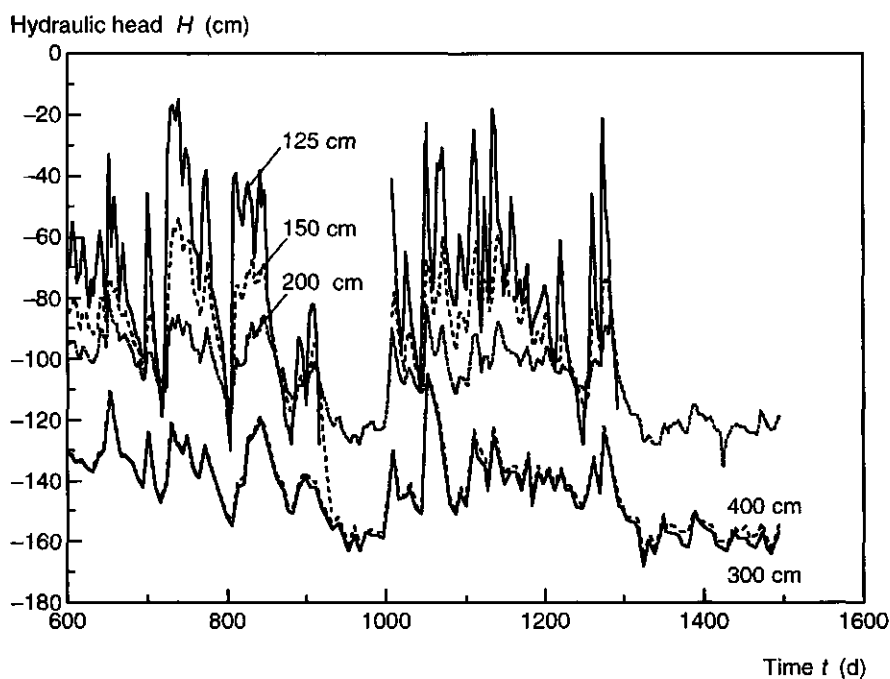


Figure 6.12 Hydraulic heads between 7 August 1993 and 24 January 1996 ($600 < t < 1500$ d) measured with piezometers at -6 m distance from experimental drain 27 at different depths.

Subsurface infiltration

In the years before 1992, the ditch water levels at the Lovinkhoeve were sometimes raised above the drain depth to provide the neighbouring fruit grower with irrigation water to prevent frost damage in the orchards. Under these conditions ditch water can infiltrate the soil profile through the subsurface drains. The water in the ditches is originating mainly from Lake IJsselmeer and partly from the larger canals in the Noordoostpolder. The average Cl concentration in the IJsselmeer water is 150 mg l^{-1} (Dienst Getijdewateren en Dienst Binnenwateren, 1990). However, for the Cl concentrations to reach 300-600 mg l^{-1} at 100-150 cm depth in the soil profile, originating from the subsurface infiltration of ditch water, the Cl concentrations in the ditch water should have been about 1000 mg l^{-1} , because a certain degree of dilution after infiltration into the soil may be expected. A Cl concentration of 1000 mg l^{-1} of the ditch water is unrealistically high compared to the Cl concentration of 150 mg l^{-1} in the

IJsselmeer water. So, subsurface infiltration did not play a substantial role and it cannot explain the gap in the Cl mass balance for the 0-120 cm depth layer.

Diffusion of chloride from the subsoil

The Cl present in the subsoil after reclamation in 1942 to a depth of about 10 m is a result of diffusion of salt into the soil during the period from about 1600 to 1932 when the sea water above the lake bottom was saline (Van der Molen, 1958). The Cl content in the 0-10 m depth soil layer amounted about 75 000 kg ha⁻¹ (Van der Molen, 1958). The situation changed after the installation of the drains because most of the Cl was leached from the top 100 cm of the soil profile. The Cl concentrations at larger depths (> 100 cm) remained high, which can also be seen in Fig. 6.7. So, the diffusion process acts now in the opposite direction: salt is transported upwards. The shape of the Cl concentration profile in Fig. 6.7 indeed shows an increase in Cl concentration with depth. Again it is assumed that the impermeable layer starts at 120 cm depth and that the water flow only occurs in the 0-120 cm depth soil layer. The diffusive Cl flux from the subsoil has to be estimated at 120 cm depth to be able to estimate the Cl mass balance. Volker and Van der Molen (1991) discussed the downward salt diffusion in the subsoil of the Noordoostpolder. From the Cl profiles in the soil they estimated a diffusion coefficient $D = 0.0146 \text{ m}^2 \text{ yr}^{-1}$ for Cl in the pores of the sediments. Using the measured Cl concentration gradient at the Lovinkhoeve at 125-145 cm depth of 1500 mg l⁻¹ m⁻¹ (Fig. 6.7) and applying Fick's law, results in an upward diffuse Cl flux of 220 kg ha⁻¹ yr⁻¹. Although the exact value of this Cl flux can differ from this estimate, due to possibly a different value of the local diffusion coefficient and changes in the Cl concentration gradient over time, it is clear that the upward Cl diffusion is a major term in the Cl mass balance. The characteristic length of the diffusion process is $l_{dif} = \sqrt{Dt}$, which results in $l_{dif} = 12 \text{ cm}$ for $t = 1 \text{ yr}$, and $l_{dif} = 85 \text{ cm}$ for $t = 49 \text{ yr}$. This length l_{dif} indicates the penetration depth of the upward Cl diffusion. In the zone where water flow plays an important role, the redistribution of Cl will be dominated by the convective transport, because the yearly water displacement of about 600 mm is an order of magnitude larger than the characteristic diffusion length l_{dif} . If the Cl concentrations in the subsoil (> 120 cm depth) are not influenced by processes like lateral groundwater flow, the upward Cl diffusion will continue for many years and the Cl concentration in the drainage water originating from this source will only slowly drop due to the depletion of the subsoil.

6.4.3 Discussion

The interpretation of the Cl mass balance of the 0-120 cm depth soil layer based on historical data and recent hydrological and chemical field data showed that all Cl initially present in the soil profile after reclamation in 1942 is discharged. There is no upward seepage at the Lovinkhoeve, and a small downward seepage might occur. However, the effect of the downward seepage on the Cl mass balance can be neglected. Upward Cl diffusion is estimated at $220 \text{ kg ha}^{-1} \text{ yr}^{-1}$ and is a major term in the Cl mass balance. Making a Cl mass balance (Eq. 6.4) for the period 1981-1991, including upward diffusion and assuming a constant Cl content in the 0-120 cm depth soil layer, results in an estimated Cl discharge of $372 \text{ kg ha}^{-1} \text{ yr}^{-1}$. The upward Cl diffusion should be quantified more precisely to make a better estimation of the Cl mass balance. The interpretation of the Cl field data turned out to be an important tool in understanding the field-scale water flow process.

6.5 Nitrogen balances and nitrate leaching 1991-1996

6.5.1 Field data 1991-1996

Various components of the nitrogen balance of the experimental field were measured during the study period 1991-1996. In spring and autumn or winter, the mineral nitrogen contents in the soil profile were measured and the crop N uptake was determined in the years 1992-1995. Nitrate leaching was monitored continuously. Table 6.2 summarises the N balances for the different leaching periods. First, the N contents of the soil profile to 100 cm depth are presented, then the cumulative N leaching and the amount of drainage water. The average NO_3 concentration in the drainage water is given for the entire leaching period. The amount of N fertiliser applied is indicated, together with the following crop. Finally, N uptake by the above-ground parts of the crop and the yield are given. Figure 6.13 shows the NO_3 concentration profiles measured before and after the leaching periods. The NO_3 concentrations were calculated by assuming that all mineral NO_3 was dissolved in the soil water. The soil samples were taken at 10-cm intervals from 0 to 100 cm depth, and Fig. 6.13 presents the NO_3

concentrations midway between these intervals (5-95 cm depth). Figures 6.14 to 6.18 give overviews of the precipitation rate, groundwater level at -6 m from the drain, drain discharge rate, and NO_3 concentration in the drainage water for the different (overlapping) parts of the study period. The successive leaching periods will be discussed individually.

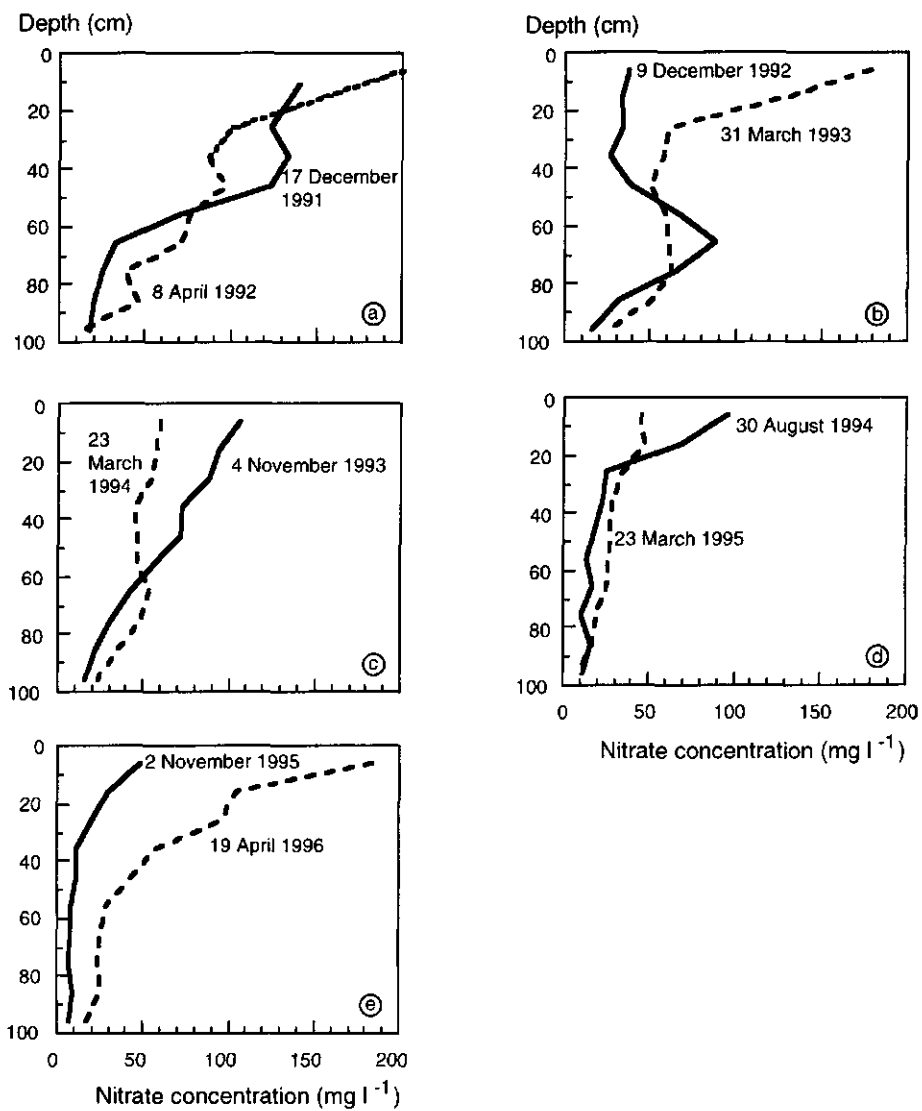


Figure 6.13 Nitrate concentration profiles at different sampling dates for five leaching periods.

6. Field data on water flow and solute transport

Table 6.2 Different components of the nitrogen balance of the experimental field at the Lovinkhoeve during the years 1991-1996. The N contents in the soil profile to 100 cm depth are measured in the autumn of the first year indicated and in the following spring. The leaching data represent data from the start of the drainage to the end of the drainage of each leaching season. The cumulative drainage and average nitrate concentration are given for the leaching periods. The fertiliser is applied in spring before sowing or planting of the crop. The N uptake of harvested crop parts, and crop yield are given.

Year (leaching period)	Autumn N content soil (kg ha ⁻¹)	Spring N content soil (kg ha ⁻¹)	N leaching (kg ha ⁻¹)	Cumulative drainage (mm)	Nitrate concentration (mg l ⁻¹)	N fertiliser applied (kg ha ⁻¹)	Crop	N uptake crop (kg ha ⁻¹)	Crop yield (t ha ⁻¹)
91-'92	69	97	12	138	39	105	Spring barley	a	a
'92-'93	45	67	35	351	44	160	Potato	219	78 b
'93-'94	55	47	50	622	35	80	Spring wheat	129	6.6 c
'94-'95	20	26	26	652	18	120	Sugar beet	146	58 b
'95-'96	10	49	0	0	-	80	Spring barley	a	a

a Not recorded

b Fresh weight

c Grain dry weight

Leaching period 1991-1992

The period ($0 < t < 114$ d) until spring barley sowing ($t = 114$ d) has already been discussed in detail in section 6.3 (Fig. 6.2). During the longer 150-d leaching period ($0 < t < 150$ d) only a small N amount of 12 kg ha^{-1} leached. However, the small 138 mm cumulative drain discharge caused a relatively high 39 mg l^{-1} average NO_3 concentration in the drainage water. Figure 6.14a shows NO_3 concentrations $> 40 \text{ mg l}^{-1}$ near the drain on 8 April 1992 ($t = 114$ d). This means that if the leaching period had been wetter, much more N leaching at high NO_3 concentrations could have occurred.

Leaching period 1992-1993

Cumulative drainage in the leaching period 1992-1993 ($300 < t < 500$ d) was 351 mm. Figure 6.15 shows maximum drain discharge rates of about 30 mm d^{-1} at $t = 393$ d and $t = 422$ d. However, fluctuations in the NO_3 concentrations in the drainage water remained small and the breakthrough of NO_3 in the drain was smooth. The initial NO_3 concentrations on 9 December 1992 ($t = 359$ d) were low, with a maximum at 65 cm depth (Fig. 6.13b). Nitrate concentrations in the topsoil were lower. After the NO_3 peak had reached the drain at $t = 365$ d, the NO_3 concentration in the drainage water remained constant. Differences in NO_3 concentrations in the soil profile were relatively small, and therefore changes in flow patterns did not have a great effect on the NO_3 concentration in the drainage water. The NO_3 profile on 31 March 1993 ($t = 471$ d) shows (Fig. 6.13b) that the NO_3 concentrations at 20-95 cm depth were nearly constant at 50 mg l^{-1} , with an increasing NO_3 concentration in the topsoil.

Leaching period 1993-1994

Cumulative drainage in the leaching period 1993-1994 ($590 < t < 910$ d, Fig. 6.16) was 622 mm, which indicates an extremely wet period. The drainage and leaching period started already in July 1993, which is very early. Potatoes were harvested on 25 October 1993 ($t = 680$ d) and the NO_3 profile was measured after harvest (Fig. 6.13c). Shallow fluctuating groundwater levels resulted in fluctuating drain discharge rates with maxima of about 30 mm d^{-1} . At $t = 651$ d an enormous peak in drain discharge rate was measured. This peak was probably partly due to an overflow of the ditch water into the drain sampling system due to an obstruction of the floating system (Fig. 4.5). The very low NO_3

6. Field data on water flow and solute transport

concentration in the drainage water at this event confirms this assumption. At $t = 680$ d, the NO_3 concentration decreased to 20 mg l^{-1} . During the small leaching event around $t = 700$ d, the NO_3 concentration increased to 30 mg l^{-1} . For $722 < t < 860$ d, the NO_3 concentration fluctuated around 45 mg l^{-1} . A substantial cumulative N amount of 50 kg ha^{-1} leached. Because the cumulative amount of drainage water was large, the average NO_3 concentration of 35 mg l^{-1} in the drainage water remained $< 50 \text{ mg l}^{-1}$. Figure 6.13c shows that on 4 November 1993 ($t = 690$ d) the NO_3 concentration in the soil decreased nearly linearly with depth. Peak flow rates for $t > 722$ d did not result in peaks in NO_3 concentrations in the drainage water. However, NO_3 concentrations larger than 40 mg l^{-1} in the drainage water indicate that a substantial part of the water originated from depths between 0 and 60 cm. For $t > 722$ d a very wet period started with a continuous shallow groundwater level, which will have caused a rapid transport of a large part of the NO_3 from the topsoil downwards.

Leaching period 1994-1995

Cumulative drainage in the leaching period 1994-1995 ($1000 < t < 1300$ d) was 652 mm, which indicates again an extremely wet leaching period. The phreatic surface sometimes reached the soil surface (Fig. 6.17b), resulting in peak discharge rates of about 30 mm d^{-1} . Although the NO_3 concentrations in the drainage water were generally low, NO_3 concentrations increased at peak discharge rates in the period $1000 < t < 1120$ d. For $1140 < t < 1225$ d NO_3 concentrations in the drainage water stabilised at 20 mg l^{-1} .

Figure 6.13d shows high NO_3 concentrations in the topsoil (0-20 cm depth) and very low NO_3 concentrations of 15 mg l^{-1} at 20-90 cm depth. This NO_3 profile indicates that maxima in NO_3 concentration in the drainage water originate from the topsoil. On 23 March 1995 ($t = 1194$ d) the NO_3 concentrations in the soil profile were rather uniform at a level of about 30 mg l^{-1} . Nitrogen fertiliser was applied on 18 April 1995 ($t = 1220$ d), and shortly afterwards a very wet period started. Rapid NO_3 transport from the topsoil downwards resulted in very high NO_3 concentration peaks in the drainage water. During this short drainage period 6 kg ha^{-1} N leached.

Leaching period 1995-1996

Figures 6.17 and 6.18 show that drain discharge ceased in June 1995 ($t > 1285$ d). During the following relatively dry winter period the groundwater level

remained below the 97.5 cm drain depth. Field measurements of groundwater levels ended in January 1996 ($t = 1500$ d). There was no discharge again until the autumn of 1996. Figure 6.13e shows the NO_3 concentration profiles in the soil. The NO_3 concentrations increased from 2 November 1995 to 19 April 1996, due to net N mineralisation throughout the entire soil profile to 100 cm depth.

6.5.2 Discussion

Water flow and nitrate transport

Figures 6.12 to 6.16 show that the groundwater levels were often shallow and fluctuated strongly as a function of the intensity of the precipitation. Groundwater levels are sometimes reaching the soil surface. Under these conditions, when the entire soil profile is nearly saturated, maximum drain discharge rates of 35 mm d^{-1} can occur. Drain discharge rates are given as actual values, while the precipitation data are given on a daily basis. So, it can occur that a drain discharge rate seems larger than the maximum precipitation rate. However, when precipitation data are presented on a hourly basis (Chapter 8), the maximum precipitation rate is always larger than the drain discharge rate.

The effect of strongly fluctuating groundwater levels and drain discharge rates on NO_3 concentrations in the drainage water depends very much on the distribution of NO_3 concentrations in the soil profile. When NO_3 concentrations in the topsoil are an order of magnitude larger than NO_3 concentrations near the drain depth, peaks in drain discharge rates can coincide with high NO_3 concentrations. The NO_3 profiles on 17 December 1991 and 30 August 1994 are examples (Fig. 6.13). When the NO_3 profiles are more uniform, differences in drain discharge rates correspond only with small fluctuations in NO_3 concentrations in the drainage water. The change in flow patterns under different hydrological conditions determines the different pathways for solute transport. The two-dimensional water flow and solute transport model SWMS_2D will be used in Chapter 8 to quantify the different components of the transport processes.

6. Field data on water flow and solute transport

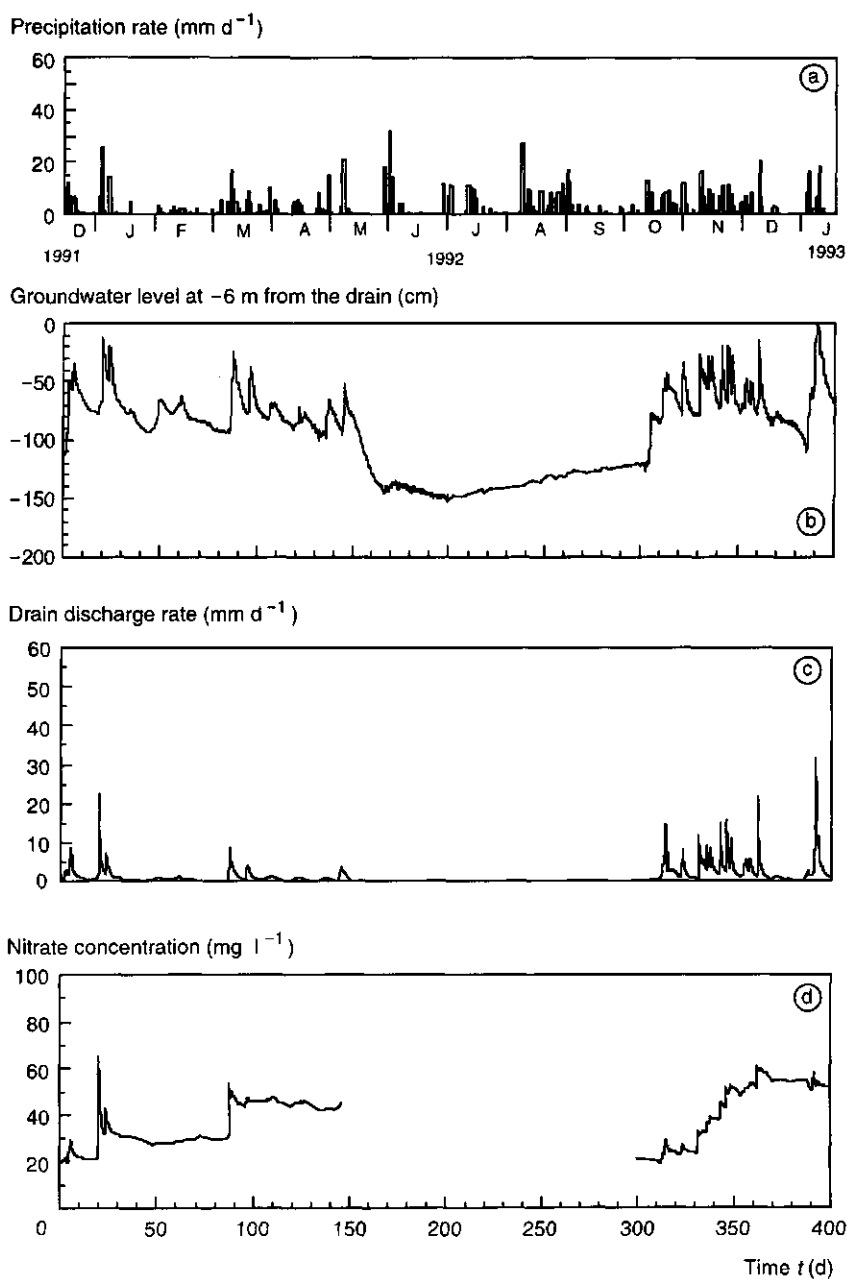


Figure 6.14 Precipitation rate (a), groundwater level at -6 m from drain 27 (b), drain discharge rate (c) and nitrate concentration in the drainage water (d) during the leaching period from 17 December 1991 ($t = 0$) to 19 January 1993 ($t = 400$ d).

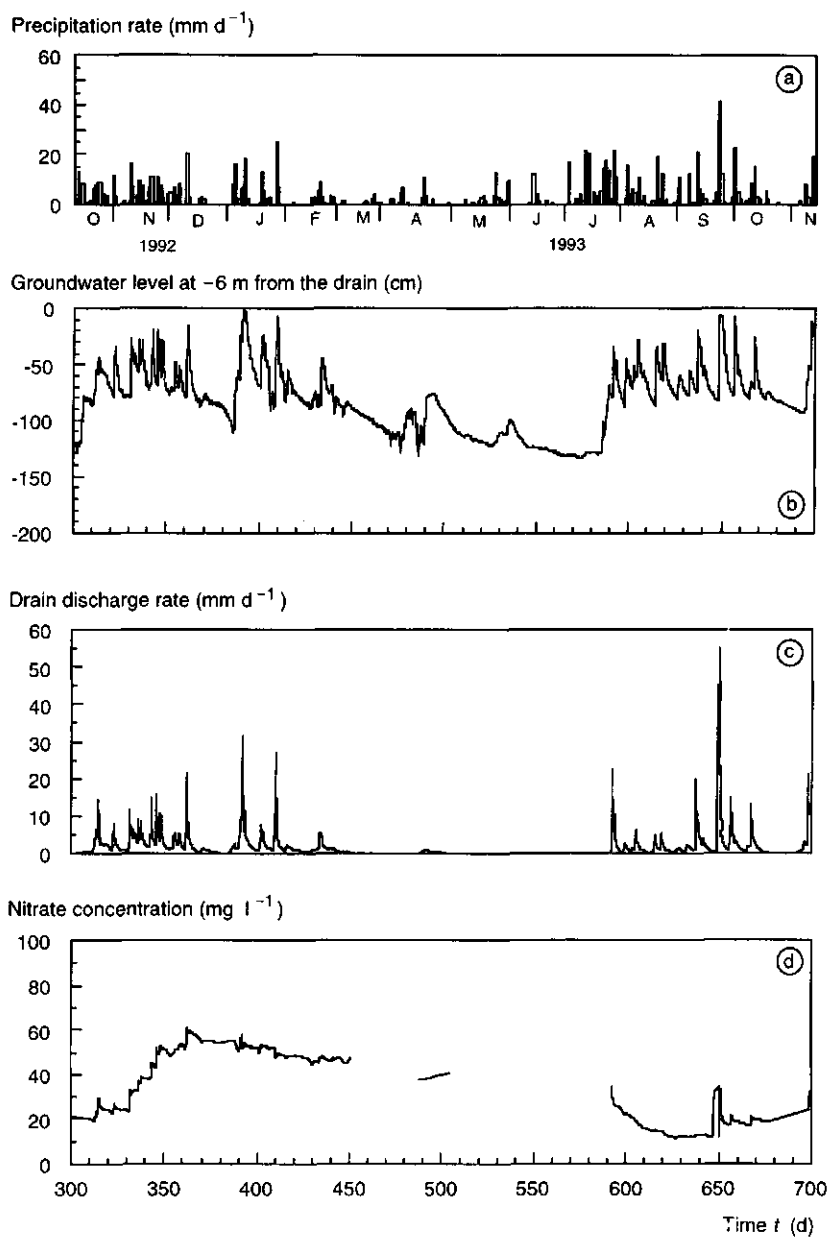


Figure 6.15 Precipitation rate (a), groundwater level at -6 m from the drain (b), drain discharge rate (c) and nitrate concentration in the drainage water (d), during the leaching period from 11 October 1992 ($t = 300 \text{ d}$) to 15 November 1993 ($t = 700 \text{ d}$).

6. Field data on water flow and solute transport

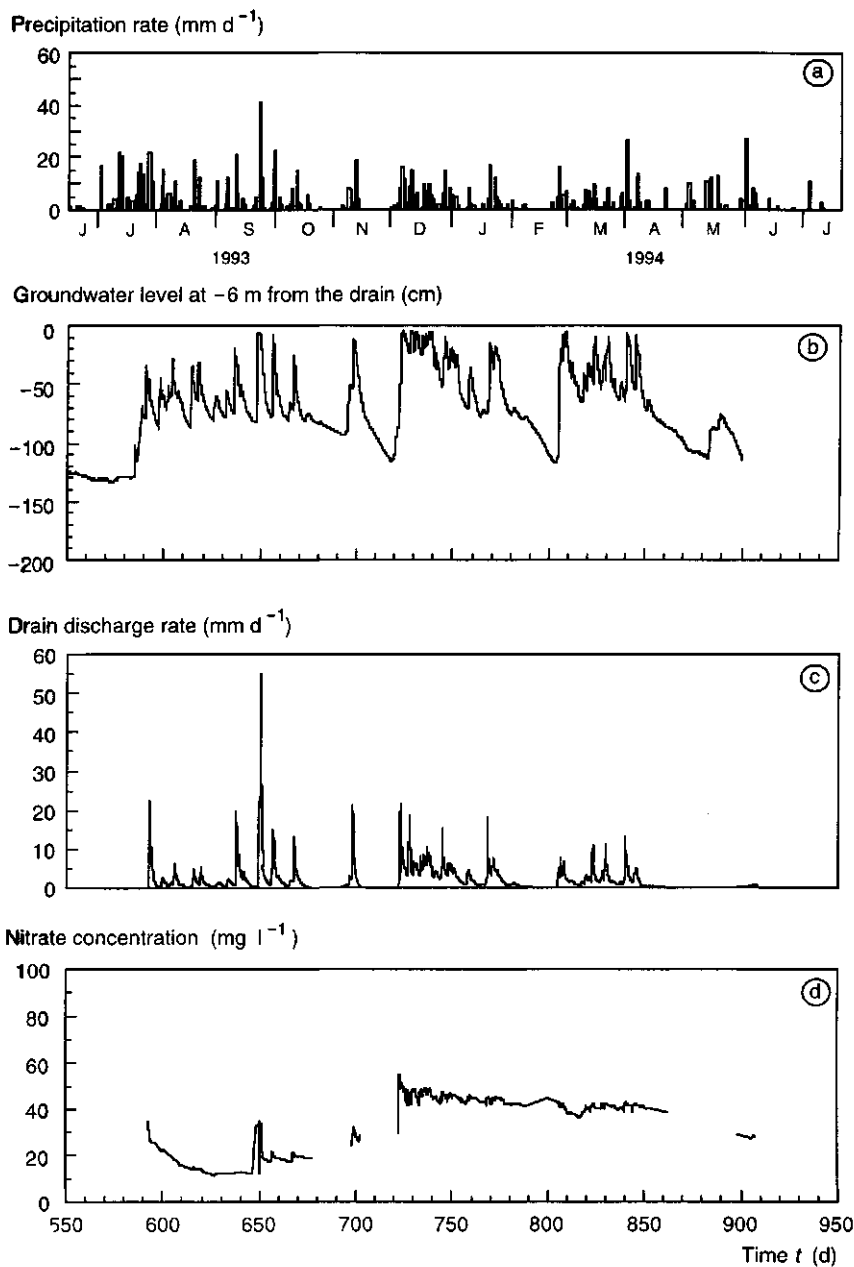


Figure 6.16 Precipitation rate (a), groundwater level at -6 m from the drain 27 (b), drain discharge rate (c) and nitrate concentration in the drainage water (d), during the leaching period from 18 June 1993 ($t = 550 \text{ d}$) to 23 July 1994 ($t = 950 \text{ d}$).

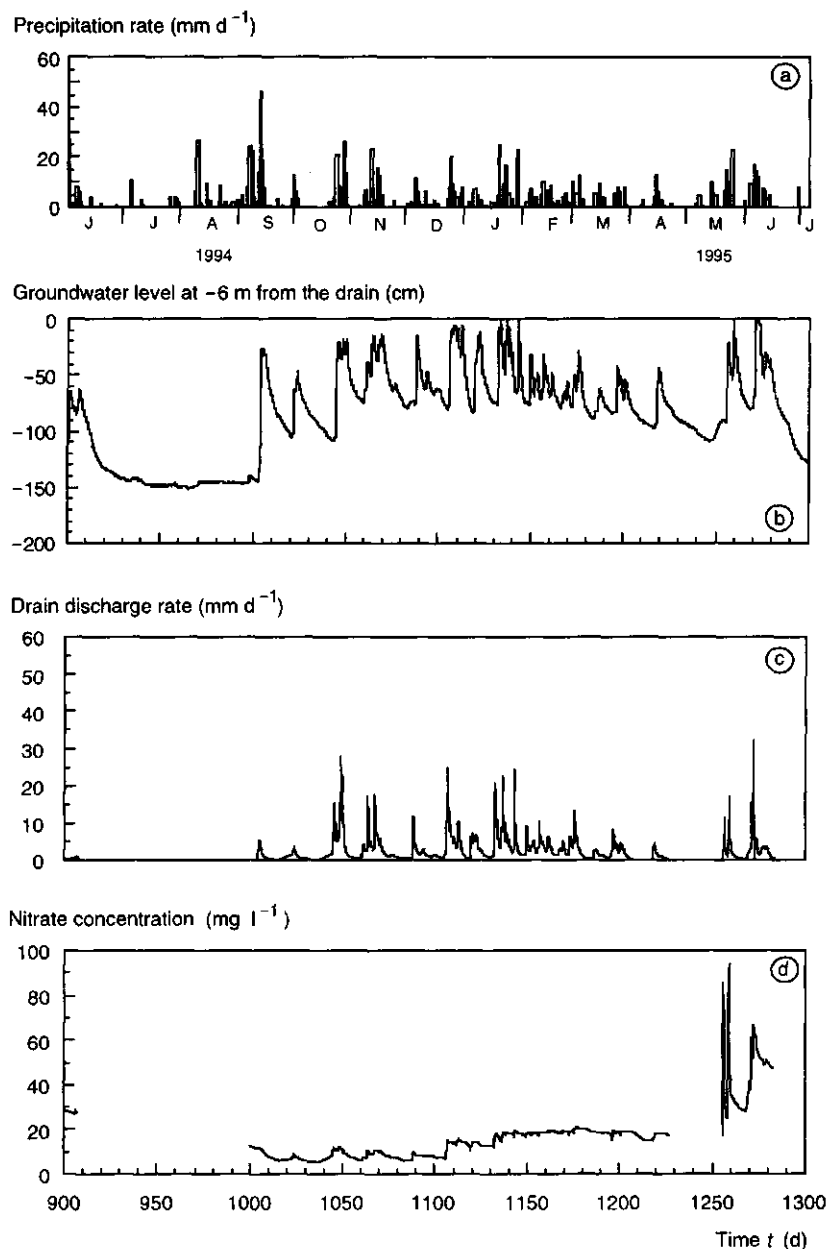


Figure 6.17 Precipitation rate (a), groundwater level at -6 m from the drain 27 (b), drain discharge rate (c) and nitrate concentration in the drainage water (d), during the leaching period from 3 June 1994 ($t = 900 \text{ d}$) to 8 July 1995 ($t = 1300 \text{ d}$).

6. Field data on water flow and solute transport

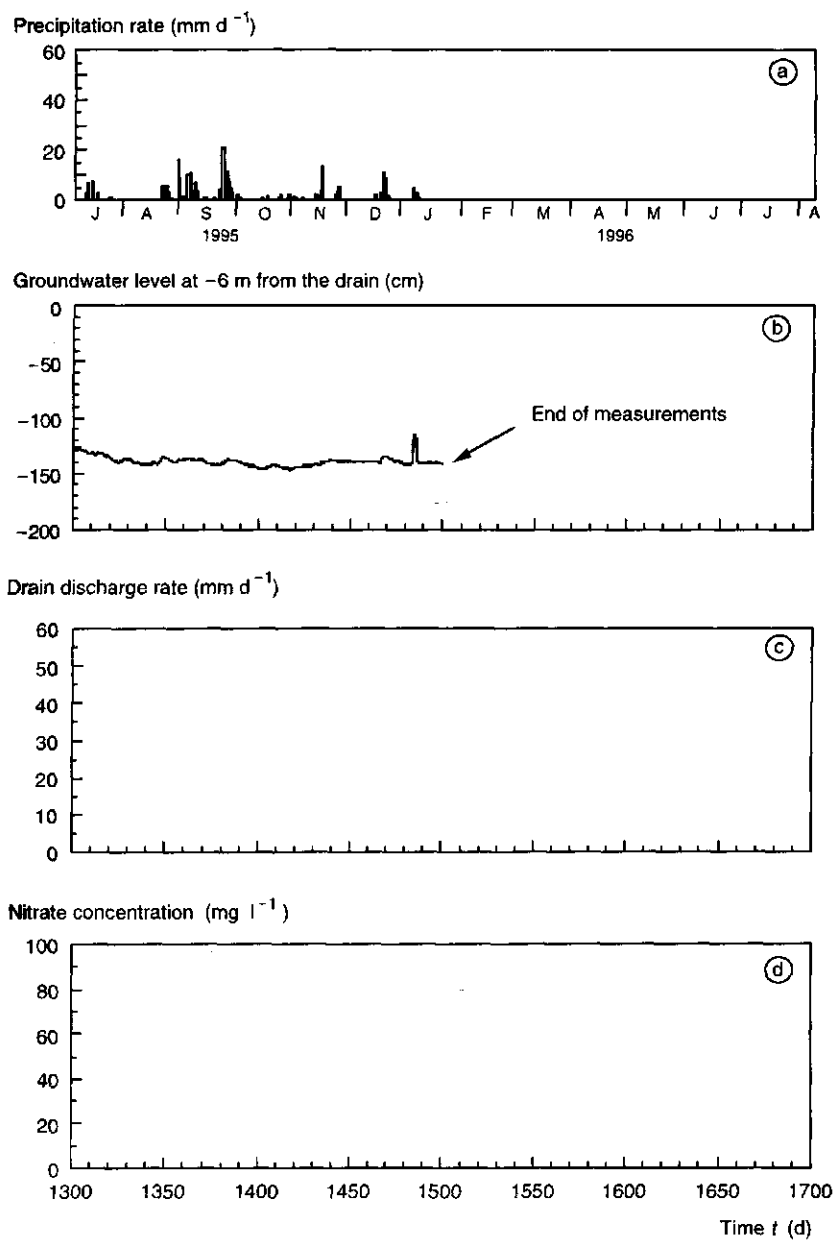


Figure 6.18 Precipitation rate (a), groundwater level at -6 m from the drain 27 (b), drain discharge rate (c) and nitrate concentration in the drainage water (d), during the leaching period from 8 July 1995 ($t = 1300 \text{ d}$) to 11 August 1996 ($t = 1700 \text{ d}$).

Relationships between drain discharge rate and groundwater level 1991-1995

Figure 6.19 shows the relationship between drain discharge rate and groundwater level for the four leaching periods. The data were calculated by first selecting the measured drain discharge rate, corresponding with an average discharge rate in the time period to collect 0.49 mm drain water. Then, the average groundwater level was calculated for the same time period. Especially at shallow groundwater levels and large drain discharge rates, these time periods can be short, i.e. 20 minutes. Measurement errors due to the response time of the groundwater tube and time synchronisation errors between different data loggers contribute to part of the variation in the data. This possible error was not analysed in detail and is thus difficult to quantify.

The relationship for the leaching period 1991-1992 has already been discussed in Par. 6.3. Figures 6.19b to 6.19d show similar relationships for the later leaching periods, although more variation in the data was found. At similar groundwater levels midway between the drains, the total water storage in the unsaturated zone can be different due to different volumetric water contents. Simulations of water flow will give an indication of the possible variation in drain discharge rates at a fixed groundwater level due to this effect. Hysteresis in the soil water retention characteristics may also contribute to the variation in water storage and consequently of drain discharge rates too. The effect of hysteresis, however, was not studied.

In situations with a shallow groundwater level, between -30 and 0 cm, the variation in drain discharge rates is large. Under these extremely wet conditions the ditch water level sometimes rose above the drain outlet, which reduces the hydraulic head gradient between the phreatic surface and the water in the ditch, resulting in a smaller drain discharge rate. From 14 November 1994 ($t = 1165$ d) onwards, the water level in the ditch was measured. However, around that time the control of the ditch water level in the polder was improved and after that time the ditch water level never again rose above the drain outlet. So, no correction for the effect of the ditch water level had to be made for this later period.

In Fig. 6.19 the drawn lines indicate Hooghoudt's equation 2.14. There was a large variation in the data, especially at shallow groundwater levels, and no attempt was made to statistically optimise the parameters of the equation. Parameters were sought to represent the extremes and the centre of the distribution of the field data. A simple Hooghoudt equation, with a hydraulic conductivity at saturation below the drain $K_{s,b} = 0$, which means that the

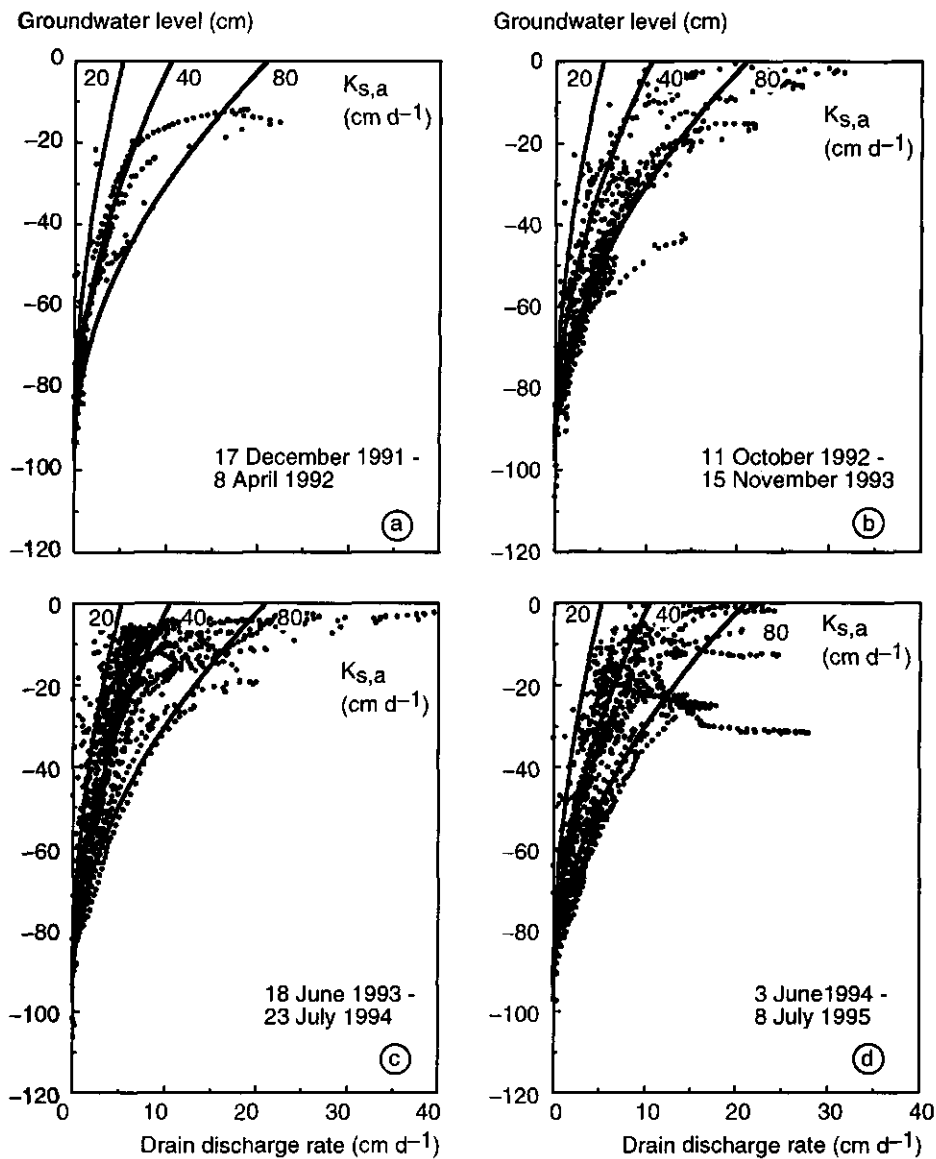


Figure 6.19 Drain discharge rates as a function of the groundwater level midway between the drains for four different leaching periods 1991-1995. The points indicate the measured data. The lines indicate the results of Hooghoudt's equation 2.14; for three hydraulic conductivities at saturation in the zone above the drain depth: $K_{s,a} = 20, 40$ and 80 cm d^{-1} .

groundwater flow below the drain depth makes no substantial contribution to the total flow to the drain, resulted in an acceptable form of the curve for deeper groundwater levels. The hydraulic conductivity at saturation above the drain $K_{s,a}$ varied between $20-80 \text{ cm d}^{-1}$ to obtain curves describing the field data. This range lies within the range of the hydraulic conductivities at saturation $10 < K_s < 100 \text{ cm d}^{-1}$ measured in the laboratory in the 0-75 cm depth soil layers (Fig. 4.16). Although the field data also differ between the leaching seasons, a Hooghoudt equation with $K_{s,a} = 40 \text{ cm d}^{-1}$ gives reasonable predictions of the drain discharge rate for groundwater levels below -30 cm.

Figure 6.19 shows a sharp increase in the drain discharge rate when the groundwater level rises above -30 cm. At shallow groundwater levels below -30 cm, the Hooghoudt equation results often in too small discharge rates, which indicates a much larger hydraulic conductivity in the topsoil. It is likely that rapid lateral water flow in the topsoil towards the drain trench and the drain occurred. The hydraulic conductivity at saturation K_s of the topsoil can vary orders of magnitude depending on the soil structure, which is influenced by the weather, by soil tillage and traffic, and by root activity and other biological activity. Direct quantification of K_s in the often loose topsoil is nearly impossible. Part of the variation in the relation between drain discharge rate and groundwater level can be attributed to variations in K_s . In future studies this aspect should be analysed in more detail. Perhaps it is possible to calculate the K_s in the topsoil from the relationship between drain discharge rate and groundwater level, using inverse methods.

Nitrate concentrations in the drainage water

For all four leaching periods the average NO_3 concentration in the drainage water was smaller than 50 mg l^{-1} . During short periods with shallow groundwater levels and high discharge rates, NO_3 concentrations larger than 50 mg l^{-1} occurred. The event of NO_3 leaching after the application of N fertiliser in June 1995 ($1250 < t < 1280 \text{ d}$) increased NO_3 concentrations in the drainage water up to 90 mg l^{-1} . In general, one might expect that for conditions with high NO_3 concentrations in the topsoil and a given amount of cumulative precipitation, a more uniform precipitation distribution would result in lower average NO_3 concentrations in the drainage water as compared to situations with high precipitation rates. For these conditions with high NO_3 concentrations in the topsoil an addition of straw or other carbon-rich material could result in NO_3

6. Field data on water flow and solute transport

fixation in organic matter and a reduction of N leaching. Also, a catch crop could be used to take up the N from the topsoil. When the peak in NO_3 concentrations is present at a greater depth, possibilities to manipulate N fixation or N uptake are limited. Under these conditions a non-uniform precipitation distribution could even result in lower N leaching. However, these situations are not likely to occur and minima in NO_3 concentrations at peak discharge rates were not measured during the 5-year monitoring period.

Drainage water is always a mixture of water originating from different zones in the soil. At discharge rates smaller than 1 mm d^{-1} , with the groundwater level below -75 cm , the drainage water originates from the $75\text{--}120 \text{ cm}$ depth soil layer. Nitrate concentrations in drainage water close to the sampling dates always correspond well the NO_3 concentrations in the soil water at these depths. Although NO_3 can be transformed in soil and can not be considered as a conservative tracer, at peak discharge rates NO_3 concentrations became so large that they had to originate from the topsoil. So, even NO_3 concentrations in the drainage water yielded information on the water flow processes in the soil.

Nitrogen patterns as a function of the distance from the drain

The nitrate profiles were measured in the blocks at different distances from the drain (Fig. 6.1) at all sampling dates. On 9 December 1992 and 4 November 1994 about 10 kg ha^{-1} more N was found at $0\text{--}1 \text{ m}$ from the drain than at greater distances from the drain. No substantial differences were measured on sampling dates in spring. However, on 19 April 1996, after the extremely dry winter, 17 kg ha^{-1} less N was found at $0\text{--}1 \text{ m}$ from the drain than at greater distances from the drain. These differences are small from an agricultural point of view. But there are other spatial differences. In the growing season differences in volumetric water content can result in differences in water and nutrient uptake by the crop. In this case a crop at a larger distance from the drain, with a shallower groundwater level, could benefit from the wetter conditions. However, the oxygen diffusion at these positions can be limiting under very wet conditions. The crop closer to the drain could benefit from the drier conditions. Field measurements at the grass field of the meteorological station of the Lovinkhoeve by Rappoldt and Corré (1997) showed that spatial differences in denitrification occurred, with a substantially higher denitrification rate at larger distances from the drain. The transport of NO_3 by convection and dispersion also plays a role in the distribution of NO_3 in the soil profile. The horizontal water flow component in the direction of

the drain will result in a net transport of NO_3 towards the drain. When no NO_3 is mineralised or applied, this transport results in a depletion of NO_3 at larger distances from the drain and an inflow of NO_3 at positions nearer to the drain. The importance of the NO_3 transport will be evaluated with the two-dimensional water flow and solute transport simulation in Chapter 8. For a detailed description of N dynamics in the soil, the N turnover has to be described in combination with the transport processes for a two-dimensional domain. Such a comprehensive approach is beyond the scope of this study. However, it is clear that spatial patterns as function of the distance to the drain play an important role in the N dynamics, due to the effect of the curved phreatic surface. In field experiments and simulations these patterns should be considered.

Nitrogen balances

Table 6.2 shows that in the 4-year crop rotation period from spring 1992 until spring 1996 a total N amount of 440 kg ha^{-1} fertiliser was applied and that 111 kg ha^{-1} leached. The N leaching of about 25% of the applied N fertiliser is a substantial component of the N balance considered from an agronomical point of view. For the total N balance, N deposition causes an extra N input of $25\text{-}40 \text{ kg ha}^{-1} \text{ yr}^{-1}$ at the soil surface (Van Faassen et al., 1994; Schröder and Vos, 1996). The N uptake by the crop is generally larger than the amount of N fertiliser applied. However, the N uptake is given for all harvested parts of the crop, i.e. leaves and tuber or grain. Normally, the leaves of for example sugar beet are left on the soil surface and are ploughed into the soil again, returning part of the N to the soil organic matter pool (see Fig. 5.18). The N uptake and yield of the crop were measured on small sample locations throughout the field. These locations were not located at the boundaries of the field or in wheel tracks. Possible yield reductions due to parcel boundaries or compaction of the soil are not considered. So, the yield must be considered as the optimum within the field. As already indicated in Par. 5.7.3, it remains difficult to quantify all terms of the N balance. Denitrification is very likely to occur under wet conditions, especially when the topsoil is still at moderate temperatures and has high NO_3 concentrations. Denitrification was not measured in this study. However, in the next section the relation between hydrological conditions, soil oxygen contents and denitrification will be evaluated. The change in soil organic matter contents and its N contents is another uncertain component in the total N balance. The NO_3 concentration profiles (Fig. 6.13) and the total soil N contents (Table 6.2) indicate that net

6. Field data on water flow and solute transport

mineralisation occurred during the leaching periods. Large increases in NO_3 concentrations and contents occurred especially in the topsoil.

6.6 Spatial patterns of hydrological conditions, soil oxygen contents and denitrification

6.6.1 Introduction

The spatial differences in N contents at various distances from the drain (Par. 6.3) measured on 17 December 1991 suggested that due to patterns in the groundwater levels differences in volumetric water contents and soil oxygen contents could occur, which could lead to spatial differences in denitrification. In this section field measurements carried out in the year 1994 are presented and interpreted to illustrate the mentioned effects. The importance of oxygen availability for soil biological processes has already been discussed in Chapter 5. The relation between oxygen contents and redox conditions will be discussed in Chapter 7 and it will be related to the occurrence of reduced forms of Fe and Mn in the drainage water.

Oxygen transport in soil

Oxygen penetrates from the atmosphere into the soil mainly by diffusion and to a lesser extent by convection. The macroscopic oxygen diffusion coefficient of the soil becomes smaller at increasing water contents. Oxygen can be consumed by soil organisms, plant roots and chemical reactions. When oxygen is respired by soil organisms, oxygen consumption depends on the availability of organic matter, the prevailing soil temperature, and other a-biotic conditions. In soil the transport of oxygen through larger pores, cracks or old root channels, can be of major importance. Oxygen can easily diffuse into these pores and then diffuse into the smaller aggregates. Rappoldt (1992) described diffusion processes in aggregated soils, assuming air at atmospheric oxygen contents in the macro-pores around aggregates of various dimensions. He showed that diffusion processes can be described with simple equivalent model soil systems in which the distribution of distances to the nearest macro-pore is the same as in the

actual soil. However, it remains difficult to characterise the soil structure with its macro-pores and soil aggregates as well as the distribution of the oxygen consumption, which corresponds to the locations of organic matter. To get an impression of the macroscopic oxygen distribution in the field, it was decided to measure the oxygen profiles (Par. 3.1.3) directly in the field.

Denitrification

Denitrification is the process which reduces NO_3^- into other nitrogen components. Denitrification in soil is predominantly an anaerobic biological process and occurs when the availability of oxygen is limited. Denitrifying micro-organisms need organic matter as an energy and food source. During denitrification, intermediate products are formed, i.e. nitrous oxide (NO_2) and dinitrous oxide (N_2O). Dinitrous oxide is a gas and can escape to the atmosphere. It is a greenhouse gas with a 200-times larger radiation absorbing capacity than CO_2 (Van der Gon and Swart, 1990). The low N_2O concentration of about 300 ppb still contributes substantially to the greenhouse effect. In the atmosphere N_2O can also be disintegrated into free nitrogen radicals, which break down ozone.

Easily decomposable organic matter, like young plant material and organic manure, is favourable for denitrification in soils (Firestone *et al.*, 1980). The NO_3^- concentration itself has an impact on denitrification. Denitrification increases at increasing NO_3^- concentrations up to about 40 mg l^{-1} (Stanford *et al.*, 1975), resulting in higher fractions of N_2O and a relative reduction of the N_2 production, especially at low pH. The optimal pH range for denitrification is 6-8. The N_2O fraction increases at lower pH. At low pH NO_3^- may be reduced to ammonium (NH_4^+). Denitrification in soils can occur at temperatures ranging from 0-75 °C, with an optimal temperature of 65 °C (Keeney *et al.*, 1979). At lower temperatures the N_2O fraction becomes relatively larger. A growing crop with its active root system can affect denitrification. Due to water uptake the soil becomes drier and oxygen transport is enhanced, and the simultaneous NO_3^- uptake reduces the amount of NO_3^- in the soil. At the same time roots respire oxygen and the organic root exudates and decaying roots can act as a carbon source for micro-organisms.

6.6.2 Hydrological conditions and soil oxygen contents

Field measurements were conducted in the integrated arable farming field in 1994 where spring barley was grown in the period from 14 April to 30 August. Pressure heads, groundwater levels (Par. 3.1.1) and soil oxygen contents (Par. 3.1.3) were measured at 95, 98 and 19 different times, respectively. TDR volumetric water contents (Par. 3.1.2) were measured on an hourly basis. However, daily averaged TDR volumetric water contents were used for making contour plots. For the contour plots (Fig. 6.20) linear interpolation was used for the time intervals between the measurements. The data are presented for only one side of the drain. The measurements at the same distance from the drain at the other side of the drain were taken, when data were missing or when the number of instruments at the other side of the drain was larger, i.e. in case of the soil oxygen measurements. It was assumed that the conditions at both sides of the drain were similar. Figure 6.20 gives an overview of precipitation rates, groundwater levels, pressure heads, volumetric water contents and soil oxygen contents at different depths as a function of the distance from the drain during 1994. The temporal variation in all quantities is large. The contour plot of groundwater levels shows the curved phreatic surface under wet conditions. A similar pattern is present in the pressure head data, especially at larger depths. The pressure heads show that the drier periods mainly occur in the growing season from April to August. Then, the spatial differences as a function of the distance from the drain are small, because the phreatic surface is deep and flat. At equilibrium with a flat phreatic surface, pressure heads at a given depth will show little variation but the corresponding water contents will reflect the variability of the soil. Local I soil properties around the TDR sensors are also variable, which means that changes in volumetric water contents are easier to measure than absolute water contents (Par. 3.2.4).

A special period occurred around mid February 1994 (Fig. 6.20), when the topsoil was frozen. The TDR measured volumetric water contents were estimated to be very low, because the relative dielectric permittivities were low in this period. No special calibration was performed in the temperature range around 0 °C (cf. Van Loon, 1991). So, the calculated low volumetric water contents are merely an indication of ice. Low oxygen contents were measured at 10 cm depth at 0 m distance from the drain, while at larger depths the oxygen contents were higher. The oxygen chamber at 10 cm depth was probably surrounded by frozen

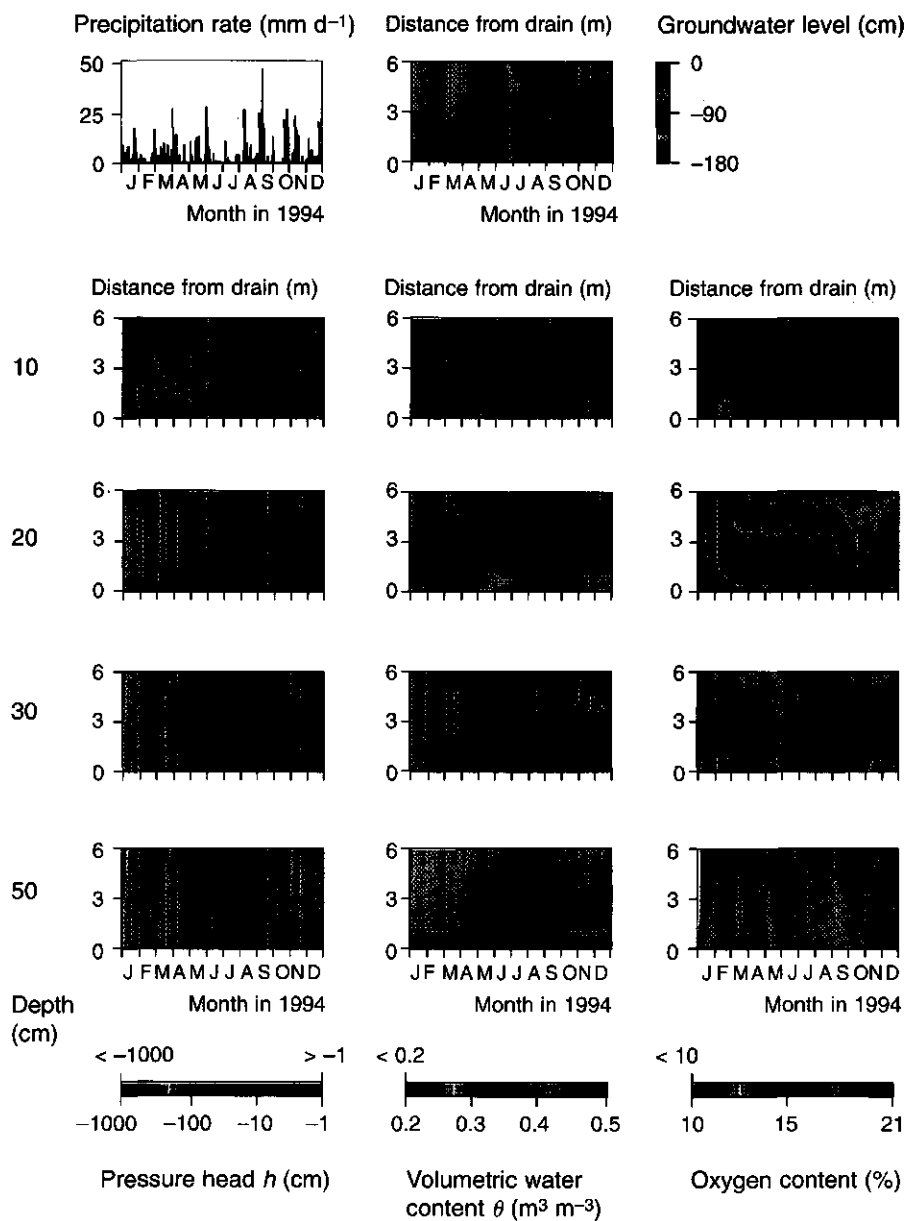


Figure 6.20 Precipitation rate, groundwater level, pressure heads (logarithmic scale), volumetric water contents and oxygen contents of the integrated arable farming field in 1994. The top contour plot shows the groundwater levels as function of the distance to the drain. The bottom contour plots show the oxygen contents, pressure heads, volumetric water contents and oxygen contents at different depths as a function of the distance from the drain.

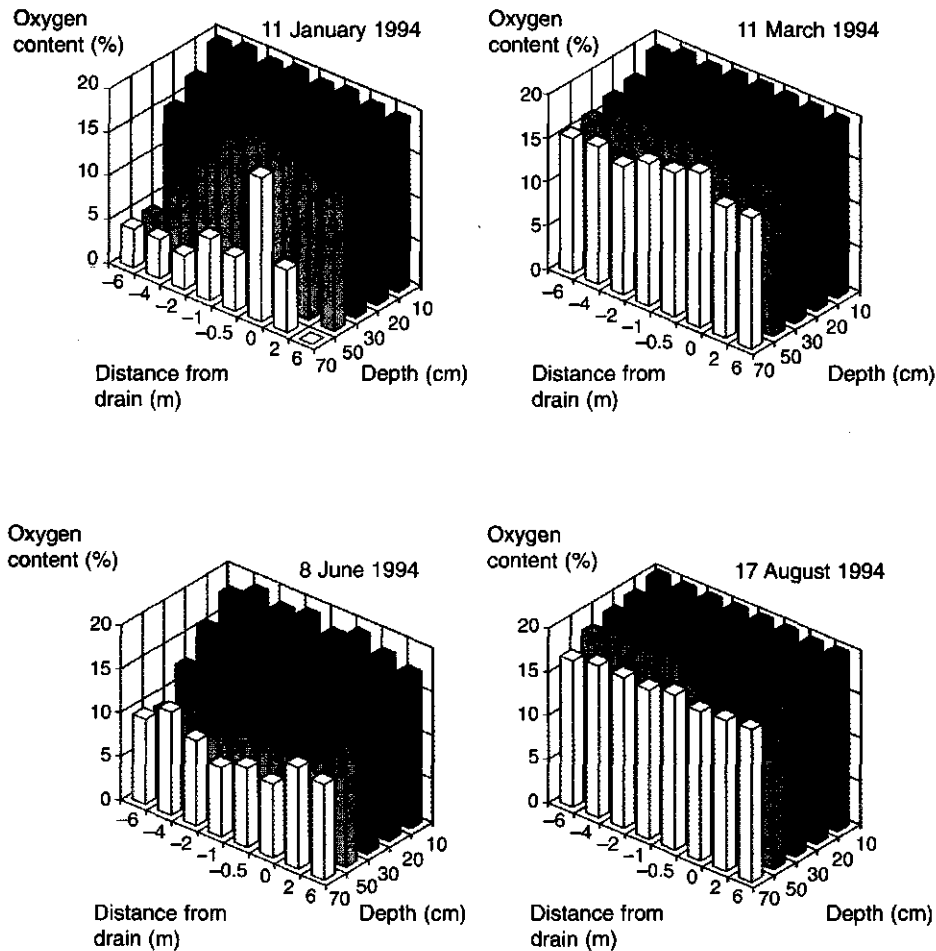


Figure 6.21 Measured oxygen contents of the integrated arable farming field at various dates throughout 1994 as functions of depth and distance from the drain. Note that the measurements are presented at equidistant distances, which means that the scales of depth and distance from the drain do not represent the real dimensions.

soil and had no connection to the atmosphere by one or more macro-pores. The capillary rise of water from the subsoil to the frozen topsoil might have increased the air content in the deeper layers. Due to diffusion of oxygen in newly formed cracks and the low biological activity in this winter period, oxygen contents in the deeper layers could become higher than those in the topsoil. Similar oxygen distributions during frost periods were measured by Rappoldt (1995) in the grass field at the meteorological station of the Lovinkhoeve.

Figure 6.21 illustrates the spatial distribution of the oxygen contents at both sides of the drain on four characteristic days during the year 1994.

On 11 January 1994 the curved phreatic surface had a distinct influence on the oxygen contents, with high oxygen contents in the topsoil and low oxygen contents at larger depths, with a clear dependence on the distance from the drain. The oxygen profiles were not entirely similar at both sides of the drain.

On 11 March 1994 the curved phreatic surface was deeper and oxygen contents ranged from 15-20% at all measurement depths. Due to the low soil temperatures on this day it can be expected that the biological activity was low, resulting in small respiration rates.

On 8 June 1994 the phreatic surface was curved and the oxygen contents decreased from about 20% close to the soil surface to 10% at 70 cm depth. No effect of distance to the drain could be observed. The biological activity might be expected to be high, due to the high soil temperatures and the presence of a growing crop.

On 19 August 1994 the oxygen contents were high, ranging from 17-20%, at all measurement depths, which indicates that the penetration of oxygen is deep. The oxygen consumption might still be expected to be high due to the high soil temperatures and the high biological activity corresponding to the barley crop with roots starting to decay. However, due to the dry conditions oxygen can easily penetrate to a large depth as a result of the high macroscopic oxygen diffusion coefficients and the presence of macro-pores.

At all four dates (Fig. 6.21) the oxygen content at 20 cm depth at 2 m distance from the drain was substantially lower than the surrounding oxygen contents. A similar behaviour can be seen at 20 cm depth at -2 m distance from the drain. These lower oxygen contents indicate a high local respiration rate or a locally low diffusion coefficient around the oxygen chambers. More detailed measurements would have been necessary to discriminate between these causes.

6.6.3 Discussion

Denitrification at the Lovinkhoeve

In all seasons denitrification will occur under wet conditions. The spatial patterns in oxygen contents will influence the denitrification patterns. So, the highest denitrification rates are expected at the wettest positions midway between the drains. Indeed, Rappoldt *et al.* (1995) showed that underneath the grass field of the meteorological station Lovinkhoeve under wet conditions N_2O losses can be an order of magnitude larger midway between the drains than above the drain. Denitrification resulted in maximum measured N loss rates of $6 \text{ kg ha}^{-1} \text{ d}^{-1}$. In this experiment the conditions for denitrification were optimal. The temperature in the topsoil was about 25°C , with apparently sufficient organic carbon available in the root zone of the grassland, and with high NO_3^- concentrations and low oxygen contents due to the shallow phreatic surface. Denitrification occurred at macroscopic oxygen contents ranging from 9 to 20%. These relatively high macroscopic oxygen contents correspond with the macroscopic length scale of the soil oxygen chambers and the O_2 contents can be interpreted as the maximum O_2 content at that depth. Local oxygen concentrations within aggregates will be lower, leading to partial anaerobiosis. The heterogeneous distribution of organic matter, roots, micro-organisms and oxygen in the complex porous soil structure, will result in a heterogeneously distributed denitrification in the soil occurring at the spatial scale of the soil aggregates.

At the Lovinkhoeve the strongly fluctuating phreatic surface has a substantial effect on denitrification under wet conditions. The spatial patterns in oxygen contents are consistent with the shape of the phreatic surface. The pH of about 7.6 (Chapter 7) in the soil is optimal for denitrification and readily decomposable organic matter can be found in the topsoil and to a lesser extent in the subsoil (Van Faassen and Lebbink, 1994). The soil temperatures show well-known seasonal fluctuations. Combining all these factors and assuming sufficient NO_3^- is available, probabilities of the occurrence of denitrification and spatial patterns can be qualitatively predicted for the different seasons of the year. In summer and in autumn the soil temperatures in the topsoil are relatively high, while in autumn the amount of organic material in the topsoil may be high, due to the incorporation of crop residues in the soil after harvest. So, high denitrification rates may be expected in the topsoil under wet conditions in autumn. In summer

there is also a high risk of denitrification, but then the growing crop extracts water from the soil, thus reducing the chance of very wet conditions in the soil as compared to autumn. Also, during the growing season the crop extracts NO_3 and a cover crop in autumn will do the same, reducing the possible level of denitrification. In winter, the soil is relatively wet and soil temperatures are low in the topsoil and moderate at larger depths. Denitrification will be low and will mainly occur at larger depths. In spring the temperatures of the topsoil are increasing and NO_3 can be formed by mineralisation from organic matter. So, denitrification can be expected to be higher in spring than in winter. Corré (1995) presented yearly N losses due to denitrification of about 20 kg N ha^{-1} for a silt loam soil comparable to the Lovinkhoeve.

Water and nutrient management

There are opportunities to influence nutrient uptake by the crop and nutrient losses by water and nutrient management. A distinction should be made between the growing season when the objective is to obtain optimal crop growth with a high nutrient use efficiency, and the leaching period when the soil is often fallow and risks of nutrient losses to the environment are high.

In the growing season the crop needs sufficient water to fulfil the transpiration demand. In dry periods irrigation can be used to reach this. A high soil water content makes nutrients better available for the crop by reducing the solute diffusion coefficient. Also, a sufficiently high water content favours N mineralisation from organic matter. Situations may occur when a crop extracts sufficient water from the relatively wet subsoil, while a nutrient limitation occurs due to dryness in the nutrient-rich topsoil. Irrigation can be a useful tool to increase the nutrient availability under such circumstances.

In a drained soil, the characteristics of the drainage system, like drain depth, and drain distance, have a substantial impact on the hydrological conditions in the soil and on the development of the crop. Van Wijk *et al.* (1988) showed the effect of the depth of the phreatic surface for a given N fertiliser application on crop yield. In general, wet conditions have a larger effect on crop yield than drier conditions. A deeper phreatic surface results in a higher yield, until a depth is reached when the water availability for the crop decreases. The effect of the hydrological conditions on crop yield may be explained by changes in N mineralisation, denitrification and N availability for the crop. However, for judging sustainable arable farming systems, information on the inputs of organic matter

6. Field data on water flow and solute transport

should be taken into account also.

In the winter leaching period Skaggs and Gilliam (1981) used controlled drainage in North Carolina (USA). Raising the outlets of the drains resulted in shallower phreatic surfaces. The increased denitrification resulted in lower NO_3 concentrations and in a smaller NO_3 leaching. Deal *et al.* (1986) reported reductions of 34% in NO_3 leaching. Controlled drainage shifts the N losses from NO_3 leaching to denitrification. By keeping the soil water contents rather high, a relatively large part of the denitrification will result in the production of N_2 , which is environmentally preferable over N_2O . However, by raising the phreatic surface the capacity of the soil to store extra infiltrating water decreases. So, after a heavy rainfall ponding and run-off can occur, with negative environmental effects by direct nutrient and sediment transport to surface waters. Under wetter conditions the topsoil is more sensitive to slaking, compaction by soil traffic, and the growing of cover crops and winter crops can become troublesome. In the growing season subsurface irrigation through drains can be used to increase crop yields. However, the possibilities of subsurface irrigation strongly depend on capillary rise in the soil profile and the presence of an impermeable subsoil which prevents downward seepage of the irrigation water. It is difficult to influence the conditions in the topsoil with subsurface irrigation when using the original drains, normally installed at about 100 cm depth.

Subsurface drains result in spatial patterns in hydrological conditions, especially under wet conditions. Differences in N losses in the field can result in differences in N availability for the crop. The a-priori information about these spatial patterns can be used in attempts to optimise the distribution of the N fertiliser over the field. One can choose to apply more fertiliser at positions where high losses are expected and aim for a uniform crop development. One can choose to apply less N fertiliser at these positions and aim for lower N losses and a non-uniform crop development over the field. These considerations are especially relevant at reduced N fertiliser application rates when a strong crop response to N fertilisation is expected. The field data showed spatial differences in N amounts of 10-30 kg ha^{-1} in the 0-100 cm depth soil layer.

6.7 Bromide tracer experiment 1994-1995

A bromide (Br) tracer experiment was conducted to evaluate whether lateral water flow and solute transport occurred in the topsoil and to measure the breakthrough curve of Br in the drain. After the application of bromide on the soil surface, Br concentrations were monitored continuously in the drainage water and were measured in the soil profile at three points in time. The experimental results will be used to gain insight into the field scale transport processes and to evaluate the possibility to simulate these processes with a two-dimensional solute transport model based on the convection-dispersion equation (Chapter 8).

6.7.1 Bromide application, sampling and analysis

Bromide application

On 17 November 1994 ($t = 1067$ d) a NaBr solution with a high Br concentration of $10\,000\text{ mg l}^{-1}$ was applied on a 2-m wide strip at 4-6 m distances, on both sides of experimental drain 27 (see Fig. 6.23a). The solution was sprayed on the soil surface, using the precision nozzles of a tractor-mounted herbicide sprayer. The application was split into three smaller applications to ensure a uniform distribution of Br on the strips. A Br amount of 87.9 kg ha^{-1} was applied on the strips, which corresponds with an average Br amount of 29.3 kg ha^{-1} for the entire experimental field. The Br application resulted in 1.1 mm of extra water applied to the soil surface of the strip.

Sampling strategy

The Br concentration in the drainage water was measured in every 10th sample, corresponding with 5 mm discharge. At peak drain discharge rates extra drainage water samples were analysed.

Soil sampling was conducted on three dates: 22 December 1994 ($t = 1102$ d), 23 March 1995 ($t = 1193$ d), and 25 July 1995 ($t = 1317$ d). The soil samples were taken in 15 rows parallel to the drain. The first date was chosen after a period with high precipitation rates and corresponding shallow groundwater levels. Under these conditions lateral water flow and Br transport could have occurred in the topsoil. Because most of the Br was still expected to be in the topsoil, the soil in the 0-50 cm depth range was sampled at 5 cm depth

6. Field data on water flow and solute transport

intervals and the soil in the 50-100 cm depth range was sampled at 25 cm depth intervals. On the later sampling dates 10-cm depth intervals were sampled to 100 cm depth. The second sampling date, 23 March 1995, was in spring just before the application of the nitrogen fertiliser. The third sampling date, 25 July 1995, was chosen in the growing season after drainage had ceased.

Bromide extraction and analysis

Bromide concentrations were measured in drainage water samples and in water extracted from soil samples. Drainage water samples were filtered in a centrifuge (0.48 µm, 3000 rpm) before the samples could be analysed using High Performance Liquid Chromatography (HPLC). Distilled water (440 ml) was added to moist soil (175 gr) taken from mixed samples. The water content of the samples was measured in the remaining soil. After a minimum shaking time of 2 hours, the soil-water solution was filtered in a centrifuge (0.48 µm, 3000 rpm) and the Br concentration was measured in the extract using the HPLC method. When the Br concentrations in the extract became smaller than 2 mg l^{-1} , the extract was concentrated by putting the extract in a stove. Evaporation of part of the water resulted in a 5-7 fold increase in the Br concentration.

The Br concentration in the filtered extract was determined with the HPLC method, using a special column to separate Br from NO_3 and NO_2 (Hamminga, pers. comm.; Harmsen, 1986). A UV-detector (205 nm) measured the concentration of the fluid in the column. Bromide standards were used to calibrate the column; the level of detection was 0.5 mg l^{-1} . The HPLC method is a precise but time-consuming method to measure Br concentrations.

6.7.2 Bromide concentrations in the drainage water

Figure 6.22 shows precipitation rate, groundwater level, drain discharge rate and Br concentration in the drainage water for the leaching period 1 November 1994 ($t = 1051 \text{ d}$) to 27 August 1995 ($t = 1352 \text{ d}$). The Br concentration in the drainage water remained low and close to the detection limit until $t = 1140 \text{ d}$. At $t = 1140 \text{ d}$ the Br breakthrough in the drain started and Br concentrations increased to 5 mg l^{-1} around $t = 1200 \text{ d}$. The variations in Br concentrations on a time scale of days are small. However, at peak discharge rates the Br concentration has local minima. For $t > 1285 \text{ d}$ the drain did no longer discharge

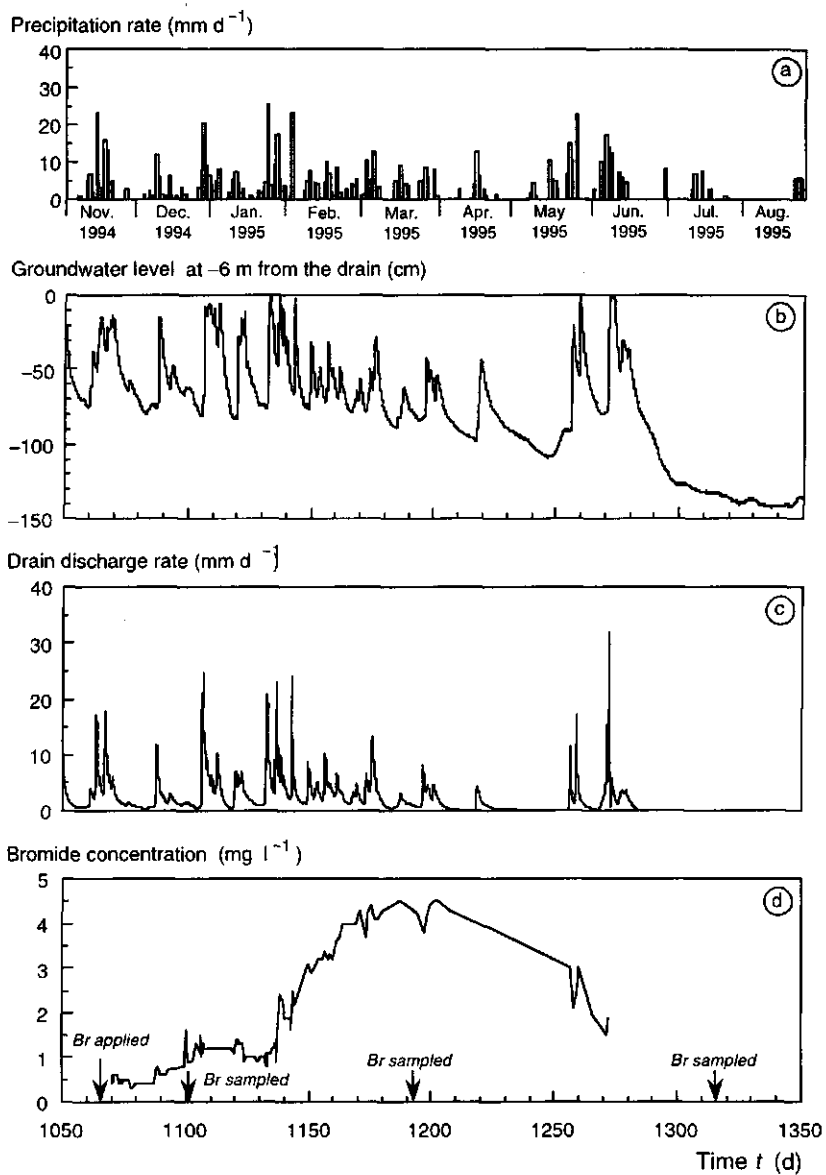


Figure 6.22 Precipitation rate (a), groundwater level at -6 m from the drain 27 (b), drain discharge rate (c) and bromide concentration in the drainage water (d), during the leaching period from 31 October 1994 ($t = 1050 \text{ d}$) to 27 August 1995 ($t = 1350 \text{ d}$).

6. Field data on water flow and solute transport

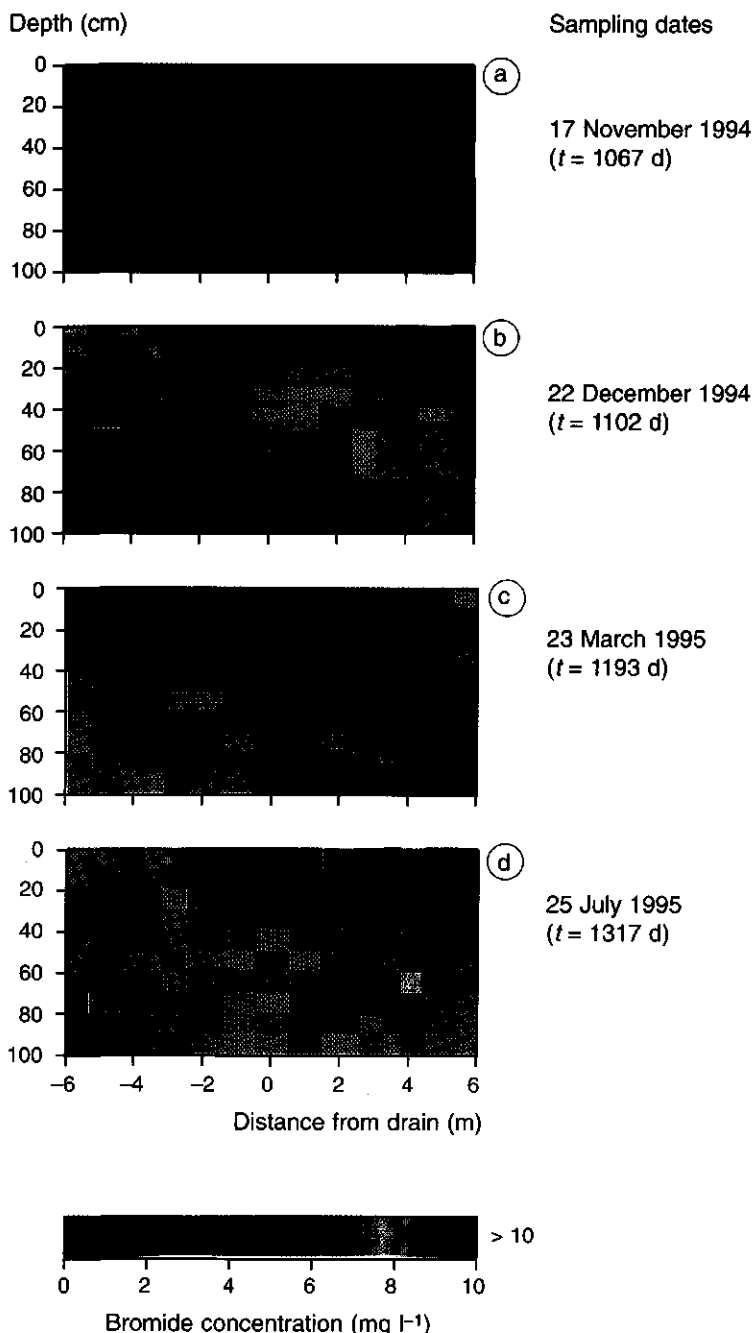


Figure 6.23 Bromide concentrations in the soil water at different soil depths as a function of the distance from the drain, at four dates during the tracer experiment.

water due to water consumption by the potato crop in the following growing season and the very dry winter 1995-1996 afterwards. In fact, drain discharge did not resume until the autumn of 1996. The Br discharge was 0.3 kg ha^{-1} from 17 November 1994 to 22 December 1994; 7.8 kg ha^{-1} from 22 December 1994 to 23 March 1995; and 3.1 kg ha^{-1} from 23 March 1995 to 25 July 1995, which corresponds with 1, 26.6 and 10.6 % of the applied Br, respectively. So, for the entire period 11.2 kg ha^{-1} (38.2%) Br was discharged. It appears that data collection should have been continued, although the Br uptake by the crop would have complicated the interpretation of the data even more.

6.7.3 Bromide concentrations in soil water

Figure 6.23a shows the initial $10\,000 \text{ mg l}^{-1}$ Br concentration in the topsoil after application on 17 November 1994 ($t = 1067 \text{ d}$).

Figure 6.23b shows the Br concentration distribution measured on 22 December 1994 ($t = 1102 \text{ d}$). In the period between 17 November 1994 and 22 December 1994 the cumulative precipitation was 62 mm. Figure 6.22b shows that in that period groundwater levels were shallow. The highest Br concentrations were found in the 0-50 cm depth layer below the strip where Br was applied. The Br concentrations of $2\text{-}10 \text{ mg l}^{-1}$ at 20-50 cm depth at -4 to -2 m and -0.5 to 4 m distance from the drain indicate lateral Br transport in the topsoil. Bromide concentrations up to 10 mg l^{-1} were found in rather erratic distribution patterns in the subsoil to 100 cm depth. The Br amount in the entire soil profile to 100 cm depth was 20 kg ha^{-1} , which is 68% of the applied Br.

Figure 6.23c shows the Br concentration distribution on 23 March 1995 ($t = 1193 \text{ d}$). In the period between 22 December 1994 and 23 March 1995 the cumulative precipitation was 325 mm. Most of the Br is vertically transported to depths between 50 and 100 cm, with the maximum Br concentration still below the strips where the Br was applied. Lateral Br movement resulted in Br concentrations of $2\text{-}10 \text{ mg l}^{-1}$ at 50-90 cm depth at -4 to -0.5 m and -1.5 to 4 m distance from the drain. In the 0-10 cm depth topsoil at 4 to 6 m distance from the drain an isolated Br concentration peak was located. The Br amount in the entire soil profile to 100 cm depth was 11.7 kg ha^{-1} , which is 38% of the applied Br.

6. Field data on water flow and solute transport

Figure 6.23d shows the Br concentration distribution on 25 July 1995 ($t = 1317$ d). In the period between 23 March 1995 and 25 July 1995 the cumulative precipitation was 254 mm. In the topsoil, between 0 and 40 cm depth, the Br concentration was relatively high, especially at -4 to 4 m distance from the drain. The dry period between June 1995 and July 1995 resulted in capillary rise of water and bromide from the deeper layers to the topsoil and an increase in the Br concentration at the soil surface was caused by soil evaporation and transpiration of water. On 25 July 1995, the Br concentration at depths larger than 50 cm became smaller than the Br concentrations at the same locations on 23 March 1995. However, the local maxima at 60-70 cm depth at -5.5 to -4.0 m and 4.0 to 5.5 m distance from the drain persisted. The Br amount in the entire soil profile to 100 cm depth was 14.4 kg ha^{-1} , which is 49 % of the applied Br.

6.7.4 Discussion

Breakthrough of Br in the drainage water occurred already after 100 mm of cumulative precipitation. The Br concentration distribution in the soil profile on 22 December 1994 ($t = 1102$ d, Fig 6.23b) indicates rapid vertical and horizontal Br transport towards the drain. Especially the rapid vertical transport to 75-100 cm depth must be caused by flow through macro-pores. The period of heavy rainfall just after the application of the Br tracer saturated nearly the entire soil profile and enhanced the possibility of this type of flow. The Br concentration distribution on 23 March 1995 ($t = 1193$ d, Fig. 6.23c) shows that Br is transported laterally from the zone with high Br concentrations below the strip where Br was applied towards the drain. The Br concentration on 25 July 1995 indicates that a redistribution of Br occurred which resulted in an increase of Br in the topsoil and a decrease of Br at greater depths. The Br concentrations in the drainage water and in the soil water around the drain at the sampling dates should be in agreement. On 22 December 1994 both the Br concentrations in the soil water (0.2 mg l^{-1}) and in the drainage water (1.5 mg l^{-1}) were low. On 23 March 1995 the Br concentrations were 0.2 mg l^{-1} in the soil water and 4.5 mg l^{-1} in the drainage water, which shows a discrepancy. However, at a small distance from the drain Br concentrations were higher; soil water at -2 to -0.5 m from the drain had Br concentrations in the 2.5 mg l^{-1} range. On 25 July 1995 the Br concentrations of 2.5 mg l^{-1} around the drain corresponded well with the 2.5

mg l⁻¹ concentration in the last drain water sample on 10 July 1995.

The local minima in the Br concentration in the drainage water at peak discharge rates could result from two possible phenomena. Firstly, when the phreatic surface rises during wet periods the macro-pores will transport water with a Br concentration which is nearly in equilibrium with the surrounding soil matrix. When the water flux densities increase, freshly infiltrated water can flow rapidly through the macro-pores without reaching an equilibrium with the surrounding soil matrix, resulting in lower Br concentrations. Secondly, the flow pattern will change during wet periods. More drainage water is originating from the zones just above the drain and the topsoil, which have relatively low Br concentrations, at least on 23 March 1995.

Some remarks can be made on the accuracy of the Br concentrations in the soil water. Bromide concentrations were measured in relatively small soil samples of about 100 ml. These 100-ml samples were obtained by mixing 5 individual 20-ml samples to average out some of the field scale variation. On the three sampling dates only 68%, 38% and 49% of the applied Br was found in the soil profile to 100 cm depth. The drainage data show that the remaining part had not yet discharged entirely. On 25 July 1995 3.2 kg ha⁻¹ more Br was found in the soil profile than on 23 March 1995. This, together with the missing 31, 34, 13% Br on the three sampling dates, indicates that a substantial part of the Br may have been transported to depths larger than 100 cm. However, the uncertainties in the Br mass balance suggest that the soil samples are not representative for the entire soil profile. Ideally, larger soil samples, i.e. 10 cm diameter, to a depth of 150 cm should have been used, including a statistical analysis of the effect of the variation of the Br concentration between the individual samples on the Br mass balance calculations. However, taking larger samples would have disturbed the small experimental field too drastically, and the Br analysis capacity limited the number of samples to be analysed.

The Br solution was applied exactly at the 4-6 m strips of the experimental field. No Br was applied at larger distances from the experimental drain. A part of the applied Br may have been transported to the adjacent drains because the position of the water divide was not exactly midway between the drains and due to lateral dispersion of Br close to the water divide. Indeed, the Br concentration distribution on 25 July 1995 (Fig. 6.23d) shows a substantial difference in Br concentrations at both sides of the drain. The Br concentrations are relatively high at positive locations from the drain and relatively low at negative locations

6. Field data on water flow and solute transport

from the drain, suggesting that a part of the Br may have been transported to distances larger than 6 m. This may explain the less than 100% recovery of Br in the soil samples.

The average bulk densities for each 10 cm depth interval were used in the Br mass balance calculation. These can differ from the actual density of the soil sample. Together with the relatively low accuracy of Br concentration measurements at the lower end of the detection scale of the HPLC method (0-2 mg l⁻¹) this may result in an uncertainty in the Br mass balance of 10-30%.

Despite the uncertainties in the interpretation of the Br data, it is evident that the high Br concentrations measured at 50-100 cm depths after a relatively small amount of precipitation show the rapid vertical Br transport. On 23 March 1995 most of the Br was transported about 50 cm downwards and the lateral spreading shows the effect of the horizontal flow components. The Br concentration distribution is not symmetrical with respect to a vertical plane through the drain, but the Br patterns are rather similar at both sides of the drain. Qualitatively, the Br concentrations in the soil water give important information on the solute transport mechanism. The Br concentrations in the drainage water quantify the average effect of the field scale transport processes more accurately than the Br concentrations measured in the soil profile.

6.8 Conclusions

Nitrate leaching was monitored on an integrated arable farming plot with reduced N fertiliser application. The soil profile at the Lovinkhoeve can be considered nearly impermeable at 120 cm depth. There is a small downward seepage of about 0.04-0.22 mm d⁻¹. This is an ideal situation for monitoring NO₃ leaching, because all NO₃ leached is discharged by the subsurface drain. The discharge is a spatial average of the NO₃ leached from the whole catchment above the drain. In the 4-year crop rotation period 1992-1996 a total N amount of 440 kg ha⁻¹ fertiliser was applied and a total N amount of 111 kg ha⁻¹ leached. Nitrogen (N) leaching varied over the years, depending on the meteorological conditions, between 0 and 50 kg ha⁻¹ yr⁻¹. High NO₃ concentrations in the drainage water were often measured during wet periods with shallow phreatic surfaces. However, yearly averaged NO₃ concentrations remained always

smaller than 50 mg l^{-1} . A flow proportional drainage water sampling method has to be used to measure NO_3 leaching accurately. Errors of about 25% can occur when NO_3 concentrations in the drainage water measurements at 30-day intervals are used to estimate cumulative N leaching. Measurements of NO_3 concentrations in the groundwater at e.g. 100 cm depth cannot be used to estimate N leaching, because drainage water does only partly originate from this groundwater.

Field data of the groundwater level - drain discharge rate relationship and the magnitude of the NO_3 concentrations in the drainage water comparable to the NO_3 concentrations in the soil profile indicate that due to the larger K_s in the topsoil a substantial part of the drainage water is originating from the topsoil during periods with a shallow phreatic surface. This conclusion is confirmed by the laboratory measurements of K_s . Two-dimensional water flow and nutrient transport, with a large lateral flow component towards the drain in the topsoil, explains the peaks in NO_3 concentrations in the drainage water. Data on chloride concentrations and results of a bromide tracer experiment also indicate the importance of the two-dimensional nature of the transport processes. However, the Br tracer experiment shows that macro-porous flow occurred.

The long-term Cl mass balance showed that all Cl initially present in the 0-120 cm depth soil layer after reclamation in 1942 is discharged. Upward Cl diffusion is estimated at $220 \text{ kg ha}^{-1} \text{ yr}^{-1}$ and is a major term in the Cl mass balance. The Cl mass balance for the period 1981-1991 results in an estimated Cl discharge of $372 \text{ kg ha}^{-1} \text{ yr}^{-1}$.

Field data on NO_3 contents in the soil profile indicate that during the winter leaching periods N mineralisation occurred, resulting in an N increase of 30-50 kg ha^{-1} . Spatial differences in N contents in the soil profile were measured as a function of the distance from the drain. Larger N amounts of 30 kg ha^{-1} were sometimes measured close to the drain. Denitrification was supposed to be the reason for these differences. Later field measurements of groundwater levels, water contents, soil oxygen contents and denitrification at the Lovinkhoeve confirmed and explained the occurrence of these spatial differences in denitrification rates at different distances from the drain. This knowledge combined with irrigation, controlled drainage and a precise application of fertiliser can be applied to optimise nutrient use efficiency and to reduce nutrient losses to the environment.

7. MULTI-COMPONENT SOLUTE TRANSPORT TO A SUBSURFACE DRAIN

7.1 Introduction

To address the problem of monitoring and modelling both reactive and non-reactive (conservative) solute transport in porous media, studies have been conducted at various spatial scales, e.g., column, field, and catchment scales. Non-reactive solutes have been used in a number of field-scale transport studies to focus on transport spatial variability, attributable mostly to soil physical properties, e.g., solute dispersion due to non-uniform distributions of fluid velocities. For example, Biggar and Nielsen (1976), Butters *et al.* (1989), and Butters and Jury (1989) demonstrated the heterogeneity of bromide (Br) breakthrough at different soil depths. Snow *et al.* (1994) concluded from lysimeter and field studies that chloride (Cl) and bromide transport were affected by local variations of solute transport properties near the soil surface, but were relatively unaffected by soil textural and structural changes between deeper soil horizons. Owens and Edwards (1992) found that Br transport to groundwater at the watershed scale depended on hydrological features such as lateral flow. These field-scale studies indicate the complexity of solute transport in soils, even when considering only a limited number of non-reactive solutes.

Addressing field-scale transport of more reactive solutes, Bjerg *et al.* (1993) and Bjerg and Christensen (1993) used chemical equilibrium modelling to describe breakthrough of solute pulses added to groundwater aquifers. They found that cation exchange processes reduced transport velocities of cations and anions in proportion to their affinities for the exchanger phase, i.e., divalent cations > monovalent cations > anions. Salama *et al.* (1993) monitored changes in groundwater and surface water qualities at the catchment scale, and noted that soil weathering processes affected solute transport. Linden *et al.* (1984) measured long-term trends of N, P, K, Na, and Cl transport within soil profiles and in groundwater under field plots with different crops and receiving municipal wastewater treatments. Differences in transport between these components depended on rate of surface application, crop uptake patterns, sorption, microbial processes, and soil structure. In addition to the role of water flow in solute transport, these studies emphasise the additional influence of chemical reaction

processes.

Transport models for reactive soil solutes were also developed. For example, Schweich *et al.* (1993a, b) used chemical equilibrium modelling to predict solute concentration waves in exchanging porous media in the presence or absence of precipitation and dissolution reactions. Gaston *et al.* (1993) coupled exchange equilibria and solute transport models to describe cation breakthrough curves for soil columns. Coupled chemical equilibrium transport models were used for performing scenario calculations of multiple, reactive component transport in soil or groundwater aquifers (Hesterberg *et al.*, 1994; Walter *et al.*, 1994). Such models should simulate the most important processes affecting the system, quantify these processes and their interactions, and be evaluated against field data.

The objectives of the present study are to provide a data set of multi-component chemical discharge from a subsurface drain and to determine the types of soil chemical processes that most strongly affect transport of these components at the study site, e.g. redox reactions, precipitation and dissolution, and cation exchange. Details of the experimental plot (Par. 6.2, Fig. 6.1), a flow-proportional drainage water sampling system (Par. 3.1.4), hydrological instrumentation (Par. 3.1), horizon boundaries (Par. 4.1.2), and some soil physical (Par. 4.2) and chemical properties (Par. 4.1.2) have already been discussed. This chapter presents results for the leaching period 1991-1992 ($0 < t < 150$ d). Chapter 6 showed already that in this period dissolved NO_3 and Cl concentrations in the drainage water varied with the drain discharge rate and showed opposite trends. These trends were related to differences in the initial distribution of these components in the soil profile and the relative contributions of water from subsurface and surface soil horizons. Thus, the chemical data contributed to the interpretation of soil physical and hydrological results. This work is extended here to include the balance of major ionic constituents in the soil solution. By combining soil physical and chemical data, results of these studies would ultimately assist in selecting, further developing, and testing solute transport models for this field situation.

7.2 Soil chemical methods

Soil mineralogy

Phyllosilicate mineralogy was determined on clay samples from each soil horizon between 0 and 109 cm depth. Soil samples were dispersed by sonifying in a 0.001 mol l⁻¹ solution of Na₂CO₃ (pH 10), and then fractionated by gravitational sedimentation (Gee and Bauder, 1986). X-ray diffraction analyses using unresolved CuK α radiation were performed on oriented clay samples prepared by smearing K- and Mg-saturated pastes onto glass slides, and then subjecting the samples to standard diagnostic pre-treatments (Whittig and Allardice, 1986). Proportions of various clay minerals were estimated by determining the fractional area of a given diagnostic diffraction peak relative to the sum of diagnostic peak areas. The *d*-spacings of diagnostic peaks used were (Whittig and Allardice, 1986; Dixon and Weed, 1989):

- i) Mg-ethylene glycol treated sample, 1.6-1.8 nm (smectite);
- ii) K-350 °C heated sample, 1.4-1.2 nm (hydroxy-interlayered 2:1-layer silicates);
- iii) K-350 °C heated sample, 0.7 nm (kaolinite, assuming negligible contribution of an 002 peak from hydroxy-interlayered minerals);
- iv) Mg-air dried sample, 1.0 nm (mica);
- v) Difference between 1.0 nm peak areas between K-air dried and Mg-air dried samples (vermiculite).

Soil carbonate was characterised using X-ray diffraction analysis of soil powder mounts of samples from horizons down to 83 cm depth. Citrate-bicarbonate-dithionite extractable Fe and Mn were determined on soil samples following the procedure of Jackson *et al.* (1986) and atomic absorption spectrometry. The mineralogical results are presented in Table 7.1.

Drainage water sampling

Results reported in this study are for flow-proportional drainage water samples (see Par. 3.1.4) collected between 17 December 1991 (*t* = 0) and 14 May 1992 (*t* = 150 d) (see Pars. 6.2 and 6.3). Sets of samples collected within several days of automatic sampling were immediately analysed for pH, then stored at 3 °C until additional chemical analyses were completed.

Table 7.1 Clay mineralogy and citrate-bicarbonate-dithionite (CBD) extractable metal concentrations in different genetic horizons of the Lovinkhoeve soil.

Depth interval (cm)	Clay Mineral Proportion*					CBD-extractable Fe (mmol kg ⁻¹)	CBD-extractable Mn (mmol kg ⁻¹)
	S	V	HIV	M	K		
0-36	0.4	0.2	0.2	0.1	0.1	90 ± 7	8.37 ± 0.04
36-46	0.5	0.1	0.2	0.1	0.1	82 ± 5	7.1 ± 0.3
46-64	0.5	0.1	0.2	0.1	0.1	93 ± 1	7.9 ± 0.8
64-83	0.5	0.0	0.2	0.2	0.1	101 ± 2	7.3 ± 0.6
83-109	0.4	0.1	0.1	0.2	0.2	99 ± 2	6.0 ± 0.5

* Approximate proportions of smectite (S), vermiculite (V), hydroxy-interlayered 2:1 phyllosilicates (HIV), mica (M), and kaolinite (K) in the phyllosilicate clay fraction.

Soil extracts

The distribution of cations and anions within the soil profile on 17 December 1991 ($t = 0$) was determined by extracting soil samples. Four sampling locations were randomly chosen within each of eight 1 to 2 m wide experimental sampling blocks representing varying distances in a perpendicular direction from the subsurface drain 27 (Fig. 6.1). Sampling locations within each block were randomly chosen with respect to distance from the field boundary (parallel to the drain) and lateral position within each sampling block (left, centre, or right one-third of the block).

Soil samples were collected at 10 cm depth intervals (0-20 cm for the shallowest samples) using stainless steel soil sampling probes. Moist samples were stored in sealed bags at 3 °C until a sub-sample was taken for moisture content determination and NO_3^- extraction. The remaining sample was dried at 40 °C, then a sub-sample of each dried sample was extracted with a 1 mol l⁻¹ solution of NH_4NO_3 (1:10 w/w, soil:solution) by shaking on a reciprocating shaker for 1 h at 2.5 s⁻¹. Samples were filtered through a non-acid Machery and Nagel MN680M filter paper (Radiometer, Corp., Zoetermeer, The Netherlands) having a 6 µm nominal pore diameter and stored at 3 °C until analysed.

Sample analyses

To monitor suspended particulates in drainage water samples, optical density (OD) at 375 nm wavelength was measured on selected samples using a UV-visible spectrophotometer with a 1 cm sample path length.

Inductively coupled plasma (ICP) spectrometry was used to measure Ca, Mg, Na, K, Fe, Mn, Al, and S in both drainage water samples and filtered soil extract samples. For the extract samples, analytical standards were prepared in a 1 mol $\text{NH}_4\text{NO}_3 \text{ l}^{-1}$ matrix. Bicarbonate in drainage water samples was measured by autotitrating with HNO_3 to the equivalence point at pH 4.5 (Rhoades, 1982). For background correction and quality control, a blank sample consisting of the deionised water used to dilute samples and a standard KHCO_3 solution sample were included in each set of samples analysed. Chloride in the drainage water and in soil extract samples was measured potentiometrically by first adding 2 ml of concentrated HNO_3 , then autotitrating with AgNO_3 (Adriano and Doner, 1982).

Dissolved organic carbon (DOC) in selected drainage water samples was measured using a Shimadzu Model TOC500 carbon analyser (Shimadzu Nederland, 's Hertogenbosch, The Netherlands) using standards of potassium hydrogen phthalate ($\text{KHC}_8\text{H}_4\text{O}_4$). Inorganic carbon was first eliminated by acidifying samples to $\text{pH} < 3.5$ with HNO_3 , then flushing for 15 minutes with high-purity $\text{N}_2(\text{g})$. Samples that contained $< 10 \text{ mg DOC l}^{-1}$ were analysed after a standard addition of 10 mg C l^{-1} of $\text{KHC}_8\text{H}_4\text{O}_4$.

Total and inorganic P measured in drainage water samples were used to calculate organic P by difference (Olsen and Sommers, 1982). After measurements on samples collected early in the study showed that inorganic P was very low (often $< 0.5 \mu\text{mol l}^{-1}$), a standard addition of $6.5 \mu\text{mol P l}^{-1}$ as KH_2PO_4 was included in later samples. Inorganic P was measured using the modified Murphrey-Riley colorimetric method given in Olsen and Sommers (1982). Total P was measured by evaporating 100 ml or less of drainage water sample using a heated sand bath. The sample residue was then digested for 1 h at 100°C in 5 ml of concentrated HNO_3 . After cooling and adding 10 drops of concentrated HClO_4 , the sample was digested for 1 h at 100°C , then heated together with 1 ml of deionised water until the HClO_4 visibly evaporated. Inorganic P was measured after adding water, phenolphthalein (pH indicator), and NaOH to neutralise the sample (Olsen and Sommers, 1982).

7.3 Composition of drainage water and soil chemical processes

Drain discharge rate

The drain discharge rates over the 1991-1992 leaching period were already presented in Par. 6.3. Figure 7.1 shows discharge rates up to $t = 150$ d and denotes times of a number of peak flow events used for reference in discussing drainage water chemistry.

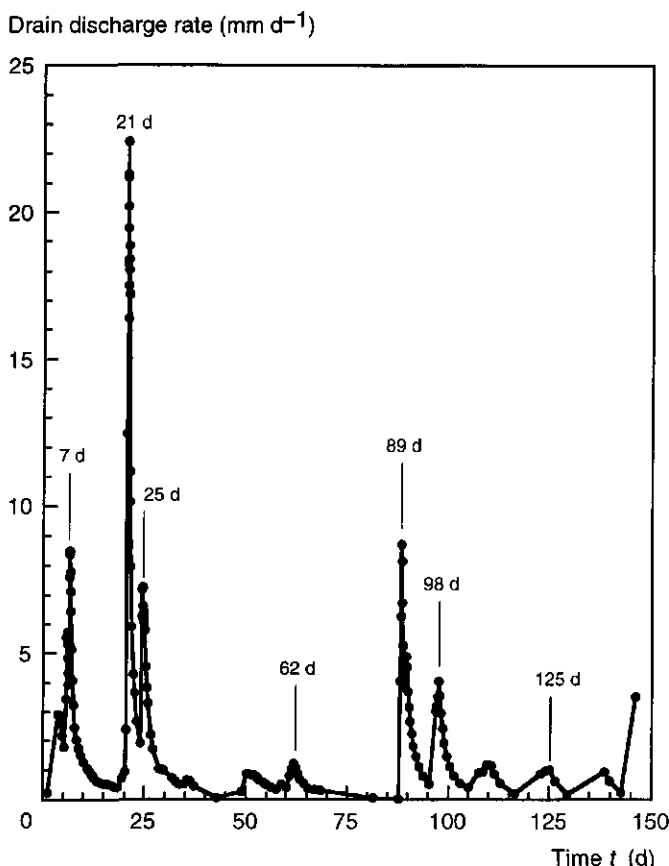


Figure 7.1 Drain discharge rate between 17 December 1991 ($t = 0$) and 14 May 1992 ($t = 150$ d). The peak discharge events presented here are also presented in the Figs. 7.2 to 7.5.

Optical density

Figure 7.2 shows the optical density (OD) measured in drainage water samples of the first 60 days of the leaching period. No measurements were made on subsequent samples. Although OD for these samples varied by a maximum of 0.01, definite peaks corresponded with peak drain discharge rates at $t = 7$, 21, and 25 d (Figs. 7.1 and 7.2). The maximum OD was found at $t = 5.3$ d, which corresponded to the minimum flow rate between peaks at $t = 4$ and 7 d (Fig. 7.1). Changes in OD may result from radiation absorption by organic matter or radiation scattering by suspended particulates (Kumada, 1987; Hiemenz, 1986). However, there were no obvious peak concentrations of DOC (data not presented) corresponding to OD peaks in drainage water samples, and there was no significant correlation ($P = 0.05$) between OD and DOC for data between $t = 0$ and 60 d ($R = 0.14$). This indicates that samples may contain some colloidal material that was not necessarily related to DOC. Light scattering from suspended particles depends on particle concentration and particle size (Hiemenz, 1986), making it difficult to quantify the amounts of particulates present. If the particulates comprised mineral colloids, then these colloids may have contributed significantly to the measured concentrations of chemical components (e.g., Al, Fe, and Mn) in the unfiltered drainage water samples.

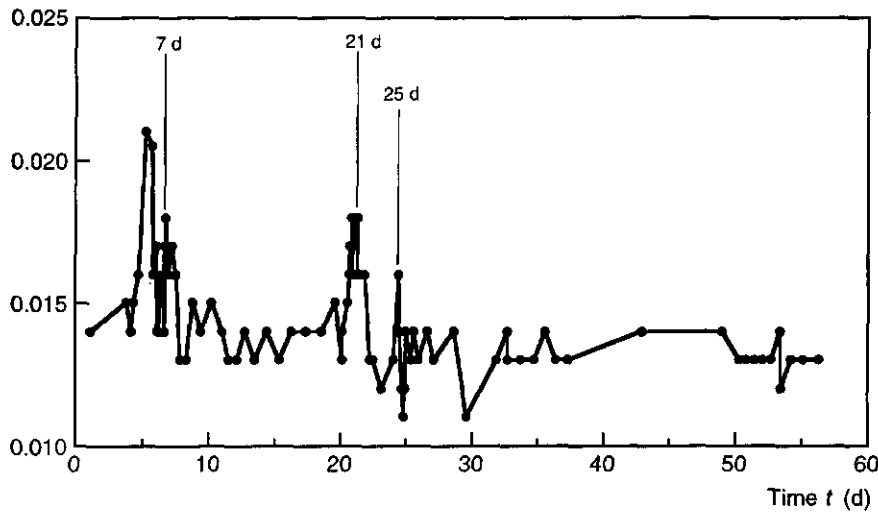
Optical density

Figure 7.2 Optical densities at 375 nm wavelength measured in selected drain discharge samples collected between 17 December 1991 ($t = 0$) and 15 February 1992 ($t = 60$ d).

Ionic balance

To determine the consistency between measured drainage water chemistry and the required condition of solution electroneutrality, an ionic balance for each sample was calculated by summing charge concentrations of the following components: Ca^{2+} , Mg^{2+} , Na^+ , K^+ , Al^{3+} , Fe^{2+} , Mn^{2+} , Cl^- , NO_3^- , HCO_3^- , SO_4^{2-} , PO_4^{3-} , and OH^- . Any charge attributable to DOC was neglected. Data for Cl^- and NO_3^- were taken from Par. 6.3. Reduced forms of Fe and Mn were chosen for samples containing detectable amounts of these components because oxidised soil forms (Fe(III), Mn(IV), and Mn(III)) are very insoluble ($< 10^{-18} \text{ mol l}^{-1}$) at $\text{pH} \geq 7.5$ (Linday, 1979; Adriano, 1986) - see pH data in Fig. 7.4. Sulphate concentrations were assumed to be equivalent to total S. The concentration of OH^- was determined from pH measurements assuming unit activity coefficients. Relative to dissolved macrocomponents, OH , PO_4 , Al , Fe , and Mn had little impact on the ionic balance. Ammonium data were excluded from the ionic balance because measurements were not made on all samples, and available data showed that $[\text{NH}_4]$ was typically very low ($0.014 \pm 0.001 \text{ mmol l}^{-1}$; $n = 76$) relative to most other cations.

Figure 7.3 shows summations of cationic, anionic, and net charge (cationic + anionic charge) determined for drainage water. The true summations of cationic and anionic charge should be mirror images on such a plot, yielding an overall ionic balance of zero. Fluctuations of the net charge about zero in Fig. 7.3 reflect deviations of measured component charge sums from their true values. The overall ionic balance was typically close to zero (mean = $0.1 \pm 1.3 \text{ mmol l}^{-1}$), which reflects the accuracy of sample analyses. The average sums of cationic and anionic charge over the 150-day drainage period were $18.7 \pm 1.6 \text{ mmol l}^{-1}$ and $-18.6 \pm 1.8 \text{ mmol l}^{-1}$, respectively.

The sums of both cationic and anionic charge decreased most noticeably during periods of peak drain discharge at $t = 7$ and $t = 21 \text{ d}$ (Fig. 7.3). In contrast, there was no apparent change in charge sum at $t = 89 \text{ d}$, when the drain discharge rate was second highest for the experimental period (Fig. 7.1). At about $t = 68 \text{ d}$, dissolved component charge decreased (Fig. 7.3) while drain discharge rate was low and essentially constant (Fig. 7.1).

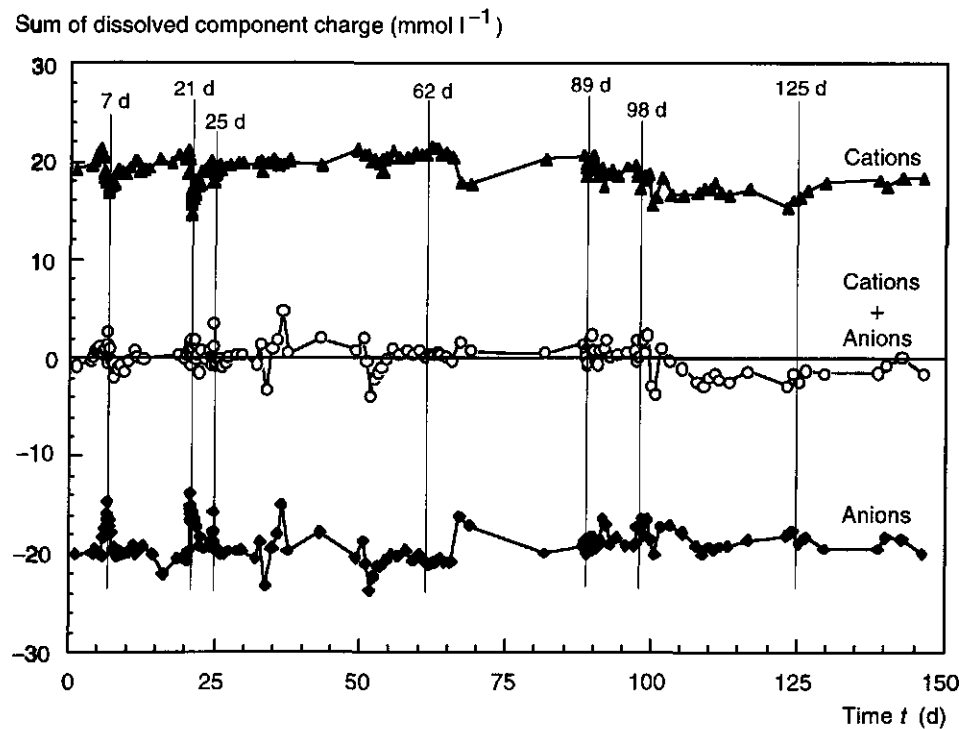


Figure 7.3 Sum of dissolved component charge calculated from chemical analyses of drain discharge samples between 17 December 1991 ($t = 0$) and 14 May 1992 ($t = 150$ d). Sums of cations, anions, and total net charge are shown separately.

pH and Dissolved Organic Carbon

Figure 7.4 shows that the drainage water pH ranged from 7.2 to 8.2 (mean $\text{pH} = 7.8 \pm 0.2$), which is representative of calcareous soils (Lindsay, 1979). The most obvious relationship between pH and drain discharge rate was that the maximum pH coincided with the peak discharge rate at $t = 21$ d (Fig. 7.4).

Measurements of DOC made on selected samples between $t = 0$ and 32 d ($n = 76$) and between $t = 80$ and 100 d ($n = 25$) showed no apparent trends related to discharge rate (data not shown). However, the mean DOC concentration of $13 \pm 2 \text{ mg l}^{-1}$ measured in samples collected between $t = 0$ and 32 d, was significantly ($P = 0.01$) higher than the mean DOC concentration of $6.4 \pm 0.4 \text{ mg l}^{-1}$ measured for the later period.

Manganese, Iron, and Aluminium

Figure 7.4 shows temporal trends in dissolved concentrations of Mn and Fe ($[Mn]$ and $[Fe]$) in drainage water samples. Between $t = 14$ and 21 d, dissolved $[Mn]$ increased steadily and peaked at a concentration of $4.4 \mu\text{mol l}^{-1}$ at $t = 21$ d at the peak in drain discharge rate (Fig. 7.4). During subsequent periods of peak flow, peak Mn concentrations were less striking or absent (e.g., at $t = 62$ or 125 d). For $t > 100$ d, dissolved $[Mn]$ was consistently lower ($\leq 0.03 \mu\text{mol l}^{-1}$) than at earlier times when $[Mn]$ was usually $> 0.1 \mu\text{mol l}^{-1}$. The Fe data (Fig. 7.4) showed very sharp concentration peaks precisely coincident with the peak drain discharge rates at $t = 21$ and 25 d. Concentration peaks also occurred at $t = 34$, 62, and 89 d. Like $[Mn]$, $[Fe]$ was consistently low for $t > 100$ d, despite the occurrence of moderate peaks in drainage flow rate (Fig. 7.4 and Fig. 7.1).

Although soil redox potential was not measured, the elevated levels of dissolved Mn and Fe usually found during periods of peak drain discharge rates (Figs. 7.1 and 7.4), indicated reduced soil conditions. Citrate-bicarbonate-dithionite extracts showed that reducible amounts of soil Fe and Mn (Table 7.1) were well in excess of total Fe and Mn discharged from the drain during this study. Thermodynamics predicts that the solubilities of Mn and Fe in equilibrium with common soil minerals are orders of magnitude lower under oxic conditions than under more reduced conditions, particularly at $\text{pH} \geq 7.2$. For example, thermodynamic data of Lindsay (1979) indicate that at $\text{pH} 7.5$ and at free electron activities (pE) of 10 and 7, the activities of aqueous Mn^{2+} in equilibrium with $\beta\text{-MnO}_2$ (pyrolusite) are 10^{-8} and 10^{-2} , respectively, while the activity of $\text{Mn}^{4+}(\text{aq})$ is 10^{-39} . At $t = 21$ d, dissolved $[Mn]$ and $[Fe]$ in drainage water samples peaked at $10^{-5.4} \text{ mol Mn l}^{-1}$ and $10^{-5.6} \text{ mol Fe l}^{-1}$ (Fig. 7.4). Also, increasing pH between $t = 8$ and 21 d (Fig. 7.4) was consistent with proton consumption accompanying soil reduction (Sposito, 1989). Furthermore, dissolved $[Mn]$ increased earlier than dissolved $[Fe]$ (Fig. 7.4), consistent with the sequence of species reduction expected for neutral soils: O_2 , NO_3^- and NO_2^- , $\text{MnO}_2(\text{s})$, $\text{FeOOH}(\text{s})$, organic matter, and finally SO_4^{2-} (Stumm and Morgan, 1981).

To determine whether elevated $[Mn]$ and $[Fe]$ in drainage water favoured precipitation of rhodochrosite (MnCO_3) or siderite (FeCO_3), ion activity products (IAPs) were determined from closed-system chemical speciation calculations, using GEOCHEM-PC (version 2.0 - Parker *et al.*, 1990; Sposito and Mattigod, 1979) and total dissolved concentrations of Mn, Fe, Ca, Mg, Na, K, HCO_3 , S, Cl, and NO_3 (and pH) in 22 selected samples corresponding to both peak and lower

7. Multi-component solute transport

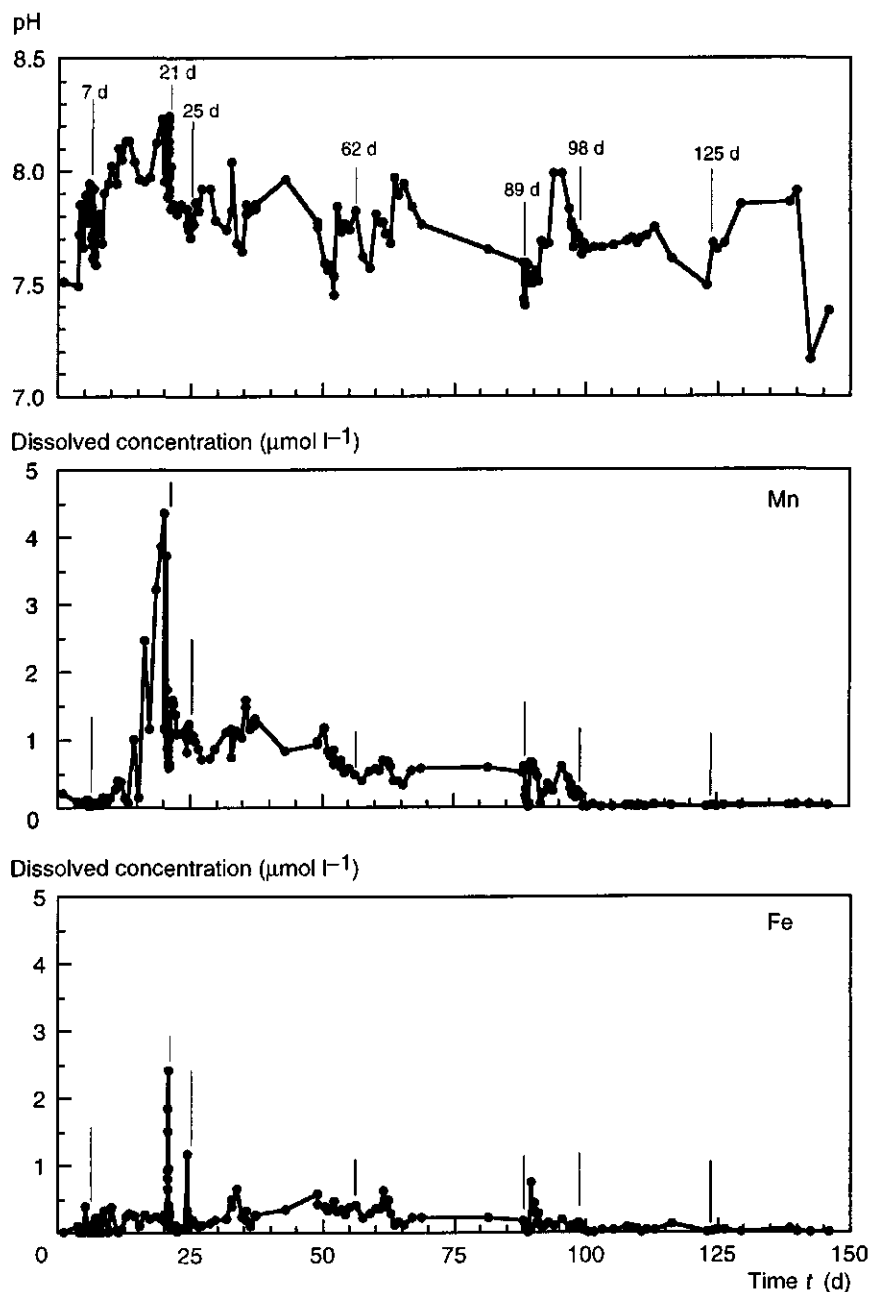


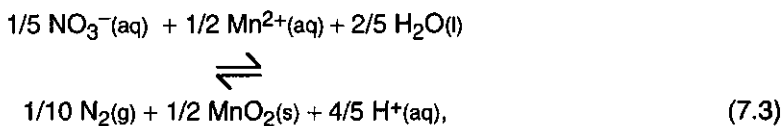
Figure 7.4 pH and dissolved concentrations of manganese and iron in drain discharge samples between 17 December 1991 ($t = 0$) and 14 May 1992 ($t = 150$ d).

drain discharge rates. Based on solubility product constants (K_{sp}) from Lindsay (1979), maximum saturation indices (SI) (Sposito, 1989) of 0.4 for $MnCO_3$ and 0.6 for $FeCO_3$ were found when $[Mn]$ and $[Fe]$ peaked near $t = 21$ d; $SI < 1$ indicates undersaturation with respect to mineral precipitation. Because the drainage water likely comprised a mixture of water originating from a reduced soil zone near the drain and water from shallower, oxic soil zones (see Chapter 6), these calculations do not rule out the possibility that Mn- and Fe-carbonate minerals formed in the reduced zone.

At the peak drain discharge rate at $t = 21$ d, both dissolved $[Mn]$ and $[NO_3^-]$ were maximised (Fig. 7.4 and Fig. 6.2). The thermodynamics of redox reactions predict that $Mn(II)$ and NO_3^- would exhibit opposite trends in dissolved concentrations. This effect can be illustrated by considering the following example reactions with respective standard-state equilibrium constants ($\log K$) of 21.1 and -20.7 (Stumm and Morgan, 1981; Sposito, 1989):



Combining reactions 7.1 and 7.2 leads to the overall reaction:



with $\log K = 0.4$. Assuming unit activities for the solid and H_2O , and an activity of $N_2(g)$ equal to its partial pressure (P_{N_2}), the following expression in terms of ion activities (in parentheses) can be derived (Lindsay, 1979) from Eq. 7.3:

$$\log (NO_3^-) = \frac{1}{2} \log P_{N_2} - \frac{5}{2} \log (Mn^{2+}) - 4 \text{ pH} - 1.6. \quad (7.4)$$

Equation 7.4 indicates that in an equilibrium solution of constant pH and P_{N_2} , concentrations of NO_3^- and Mn^{2+} would vary inversely. The denitrification

reaction pathway actually involves sequential reduction of NO_3^- to produce NO_2^- , N_2O (g), and finally N_2 (g) (Payne, 1981; Par. 6.6, this thesis); however, even the first reduction step would involve the loss of NO_3^- . Elevated levels of both NO_3 and Mn during early peak drain discharge periods supports the judgement that drainage water at these times comprised a mixture of reduced soil solution of higher [Mn] originating near the drain and more oxidised solution of higher $[\text{NO}_3]$ from shallower depths (see Chapter 6). Fluctuations in dissolved [Mn] and [Fe] measured during the first 100 days of the study (Fig. 7.4) are probably due to water with a high nitrate concentration raising the redox potential of the reduced zone.

The mean NO_3 concentration in drainage water samples increased from $0.47 \pm 0.04 \text{ mmol l}^{-1}$ between $t = 30$ and 88 d to $0.76 \pm 0.05 \text{ mmol l}^{-1}$ between $t = 89$ to 146 d, probably because elevated levels of NO_3 initially occurring in the upper 50 cm of soil reached a depth near the drain for $t > 89$ d (see Par. 6.3). Consistent with Eq. 7.4, a decrease in drainage water [Mn] and [Fe] between $t = 100$ and 150 d (Fig. 7.4) suggests that NO_3 increased the redox potential of the reduced zone near the drain, causing oxidation and precipitation of insoluble Fe- and Mn-oxide minerals.

Temporal variations in dissolved [Al] in drainage water samples (data not shown) were usually similar to dissolved [Fe]. Sharp [Al] peaks of 4.4 and $2.4 \mu\text{mol l}^{-1}$ occurred at $t = 21$ and 25 d. Data showed an overall significant correlation between dissolved [Fe] and [Al] ($R = 0.71$, $n = 167$), suggesting that there was an association between these metals in mineral assemblages being dissolved (or dispersed) when these metals occurred at elevated levels.

Macrochemical components

Figure 7.5 shows concentrations of HCO_3 , Ca, Na, Mg, K, and S in drainage water. Concentrations of Cl and NO_3 were presented in Par. 6.3. Dissolved concentrations of Ca, HCO_3 , Na, S, and Cl were typically in the range of 1 to 8 mmol l^{-1} while Mg, K, and NO_3 were in the range of 0.1 to 1.5 mmol l^{-1} . Differences in temporal variation between discharged chemical components are apparent from data sets plotted at the same scale in Fig. 7.5. Initial soil profile distributions of extractable Na, Mg, K, and S are shown in Fig. 7.6.

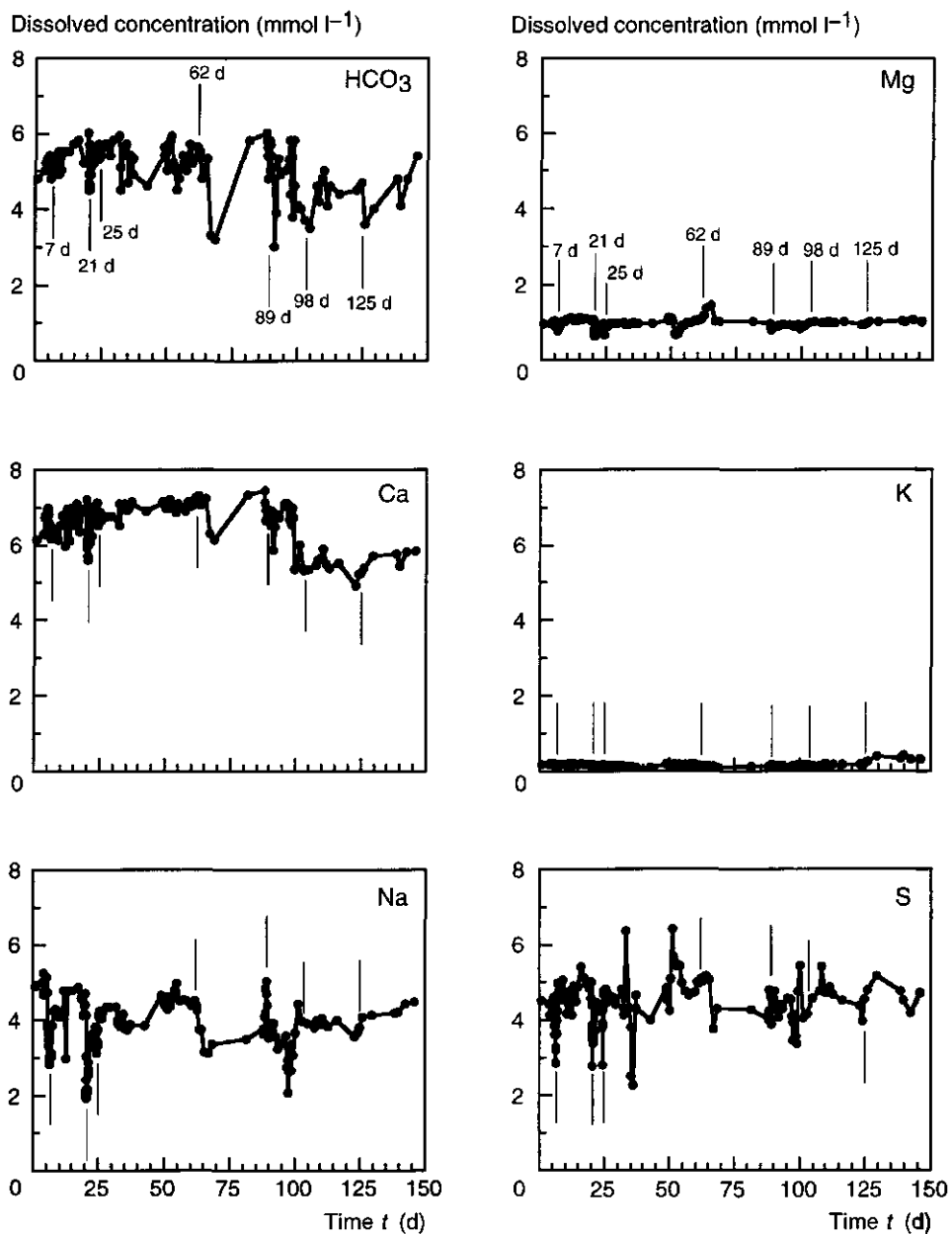


Figure 7.5 Dissolved concentrations of bicarbonate (HCO_3), calcium (Ca), sodium (Na), magnesium (Mg), potassium (K), and sulphur (S) measured in drain discharge samples between 17 December 1991 ($t = 0$) and 14 May 1992 ($t \approx 150$ d).

Calcium and bicarbonate

Discharged concentrations of Ca and HCO_3 followed similar temporal trends (Fig. 7.5), as expected if CaCO_3 (calcite) controlled their solubilities. Statistically, there was a significant correlation ($P = 0.01$; $R = 0.66$, $n = 168$) between dissolved [Ca] and $[\text{HCO}_3]$, and results were consistent with the pH effect on calcite solubility (Lindsay, 1979). For example, the elevated pH at $t = 21$ d (Fig. 7.4), which is supposed to be attributed to Mn reduction, corresponded with minima in [Ca] and $[\text{HCO}_3]$ (Fig. 7.5). Also, while pH first increased, then steadily decreased between $t = 62$ and 89 d (Fig. 7.4), both [Ca] and $[\text{HCO}_3]$ first decreased then increased.

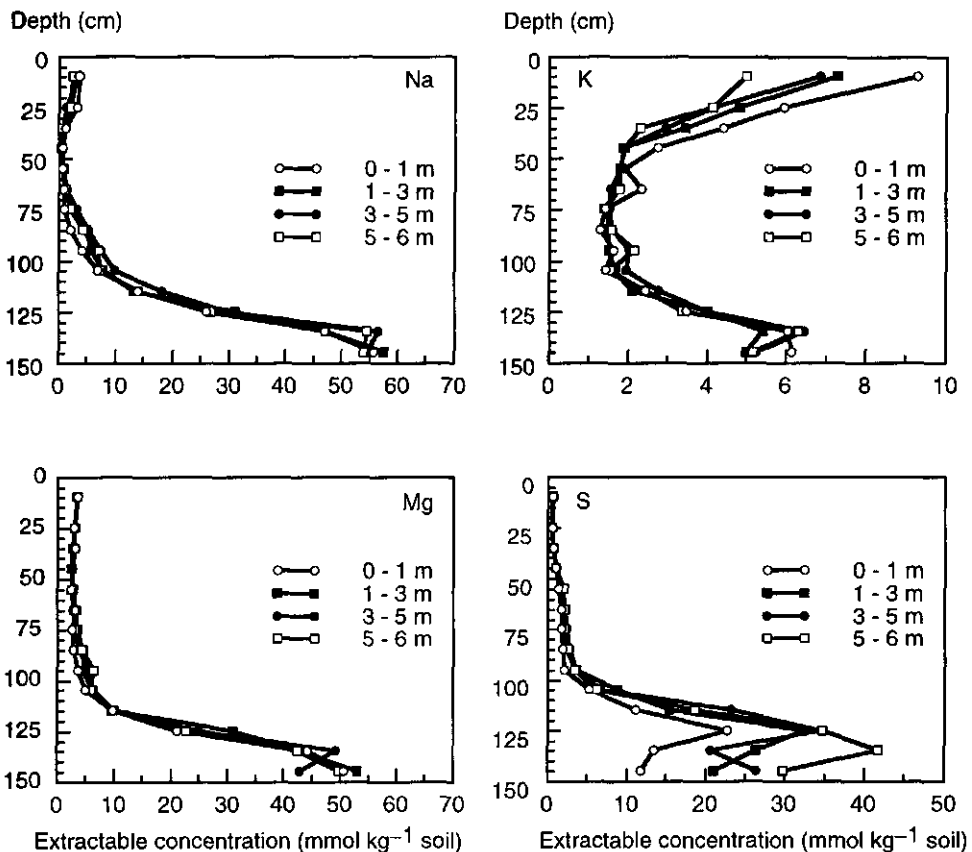


Figure 7.6 Extractable concentrations of sodium (Na), magnesium (Mg), potassium (K), and sulphur (S) in the soil profile measured at different lateral distance intervals from the drain.

To evaluate drainage water samples for the degree of saturation with respect to calcite, activities of Ca^{2+} and CO_3^{2-} were determined from GEOCHEM-PC calculations for the 22 selected samples discussed above. Values of IAP (Ca^{2+}) (CO_3^{2-}) ranged from $10^{-8.01}$ to $10^{-7.13}$, with an average value of $10^{-7.48}$. Given $K_{sp} = 10^{-8.41}$ for calcite (Lindsay, 1979), the samples were 2.5 to 19 times supersaturated with respect to pure calcite.

X-ray diffraction analyses indicated that the soil contained high-Mg calcite. The d -spacing corresponding to the most intense (112) diffraction peak for four samples analysed ranged from 0.300 to 0.299 nm, indicating that the calcite contained between 0.12 and 0.16 mole fraction of Mg (Doner and Lynn, 1989). Also, differences in calcite crystallite size at different soil depths were indicated by the 112 peak being sharpest for the sample from the 64-83 cm depth interval in which less intense diagnostic calcite peaks were also discernible, and broadest for the 36-46 cm depth interval sample (Doner and Lynn, 1989; Inskeep and Bloom, 1986). Calcite containing 0.12 to 0.16 mole fraction of Mg would have about a three- to four-fold higher solubility than pure calcite (Bathurst, 1971), which explains part of the apparent supersaturation. In addition, crystallite size and interaction with DOC could contribute to altered calcite solubility, while exclusion of dissolved Ca-DOC complexes in the speciation calculations may have resulted in an overestimation of IAP (Suarez *et al.*, 1992; Amrhein and Suarez, 1987; Inskeep and Bloom, 1986).

Sodium, magnesium and potassium

Concentrations of Na, Mg, and K in drainage water (Fig. 7.5) were lower than dissolved Ca and were probably controlled by cation exchange reactions. Although some Mg was associated with calcite, no significant correlation was found between dissolved Ca and Mg ($P = 0.05$, $R = 0.14$, $n = 168$). If congruent dissolution of high-Mg calcite throughout the soil profile controlled both Mg and Ca solubilities, then drainage water concentrations of these components would be correlated.

During peak discharge events between $t = 0$ and 25 d, dissolved [Na] and [Mg] distinctly decreased (Fig. 7.5). This result was consistent with the behaviour of Cl and opposite to NO_3 (see Chapter 6). At peak discharge events for $t > 25$ d, dissolved macrochemical components sometimes decreased (e.g., [Mg] at $t = 89$ d and [Na] at $t = 98$ d - Fig. 7.5), increased (e.g., [Na] at $t = 89$ d - Fig. 7.5), or remained fairly constant (e.g., [K] at most times - Fig. 7.5). Also, during periods of

steady drain discharge rate, water chemistry sometimes changed (see e.g., data from $t = 62$ to 89 d in Fig. 7.5). In contrast, discharged Cl concentration showed nearly an exact inverse relationship to discharge rate over the entire 120-d period for which data are reported in Chapter 6. These data indicate the conservative (nonadsorbing) nature of Cl in this soil, which contained mainly smectite, vermiculite, and hydroxy-interlayered minerals (Table 7.1) in the clay fraction, and had pH levels equal to or larger than the point of zero net charge for common oxide minerals (Sposito, 1989). The fact that both discharged and extractable Na and Cl concentrations were of comparable magnitude (Figs. 7.5 and 7.6, and Figs. 6.6 and 6.7) indicates that Na was also weakly bound to the soil exchanger phase.

Differences in drainage water concentrations of Na and Mg were qualitatively consistent with expectations based on cation exchange models. Initial concentrations of extractable Na and Mg throughout the soil profile were nearly identical (Fig. 7.6). In drainage water samples, dissolved [Na] was approximately four times greater than dissolved [Mg]. A conditional cation exchange selectivity coefficient ($K_{\text{Na},\text{Mg}}$) for Na-Mg exchange as a function of the charge fractions of exchangeable cations, X_M , where $M = \text{Na}^+$ or Mg^{2+} , and solution charge concentrations in $\text{mol}_c \text{ l}^{-1}$ (C_M) can be written as (Gaston *et al.*, 1993):

$$K_{\text{Na},\text{Mg}} = (X_{\text{Mg}} / X_{\text{Na}}^2) (C_{\text{Na}}^2 / C_{\text{Mg}}). \quad (7.5)$$

As a first approximation, an effective value of $K_{\text{Na},\text{Mg}}$ can be calculated from the field data. Given essentially equivalent extractable molar concentrations of soil Na and Mg throughout the profile (at least initially - Fig. 7.6), and assuming that extractable Mg is equivalent to Mg in the exchanger phase and not from high-Mg calcite dissolution, then $X_{\text{Mg}} / X_{\text{Na}} = 2$, and Eq. 7.5 can be simplified to:

$$K_{\text{Na},\text{Mg}} = (2 / X_{\text{Na}}) (C_{\text{Na}}^2 / C_{\text{Mg}}). \quad (7.6)$$

From average concentrations of Mg and Na in Fig. 7.5, $C_{\text{Mg}} = (1.8 \pm 0.2) 10^{-3} \text{ mol}_c \text{ l}^{-1}$ and $C_{\text{Na}} = (3.8 \pm 0.8) 10^{-3} \text{ mol}_c \text{ l}^{-1}$. The choice of X_{Na} is somewhat arbitrary, but at the 97.5 cm drain depth, extractable soil Na concentration is 6 mmol kg^{-1} (Fig. 7.6). Dividing extractable soil Na by a CEC of 220 mmol kg^{-1} for this soil zone (Par. 4.1.2, Fig. 4.6), gives $X_{\text{Na}} = 0.0273$. Using these numbers in

Eq. 7.6 gives $K_{\text{Na},\text{Mg}} = 0.59$, indicating a preference for Na exchange over Mg under these field conditions. Based on ternary (Ca-Mg-Na) cation exchange data of Fletcher *et al.*, (1984 - Table 1) for a montmorillonitic soil separate at pH 7, $K_{\text{Na},\text{Mg}}$ ranged from 4 to 17 (preference for Mg), with an average value of 7 ± 4 . The large discrepancy between $K_{\text{Na},\text{Mg}}$ calculated from the field data versus published laboratory results might be attributable to the approximate nature of the former calculation, or to the fact that typically larger values of X_{Na} and X_{Mg} were used in the laboratory experiments (Fletcher *et al.*, 1984). Nevertheless, it is apparent that any reactive model for predicting the transport of these components must include a value of $K_{\text{Na},\text{Mg}}$ appropriate for the prevailing background of Ca in the system, and account for the degree that high-Mg calcite contributes to Mg behaviour in the soil.

Dissolved [Na] in drainage water was more than 4-fold higher than [K], consistent with the lower level of extractable soil K at depths greater than 75 cm (Fig. 7.6). Unlike Na and Mg, extractable K concentration was elevated in the top 50 cm as well as under the drain, probably due to inputs of K-containing soil amendments during the cropping season prior to this study and K already present in the subsoil after reclamation (see Par. 4.1.1). In comparison to other macrochemical components, the lower dependence of drainage water [K] on discharge rate is reasonable if both surface and subsurface soil horizons contributed dissolved K during peak discharge events. A discernible increase in discharged [K] for $t > 125$ d (Fig. 7.5) appears to be breakthrough of K that was initially present in the top 50 cm of soil (Fig. 7.6). Breakthrough of NO_3^- at $t = 89$ d (Fig. 6.2) preceded K^+ breakthrough, which was qualitatively consistent with cation exchange retarding transport of K^+ relative to Cl^- . For example, field results of Bjerg and Christensen (1993) showed that non-adsorbing anion (Cl^-) transport velocities were two-fold to ten-fold higher than K^+ and Na^+ velocities. Of course, relative transport rates of these ions will depend on the ion-exchange characteristics of a particular soil.

The extractable K^+ data in Fig. 7.6 suggest a trend of increasing [K] with decreasing distance from the drain in the topsoil. A similar trend was observed for extractable NO_3^- (Fig. 6.5). Multiple comparisons of all extractable K means at each soil depth using the Tukey-Kramer HSD procedure (Snedecor and Cochran, 1967) showed significant differences in extractable K ($P = 0.05$ or 0.01) between samples taken at different distances from the drain, particularly at 0 to 50 cm depths. Unlike NO_3^- , K^+ is not transformed to other chemical forms. Thus,

these data support the hypothesis that lateral transport of solutes was significant in the topsoil (see Chapter 6).

Sulphur

Analogous to dissolved [Cl], [Na], and [Mg], dissolved [S] in drainage water decreased during periods of peak discharge rates between $t = 0$ and 25 d (Fig. 7.5 and Fig. 6.6). However, fluctuations in dissolved S were more erratic and less related to discharge rate than for [Cl]. It is noteworthy that there was a correspondence between fluctuations in dissolved [S] between $t = 30$ and 60 d (Fig. 7.5) and deviation of the calculated ionic balance from neutrality (Fig. 7.3). This relationship suggests that either measured concentrations of dissolved S or the assumption that SO_4^{2-} was the dominant S species were questionable for some samples.

Phosphorus

Although P concentrations were very low in the drainage water, the importance of this soil component as a potential surface water contaminant warrants summarising the results. The average concentrations of inorganic and organic P in drainage water over the 150-day leaching period were 0.2 ± 0.1 and $14 \pm 13 \mu\text{mol l}^{-1}$. On a per-sample basis, the average fraction of organic P relative to total P was 0.6 ± 0.3 .

7.4 Conclusions

Multi-component solute discharge from a subsurface drain was affected by oxidation-reduction, precipitation-dissolution, ion exchange and hydrological conditions. The initial distribution of a component within the soil profile largely influenced how the drain discharge rate affected the drainage water chemistry. Although increased dissolved [Mn] occurring during initial stages of shallow groundwater levels and high drain discharge rates indicated reduced conditions near the drain, NO_3^- originating from shallower oxic zones was discharged from the drain at elevated concentrations. However, later in the study period, consistently higher nitrate concentrations near the drain apparently increased the redox potential of this zone and decreased the reductive dissolution of Mn and Fe. Precipitation and dissolution reactions involving Ca and HCO_3^- probably

controlled the solubility of these components, although drainage water samples appeared to be on the average supersaturated with respect to high-Mg calcite. Concentrations of Na, Mg, and Cl in the drainage water were related to their relative affinities for the exchanger phase.

8. MODELLING TWO-DIMENSIONAL WATER FLOW, AND NITRATE, CHLORIDE AND BROMIDE TRANSPORT TO A SUBSURFACE DRAIN

In this chapter the modelling of water flow and solute transport to a subsurface drain is presented for the specific hydrological situation at the Lovinkhoeve. Literature on two-dimensional modelling is discussed, and the choice for the finite element model SWMS_2D (Simunek *et al.*, 1994) is justified. Special attention is given to the description of a subsurface drain in the finite element model and to the hydraulic conductivity characteristic close to saturation. The calibration of the model is based on the soil physical characteristics presented in Par. 4.2 and field data of the first 40 days of the leaching experiment 1991-1992 (Par. 6.2). The calibrated model is applied to simulate the later nitrate leaching (1991-1995), chloride leaching (1991-1992) and bromide tracer (1994-1995) experiments. In these winter-leaching periods, no crops are grown and the soil surface is bare. Finally, the model is used to quantify the effects of changes in meteorological conditions, drain spacing, downward seepage and N mineralisation on NO_3 leaching.

8.1 Two-dimensional water flow and solute transport models

Overview of the literature

For two-dimensional modelling of water flow and solute transport to a drain nearly always finite element models are used. Such models are very flexible in describing different geometries using a triangular grid, in which changes in grid density can be incorporated easily.

Fipps *et al.* (1986) compared four models to describe a subsurface drain in finite element water balance models for steady state conditions, focusing on the saturated zone of the soil. Comparisons were made with the analytical solution of Kirkham (1949) for steady water flow in a homogeneous, isotropic soil under ponded conditions. Two other flow situations were considered also.

The *first* model had a high grid density near the drain and was used as a reference. The drain was described as a cylindrical hole with an effective drain radius. The calculated Darcian fluxes at the drain boundary resulted in mass balance errors of 5%. The reason for these errors was the sensitivity of the model

to small errors in hydraulic head H close to the drain. The errors could be reduced to 1.4% by calculating the Darcian flux to the drain not by assuming a radial flow field near the drain, using the H gradient between the drain and the nodal points closest to the drain, but by the H gradient between the drain, which had a uniform H over its circumference, and a nodal point a few centimetres away from the drain.

The *second* model calculated the drain flow rate based on the equation of Kirkham (1949). By using this drain flow rate as a flux boundary condition, a coarse grid could be used in the vicinity of the drain. The application of this model is limited to steady state conditions.

The *third* model simulated the drain as one nodal point with a constant H . The density of the grid around this node, which acts as a sink, must be very high to obtain accurate results. The phreatic surface in the vicinity of the drain was not well described and simulated drain discharge rates were too large compared to the results of the reference model.

The *fourth* model was based on an electrical network (Vimoke *et al.*, 1963), consisting of connected square elements and resistance adjustment factors close to the drain, which was described as a single node. This model calculated accurate drain discharge rates compared to the reference model.

Fipps *et al.* (1986) concluded that the reference model with a high grid density around the drain is an appropriate choice when an accurate description of H in the whole flow domain is important. In the vicinity of the drain water flows in a radial direction, with a logarithmic hydraulic head distribution as a function of the radial distance from the drain centre. In numerical models generally a constant H gradient is assumed between two adjacent nodal points. The logarithmic H distribution can be approached by using a large number of nodal points with constant H gradients between the nodal points. This explains the need for a high grid density around the drain. In fact, this applies generally for all zones with variable H gradients.

The comparisons made by Fipps *et al.* (1986) referred to water flow in the saturated zone of the soil only. Zaradny and Feddes (1978) took the entire unsaturated-saturated zone into account, and studied transient flow with different boundary conditions for a drain. Steady flow solutions for a homogeneous, isotropic soil were finally obtained. The drain was described as an ideal drain (outer diameter = 5 cm) without an entrance resistance. Two boundary conditions along the drain surface were distinguished. When a drain is completely filled with

water, H in the drain is constant, and the wall of the drain is an equipotential. In general, a drain is a seepage face. The part in the unsaturated zone is a "no flow" boundary, and the part of the drain in the saturated zone is an equipotential boundary. In the examples with a prescribed flux at the soil surface, the differences between the calculated phreatic surfaces for these two methods describing the drain were small. The total flux through the soil surface must correspond to the drain flow rate. Because the boundary conditions were different, it is not possible to compare these results with the findings of Fipps *et al.* (1986). Zaradny and Feddes (1978) showed that the streamlines already bent significantly towards the drain in the unsaturated zone.

The importance of anisotropy of the hydraulic conductivity in the saturated zone was demonstrated by Gureghian and Youngs (1975), who considered a case of steady flow. The anisotropy was introduced in the model by using isotropic horizontal layers with a different K_s . For a two-layer system, with water flow to a subsurface drain, a relatively larger K_s in the top layer causes faster horizontal flow in the top layer in the direction of the drain, as compared to a situation with isotropic hydraulic conductivities in the entire soil profile. For a situation with a backfill over a tile drain, which creates a zone with larger hydraulic conductivity, water flow and solute transport from the top layer to the drain will become even faster.

Munster *et al.* (1994) adapted and applied successfully a two-dimensional finite difference model to describe transport of a pesticide to a subsurface drain. This model solves Richards' equation for water flow and the convection-dispersion equation for chemical transport. The layering of the soil profile and local anisotropy within these layers was taken into account. However, this model ran on a mainframe computer and did not have the flexibility of finite elements concerning local variations in grid densities.

A water flow and solute transport model for the Lovinkhoeve

Modelling the overall water balance receives much attention in the drainage literature, which means that drain discharge rates must be calculated accurately. To calculate solute transport, the water fluxes within the soil must be described accurately also. To cope with the situation at the Lovinkhoeve, a model must be able to simulate the strongly fluctuating groundwater levels, which lead to large peaks in solute concentrations in the drainage water (Chapters 6 and 7). The large differences in K_s between the layers (Fig. 4.16) indicate that anisotropy of

the soil profile can play an important role. The unsaturated zone can have a substantial effect on the water flow to the drain, directly by the horizontal component of the water flow in the unsaturated zone and indirectly by the water retention. The two-dimensional finite element model SWMS_2D (Simunek *et al.*, 1994), describing the dynamics of water flow and solute transport in the saturated and unsaturated zones, was chosen as the most appropriate model. The model is well documented, runs on PC's as well as mainframe computers, and the generation of the grid, input and output are well organised (Simunek *et al.*, 1996). The characteristics of SWMS_2D have already been described in Par. 2.1.3 and Par. 2.2.

8.2 Modelling the Lovinkhoeve field

8.2.1 Flow domain and finite element grid

Water flow and solute transport were modelled in the flow domain of 6 m width, representing half the drain spacing, and a depth of the soil profile of 2 m (Fig. 8.1). The bottom of the soil profile was assumed to be impermeable. The drain was located at 97.5 cm depth, and was described as a half circular hole with the real physical dimensions (inner diameter = 5 cm). The inner wall of the drain was described as a seepage face, implying that the drain is always practically empty. A finite element grid was created with the triangular elements forced to be stratified according to the layered soil profile (Fig. 8.1). The distribution of the triangles was generated using an automatic grid generator (Simunek *et al.*, 1996). The density of the grid was then evaluated using the first 40 days of the leaching period 1991-1992 ($0 < t < 40$ d) as test period. The grid density was judged to be sufficient when a converging solution and a small water balance error (< 1%) was found. This percentage represents the errors in summed changes in volumetric water contents in the entire flow domain relative to the water fluxes over the boundaries of the flow domain. A trial and error method was used until the grid presented in Fig. 8.1 was found. High densities of the grid were used close to the soil surface and close to the drain, because gradients in hydraulic head are large and variable in these zones. In the subsoil, especially further away from the drain, lower grid densities could be used.

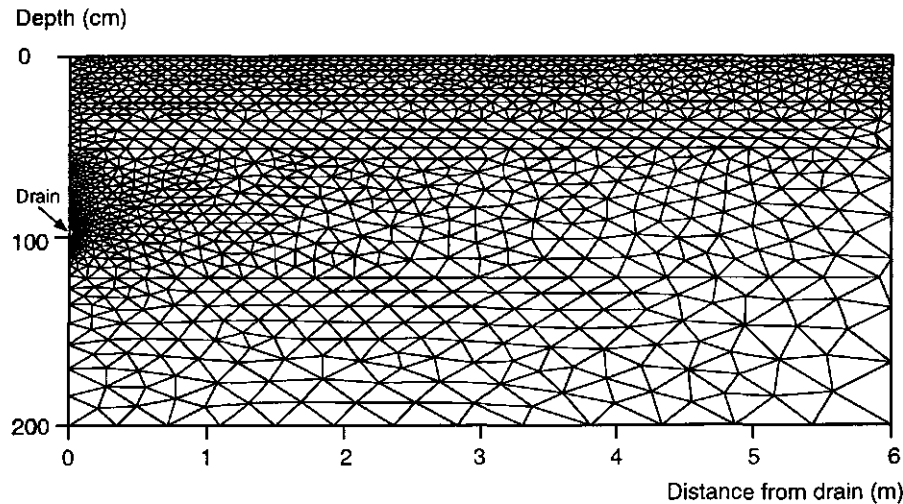


Figure 8.1 The finite element grid in the flow domain representing half the drain spacing. A detail is given of the grid close to the drain. The entire grid consists of 2563 triangles and 1352 nodes.

Water flow and nutrient transport in a layered silt loam soil

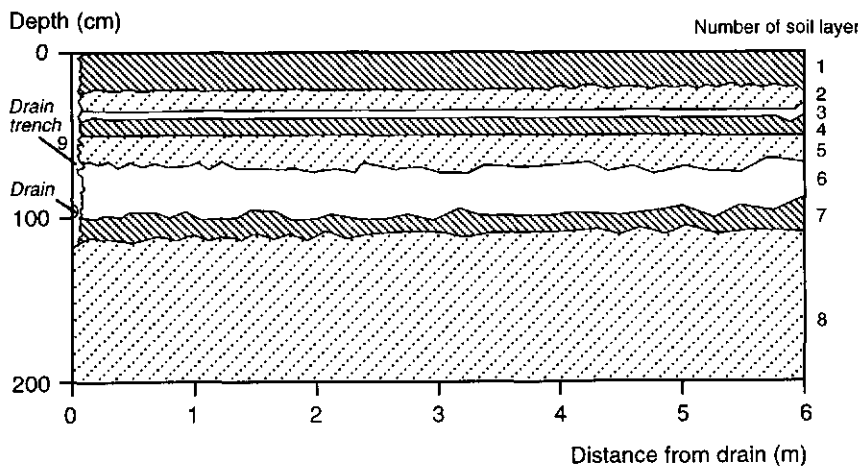


Figure 8.2 Distribution of the different soil layers in the flow domain, including a drain trench in the zone above and below the drain. The (small) numbers of the soil layers on the right-hand side and of the drain trench (9) correspond to the hydraulic characteristics mentioned in the text and in Tables 8.1, 8.2, and 8.3.

Table 8.1 Hydraulic characteristics of the different soil layers used in the initial simulations. Parameters in the analytical expressions of Van Genuchten (Eq. 2.16) and Mualem (Eq. 2.17) for describing the hydraulic characteristics of the different layers of the Lovinkhoeve soil (see Fig. 8.2): θ_r = residual volumetric water content ($\text{m}^3 \text{m}^{-3}$), θ_s = volumetric water content at saturation ($\text{m}^3 \text{m}^{-3}$), K_s = hydraulic conductivity at saturation (cm d^{-1}), α (cm^{-1}), n and L are empirical parameters, θ_k = volumetric water content at transition point in hydraulic conductivity characteristic close to saturation ($\text{m}^3 \text{m}^{-3}$), K_k = hydraulic conductivity at transition point (cm d^{-1}).

Zone	Layer	Depth (cm)	θ_r ($\text{m}^3 \text{m}^{-3}$)	θ_s ($\text{m}^3 \text{m}^{-3}$)	K_s (cm d^{-1})	α (cm^{-1})	n	L	θ_k ($\text{m}^3 \text{m}^{-3}$)	K_k (cm d^{-1})
1	1	0-25	0.04040	0.43709	2.038	0.00436	1.30740	-2.02754	0.43709	2.038
2	2	25-35	0.08165	0.47303	1.624	0.00525	1.62422	-1.84898	0.47303	1.624
	3	35-40	0.08165	0.47303	1.624	0.00525	1.62422	-1.84898	0.47303	1.624
3	4	40-50	0.10060	0.51506	0.373	0.00207	1.91432	-1.46461	0.51506	0.373
	5	50-70	0.10060	0.51506	0.373	0.00207	1.91432	-1.46461	0.51506	0.373
	6	70-95	0.10060	0.51506	0.373	0.00207	1.91432	-1.46461	0.51506	0.373
	7	95-120	0.10060	0.51506	0.373	0.00207	1.91432	-1.46461	0.51506	0.373
	8	120-200	0.10060	0.51506	0.373	0.00207	1.91432	-1.46461	0.51506	0.373
	9	Trench	0.08165	0.47303	1.624	0.00525	1.62422	-1.84898	0.47303	1.624

8.2.2 Hydraulic characteristics close to saturation

In Fig. 8.2 the small numbers 1-8 on the right-hand side and 9 on the left-hand side indicate the different soil layers and corresponding different soil hydraulic characteristics that were used as the initial characteristics (Table 8.1) before the calibration of the water flow part of the model. The soil profile is divided into the three main depth zones: 0-25 cm depth topsoil, 25-40 cm depth intermediate layer, 40-200 cm depth subsoil; and the drain trench (Fig. 8.2, number 9). Within the intermediate layer and the subsoil, a distinction is made between different soil layers (Fig. 8.2 and Table 8.1). The difference between the two intermediate layers 2 and 3 is only in the K_s value (Table 8.2); the water retention characteristic ($h - \theta$) and the unsaturated part of the hydraulic conductivity characteristics of these layers are identical. The same applies to the subsoil layers 4, 5, 6, 7 and 8 (Table 8.2). For the drain trench, the soil hydraulic characteristics of the intermediate layer were used, with a relatively large K_s value. The hydraulic characteristics for the unsaturated zone were identical to plot 16A presented in Par. 4.2.3. However, the values of K_s , which can differ orders of magnitude from the values of K in the unsaturated zone, have to be incorporated into the hydraulic conductivity characteristics.

To obtain a smooth transition between K in the unsaturated and saturated zones, the option in the SWMS_2D model is used to define a volumetric water content θ_k with corresponding pressure head h_k above which the hydraulic conductivity characteristic varies linearly between K_k and K_s . This procedure is intended to reduce the numerical problems for calculations at nodal points close to saturation. The original Mualem equation (Eq. 2.17) is used for water contents $\theta < \theta_k$. As an example, the hydraulic conductivity characteristics for three soil layers are given in Fig. 8.3, which represent the results of the calibration procedure described in the next paragraph. Figure 8.4 shows the relative hydraulic conductivity $K_r = K / K_s$ close to saturation as a function of pressure head h for the same soil layers. A threshold $h_k = -20$ cm was chosen for the linear part of the hydraulic conductivity characteristics. The only difference between the hydraulic conductivity characteristics of the layers 4, 5, 6, 7 and 8 is the value of K_s (Table 8.2) and the corresponding steepness of K between $h = h_k$ and $h = 0$.

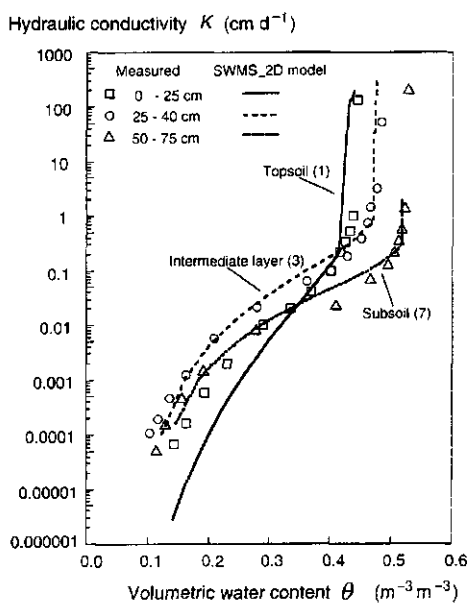


Figure 8.3 Example of the hydraulic conductivity characteristics for soil layers: Topsoil (1): 0-25 cm; Intermediate layer (3): 35-40 cm; and Subsoil (7): 95-120 cm depth. The lines show the description of the hydraulic conductivity characteristics in SWMS_2D, the symbols indicate laboratory measurements at the indicated depths (see Table 8.1, Fig. 8.2, and Fig. 4.12).

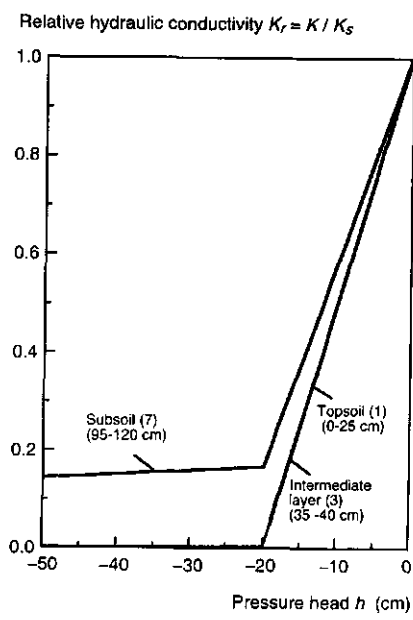


Figure 8.4 Relative hydraulic conductivity characteristics close to saturation for three soil layers: Topsoil (1): 0-25 cm; Intermediate layer (3): 35-40 cm; and Subsoil (7): 95-120 cm depth, as a function of pressure head, as used in SWMS_2D. The relative hydraulic conductivity K_r is expressed as a fraction of K_s . (see Table 8.1 and Fig. 8.2)

8.2.3 Calibration of the water flow part of the model

To calibrate the SWMS_2D model, first steady state conditions were considered. The drain discharge rate - groundwater level data measured in the field in the leaching period 1991-1992 ($0 < t < 160$ d; Fig. 6.11) were used to evaluate the simulations. The hydraulic conductivities at saturation K_s for all soil layers were varied to calibrate the SWMS_2D model. However, the values of K_s have to be in the range of the measured values (Fig. 4.16). This method of calibration assumes that the saturated zone below the phreatic surface dominates the water flow to the drain and that water flow in the unsaturated zone makes a much smaller contribution, limited to the zone where the hydraulic conductivity linearly increases: $-20 < h < 0$ cm. The large differences in measured hydraulic conductivities between the saturated and the unsaturated zones (Figs. 8.3 and 8.4) justifies this assumption. For the later dynamic simulations with transient boundary conditions, the effect of the unsaturated zone will become more important due to the water retention in this zone.

To calibrate K_s for the subsoil, the calibration procedure started with a low uniform infiltration rate at the soil surface, which corresponded to a low drain discharge rate. By increasing the infiltration rate, the phreatic surface rose and shallower soil layers became saturated and their K_s values were calibrated. The calibration of the shallower layers depended on the results of the underlying layers. In the calibrations, the K_s of the drain trench was fixed at $K_s = 200$ cm d⁻¹ and a possible entrance resistance of the drain was ignored.

Steady infiltration rates of 1, 2, 3, 6, 8, 10, 15, 20, and 25 mm d⁻¹ were used to find the values of K_s for the different layers. The K_s values for the soil layers were optimised by comparing the simulated groundwater level at the fixed drain discharge rates with the field data for the leaching period 1991-1992 ($0 < t < 150$ d; Fig. 8.5). A decrease in K_s with depth was used as a criterion, because this trend was found in the laboratory data (Fig. 4.16). An automated optimisation procedure was too complex and time-consuming due to the long computation times for each simulation and the dependence of the calibration of the shallower layers on the results of the deeper layers. Table 8.2 gives the final K_s data after the calibration procedure. Figure 8.5 shows the measured and simulated points of the relationship between drain discharge rate and groundwater level. Simulated drain discharge rates were close to the field data, although the field data do not really represent steady state conditions.

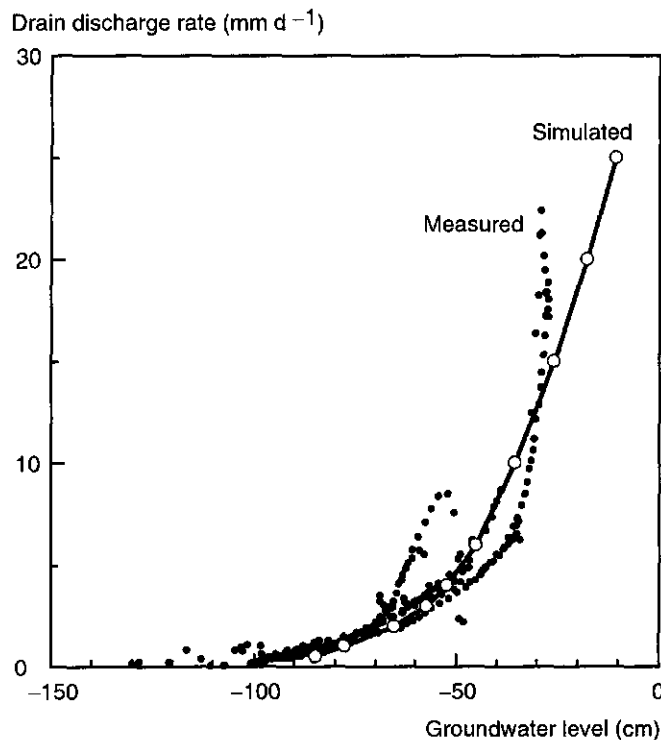


Figure 8.5 Measured and simulated data of the relationship between drain discharge rate and groundwater level for the leaching period from 17 December 1991 to 25 May 1992 ($0 < t < 160$ d). The groundwater data represent the position midway between two drains, i.e. at -6 m from the drain. The simulated data are obtained for steady state conditions.

Table 8.2 Hydraulic characteristics of the different soil layers after the K_s calibration procedure. For further details see legend Table 8.1.

Zone	Layer	Depth (cm)	θ_r ($\text{m}^3 \text{m}^{-3}$)	θ_s ($\text{m}^3 \text{m}^{-3}$)	K_s (cm d^{-1})	α (cm^{-1})	n	L	θ_k ($\text{m}^3 \text{m}^{-3}$)	K_k (cm d^{-1})
1	1	0-25	0.04040	0.43709	200	0.00436	1.30740	-2.02754	0.41072	2.038
2	2	25-35	0.08165	0.47303	200	0.00525	1.62422	-1.84898	0.46923	0.949
	3	35-40	0.08165	0.47303	300	0.00525	1.62422	-1.84898	0.46923	0.949
3	4	40-50	0.10060	0.51506	120	0.00207	1.91432	-1.46461	0.51461	0.334
	5	50-70	0.10060	0.51506	40	0.00207	1.91432	-1.46461	0.51461	0.334
	6	70-95	0.10060	0.51506	20	0.00207	1.91432	-1.46461	0.51461	0.334
	7	95-120	0.10060	0.51506	10	0.00207	1.91432	-1.46461	0.51461	0.334
	8	120-200	0.10060	0.51506	2	0.00207	1.91432	-1.46461	0.51461	0.334
	9	Trench	0.08165	0.47303	200	0.00525	1.62422	-1.84898	0.46923	0.949

8. Modelling two-dimensional water flow and solute transport

Figure 8.6 shows the distribution of the water flux densities for two different steady state conditions. The water flow in the unsaturated zone is mainly vertical until the phreatic surface is approached. In the unsaturated zone just above the phreatic surface, there is a substantial horizontal component in the flux density due to the increase in the hydraulic conductivity. The horizontal flux density is dominant in the saturated zone. Radial flow, with high flux densities, occurs in the zone close to the drain as a result of the convergence of the flow towards the drain.

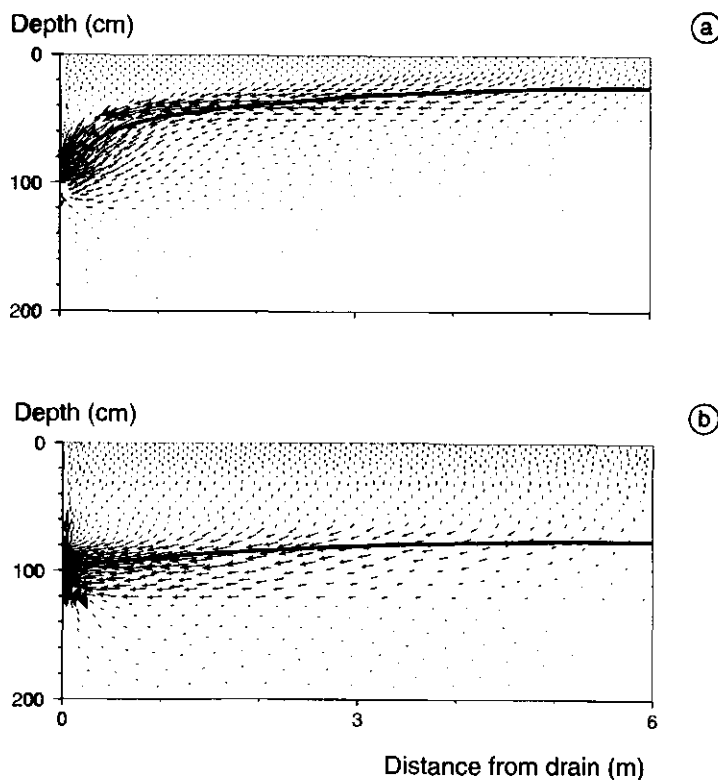


Figure 8.6 Distribution of the water flux densities in the flow domain for steady infiltration rates of 15 mm d^{-1} (a) and 1 mm d^{-1} (b), respectively. The lengths of the arrows indicate the magnitude of the flux density relative to the maximum. At the same arrow length, the absolute flux densities are twenty times larger in the top figure than in the bottom figure. The thick lines show the depth of the phreatic surface.

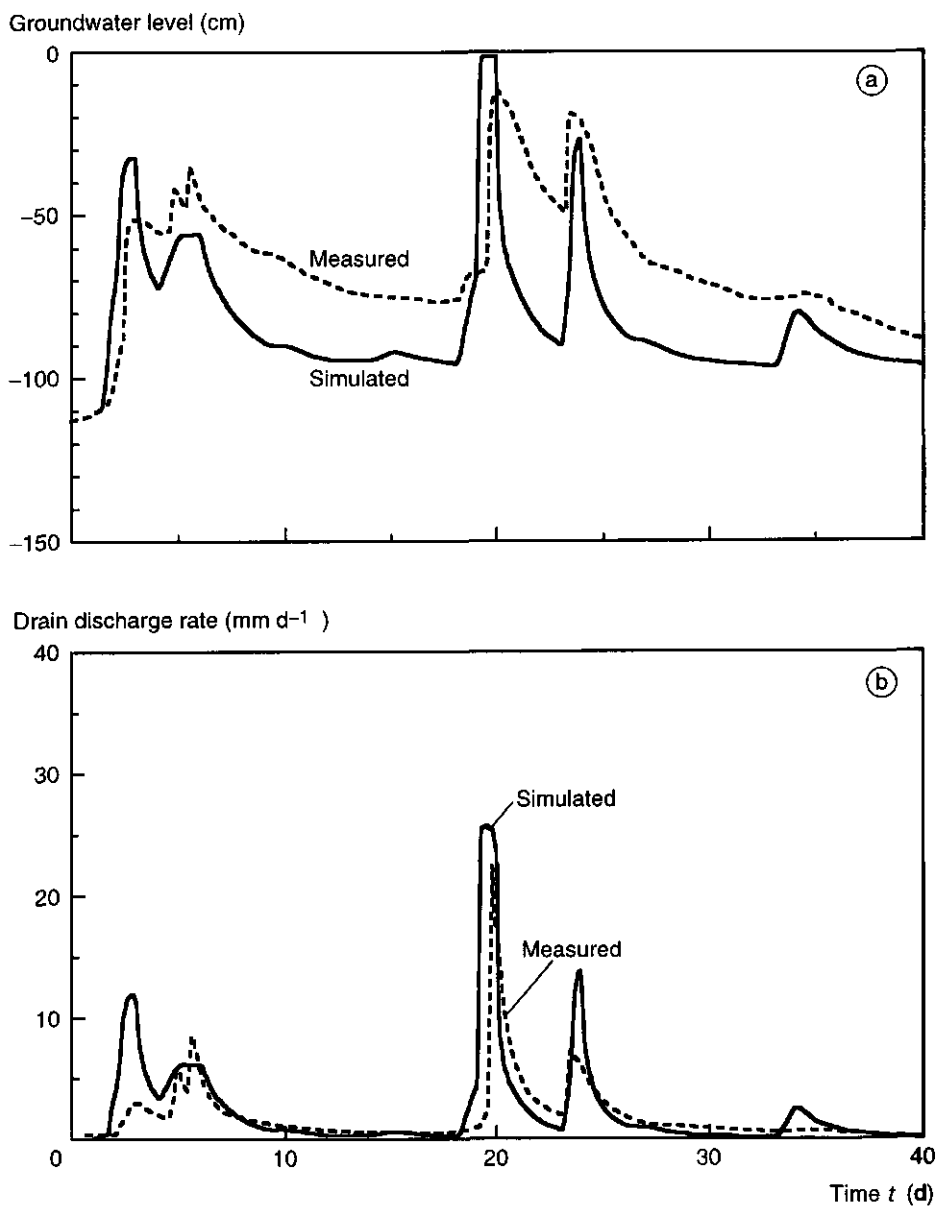


Figure 8.7 Measured and simulated groundwater levels at -6 m from the drain (a), and drain discharge rates (b), for the leaching period 17 December 1991 to 26 January 1992 ($0 < t < 40$ d). The simulation results were obtained using the laboratory hydraulic characteristics, with $\alpha = 0.00438 \text{ cm}^{-1}$, for the steady state calibration, and using *daily* precipitation data.

To calibrate the model under transient conditions, the field data of the leaching period 17 December 1991 - 25 January 1992 ($0 < t < 40$ d) (see Par. 6.2) were used. The hydraulic conductivity characteristics were not changed, but the effect of the water retention curve on the dynamics of both the drain discharge rate and the groundwater level was considered. In the simulations no ponding at the soil surface was allowed. A horizontal phreatic surface at 116 cm depth with pressure heads in equilibrium with this phreatic surface was used as initial condition. The transient calculations were performed with daily precipitation and potential evaporation data as boundary condition at the soil surface. Simulations using the hydraulic characteristics obtained from the steady state calibrations (Table 8.2), resulted in too fast reactions of the groundwater level and the drain discharge rates to precipitation events (Fig. 8.7), as compared to the field data. During periods with high precipitation rates around $t = 21$ d, the simulated phreatic surface nearly intersected the soil surface (Fig. 8.7). The slower dynamics of the field data indicate that the differential water capacity C in the field was larger than in the simulations. The largest changes in pressure heads can be expected in the topsoil. So, the sensitivity of the overall dynamics of the water balance can be studied best by varying the water retention characteristic in this zone. The laboratory water retention characteristic of the 0-25 cm depth topsoil, together with field data, is given in Fig. 8.8. The field data show that at similar pressure heads volumetric water contents are lower compared to the laboratory water retention data. This can be attributed to air entrapment or hysteresis, as mentioned before (Par. 4.2.1). Increasing the α parameter in Eq. 2.16 by a factor 5 to $\alpha = 0.02190 \text{ cm}^{-1}$ results in an analytical description of the water retention curve which fits the field data better (Fig. 8.8). With an increase of α with a factor 10 to $\alpha = 0.04380 \text{ cm}^{-1}$, the outer boundary of the field water retention data ("field absorption curve") is approached. The shape of the water retention curve for larger values of α resulted in larger differential water capacities in the important pressure head range $-100 < h < 0$ cm. Because the shape of the water retention curve was changed, the description of the hydraulic conductivity characteristic using Eq. 2.17 had to be adapted. For the topsoil, a new fit was performed on the laboratory hydraulic conductivity data, using the fixed parameters of the water retention curve, to find new L and K_k parameters (Table 8.3). The increased differential water capacity C results in a damping out of the changes in the groundwater level and corresponding drain discharge rates. The simulations with $\alpha = 0.02190 \text{ cm}^{-1}$ were close to the field data.

However, the dynamics at the peak precipitation event at $t = 21$ d and the two small peaks around $t = 8$ d were not simulated well. This appears to be due to the input of precipitation data at daily intervals. Using the changed water retention characteristic together with the hourly precipitation and daily evaporation data resulted in simulated groundwater levels (Fig. 8.9a) and drain discharge rates (Fig. 8.9b) in close agreement with the measurements.

The transient simulations of the soil water balance were precise with respect to the overall water balance. At daily intervals the error in the water mass balance was typically $< 1\%$. This percentage represents the errors in summed changes in volumetric water contents in the entire flow domain relative to the water fluxes over the boundaries of the flow domain, and can be considered as a very strict criterion. The computation time for the transient simulations for the 40-day

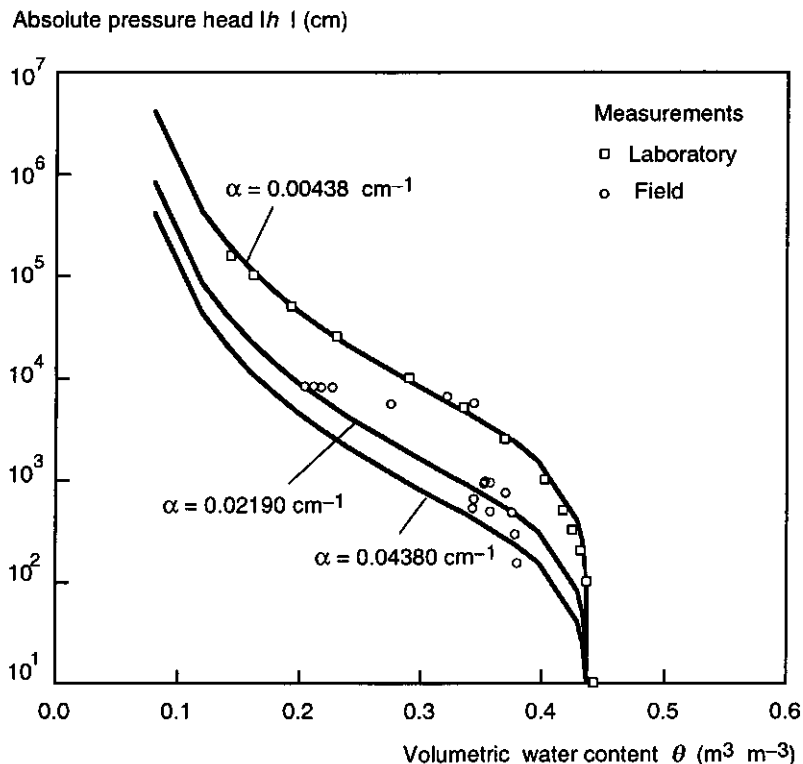


Figure 8.8 Laboratory and field water retention characteristics for the 0-25 cm depth topsoil of the Lovinkhoeve. The fits for three α parameters (Eq. 2.16) are shown.

calibration period was typically 10 hours on a 75 MHz IBM-type personal computer. This long computation time is mainly caused by the periods with high infiltration rates and shallow phreatic surfaces. The numerical calculations are very sensitive to small changes in pressure head, because the hydraulic conductivity characteristic close to saturation is still steep. The iteration procedure used to find a converging solution automatically reduces the computational time steps, leading to long computation times. The layered soil profile and the drain trench with different hydraulic properties make hydraulic head gradients more variable and thus convergence slower. Even for steady state conditions at high infiltration rates larger than 10 mm d^{-1} , the numerical calculations take hours, indicating the sensitivity of the solution for very small changes in pressure head.

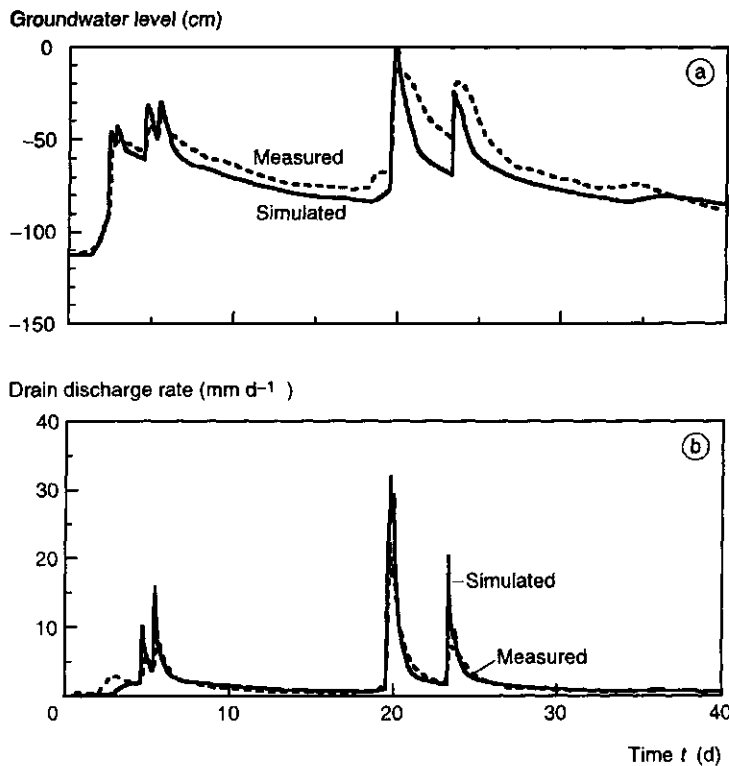


Figure 8.9 Measured and simulated groundwater levels at -6 m distance from the drain (a); and the drain discharge rates (b). The simulation results were obtained using the adapted water retention characteristic for the $0\text{--}25 \text{ cm}$ depth topsoil ($\alpha = 0.02190 \text{ cm}^{-1}$) and hourly precipitation data.

Table 8.3 Hydraulic characteristics of the different soil layers after the K_s calibration procedure and the adaptation of the water retention characteristic of the 0-25 cm topsoil. For further details see legend Table 8.1.

Zone	Layer	Depth (cm)	θ_r ($\text{m}^3 \text{m}^{-3}$)	θ_s ($\text{m}^3 \text{m}^{-3}$)	K_s (cm d^{-1})	α (cm^{-1})	n	L	θ_k ($\text{m}^3 \text{m}^{-3}$)	K_k (cm d^{-1})
1	1	0-25	0.04040	0.43709	200	0.02190	1.30740	-2.02754	0.41072	0.206
2	2	25-35	0.08165	0.47303	200	0.00525	1.62422	-1.84898	0.46923	0.949
	3	35-40	0.08165	0.47303	300	0.00525	1.62422	-1.84898	0.46923	0.949
3	4	40-50	0.10060	0.51506	120	0.00207	1.91432	-1.46461	0.51461	0.334
	5	50-70	0.10060	0.51506	40	0.00207	1.91432	-1.46461	0.51461	0.334
	6	70-95	0.10060	0.51506	20	0.00207	1.91432	-1.46461	0.51461	0.334
	7	95-120	0.10060	0.51506	10	0.00207	1.91432	-1.46461	0.51461	0.334
	8	120-200	0.10060	0.51506	2	0.00207	1.91432	-1.46461	0.51461	0.334
4	9	Trench	0.08165	0.47303	200	0.00525	1.62422	-1.84898	0.46923	0.949

8.2.4 Calibration of the solute transport part of the model

The hydraulic properties of the final calibration of the water flow part of the model (Table 8.3) were used for the simulations including solute transport. As initial condition the measured nitrate concentrations on 17 December 1991 ($t = 0$) were used. A longitudinal dispersivity $a_l = 10 \text{ cm}$ and a transversal dispersivity $a_t = 1 \text{ cm}$ were initially chosen. Nitrate was considered to be a conservative solute, so no production, transformations or exchange was taken into account. Figure 8.10 shows that the dynamics of the nitrate concentrations in the drainage water are simulated well, although the concentrations were overestimated. The sensitivity of the results for the choice of the dispersivities was evaluated by reducing the dispersivities by a factor 10 and 100, respectively. The smaller dispersivities resulted in less spreading of the nitrate and lower nitrate concentrations in the drainage water (Fig. 8.10). The nitrate concentrations in the drainage water became larger at larger dispersivities because the peak of the nitrate concentration had not reached the drain yet, and under these conditions an extra spreading of nitrate leads to a faster breakthrough of part of the nitrate in the drain. Also at smaller dispersivities the simulated concentrations were larger than the measured concentrations. However, the dynamics of the nitrate concentration in the drainage water is dominated by the changes in flow patterns

under different hydrological conditions. The convective part of the solute transport determines the peaks in nitrate concentrations. Because the very small values of $a_l = 0.1$ cm and $a_t = 0.01$ cm resulted sometimes in numerical instability, $a_l = 10$ cm and $a_t = 1$ cm were used as representative values in the later simulations. The order of magnitudes of these dispersivities corresponds to the dispersivities of 5-20 cm given by Van Hoorn *et al.* (1981) for field-scale solute transport.

The transient simulations of solute transport were precise with respect to the solute mass balance. At daily intervals errors were typically $< 0.1\%$. This percentage represents the errors in amounts of solutes in the flow domain relative to the change in total solute amounts. The computation time for the transient solute transport simulations for the 40-day calibration period was typically 16 hours on a 75 MHz IBM-type personal computer.

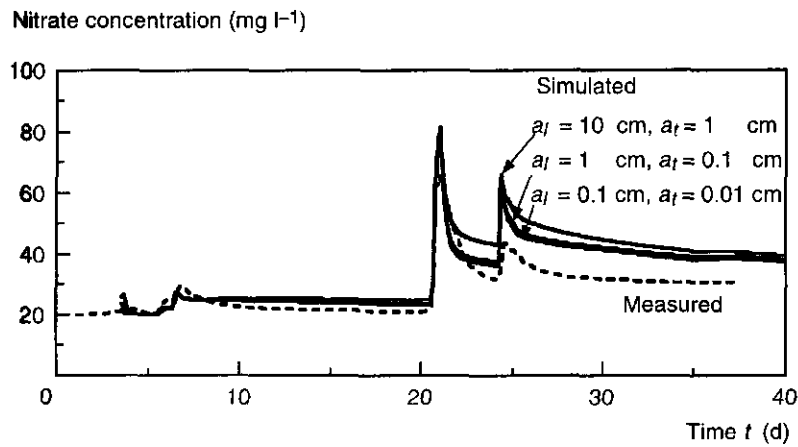


Figure 8.10 Measured and simulated NO_3 concentrations in the drainage water. The simulation results were obtained using the adapted water retention characteristic for the 0-25 cm depth topsoil with $\alpha = 0.02190 \text{ cm}^{-1}$, using different values for the longitudinal dispersivity a_l and transversal dispersivity a_t .

8.3 Simulation of nitrate transport

The soil hydraulic properties presented in the former paragraphs were used for the simulations of all leaching periods (Table 8.3). As atmospheric conditions hourly precipitation and daily potential Makkink evaporation data were used. In the calculation of the reference soil evaporation no reduction factor was used (see Par. 6.3.2). The simulations started at the time of the sampling of NO_3 concentration in autumn or winter. The results of these measurements were used as initial conditions for solute transport. The spatial distribution of NO_3 concentration as a function of the distance from the drain was only accounted in the initial condition at 17 December 1991 ($t = 0$; see Fig. 8.12a). The groundwater level midway between the drains was taken as representative for the depth of the initial phreatic surface. A flat phreatic surface could be used, because the phreatic surface was nearly always below the drain depth at the instants samples were collected to measure the NO_3 concentrations. An equilibrium in hydraulic head was assumed with this phreatic surface to calculate initial pressure heads. Table 8.4 summarises the overall results for all leaching periods. The "leaching period" 1995-1996 was not simulated because there was no drain discharge.

Table 8.4 Overview of the simulation results of the different leaching periods and the field measurements of the same period.

Leaching period	Time interval (d)	Cumulative drain discharge (mm)	Cumulative N discharge (kg ha^{-1})	Cumulative N discharge (kg ha^{-1})	
	Measured	Simulated	Measured	Simulated	
1991-1992	0-160	138	153	12	17
1992-1993	359-500	184	165	22	13
1993-1994	689-940	392	383	38	27
1994-1995	988-1250	578	577	19	17
1994-1995	1250-1350	60	66	7	3

Leaching period 1991-1992

The leaching period from 17 December 1991 to 25 May 1992 ($0 < t < 160$ d) was simulated using the measured NO_3 concentration profile on 17 December 1991 ($t = 0$) as initial condition, including the spatial distribution of NO_3 as a function of the distance to the drain. Groundwater levels are generally simulated at larger depths than the measurements, except for situations with high precipitation rates, i.e. around $t = 7$ d and $t = 21$ d (Fig. 8.11a). Simulated and measured drain discharge rates in the course of time correspond well (Fig. 8.11b). Peak discharge rates are sometimes simulated larger than measured discharge rates. However, in dry periods, i.e. $40 < t < 80$ d, the simulated drain discharge starts later than that measured, which is related to the deeper simulated groundwater level and the corresponding larger water storage capacity.

Nitrate concentrations in the drainage water are overestimated for $0 < t < 90$ d, and are close to the measured data for $t > 90$ d (Fig. 8.11c). The changes in NO_3 concentrations in the drainage water in the course of time are simulated well. Figure 8.12 presents the simulated NO_3 concentration distribution at three characteristic times, showing the vertical displacement and dilution of NO_3 . At high infiltration rates the NO_3 just above the drain is transported downwards rapidly.

Measured and simulated cumulative drain discharges were 138 and 153 mm, and cumulative N discharges were 12 and 17 kg ha^{-1} , respectively (Table 8.4).

Leaching period 1992-1993

The leaching period from 1 December 1992 to 31 March 1993 ($350 < t < 470$ d) was simulated using the measured NO_3 concentration profile on 9 December 1992 ($t = 359$ d) as initial condition. The period before the sampling date was not simulated, although the drain discharge already occurred (Fig. 6.15). The groundwater levels and drain discharge rates are simulated equally well as in the 1991-1992 leaching period (data not shown). The measured and simulated cumulative drain discharges were 184 and 165 mm, respectively (Table 8.4).

The simulated NO_3 concentrations in the drainage water are too low (Fig. 8.13). The net production of NO_3 in the soil profile during the leaching period could be an explanation for the difference between measured and simulated NO_3 concentrations. Figure 6.13 shows a substantial increase in NO_3

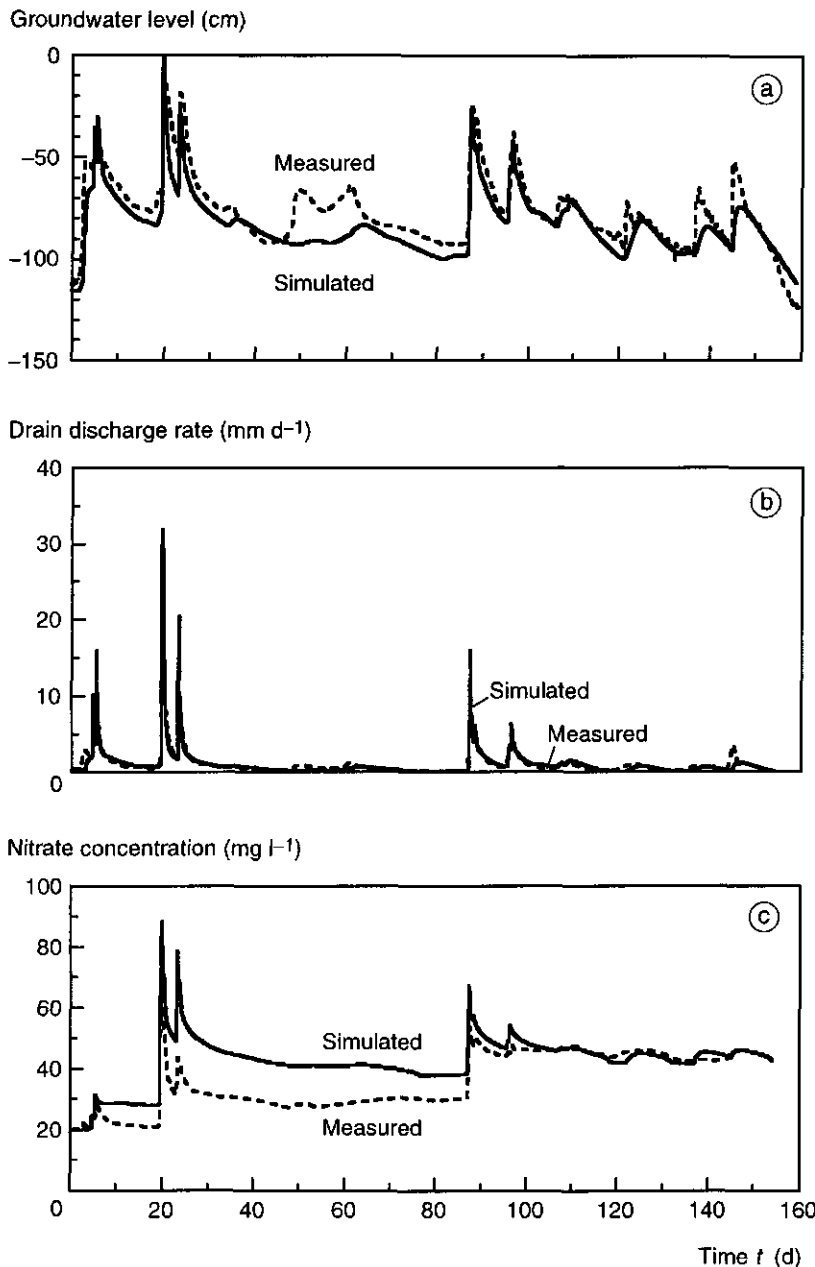


Figure 8.11 Measured and simulated groundwater levels at -6 m distance from the drain (a), drain discharge rates (b), and NO_3^- concentrations in the drainage water (c), for the leaching period from **17 December 1991** to **25 May 1992** ($0 < t < 160$ d).

concentrations in the top 20 cm of the soil, most likely due to mineralisation and deposition. Table 6.2 shows that total N content to a depth of 100 cm increased from 45 kg ha^{-1} at $t = 359 \text{ d}$ to 67 kg ha^{-1} at $t = 471 \text{ d}$. However, in the simulations the N content decreased to 37 kg ha^{-1} at $t = 471 \text{ d}$, because no N mineralisation was accounted for. Especially at peak discharge rates, when water is originating from the topsoil, large errors occur in the simulated NO_3 concentrations. The simulated NO_3 concentrations in the topsoil decrease due to fresh water infiltrating at the soil surface, while in the field an increase in NO_3 concentrations occurs. However, the large differences in simulated and measured concentrations at the start of the simulation period cannot be explained by N mineralisation. The measured and simulated cumulative N discharge were 22 and 13 kg ha^{-1} , respectively (Table 8.4).

Leaching period 1993-1994

The leaching period 4 November 1993 to 25 April 1994 ($689 < t < 860 \text{ d}$) was simulated using the NO_3 concentration profile measured on 4 November 1993 ($t = 689 \text{ d}$) as initial condition. Figure 8.14 shows that the simulated NO_3 concentration in the drainage water around $t = 700 \text{ d}$ starts too low, but changes in NO_3 concentrations are simulated at the right times. For $730 < t < 820 \text{ d}$ the simulated concentrations are close to the measurements, although the peaks in NO_3 concentrations are more extreme in the simulations. For $t > 820 \text{ d}$ the NO_3 concentrations are substantially lower than the measurements. Measured and simulated cumulative drain discharges were 392 and 383 mm, and cumulative N discharges were 38 and 27 kg ha^{-1} , respectively. Table 6.2 shows that to a depth of 100 cm an N amount of 42 kg ha^{-1} was formed by net N mineralisation or deposition during the leaching period. This was not accounted for in the simulations.

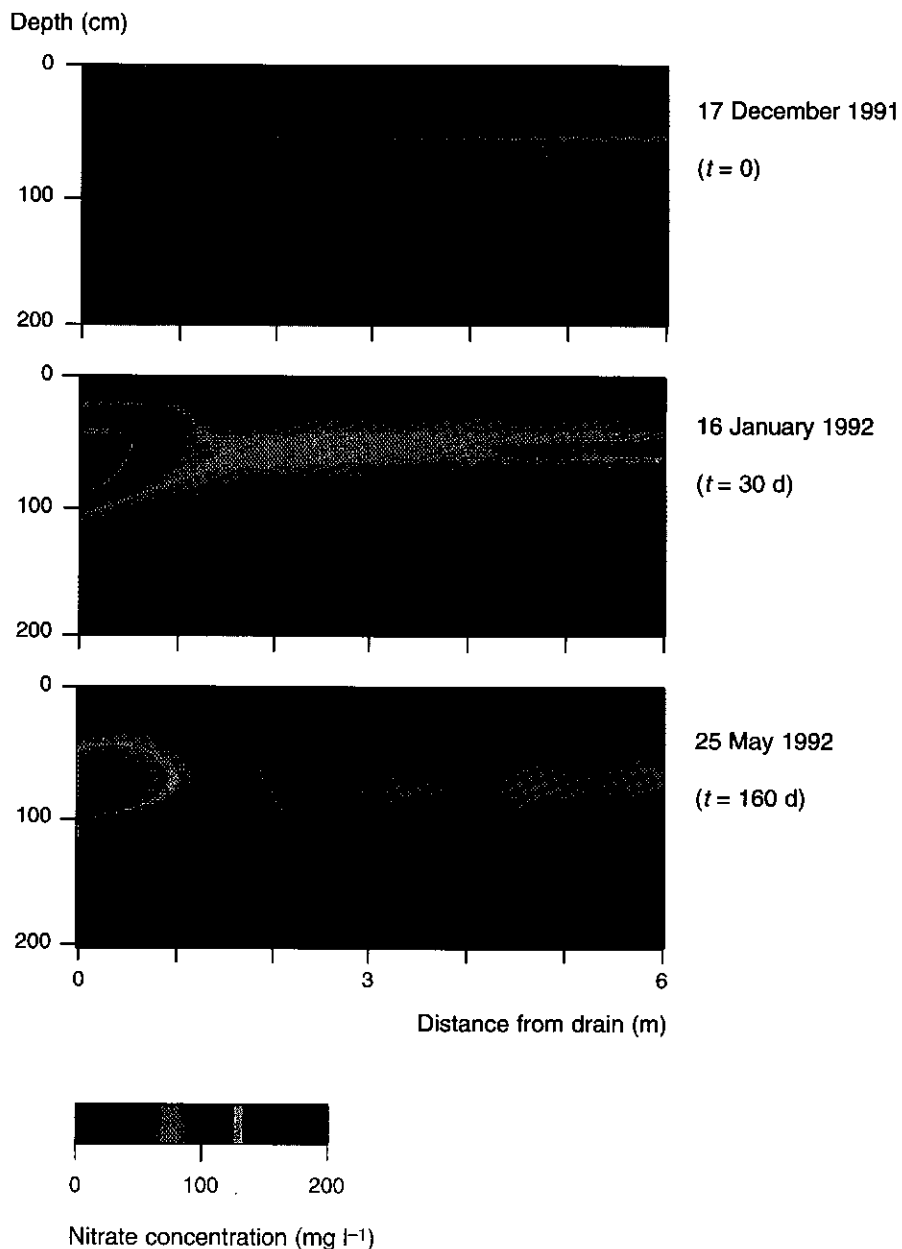


Figure 8.12 Simulated NO_3 concentration distribution in the flow domain for three characteristic times during the leaching period from 17 December 1991 to 25 May 1992 ($0 < t < 160$ d).

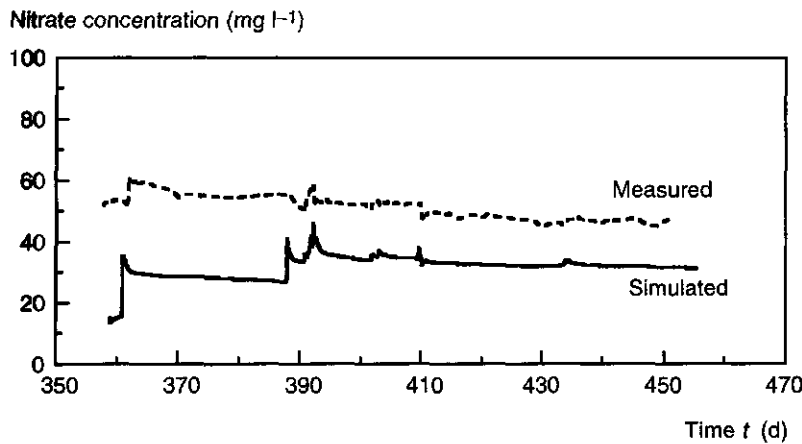


Figure 8.13 Measured and simulated NO_3 concentrations in the drainage water for the leaching period 1 December 1992 to 31 March 1993 ($350 < t < 470$ d).

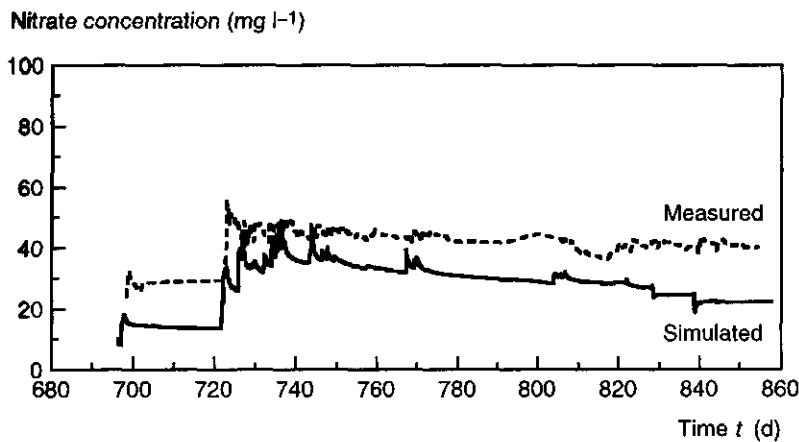


Figure 8.14 Measured and simulated NO_3 concentrations in the drainage water for the leaching period from 4 November 1993 to 25 April 1994 ($689 < t < 860$ d).

Leaching period 1994-1995

The leaching period from 30 August 1994 to 28 August 1995 ($988 < t < 1350$ d) was simulated using the measured NO_3 concentration profile on 30 August 1994 ($t = 988$ d) as initial condition. Figure 8.15 shows that in the period $988 < t < 1110$ d the simulated NO_3 concentrations were overestimated, and underestimated in the period $1110 < t < 1250$ d. Both simulations and measurements show low NO_3 concentrations. Measured and simulated cumulative N discharges were 19 and 17 kg ha^{-1} , respectively (Table 8.4).

The period after the application of fertiliser in spring 1995 ($t > 1250$ d) was simulated separately, using the measured NO_3 profile data and the applied fertiliser as new initial conditions. The fertiliser was assumed to be distributed homogeneously through the first 20 cm of the topsoil. The high NO_3 concentration peaks in the drainage were not simulated well. Although small peaks were simulated, the main part of the applied NO_3 had not been transported to the drain yet. The measured and simulated cumulative N discharges in this period were 6.9 and 2.8 kg ha^{-1} , respectively (Table 8.4).

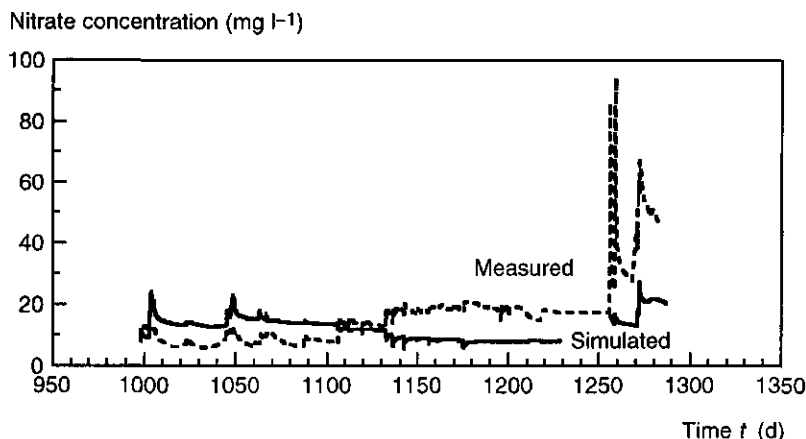


Figure 8.15 Measured and simulated NO_3 concentrations in the drainage water for the leaching period from 30 August 1994 to 28 August 1995 ($988 < t < 1350$ d).

8.4 Simulation of chloride leaching and the bromide tracer experiment

Chloride leaching 1991-1992

The simulation of the water balance for Cl transport in the leaching period from 17 December 1991 till 15 April 1992 ($0 < t < 120$ d) was the same as the water balance used for NO_3 transport (Par. 8.3). The measured Cl distribution in the field (Fig. 6.7) was used as initial condition. So, initial Cl concentrations were relatively high in the subsoil and relatively low in the topsoil. The simulated Cl concentrations in the drainage water are a factor of about 1.5 larger than the measured Cl concentrations (Fig. 8.16). However, the relative changes in Cl concentrations are simulated very well. The minimum in Cl concentrations correspond with high drain discharge rates; the maximum in Cl concentrations correspond with low drain discharge rates. The cumulative Cl discharges for the measurements and simulations were 180 and 353 kg ha^{-1} , respectively.

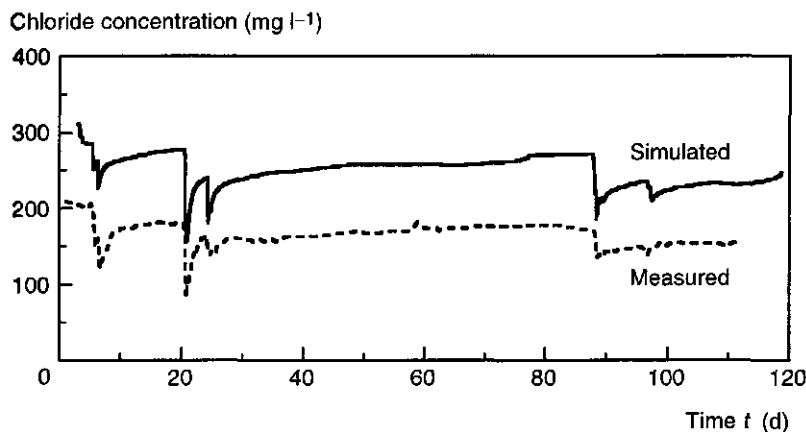


Figure 8.16 Measured and simulated Cl concentrations in the drainage water for the leaching period from 17 December 1991 to 15 April 1992 ($0 < t < 120$ d).

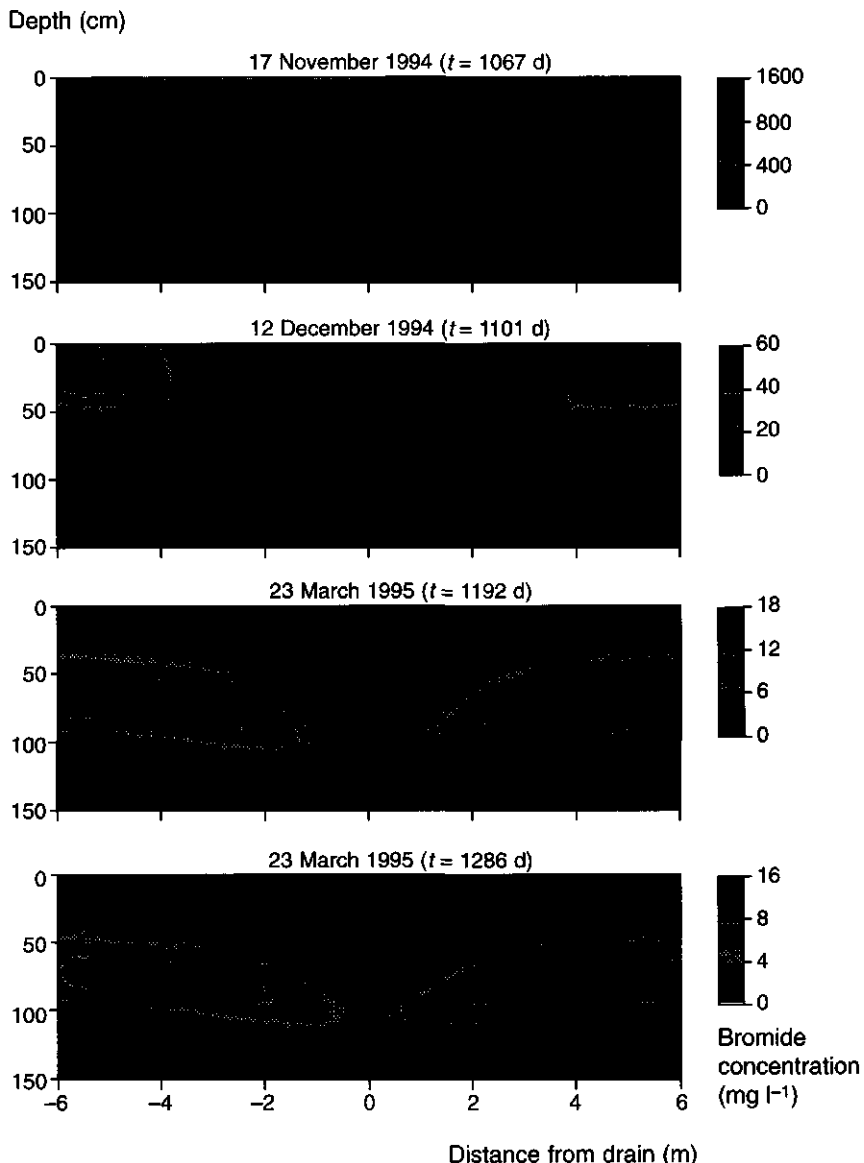


Figure 8.17 Simulated Br concentration distribution in the flow domain for four characteristic times during the leaching period 17 November 1994 to 9 July 1995 ($1067 < t < 1300$ d). The first three times correspond with the measurements presented in Fig 6.23.

Bromide tracer experiment

The Br leaching period 17 November 1994 to 26 July 1995 ($1067 < t < 1317$ d) was simulated using the soil hydraulic properties presented in Table 8.3, while using hourly precipitation and daily potential Makkink evaporation data. The initial Br distribution in the soil profile in the simulation was obtained by defining a maximum concentration at the nodal points of the soil surface at 4-6 m from the drain. The SWMS_2D model assumes linear gradients in concentrations between all nodal points, which results in a smoothing of the Br pulse applied to the soil surface. The maximum Br concentration was chosen in such a way that a correct total Br mass in the surface layer was obtained.

The groundwater levels and drain discharge rates seems to be simulated equally accurate as in the leaching periods discussed before (data not shown). However, the measured and simulated cumulative drain discharge were 482 and 425 mm, respectively. This 11% difference was larger than in the other leaching periods. It appeared that the soil evaporation became rather high during dry periods. Therefore, potential soil evaporation was reduced by a factor 0.67 for the entire period. Now, the simulated cumulative drain discharge was 483 mm, which is close to the measured 482 mm.

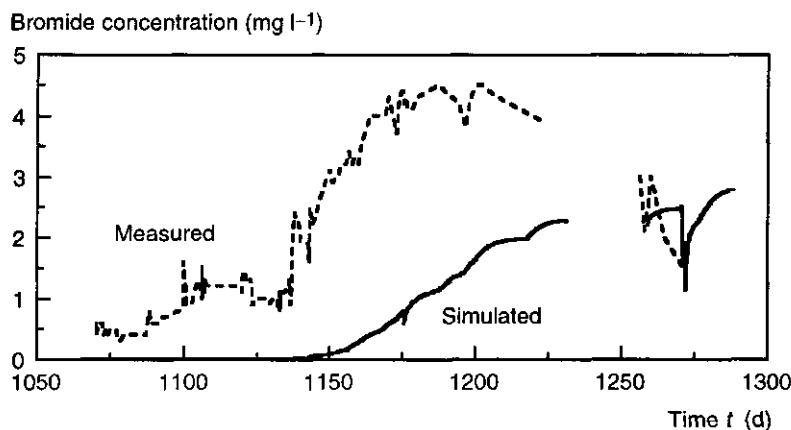


Figure 8.18 Measured and simulated Br concentrations in the drainage water for the leaching period 17 November 1994 to 9 July 1995 ($1067 < t < 1300$ d).

Figure 8.18 shows the simulated and measured Br concentration in the drainage water. The simulated Br breakthrough occurred later and Br concentrations were underestimated. The maximum Br concentration in the drainage water was measured around $t = 1200$ d, while in the simulations the maximum was not yet found. Figure 8.17 shows the simulated Br concentration distribution in the soil profile at the same times that soil samples were taken (see Fig. 6.23). Bromide was transported vertically and horizontally towards the drain. Bromide concentrations below the application zone remain relatively high. The maximum Br concentration in the soil decreases rapidly, due to mixing with fresh water. Bromide concentrations remain relatively low in the zone above the drain, because when the phreatic surface is shallow fresh water infiltrated at the soil surface flowed rapidly to this zone. Also in the zone far from the drain, close to the watershed of the catchment area of the drain (6 m from the drain), Br concentrations decrease because Br is transported away from this zone. Although the simulated Br concentrations in the soil profile are overestimated, the simulated Br distribution pattern resembles the field data (Fig. 6.23). The very dry period for $t > 1286$ d could not be simulated, probably because the finite element grid near the soil surface was not dense enough to find converging solutions at variable H gradients. This is why Fig. 8.17 presents the final Br concentration distribution at $t = 1286$ d instead of at $t = 1316$ d, corresponding with Fig. 6.23.

The overall Br mass balance of the simulations results in a cumulative drain discharge of 2.5 kg ha^{-1} , which is much lower than the 11 kg ha^{-1} discharge measured in the field. In the simulations the background Br concentration was assumed to be zero. However, the Br concentration in the drainage water measured at $t = 1060$ d, when no applied Br is expected in the drain yet, indicates a background Br concentration of 0.5 mg l^{-1} . Adding this background concentration results in a Br discharge of 2.5 kg ha^{-1} for the entire leaching period. Correcting the simulated Br discharge for this amount, would result in a total simulated Br discharge of 5 kg ha^{-1} .

8.5 Discussion

Description of the drain

The subsurface drain is described as a half circular hole with all or part of its inner wall functioning as a seepage face. The pressure head is $h = 0$ at parts of the drain which are below the phreatic surface and which are actually draining. It was observed in the field that the ditch water level could rise above the drain outlet under extremely wet conditions. Then, the $h = 0$ boundary condition in the drain is no longer valid. The whole drain is filled with water and the hydraulic head in the drain can be assumed to be equal to the hydraulic head in the ditch, ignoring the hydraulic head loss over the length of the drain itself. This situation results in smaller drain discharge rates at given groundwater levels midway between the drains than for situations with a deeper ditch water level. Some of the variation in the measured relationship between drain discharge rate and groundwater level (Fig. 8.5) can be attributed to this effect. In the SWMS_2D model a varying hydraulic head in the drain can be taken into account by using a variable prescribed pressure head as boundary condition at the inner wall of the drain. However, this means that the pressure head has to be measured in the field at time intervals of about 15 minutes. Such data were not available for the first part of this study, and later the ditch water level always remained below the drain depth, hence this option could not be implemented in the model. Because the highest water and nitrate discharge rates occur during periods when the ditch water level may be high, this feature should be accounted for in future research.

The drain depth is taken at 97.5 cm depth. However, in the experimental field the drain depth ranges from 91-104 cm depth over the length of the field (see Par. 4.1.3). This difference in depth means that the drainage can still continue when the groundwater level in the centre of the field drops below the drain depth, because part of the field close to the ditch with a larger drain depth can still discharge water. Especially for phreatic surfaces close to the drain depth, the difference of a few centimetres in drain depth will have a considerable effect on the small hydraulic head gradient. However, the hydraulic conductivities in the subsoil are low and the drain discharge rates are low. Consequently, the errors relative to drain discharge in the entire leaching period remain small.

The drain trench with its relatively large K_s enhances fast vertical transport to the drain. In the field the drain trench was clearly visible when a soil pit was dug, because it had a different colour and no layering, as compared to the

undisturbed soil. Figure 4.16 shows that K_s in the drain trench is large. This large K_s only plays a role when the drain trench is saturated or close to saturation. Due to this large K_s the simulated groundwater levels above the drain remain close to the drain depth under most conditions.

The drain is assumed to be ideal, which means that no extra resistance is taken into account explicitly for hydraulic head losses due to its limited inlet area relative to its outer area. Stuyt (1992) found that the larger pores connecting a drain with the surrounding soil dominate the functioning of the drain. Then, the concept of potential flow to a drain is not valid. However, in the calibration procedure of K_s for the different soil layers a possible entrance resistance would result in larger values of K_s for the soil layers to achieve a comparable relationship between groundwater level and drain discharge rate. Especially, the K_s of the drain trench and a possible entrance resistance are closely linked. This K_s was fixed, and it was decided to ignore the effects of a specific entrance resistance to reduce the degrees of freedom in the calibration procedure. The simulated drain discharge rates at shallow phreatic surfaces were smaller than the measured data. This was an extra reason to ignore the entrance resistance.

Description of the hydraulic conductivity characteristic

The hydraulic conductivity characteristic close to saturation was adapted to create a smooth transition in K from the saturated to the unsaturated zone. Nevertheless, the steepness of this characteristic for the topsoil close to saturation resulted in numerical problems during high infiltration rates when the phreatic surface was shallow. The choice of $h_k = -20$ cm as a threshold value was based on practical considerations. This h_k has to be chosen as close as possible to $h = 0$, but on the other hand the numerical calculations have to converge. Creating a denser grid would perhaps allow a less negative h_k , i.e. $h_k = -10$ cm. However, this denser grid would lead to longer computation times.

The consequence of the linear increase of K close to saturation is that the zone with a thickness of about $|h_k| = 20$ cm above the phreatic surface will contribute substantially to the horizontal water flow and will behave somewhat like a saturated part of the soil. The choice of h_k has a direct effect on the position of the phreatic surface. When a discontinuous change in hydraulic conductivity to K_s is assumed at $h = 0$, the phreatic surface has to be about $|0.5 h_k| = 10$ cm higher as compared to the situation with a linear increase in K to achieve similar discharge rates. The more negative h_k is chosen, the deeper the phreatic surface

will be simulated. The drain discharge rate is determined by both the distribution of K and the hydraulic head gradients, and is thus less sensitive to the exact position of the phreatic surface. In the comparison of measured versus simulated data, the drain discharge rate data should be weighted more than the groundwater level data.

Numerical problems in SWMS_2D

This chapter presents simulation results of SWMS_2D. However, sometimes numerical problems in the calculations occurred. In particular when the soil evaporation rate was high during a few days no converging solutions were found. Probably, this can be solved by increasing the grid density close to the soil surface to be able to simulate the strongly varying hydraulic head gradients. No attempt was made to optimise the grid density for these situations, because converging solutions in the wetter leaching periods were considered as more relevant. So, it could happen that simulation periods were shorter than the measurement periods. For example the dry period at the end of the Br tracer experiment could not be simulated. In fact, in that period a potato crop was already growing in the field, for which water and Br uptake should be simulated also.

At relatively small dispersivities, the numerical dispersion occurring in the computations became apparent in the simulated concentration distributions. The distances between the nodes of the finite element grid were in the order of centimetres, while dispersivities $a_l = 1$ cm and $a_t = 0.1$ cm were an order of magnitude smaller. This resulted in erratic distributions of the solute concentration. Using larger values of a_l and a_t , i.e. $a_l = 10$ cm and $a_t = 1$ cm, resulted in smooth concentration distributions as shown in Figs. 8.12 and 8.17.

Darcian flow and the convection-dispersion description for solute transport

The overall water balance and the Darcian water fluxes are simulated satisfactorily. The large values of K_s are realistic for the Lovinkhoeve soil. However, the origin of the large K_s values is related to the occurrence of macropores, worm holes, old root channels and small cracks. Evidence for the functioning of these larger pores was found during the K_s measurements (Par. 4.2.4) and the Br tracer experiment (Par. 6.7). This means that the water flow is not homogeneously distributed over the soil at the microscopic scale. Under saturated conditions, water flow at the macroscopic scale can still be described

well by large K_s values and Darcian flow.

The consequences of using macroscopic effective hydraulic conductivities are much more important for solute transport. Under saturated conditions the main flow is through the larger pores. The solutes will not reside only in these larger pores but also in the soil matrix. Then, the dynamics of solute transport depends on the rate of solute exchange between the soil matrix and the larger pores. These exchange processes could be described by introducing an absorption-desorption term in the solute transport equations or by using complex dual porosity transport models (Van Genuchten *et al.*, 1984; Nieber and Misra, 1993). In this study the possible exchange processes were ignored. The limited objective was to evaluate how well a two-dimensional Darcian water flow model could describe the field scale processes, using the convection-dispersion approach for solute transport.

The temporal patterns of nitrate and chloride concentrations in the drainage water are simulated well, which indicates that water flow is dominant and well described. However, the absolute levels of nitrate and chloride concentrations in the drainage water are both simulated too high in the period $0 < t < 100$ d (Figs. 8.11c and 8.16). Periods with high flow rates are decisive for the solute transport to drains and the changes in solute distributions in the soil profile. In these periods the water in the larger pores could have lower solute concentrations than the soil matrix due to the lack of time for solute exchange with the soil matrix. Because this exchange is not accounted for, the simulated solute concentrations in the drainage water could be larger than the field data. Both nitrate and chloride concentrations are simulated too high, while their initial distributions in the soil profile were opposite. So, it is not likely that errors in simulated water flow and corresponding errors in the flow paths of solutes are the source of the deviation. In that case only one of the concentrations of NO_3 or Cl would have been simulated too high, and the other too low.

The simulations of Br and Cl transport indicated that the applicability of the convection-dispersion approach for the Lovinkhoeve field is limited. Especially, the Br field data showed rapid vertical transport, which could not be simulated with the convection-dispersion model. Bromide breakthrough was simulated later than measured. In contrast to NO_3 and Cl , the Br concentrations in the drainage water were simulated too low. However, there is a large difference between the distribution of Br present in the soil and NO_3 and Cl . Bromide was recently applied to the soil surface and was transported rapidly downwards during a wet

period just after the Br application. It is not likely that Br was homogeneously distributed in the soil already, but it would have been located close to the larger pores through which it was transported downwards. The chance to be transported with water flowing through these same large pores at later times is then larger for Br than for solutes like NO_3 and Cl, which are probably more homogeneously distributed. Under these conditions the measured Br concentrations will be larger than simulated with a convection-dispersion model.

It was not tried to optimise the simulation results using the NO_3 leaching data of the later leaching periods. The SWMS_2D model has many degrees of freedom related to water flow and solute transport, and it was already difficult to obtain converging solutions for the complex saturated-unsaturated water flow problem, due to the strong non-linearities in hydraulic conductivities in the layered soil profile. Uncertainties in N mineralisation made it difficult to improve the NO_3 transport part. More complex models, taking into account macro-pore flow and exchange between the soil matrix and larger pores, should be tried to simulate the Lovinkhoeve field situation. However, for these models even more soil physical information is needed, and still the two-dimensional character of the water flow and transport processes has to be described. Such an approach was beyond the scope of this thesis.

Diffusion was not taken into account in the simulations of solute transport. Especially for Cl transport the upward diffusion is a major component of the long-term Cl mass balance (Par. 6.4). Incorporation of upward diffusion in the simulations would result in even higher simulated Cl concentrations in the drainage water. A more detailed study of the nature of Cl transport and of the quantification of the upward Cl diffusion from the subsoil is necessary to simulate Cl transport more accurately. A 120 cm depth for the impermeable layer in the simulation instead of 200 cm depth could improve the simulations, because then the Cl at high concentrations in the 120-200 cm depth zone can be transported upwards only by diffusion. Although the hydraulic conductivity at saturation in the 120-200 cm depth layer $K_s = 2 \text{ cm d}^{-1}$ was small, still a substantial amount of solutes could reach this zone (Fig. 8.12 and Fig. 8.17).

Theories on water flow and solute transport

In the literature there is much emphasis on dual porosity models and preferential flow. The dual porosity theory distinguishes between mobile and immobile water and exchange processes between the two domains of macro-pores and aggregates (Raats, 1981a; Van Genuchten *et al.*, 1984). In the Lovinkhoeve silt loam soil aggregates are present, and a dual porosity description of the transport mechanisms could be appropriate. However, especially for field situations, the characterisation of dual porosity flow properties is complex and not standard (Roth *et al.*, 1990). Bootink (1993) studied field transport processes in the Flevopolder, where the soil has a higher clay content than in the Noordoostpolder. He showed that under conditions with free water on the soil surface, the large, vertical, continuous cracks connecting the topsoil with the subsoil resulted in rapid solute transport to the subsurface drains. Under drier conditions these cracks and macro-pores will not contribute to water flow. Bronswijk (1988) developed a transport model including preferential flow due to shrinkage cracks in heavy clay soils. Although there is limited swelling and shrinkage at the Lovinkhoeve, the research approaches of Bootink (1993) and Bronswijk (1988) appears to be more appropriate for heavy clay soils than for the Lovinkhoeve silt loam soil.

Two-dimensional model

It is clear that the two-dimensional flow patterns have a dominant effect on solute transport. Especially water flow below and just above the phreatic surface contributes substantially to horizontal solute transport. Therefore, much attention was focused on the saturated zone and the hydraulic conductivity near saturation, and less on the unsaturated zone. The groundwater level - drainage discharge rate was optimised using eight soil layers and a drain trench with different hydraulic characteristics. Probably a reduction of the number of soil layers is possible without loosing too much detail of the water flow patterns. However, a sensitivity analysis for the effect of the number of soil layers on, e.g., the relationship between groundwater level and drainage discharge rate was too time-consuming to be carried out in this study.

This study focused on NO_3 leaching and no special attention was given to the optimisation of the simulated soil physical conditions in the unsaturated zone. The conditions in the unsaturated zone depend largely on the choice of K_s of the deeper layers. If, instead of water movement and solute transport, the soil

physical conditions in the unsaturated zone are subject of study, for example in studies on oxygen transport or biological studies, a one-dimensional model would be appropriate. By using the boundary conditions at the bottom of the soil profile, for example measured groundwater levels, one-dimensional simulations can be carried out at different distances from the drain. Under wet conditions, when the largest spatial differences occur, the hydraulic heads in the unsaturated zone will be close to the equilibrium with the phreatic surface. Then, this equilibrium can be used directly as a very simple model to infer the soil physical conditions in the field (Assinck, 1995).

Modelling NO₃ leaching

Nitrogen dynamics plays an important role in determining actual NO₃ concentrations in the soil profile. Considering NO₃ as a conservative solute leads to errors of simulated NO₃ concentrations in the drainage water. Field data of the N balance (Fig. 6.13 and Table 6.2) show that also during winter leaching periods considerable increases in NO₃ contents occurred due to net mineralisation and deposition; especially during relatively dry periods. Other processes like immobilisation and denitrification make the description of the N dynamics even more complex, as already discussed in Chapter 6. Of course it was known before the start of the experiments and the modelling that only considering convective and dispersive NO₃ transport is a great simplification. Despite the limitations in modelling solute transport in general and NO₃ transport in particular, the next section describes some explorative simulations to illustrate the effect of different atmospheric conditions, hydrological boundary conditions and N mineralisation on NO₃ leaching.

8.6 Explorative two-dimensional simulations

In this section examples are given of two-dimensional simulations of water flow and nitrate transport, using different meteorological conditions, a downward seepage rate at the bottom of the soil profile, a smaller drain spacing, and N mineralisation. The aim of the simulations is to get a better understanding of the transport processes and to quantify changes in NO₃ leaching. Simulations can help to evaluate the effect of possible measures to reduce NO₃ leaching. The simulations of the leaching period 1991-1992 ($0 < t < 160$ d) were used as

reference simulation (Par. 8.2). The measured distributions in the field on 17 December 1991 ($t = 0$) were taken as initial NO_3 concentrations, including the spatial NO_3 distribution as a function of the distance from the drain (Fig. 6.5). Table 8.5 summarises the inputs and results for the different simulations. To illustrate the effect of N mineralisation on N leaching, the leaching period 1993-1994 was chosen, because Table 6.2 indicates that the N mineralisation was large in this period.

Table 8.5 Initial conditions with respect to the NO_3 distributions as function of the distance from the drain, and the simulation results of the different leaching periods and the field measurements for the same period.

Simulation	Leaching period	Initial NO_3 distribution	Cumulative drain discharge (mm)	Cumulative N discharge (kg ha^{-1})
Reference	1991-1992	Spatial pattern	153	17.3
Uniform precipitation	1991-1992	Spatial pattern	143	11.1
Meteo 1992-1993	1991-1992	Spatial pattern	340	38.4
Downward seepage	1991-1992	Spatial pattern	120	14.3
6 m drain spacing	1991-1992	Uniform	157	12.2
N mineralisation	1992-1993	Uniform	165	14.3

8.6.1 Results of the simulations

Uniform distribution of precipitation

In this example the cumulative amount of measured precipitation of the 160 d leaching period 1991-1992 was distributed uniformly over this period, resulting in an average precipitation rate of 1.7 mm d^{-1} . The steady infiltration at the soil surface results in a slow rise of the groundwater level in the period $0 < t < 20 \text{ d}$ (Fig. 8.19a) and a slow fall of the groundwater level for $t > 60 \text{ d}$, which is the period when soil evaporation increased. The drain discharge rate remains nearly constant for $20 < t < 100 \text{ d}$ and decreases slowly for $t > 120 \text{ d}$ (Fig. 8.19b). The breakthrough of NO_3 in the drainage water is smooth (Fig. 8.19c), and NO_3 concentrations remain relatively low. The cumulative N leaching is 11.1 kg ha^{-1} , which is 36% lower than the 17.3 kg ha^{-1} N leaching simulated for the reference situation with the actual precipitation distribution (Table 8.5).

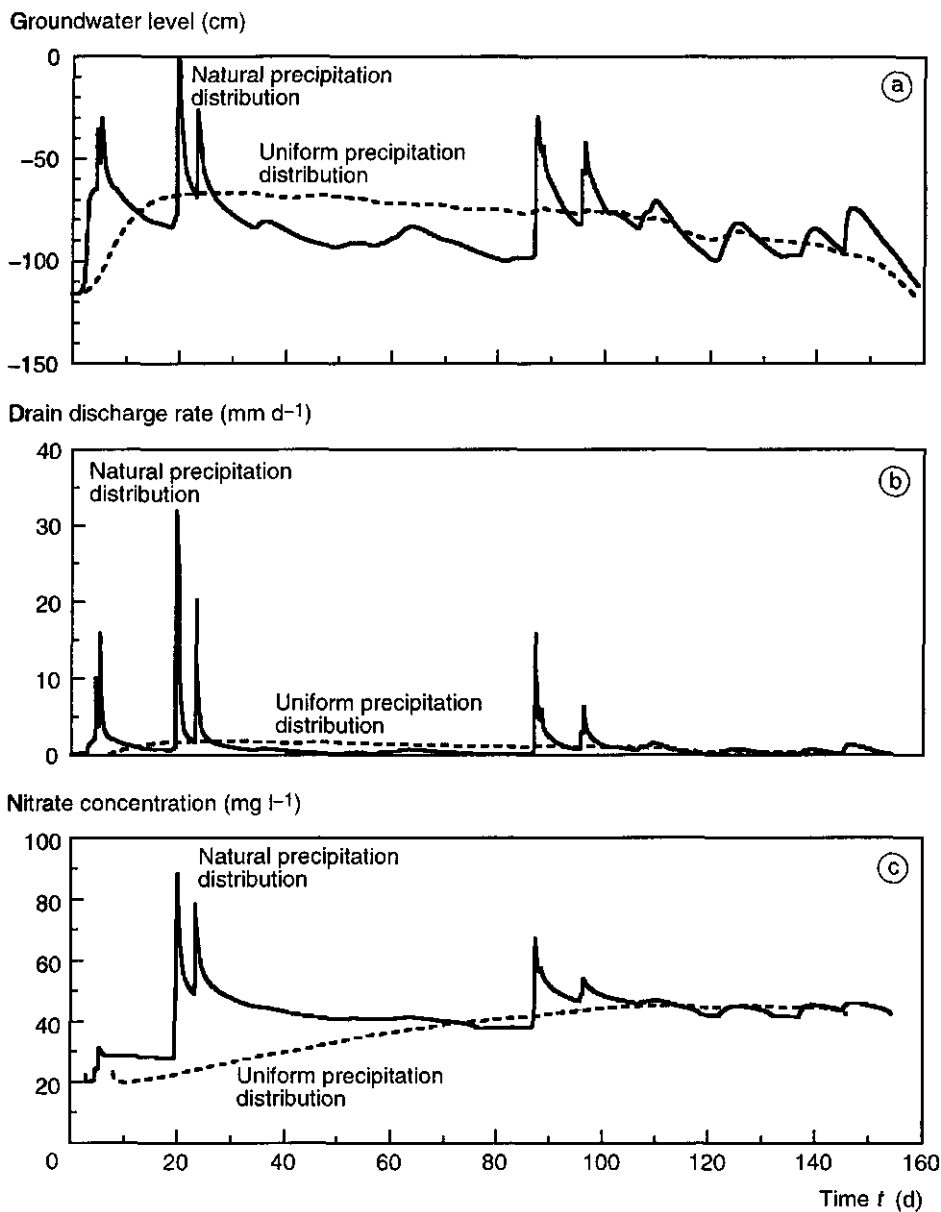


Figure 8.19 Two-dimensional simulations of groundwater levels at -6 m distance from the drain (a), drain discharge rates (b), and NO_3 concentrations in the drainage water (c). The natural precipitation distribution of the leaching period from 17 December 1991 to 25 May 1992 ($0 < t < 160$ d) is used and a uniform redistribution of the same amount of precipitation over the whole period.

Meteorological conditions of leaching periods 1992-1993

In this example the meteorological conditions of the first 160 days of the leaching period 1992-1993 are used as atmospheric boundary conditions in the simulations (see Fig. 6.15a). These conditions can be considered as more representative average hydrological conditions than the meteorological conditions in the relatively dry leaching period 1991-1992. Shallower groundwater levels are simulated with more peaks of the groundwater level reaching the top 25 cm of the soil profile (Fig. 8.20a). This results in higher drain discharge rates (Fig. 8.20b). Peaks in NO_3 concentrations in the drainage water (Fig. 8.20c) correspond with peaks in groundwater level and drain discharge rates. The fluctuations in NO_3 concentrations are dominated by convective transport. At the end of the simulation period most of the NO_3 has been transported downwards or discharged, and later peaks in the groundwater level ($t > 100$ d) result in a decrease of NO_3 concentrations in the drainage water, because this water mainly originates from the topsoil where the NO_3 concentrations are then low. The cumulative drain discharge using the meteorological conditions of 1992-1993 is 340 mm, which is 220% larger than the 153 mm simulated for the reference situation. The cumulative N leaching was 38.4 kg ha^{-1} which is 220% larger than the 17.3 kg ha^{-1} simulated for the reference situation (Table 8.5).

Downward seepage

A maximum downward seepage of 25 mm during the first 112 days of the leaching period was estimated from the field water balance (Par. 6.3.2). In the reference simulation the boundary at 2 m depth is an impermeable ("no flow") boundary. To illustrate the effect of downward seepage on NO_3 transport, a constant water flux density of 0.22 mm d^{-1} was used as a boundary condition at 2 m depth. The small downward seepage results in a deeper phreatic surface (Fig. 8.21a) and the drain discharge rates become smaller (Fig. 8.21b), because part of the water leaves the soil profile at 2 m depth. The simulated cumulative drain discharge for the 160-day simulation period decreases from 153 mm for the reference situation to 120 mm with downward seepage. The simulated NO_3 concentrations in the drainage water increase due to the extra downward water and NO_3 movement (Fig. 8.21c), although at peak discharge rates the maximum NO_3 concentrations decrease. The total NO_3 leaching amounts to 14.3 kg ha^{-1} , which is 17% smaller than the 17.3 kg ha^{-1} for the reference simulation (Table

8. Modelling two-dimensional water flow and solute transport

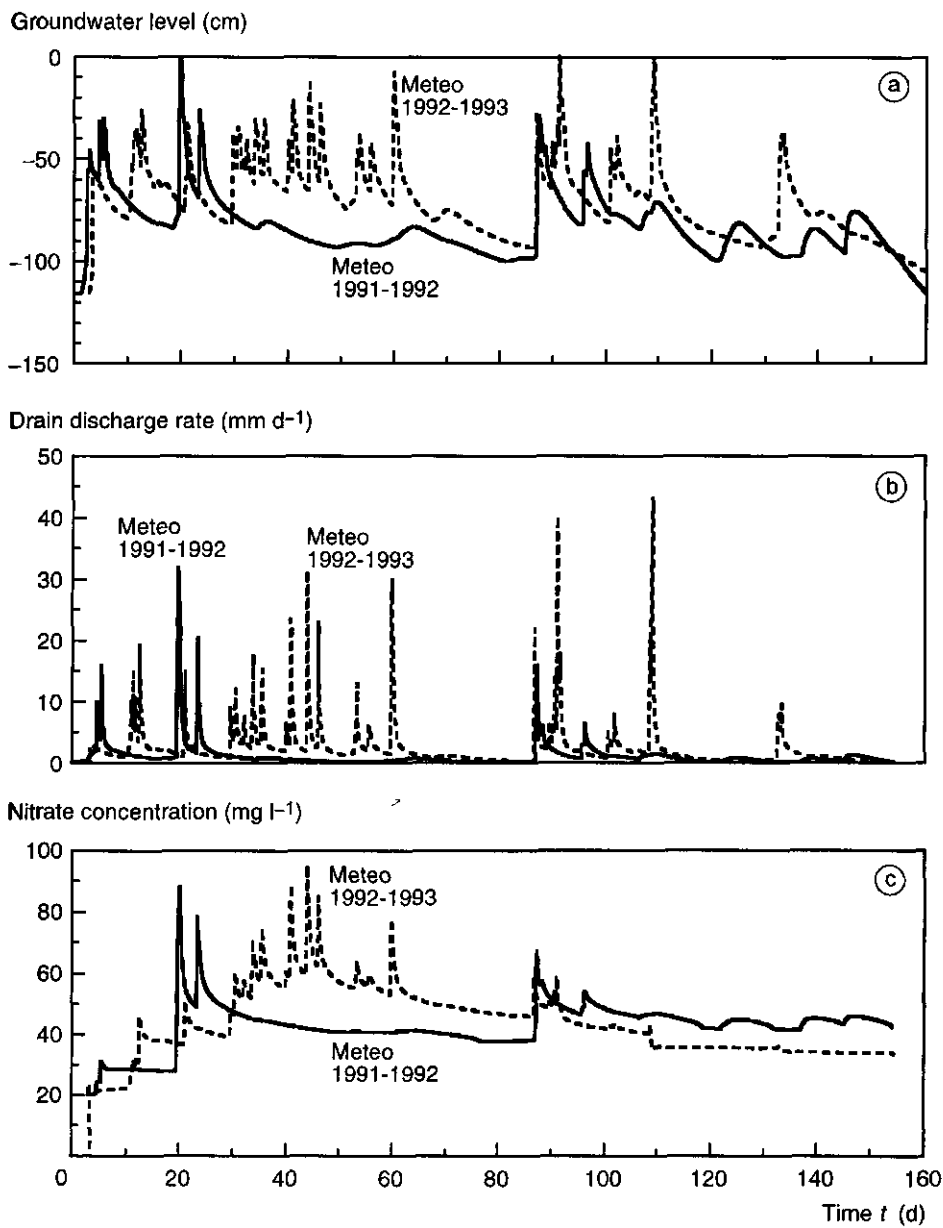


Figure 8.20 Two-dimensional simulations of groundwater levels at -6 m distance from the drain (a); drain discharge rates (b); and NO_3 concentrations in the drainage water (c). The actual meteorological conditions of the leaching period from 17 December 1991 to 25 May 1992 ($0 < t < 160$ d) were used, as well as the meteorological conditions of the first 160 days of the leaching period 1992-1993.

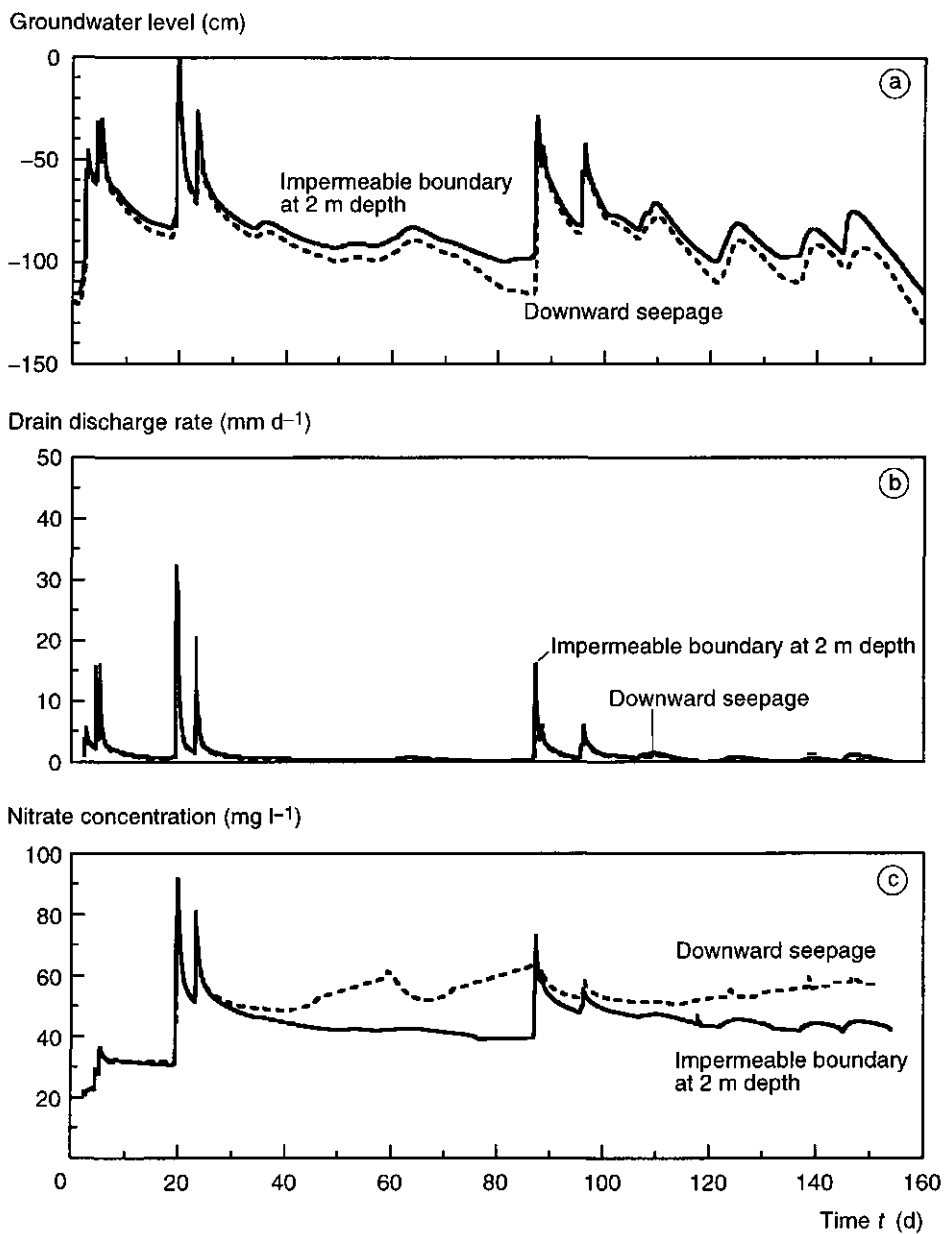


Figure 8.21 Two-dimensional simulations of the groundwater levels at -6 m distance from the drain (a); drain discharge rates (b); and NO_3 concentrations in the drainage water (c). The meteorological conditions of the leaching period from 17 December 1991 to 25 May 1992 ($0 < t < 160$ d) were used, for a situation with an impermeable boundary at 2 m depth, as well as for an uniform and constant downward water flux density of 0.22 mm d^{-1} at 2 m depth.

8.5). For a situation with high NO_3 concentrations in the topsoil a small downward seepage decreases the chance of NO_3 leaching to the drain for meteorological conditions with large variations in precipitation rates.

Reduction of the drain spacing from 12 m to 6 m

At 12 m drain spacing, field measurements and simulations show very shallow groundwater levels. It is common practice to install extra drains between the existing drains to lower the phreatic surface. A smaller drain spacing will also have an effect on the dynamics of NO_3 leaching. To compare NO_3 leaching for 6 m and 12 m drain spacing, the average NO_3 profile distribution of 17 December 1991 ($t = 0$) was used as initial condition, without a spatial distribution as a function of the distance to the drain. A new finite-element grid similar to the grid presented in Fig. 8.1 was generated for the simulation with the 6 m drain spacing, because the dimensions of the flow domain changed.

The groundwater levels midway between the drains are substantially lower for the 6 m drain spacing and the drop of the groundwater level is much faster, *i.e.* $t = 21$ d and $t = 24$ d (Fig. 8.22a). Peak discharge rates are larger and the decrease of the drain discharge rate is more rapid for the 6 m drain spacing than for the 12 m drain spacing (Fig. 8.22b). The smaller flow resistance due to the shorter flow paths to the drain explains this effect (see Eq. 2.14). Figure 8.22c shows lower NO_3 concentrations for the 6 m drain spacing than for the 12 m drain spacing. Because the phreatic surface remains deeper, less NO_3 from the topsoil will be transported rapidly to the drain. In general, a deeper phreatic surface will reduce the chance of high NO_3 concentrations in the drainage water in a layered soil profile with a relatively high hydraulic conductivity in the topsoil. The cumulative N leaching for the 6 m drain spacing was 12.2 kg ha^{-1} , which is 29% smaller than the 17.3 kg ha^{-1} for 12 m drain spacing of the reference simulation (Table 8.5).

N mineralisation

N mineralisation is simulated for the leaching period 1992-1993. It can be inferred from Table 6.2 that there was an N production of 57 kg ha^{-1} in the soil profile from 9 December 1992 ($t = 359$ d) to 31 March 1993 ($t = 471$ d), which is caused by net mineralisation and deposition. Figure 8.13 shows that the simulated NO_3 concentrations in the drainage water were too low.

In this simulation it is assumed that an amount of 57 kg ha^{-1} is mineralised

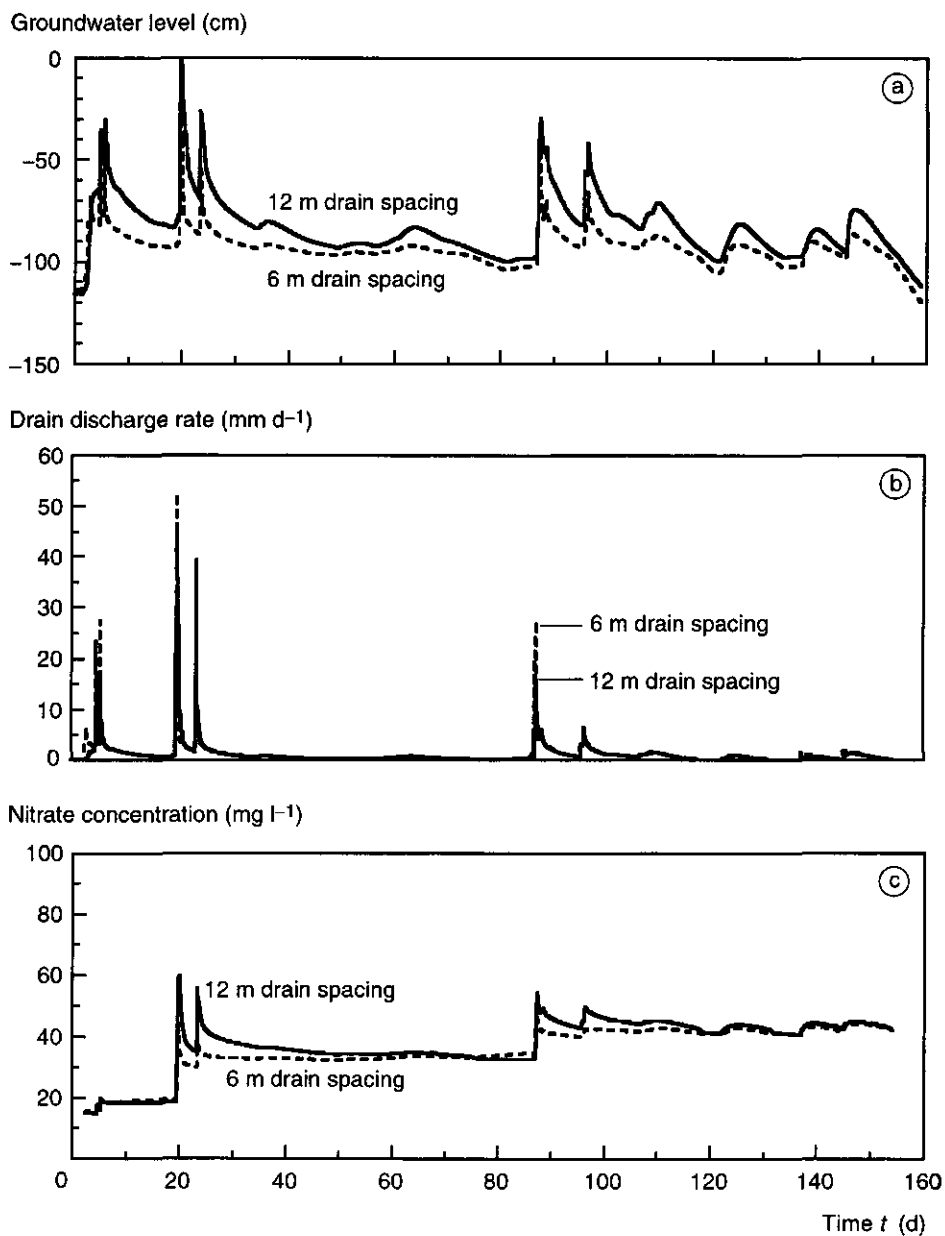


Figure 8.22 Two-dimensional simulations of the groundwater levels at -3 and -6 m from the drain (midway between the drains) (a); drain discharge rates (b); and NO_3^- concentrations in the drainage water (c). The actual meteorological conditions of the leaching period from 17 December 1991 to 25 May 1992 ($0 < t < 160$ d) were used, for a 6 m and a 12 m drain spacing.

in the top 25 cm of the soil profile. A constant production term is incorporated into the solute transport simulations. Figure 8.23 shows an increase in the simulated NO_3 concentrations for $t > 359$ d, as compared to the simulations without a mineralisation term. The cumulative N discharge rates with and without N mineralisation were 14.3 and 12.7 kg ha^{-1} , respectively. Although simulation of N mineralisation increased the NO_3 leaching by 13%, a large difference with the measured 21.5 kg ha^{-1} remains.

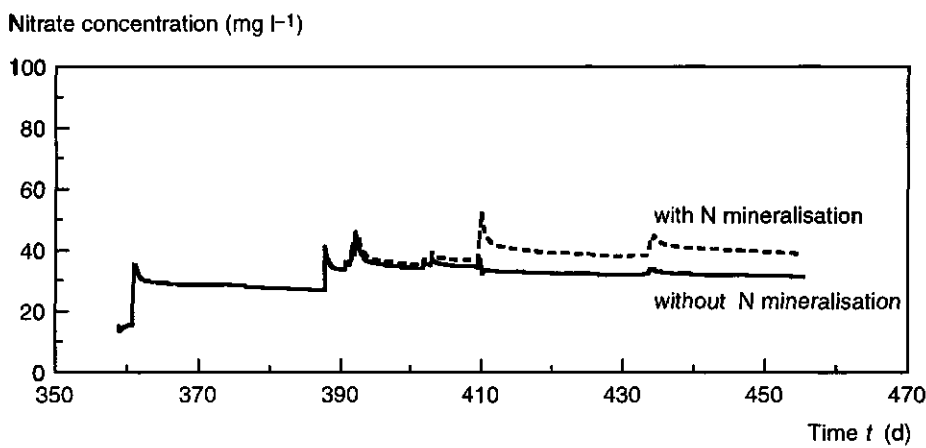


Figure 8.23 Two-dimensional simulations of NO_3 concentrations in the drainage water. The actual meteorological conditions of the leaching period 1 December 1992 to 31 March 1993 ($350 < t < 470$ d) were used, for a situation with and without N mineralisation in the 0-25 cm topsoil.

8.6.2 Discussion

The explorative simulations for the layered soil profile of the Lovinkhoeve demonstrated once more the large impact of the dynamics of water flow on NO_3 leaching. The simulations with a uniform precipitation distribution showed that NO_3 discharge is not proportional to the amount of water discharged, but depends on the NO_3 distribution in the soil profile and the actual distribution of precipitation over time. The simulations with downward seepage and a reduced drain spacing illustrated that the initial distribution of NO_3 over the soil profile,

combined with a proper two-dimensional description of the flow and transport processes, are essential for the prediction of the effects of changes in boundary conditions on NO_3 leaching. A reduced drain spacing decreases the chance that high NO_3 concentrations in the topsoil can be transported rapidly to the drain, and thus reduces NO_3 leaching for these typical situations. N mineralisation increases the NO_3 concentrations in the soil profile and this may lead to an increase of NO_3 leaching.

The explorative simulations were meant to illustrate the effect of different conditions on NO_3 leaching. The absolute values of the simulated N leaching will not be very accurate (see Par. 8.4), but the changes in NO_3 leaching under different conditions give useful information on possible measures to reduce NO_3 leaching.

8.7 Conclusions

The dynamics of the water balance of the Lovinkhoeve is well described by the two-dimensional SWMS_2D model based on the Darcy equation. To be able to model the saturated and unsaturated zone simultaneously, it was necessary to use a linear transition in the hydraulic conductivity characteristics close to saturation. The layering of the soil profile had a pronounced effect on the flow paths to the drain under different atmospheric conditions. Under dry conditions with a relatively deep phreatic surface, drainage water mainly originated from the zone close to the drain depth. Under extremely wet conditions, the major part of the drainage water originated from the topsoil. Due to the relatively high hydraulic conductivity in this zone, rapid lateral transport occurred towards the drain. After calibration of the water flow part of the SWMS_2D model, simulated and measured groundwater levels and drain discharge rates compared well.

Based on the convection-dispersion equation, solute transport was simulated with SWMS_2D. The convective transport component dominated the occurrence of peaks in solute concentrations in the drainage water. However, it was difficult to obtain accurate quantitative simulation results for solute transport. The simulated NO_3 and Cl concentrations over the leaching period 1991-1992 were both larger than the measured concentrations, while their initial distributions in the soil profile were opposite. Water flow and solute transport

8. Modelling two-dimensional water flow and solute transport

through the larger pores and possible solute exchange between the soil matrix and water in these pores appeared to play an important role. Simulated Br concentrations over the leaching period 1994-1995 were too low. Bromide, which had recently been applied to the soil surface as a tracer, appeared to be close to the larger pores which dominated water flow. Field measurements on solute transport gave important information on the nature of water flow and were essential in evaluating the simulation results. More complex models, taking into account macro-pore flow and solute exchange between the soil matrix and larger pores, should be tried to simulate solute transport at the Lovinkhoeve.

Nitrate concentrations in the soil profile were underestimated at the end of simulation periods. Nitrogen mineralisation, N deposition and denitrification have to be accounted for to allow a better description of N leaching. An explorative simulation illustrated the increase in N leaching due to N mineralisation in the topsoil. Other simulations showed that N leaching is not proportional to the cumulative drain discharge, but rather depends on the distribution of precipitation. A smaller drain spacing reduces the N leaching for the typical situation when NO_3 concentrations are high in the topsoil.

SUMMARY

Environmental problems related to agriculture have been an important issue for more than two decades (Chapter 1). Leaching of nitrate (NO_3) and phosphate (PO_4) from the soil to groundwater and surface water is a major problem, especially in The Netherlands. Water flow in the soil is the vehicle for the nutrient leaching. This thesis presents a combination of theory, numerical models and field and laboratory measurements to understand, describe and predict water flow and nutrient transport in the layered silt loam soil of the Lovinkhoeve experimental farm in the Noordoostpolder, The Netherlands. Models can help to understand the processes and their interactions. Field measurements are necessary to quantify the processes and validate the simulation results. The objective of this thesis is to evaluate how well one- and two-dimensional models based on the Darcy equation for water flow and the convection-dispersion equation for solute transport can describe the field-scale water flow and nutrient transport processes in a layered, anisotropic soil profile. Based on these results, ideas for improved agricultural management practices and new strategies for environmental protection or regulation can be generated. Also, recommendations for good measurement methods to quantify NO_3 leaching can be given.

Chapter 2 describes the theory for water flow and solute transport in soil, together with the numerical models that are used in this thesis. For water flow the Darcy equation (Eq. 2.2) is used. In the unsaturated zone, the water retention and hydraulic conductivity characteristics define the hydraulic properties of the soil. The analytical functions of Van Genuchten and Mualem are introduced to describe these characteristics. The SWATRE model, a one-dimensional finite difference model for water flow in the unsaturated zone, is presented. Water flow in the saturated zone can be described by a relatively simple equation (Eq. 2.12), and some drainage equations are discussed as special solutions of this equation. The SWMS_2D model, a two-dimensional finite element model for water flow in the combined saturated-unsaturated zone, is presented. Solute transport is described by the convection-dispersion equation (Eq. 2.20). The characteristics of the solute transport part of the SWMS_2D model are presented. Also, theories on residence times of solutes in aquifers are briefly discussed.

Chapter 3 describes the field and laboratory methods. Standard field measurements of pressure head, groundwater level, hydraulic head, soil temperature and bulk density are briefly discussed. The theory of Time Domain Reflectometry (TDR) is treated in more detail and attention is given to new types of TDR sensors that are installed at several depths from the soil surface under an angle of 45°. A method to measure macroscopic soil oxygen contents in the field is presented. A flow-proportional drain water sampling device with compensation for a fluctuating ditch water level, that was specially developed for this study, is described. A meteorological station was set up at the Lovinkhoeve and the specifications of all meteorological measurements are presented.

The standard laboratory methods to determine the water retention and hydraulic conductivity characteristics are discussed briefly. An improved laboratory method to measure the hydraulic conductivity at saturation K_s is introduced. When the bottom of the soil sample remained saturated, which is different from the standard method involving outflow into the atmosphere, larger K_s values were measured. The procedure to calibrate TDR water contents in the laboratory using repacked soil columns is presented.

The characteristics of the Lovinkhoeve experimental farm are given in Chapter 4. The geological history describing the influence of the former sea and lake on the soil-formation processes, explains the nature of the layered soil profile. The calcareous silt loam topsoil now has a relatively high organic matter content (2.2-2.8%) and is a fertile soil with respect to nutrient availability. However, individual plots may have different organic matter and nutrient contents due to different management of the plots in the past. The fields of the Lovinkhoeve have subsurface drains at about 1 m depth and at 12 m spacing. The lay-out of the experiments described in this thesis is given.

Different calibration curves were tested to describe the TDR calibration data. The De Loor-model was able to predict differences between the calibration curves for the different soil layers based on differences in clay minerals and bulk densities. Close to saturation, the laboratory TDR measurements deviated from the Topp-model and the De Loor-model. For each depth interval a linear relationship between the refractive index n_a and θ was used as model, because this model described the calibration data well in the entire water content range. The TDR field measurements were corrected for changes in soil temperatures.

The water retention and hydraulic conductivity characteristics were

Summary

measured for fields with different arable farming systems in samples from the soil layers at 0-25, 25-40, and 50-75 cm depth. Especially, differences between the water retention characteristics for the topsoil (0-25 cm depth) were substantial, which was probably related to differences in organic matter content between the fields. However, differences in hydraulic characteristics between the soil layers were more distinct. The hydraulic conductivity at saturation K_s showed a large variation, but it was clear that $K_s \approx 200 \text{ cm d}^{-1}$ in the 0-25 cm depth topsoil was much larger than $K_s \approx 10 \text{ cm d}^{-1}$ in the 95-120 cm depth subsoil. The drain trench had also a large $K_s \approx 200 \text{ cm d}^{-1}$. The consequences of these differences for water flow and solute transport are evaluated in the later chapters.

In the first research period 1986-1990, this study focused on the characterisation and monitoring of the soil physical environment with respect to soil biological processes in conventional and integrated arable farming systems (Chapter 5). A hypothesis was that different arable farming systems with a different organic matter input and soil tillage depth would result in different soil physical characteristics in the topsoil. It turned out to be difficult to find differences between the hydraulic characteristics of the fields. The uncertainty and variability in the results were large. Differences in the hydraulic characteristics of the different soil layers were more pronounced than between the topsoils of the different fields. A direct measurement of the soil physical field conditions was a more successful approach to detect differences between the fields. The average bulk densities in the years 1986-1990 for different plots were 1345, 1395, 1400 kg m^{-3} , as a result of the historical differences in organic matter contents of 2.8, 2.3 and 2.2%, respectively. In all growing seasons the time-scale of the fluctuations in pressure heads was in the order of days, except after heavy rainfall when the pressure heads in the topsoil reacted more quickly. Especially the plot with minimum tillage showed lower pressure heads in the topsoil and larger pressure heads in the subsoil compared to the other plots. It appeared that the crop development and the water uptake pattern by the roots dominated the differences in pressure heads between the fields.

Simulations of the Lovinkhoeve field water balance using the one-dimensional SWATRE model resulted in too large simulated pressure heads. The hydraulic conductivity characteristic of the subsoil had a substantial impact on the water balance and strongly influenced the soil physical conditions in the topsoil. Using the field water retention characteristic for the topsoil and a reduced

hydraulic conductivity in the subsoil improved the simulations, but even then large differences between simulations and measurements remained.

The soil biological results of the Dutch Programme on Soil Ecology of Arable Farming Systems were evaluated. N mineralisation is dominated by bacteria decomposing organic matter and bacterivorous protozoans and nematodes predating the bacteria. The net mineralisation in the topsoil (0-25 cm depth) was estimated to be 101 kg N ha⁻¹ yr⁻¹ in an integrated plot and 78 kg N ha⁻¹ yr⁻¹ in a conventional plot. The larger mineralisation at the integrated plot compared to the conventional plot is a result of the higher organic matter input and the higher biological activity. The Lovinkhoeve food web model interrelates different functional groups of soil organisms. Simulated N mineralisation for an integrated and conventional plot compared well with the field measurements. Field measurements and N balance estimates for integrated and conventional plots indicated yearly averaged N losses of 45 and 72 kg N ha⁻¹ yr⁻¹, respectively. However, small changes in the organic matter pool of the soil have a major impact on the estimated N losses. It is necessary to quantify the NO₃ leaching by direct measurements, because the calculation of NO₃ leaching as the rest term of the overall field N mass balance is not accurate and does not yield information on the dynamics of the leaching process. A two-dimensional model for water flow and nutrient transport has to be used to describe the field scale transport processes at the Lovinkhoeve. These conclusions were the starting point for the research focusing on NO₃ leaching presented in the following chapters.

Nitrate leaching was monitored on an integrated arable farming plot with a reduced N fertiliser application (Chapter 6). The soil profile at the Lovinkhoeve is nearly impermeable at 120 cm depth. There may be a small downward seepage of about 0.04-0.22 mm d⁻¹. This is an ideal situation for monitoring NO₃ leaching, because all NO₃ leached is discharged by the subsurface drain and is a spatial average of the whole catchment above the drain. In the 4-year crop rotation period 1992-1996 a total N amount of 440 kg ha⁻¹ fertiliser was applied and a total N amount of 111 kg ha⁻¹ leached. Depending on the meteorological conditions, nitrogen (N) leaching varied over the years between 0 and 50 kg ha⁻¹ yr⁻¹. High NO₃ concentrations in the drainage water were often measured during wet periods with shallow phreatic surfaces. However, yearly averaged NO₃ concentrations remained always lower than 50 mg l⁻¹. A flow-

Summary

proportional drainage water sampling method has to be used to measure NO_3 leaching accurately. Errors of about 25% may occur when NO_3 concentration measurements in the drainage water at 30-day intervals are used to estimate cumulative N leaching. Measurements of NO_3 concentrations in the groundwater cannot be used to estimate N leaching, because drainage water is only partly originating from this groundwater.

Two-dimensional water flow and nutrient transport, with a large lateral flow component towards the drain in the topsoil, explains the peaks in NO_3 concentrations in the drainage water. Data on chloride (Cl) concentrations and results of a bromide (Br) tracer experiment also indicate the importance of the two-dimensional nature of the transport processes. The Br tracer experiment shows that macro-porous flow occurred also.

The long-term Cl mass balance showed that all Cl initially present in the 0-120 cm depth soil layer after reclamation in 1942 is discharged. Upward Cl diffusion in 1991 is estimated at $220 \text{ kg ha}^{-1} \text{ yr}^{-1}$ and is a major term in the Cl mass balance. The Cl mass balance for the period 1981-1991 results in an estimated Cl discharge of $372 \text{ kg ha}^{-1} \text{ yr}^{-1}$.

Field data on NO_3 contents in the soil profile indicate that during the winter leaching periods N mineralisation occurred, resulting in an N increase of 30-50 kg ha^{-1} . Spatial differences in N contents in the soil profile were measured as a function of the distance from the drain. Larger N amounts of 30 kg ha^{-1} were sometimes measured close to the drain. Denitrification was supposed to be the cause of these differences. Later field measurements of groundwater levels, water contents, soil oxygen contents and denitrification at the Lovinkhoeve confirmed and explained the occurrence of these spatial differences in denitrification rates.

Multi-component solute discharge from a subsurface drain (1991-1992) was affected by oxidation-reduction, precipitation-dissolution, ion exchange and hydrological conditions. The initial distribution of a component within the soil profile largely influenced how the drain discharge rate affected the drainage water chemistry. The ionic balance for all elements showed electroneutrality of the drainage water, indicating a good quality of the chemical measurements. Although increased dissolved manganese (Mn) concentrations occurring during initial stages of shallow groundwater levels and high drain discharge rates indicated reduced conditions near the drain, NO_3 originating from shallower oxic

zones was discharged from the drain at elevated concentrations. However, later in the study period, consistently higher NO_3^- concentrations near the drain apparently increased the redox potential of this zone and decreased the reductive dissolution of Mn and Fe. Precipitation and dissolution reactions involving Ca and HCO_3^- probably controlled the solubility of these components, although drainage water samples appeared to be on the average supersaturated with respect to high-Mg calcite. Concentrations of Na, Mg, and Cl in the drainage water were related to their relative affinities for the exchanger phase. A more detailed soil chemical study is necessary to be able to allow a better description of these chemical interactions.

The dynamics of water flow at the Lovinkhoeve are well described by the two-dimensional model SWMS_2D based on the Darcy equation (Chapter 8). To be able to model the saturated and unsaturated zones simultaneously, it was necessary to use a linear transition in the hydraulic conductivity characteristics close to saturation. The layering of the soil profile had a pronounced effect on the flow paths to the drain under different atmospheric boundary conditions. Under dry conditions, with a relatively deep phreatic surface, drainage water mainly originated from the zone close to the drain. Under extremely wet conditions, the major part of the drainage water originated from the topsoil. Due to the relatively high hydraulic conductivity in this zone, rapid lateral transport occurred towards the drain. After calibration of the water flow part of the SWMS_2D model, simulated and measured groundwater levels and drain discharge rates compared well.

The convective transport component of solute transport dominated the occurrence of peaks in solute concentrations in the drainage water. However, the simulated NO_3^- and Cl concentrations in the leaching period 1991-1992 were both larger than the measured concentrations, while their initial distributions in the soil profile were opposite. Water flow and solute transport through the larger pores and possible solute exchange between the soil and water in these pores appeared to play an important role. Bromide concentrations simulated in the leaching period 1994-1995 were too low. Bromide, which was recently applied to the soil surface as a tracer, appeared to be close to the larger pores which dominated water flow. Field measurements on solute transport gave important information on the nature of water flow and were essential in evaluating the simulation results. More complex models, taking into account macro-pore flow

Summary

and solute exchange between the soil matrix and water in these larger pores should be tried to simulate solute transport at the Lovinkhoeve.

At the end of simulation periods NO_3 concentrations in the soil profile were underestimated. To improve the description of N leaching, N mineralisation and N deposition and denitrification have to be accounted for. An explorative simulation illustrated the increase in N leaching due to N mineralisation in the topsoil. Other simulations showed that N leaching is not proportional to the cumulative drain discharge, but rather depends on the distribution of precipitation. A smaller drain spacing reduces the N leaching for the typical situation when NO_3 concentrations are high in the topsoil.

New insight is gained into the nature of two-dimensional water flow and the effects of anisotropy in the hydraulic characteristics of the soil profile on solute transport. The two-dimensional model SWMS_2D or similar models can be used in future studies to improve nutrient use efficiency. Spatial patterns in soil physical conditions can be a result of drainage. These patterns can be predicted and their impact on the N transformations can be quantified. For these types of studies the transport models have to be linked with models describing N dynamics, especially N mineralisation, denitrification and N uptake by the crop, including a detailed description of the root distribution. For studying transport processes in a complex porous medium like a natural soil, a balanced combination of models and measurements is the best way to progress.

The limits for NO_3 concentrations in groundwater and surface waters are still under discussion, but it is likely that they will become stricter. The average NO_3 concentrations in the drainage water measured in this study always remained below the 50 mg l^{-1} EU criterion for groundwater. However, in The Netherlands a stricter criterion of 10 mg l^{-1} is under debate for surface waters. It will be very hard to reach this goal from an agronomical point of view. An integrated model as described above can be used to simulate the agronomical and environmental benefits of different water and nutrient management strategies. Precise application of fertilisers and irrigation water to improve the nutrient use efficiency, and controlled drainage to reduce NO_3 leaching to surface waters, are promising measures to achieve these goals.

SAMENVATTING

De laatste twintig jaren hebben milieuproblemen in relatie tot landbouw veel aandacht gekregen (Hoofdstuk 1). Uitspoeling van nitraat (NO_3) en fosfaat (PO_4) vanuit de bodem naar grond- en oppervlaktewater is een groot probleem, zeker in Nederland. Het bodemwater is het transportmedium voor de nutriënten. Dit proefschrift combineert theorie, numerieke modellen, en veld- en laboratoriummetingen om waterstroming en nutriënttransport te begrijpen, te beschrijven en te voorspellen voor de gelaagde zavelgrond van de proefboerderij Dr. H.J. Lovinkhoeve in de Noordoostpolder. Theorie en modellen kunnen helpen bij het begrijpen en kwantificeren van de processen en hun onderlinge interacties. Veldmetingen zijn noodzakelijk om de processen te kwantificeren en om de resultaten van modelberekeningen te valideren. Het doel van deze studie is te onderzoeken hoe goed transportprocessen in een gelaagd, anisotrop bodemprofiel kunnen worden beschreven met de Darcy-vergelijking voor waterstroming en de convectie-dispersievergelijking voor stoffentransport. De bedoeling is dat ideeën worden verkregen over een verbeterde agrarische bedrijfsvoering met nieuwe strategieën om aan milieunormen te voldoen, en dat verantwoorde methoden worden aangegeven om nitraatuitspoeling te meten.

Hoofdstuk 2 behandelt de theorie van waterstroming en stoffentransport in de bodem, in samenhang met de numerieke modellen die later zullen worden toegepast. De Darcy-vergelijking (Vgl. 2.2) wordt gebruikt voor waterstroming. In de onverzadigde zone van de bodem bepalen de waterretentie- en de waterdoorlatendheidskarakteristiek de hydraulische eigenschappen. Deze karakteristieken worden respectievelijk beschreven met de functies van Van Genuchten en Mualem. Het SWATRE-model wordt gepresenteerd als een eendimensionaal eindig differentie-model voor waterstroming in de onverzadigde zone. Waterstroming in de verzadigde zone kan met een eenvoudige vergelijking (Vgl. 2.12) worden beschreven. Enkele drainageformules worden besproken als bijzondere oplossingen van deze vergelijking. Het SWMS_2D-model wordt gepresenteerd als tweedimensionaal eindig elementen-model voor waterstroming in de gecombineerde verzadigde en onverzadigde zone. Stoffentransport wordt beschreven met de convectie-dispersievergelijking (Vgl. 2.20) en de karakteristieken van het SWMS_2D model met betrekking tot het stoffentransport worden toegelicht. Theorieën over

verblijftijden van stoffen in begrensde watervoerende systemen worden kort besproken.

Hoofdstuk 3 behandelt veld- en laboratoriummeetmethoden. Standaard veldmetingen van drukhoogte, grondwaterstand, stijghoogte, bodemtemperatuur en bulkdichtheid worden kort toegelicht. De theorie van Time Domain Reflectometry (TDR) wordt uitgebreid behandeld. Besproken worden nieuwe TDR-sensoren, die onder een hoek van 45° vanaf het bodemoppervlak op verschillende dieptes kunnen worden geïnstalleerd. Het meten van het macroscopische bodemzuurstofgehalte en een speciaal ontwikkeld debietsproportioneel drainbemonsteringssysteem met een compensatie voor fluctuerende slootwaterstanden worden behandeld. Het op de Lovinkhoeve ingerichte weerstation wordt beschreven en de specificaties van de meteorologische metingen worden gegeven.

De standaardmeetmethoden voor de waterretentie- en waterdoorlatendheidskarakteristiek worden kort toegelicht. Een verbeterde versie voor de bepaling van de waterdoorlatendheid bij verzadiging wordt geïntroduceerd. De waterstroming door een monster bleek groter te zijn als het verzadigde monster aan de onderzijde volledig in contact is met water, ten opzichte van de standaardmethode waarbij het water vrij in de atmosfeer uitstroomt. De laboratoriummethode voor de ijking van TDR-watergehalten met behulp van kolommen gevuld met Lovinkhoeve-grond wordt uiteengezet.

De karakteristieke eigenschappen van de proefboerderij Lovinkhoeve worden in Hoofdstuk 4 besproken. De geologische geschiedenis laat de invloed zien van de voormalige Zuyderzee en het latere IJsselmeer op de bodemvormingsprocessen. Deze invloeden verklaren de gelaagde opbouw van het bodemprofiel. De kalkrijke zavel-bovengrond (0-25 cm diepte) heeft een hoog organische-stofgehalte (2.2-2.8%) en is een vruchtbare grond met betrekking tot nutriëntenbeschikbaarheid. Tussen de diverse proefvelden bestaan verschillen in organische-stofgehalten door historische verschillen in landbouwkundige behandelingen. De proefvelden zijn gedraaineerd op circa 1 m diepte en de drainafstand is 12 m.

Voor de beschrijving van de TDR-ijkingen zijn verschillende modellen getest. Het De Loor-model, gebaseerd op bulkdichtheid en lutumgehalte, voorspelde de verschillen tussen de ijklijnen van de diverse bodemlagen goed.

Samenvatting

Maar dichtbij verzadiging vertoonden zowel het De Loor-model als het empirische Topp-model afwijkingen ten opzichte van de meetgegevens. Uiteindelijk is gekozen voor het lineaire verband tussen refractie index n_a en het volumetrische watergehalte θ , omdat dit model in het hele watergehaltebereik goede resultaten opleverde. De TDR-veldmetingen werden gecorrigeerd voor veranderingen in bodemtemperatuur.

De waterretentie- en waterdoorlatendheidskarakteristieken werden bepaald aan monsters uit de 0-25, 25-40 en 50-75 cm bodemlagen van de verschillende akkerbouwsystemen. Er waren verschillen tussen de karakteristieken van de bovengronden (0-25 cm diepte), die waarschijnlijk werden veroorzaakt door verschillen in organische-stofgehalten. De karakteristieken van de drie bodemlagen vertoonden veel grotere verschillen. De waterdoorlatendheid bij verzadiging K_s varieerde sterk, maar $K_s \approx 200 \text{ cm d}^{-1}$ in de bovengrond (0-25 cm diepte) was veel groter dan $K_s \approx 10 \text{ cm d}^{-1}$ in de ondergrond (95-120 cm diepte). De drainsleuf had ook een hoge $K_s \approx 200 \text{ cm d}^{-1}$. De gevolgen van deze verschillen voor waterstroming en stoffentransport worden in de volgende hoofdstukken beschouwd.

In de periode 1986-1990 richtte het onderzoek zich op het karakteriseren en volgen van de bodemfysische toestand in relatie tot bodembiologische processen in gangbare en geïntegreerde akkerbouwsystemen (Hoofdstuk 5). Verschillende hoeveelheden organische bemesting en verschillende grondbewerkingsdiepten zouden kunnen resulteren in verschillen in hydraulische eigenschappen. Het bleek moeilijk om deze verschillen aan te tonen (Hoofdstuk 4). Directe veldmetingen van de bodemfysische toestanden lieten wel verschillen tussen de akkerbouwsystemen zien. De gemiddelde bulkdichthesen in de jaren 1986-1990 waren 1345, 1395, 1400 kg m^{-3} ten gevolge van historische verschillen in organische-stofgehalten van respectievelijk 2,8%, 2,3% and 2,2%. Drukhoogteveranderingen in het groeiseizoen werden op dagbasis gemeten. Maar na zware neerslag was de tijdschaal van substantiële drukhoogteveranderingen veel korter. Een akker waar minimale grondbewerking werd uitgevoerd had lagere drukhoogten ("droger") in de bovengrond en hogere drukhoogten ("natter") in de ondergrond dan alle overige akkers. De ontwikkeling van het gewas en het wateropnamepatroon van de wortels bepaalden de verschillen in drukhoogten tussen de akkers met verschillende akkerbouwsystemen. Eendimensionale

waterbalanssimulaties met SWATRE gaven te hoge drukhoogten ("te nat"). De waterdoorlatendheid in de ondergrond bleek een grote invloed te hebben op de waterbalans en op de bodemfysische toestanden in de bovengrond. Het gebruik van de veldwaterretentiekarakteristiek en een lagere waterdoorlatendheid in de ondergrond verbeterde de simulaties, maar er bleven grote verschillen ten opzichte van de gemeten drukhoogten.

De bodembiologische resultaten, die in dezelfde onderzoeksperiode werden verkregen, zijn vanuit een bodemfysisch perspectief beschouwd. Stikstof-mineralisatie werd grotendeels bepaald door bacteriën die organisch materiaal afbraken en de predatie van deze bacteriën door bacterivore protozoën en nematoden. De netto-mineralisatie in de bovengrond (0-25 cm diepte) bedroeg in de geïntegreerde akkers $101 \text{ kg N ha}^{-1} \text{ jr}^{-1}$ en in de gangbare akkers $78 \text{ kg N ha}^{-1} \text{ jr}^{-1}$. De hogere mineralisatie in de geïntegreerde akkers werd veroorzaakt door een hogere organische bemesting en een hogere biologische activiteit. Het voedselwebmodel van de Lovinkhoeve beschrijft de relaties tussen de verschillende functionele groepen bodemorganismen. Gesimuleerde stikstof-mineralisatie voor een geïntegreerde en een gangbare akker kwamen goed overeen met de veldmetingen. Uit een combinatie van veldmetingen en een stikstofbalans werden jaargemiddelde stikstofverliezen berekend van $45 \text{ kg N ha}^{-1} \text{ jr}^{-1}$ voor een geïntegreerde akker en $72 \text{ kg N ha}^{-1} \text{ jr}^{-1}$ voor een gangbare akker. Deze berekeningen zijn echter erg gevoelig voor kleine veranderingen in het organische-stofgehalte. De berekening van stikstofuitspoeling als restterm van de stikstofbalans is onnauwkeurig. Het direct meten van de stikstofuitspoeling is dus noodzakelijk en levert inzicht in de dynamiek van dit proces. Voor de situatie op de Lovinkhoeve moet een tweedimensionale beschrijving van transportprocessen in het veld worden gebruikt. Deze conclusies waren het uitgangspunt voor het verdere onderzoek, dat zich vooral richtte op nitraatuitspoeling.

Van een geïntegreerde akker waaraan een relatief lage stikstofbemesting werd toegediend, werd continu de nitraatuitspoeling gemeten (Hoofdstuk 6). Op 120 cm diepte is de bodem van de Lovinkhoeve nagenoeg ondoorlatend voor water. De weging is circa $0,04 - 0,22 \text{ mm d}^{-1}$. Dit levert een ideale situatie op om uitspoeling te meten, aangezien alle stoffen via de drains afgevoerd worden. Drainagewater en daarin voorkomende stoffenconcentraties zijn tevens een ruimtelijk gemiddelde over het afvoergebied van de drain. Voor de vierjarige

gewasrotatie 1992-1996 werd 440 kg ha^{-1} stikstof (N) toegediend en was de totale N-uitspoeling 111 kg ha^{-1} . De jaarlijkse N-uitspoeling varieerde van 0 tot 50 kg $ha^{-1} jr^{-1}$, afhankelijk van de meteorologische omstandigheden. Tijdens perioden met een ondiepe grondwaterspiegel werden hoge NO_3^- -concentraties in het drainagewater gemeten. Toch bleven de gemiddelde NO_3^- -concentraties op jaarbasis altijd lager dan 50 mg l^{-1} . Een debietsproportionele bemonstering van het drainagewater is noodzakelijk voor het nauwkeurig kwantificeren van de NO_3^- -uitspoeling. Bij het meten van deze NO_3^- -concentraties op een vast tijdinterval van bijvoorbeeld 30 dagen en het vervolgens schatten van de N-uitspoeling, kunnen fouten van 25% worden gemaakt. Het meten van NO_3^- -concentraties in het diepere grondwater op de Lovinkhoeve en in de IJsselmeerpolders is niet bruikbaar als methode om stikstofuitspoeling te voorspellen, aangezien het drainagewater maar voor een klein gedeelte uit deze zone afkomstig is.

Het tweedimensionale karakter van de waterstroming en het nutriënten-transport, met een grote laterale component in de richting van de drain, verklaart de gemeten pieken in NO_3^- -concentraties in het drainagewater. Gemeten concentraties van chloride (Cl) en bromide (Br) bevestigen de gevolgen van de tweedimensionale transportprocessen. De resultaten van het Br-tracer-experiment laten zien dat transport door macroporiën een belangrijke rol speelde. Chloride, dat zich na drooglegging van de polder in 1942 in de 0-120 cm bodemlaag bevond, is grotendeels uitgespoeld. Opwaartse diffusie van Cl was in 1991 circa 220 kg $ha^{-1} jr^{-1}$, en dit is een aanzienlijke bijdrage aan de totale massabalans voor Cl. Voor de periode 1981-1991 wordt een jaarlijkse Cl-afvoer via de drains berekend van 372 kg $ha^{-1} jr^{-1}$.

Gemeten N-gehalten in het bodemprofiel geven aan dat er gedurende uitspoelperioden N-mineralisatie van 30-50 kg ha^{-1} plaatsvindt. Ook treden er ruimtelijke verschillen in N-gehalten op als functie van de afstand tot de drain. Verschillen in denitrificatie zijn hiervoor waarschijnlijk verantwoordelijk. Latere veldmetingen van grondwaterstanden, watergehalten en bodemzuurstofgehalten bevestigden en verklaarden verschillen in denitrificatiesnelheid.

De chemische samenstelling van het drainagewater (1991-1992) werd sterk bepaald door oxidatie-reductiereacties, het neerslaan en in oplossing gaan van zouten, ionen-uitwisseling en de hydrologische toestand. De initiële verdeling van de stoffen in het bodemprofiel had grote invloed op het verschijnen van deze stoffen in het drainagewater. Uit de sommatie van de lading van alle elementen

bleek een berekende elektro-neutraliteit van het drainagewater. Hieruit werd afgeleid dat de chemische bepalingen voldoende nauwkeurig waren. Hoge concentraties mangaan (Mn) gaven aan dat er gereduceerde omstandigheden in het bodemprofiel optradën. Op hetzelfde moment werden hoge NO_3^- -concentraties gemeten. Het is waarschijnlijk dat dit NO_3^- uit een andere, oxische, zone in de bodem afkomstig was. In een later stadium daalden de Mn-concentraties in het drainagewater. Door neerwaarts NO_3^- -transport is de redoxpotentiaal op de plaatsen waar Mn zich bevond waarschijnlijk toegenomen, zodat Mn niet meer in oplossing ging. Het neerslaan en in oplossing gaan van calcium (Ca) en waterstofcarbonaat (HCO_3^-) leek hun oplosbaarheid te bepalen. De drainagewatermonsters waren oververzadigd met magnesiumcalciet (Mg-CaCO_3). De concentraties van Na, Mg en Cl konden gerelateerd worden aan hun respectievelijke voorkeuren voor het uitwisselingsoppervlak. Een meer gedetailleerde bodemchemische studie is nodig om al deze chemische interacties onder sterk wisselende hydrologische omstandigheden beter te beschrijven.

Om met het tweedimensionale model SWMS_2D zowel waterstroming in de verzadigde als in de onverzadigde zone te kunnen simuleren werd gebruik gemaakt van een lineaire toename van de waterdoorlatendheid nabij verzadiging. De gelaagdheid van het bodemprofiel had een groot effect op de stroombanen naar de drain onder verschillende atmosferische randvoorwaarden. Onder droge omstandigheden, met een relatief diep freatisch vlak, was het drainagewater voornamelijk afkomstig uit zones in de buurt van de 97.5 cm draindiepte. Onder zeer natte omstandigheden was het grootste gedeelte van het drainagewater afkomstig uit de bovengrond. De hoge waterdoorlatendheid in de bovengrond leidde tot een snel lateraal transport naar de drain. Na calibratie van het SWMS_2D-model werden grondwaterstanden en drainafvoeren goed gesimuleerd.

Het convectieve stoffentransport bepaalde de pieken in concentraties in het drainagewater. De gesimuleerde NO_3^- - en Cl-concentraties in de uitspoelperiode 1991-1992 waren echter beider te hoog, ondanks hun tegenovergestelde concentratieverdelingen in het bodemprofiel. Waterstroming en stoffentransport door grotere poriën leek een belangrijke rol te spelen. Simulaties van Br-concentraties in de uitspoelperiode 1994-1995 leverden te lage Br-concentraties in het drainagewater op. Bromide was kort voor het begin van deze

Samenvatting

uitspoelperiode op het bodemoppervlak toegediend en is vervolgens snel naarwaarts getransporteerd en bevond zich blijkbaar nog dicht bij de grotere poriën die de waterstroming onder natte omstandigheden domineerden. Veldmetingen leverden essentiële informatie over de aard van de waterstroming en waren noodzakelijk om de modelberekeningen op hun waarde te kunnen schatten. Om stoffentransport op de Lovinkhoeve nog beter te beschrijven kunnen complexere modellen worden geprobeerd die rekening houden met de uitwisseling van water en stoffen in de macroporiën en in de bodemmatrix.

Aan het einde van de uitspoelperioden werden de NO_3 -concentraties in het bodemprofiel te laag gesimuleerd. De N-uitspoeling kan beter worden beschreven door ook N-mineralisatie en denitrificatie te beschouwen. Een voorbeeldberekening laat de toename van N-uitspoeling ten gevolge van N-mineralisatie zien. Andere simulaties laten zien dat N-uitspoeling niet evenredig is met het neerslagoverschot, maar sterk afhangt van de neerslagverdeling. Een kleinere drainafstand leidt tot verminderde N-uitspoeling, vooral als de N zich bovenin het bodemprofiel bevindt.

Er zijn nieuwe inzichten verkregen in het karakter van tweedimensionale stroming en de gevolgen van de anisotropie van een gelaagd bodemprofiel voor stoffentransport. Tweedimensionale modellen zoals SWMS_2D kunnen in toekomstige studies worden gebruikt om de benutting van nutriënten te optimaliseren. Ruimtelijke patronen in bodemfysische toestanden kunnen optreden als gevolg van drainage. Deze patronen kunnen worden voorspeld en stikstofomzetten kunnen vervolgens worden berekend. Voor dit type studies moeten de transportmodellen worden gecombineerd met modellen die de stikstofdynamiek beschrijven, met name N-mineralisatie, denitrificatie, en N-opname door een gewas, inclusief een gedetailleerde beschrijving van de beworteling. Om verdere vooruitgang te boeken bij het bestuderen van transportprocessen in een complex poreus medium als een natuurlijke bodem, is een gecombineerd gebruik van modellen en veldmetingen de beste weg.

Er is nog steeds veel discussie over de normen voor NO_3 -concentraties in grond- en oppervlaktewater, en het is waarschijnlijk dat de normen strenger zullen worden. De gemiddelde NO_3 -concentraties in het drainagewater bleven in dit onderzoek altijd onder de EU-norm voor grondwater van 50 mg l^{-1} . In Nederland wordt echter voor oppervlaktewater al over een norm van 10 mg l^{-1} gesproken. Vanuit een landbouwkundig oogpunt zal het zeer moeilijk zijn om

aan zo'n scherpe norm te voldoen. Met bovengenoemde geïntegreerde modellen is het mogelijk om landbouwkundige en milieukundige voor- en nadelen van verschillende strategieën van water- en nutriëntenbeheer te simuleren. Precieze toediening van nutriënten en water om de nutriëntenbenutting te verhogen en gecontroleerde drainage om nitraatuitspoeling te verminderen zijn veelbelovende mogelijke maatregelen om aan deze strengere milieunormen te voldoen.

REFERENCES

REFERENCES

Addiscott, T.M., A.P. Whitmore and D.S. Powlson, 1991. Farming, fertilizers and the nitrate problem. Rothamsted Experimental Station, Harpenden, United Kingdom.

Addiscott, T.M. and D.S. Powlson, 1992. Partitioning losses of nitrogen fertilizer between leaching and denitrification. *J. Agric. Sci.* 118: 101-107.

Adriano, D. C., 1986. Trace elements in the terrestrial environment. Springer-Verlag, New York.

Adriano, D. C. and H. E. Doner, 1982. Bromine, chlorine, and fluorine. In: A. L. Page, R. H. Miller, and D. R. Keeney (Eds.), *Methods of soil analysis*, part 2, ASA-SSSA., Madison, Wisconsin, pp. 449-483.

Amrhein, C. and D. L. Suarez, 1987. Calcite supersaturation in soils as a result of organic matter mineralisation. *Soil Sci. Soc. Am. J.* 51: 932-937.

AMWO, 1988. Programma van eisen van het Agrometeorologische Waarnemingsnetwerk voor Onderzoek (AMWO). Eindrapport van de werkgroep AMWO, Wageningen, The Netherlands (in Dutch).

Arya, L.M., D.A. Farrell and G.R. Blake, 1975. A field study of soil water depletion patterns in presence of growing soybean roots. I. Determination of hydraulic properties of the soil. *Soil Sci. Soc. Am. Proc.* 39: 424-430.

Assinck, F., 1995. De invloed van de waterbalans op ruimtelijke denitrificatiepatronen. Afstudeerrapport Van Hall Instituut no. 95MI03 (in Dutch).

Bathurst, R. G. C, 1971. Carbonate sediments and their diagenesis. Elsevier Publ. Co., Amsterdam.

Bear, J., 1972. Dynamics of fluid in porous media. Elsevier, New York.

Bear, J. and A. Verruijt, 1992. Modeling groundwater flow and pollution. D. Reidel Publishing Company, Dordrecht, The Netherlands.

Belmans, C., J.G. Wesseling and R.A. Feddes, 1983. Simulation model of the water balance of a cropped soil : SWATRE. *J. Hydrol.* 63: 271-286.

Bieleman, J., 1993. Landbouw in een spanningsveld. In: J. van den Noort (Ed.) *Onvoltooid verleden tijd: geschiedenis en milieu*, Rotterdam, The Netherlands, pp. 17-31 (In Dutch).

Biggar, J. W. and D. R. Nielsen, 1976. Spatial variability of the leaching characteristics of a field soil. *Water Resour. Res.* 12: 78-84.

Bjerg, P. L. and T. H. Christensen, 1993. A field experiment on cation exchange-affected multicomponent solute transport in a sandy aquifer. *J. Contam. Hydrol.* 12: 269-290.

Bjerg, P. L., H. C. Ammentorp and T. H. Christensen, 1993. Model simulations of a field experiment on cation exchange-affected multicomponent solute transport in a sandy aquifer. *J. Contam. Hydrol.* 12: 291-311.

Bloem, J., G. Lebbink, K.B. Zwart, L.A. Bouwman, S.L.G.E. Burgers, J.A. De Vos and P.C. De Ruiter, 1994. Dynamics of microorganisms, microbivores and nitrogen mineralisation in winter wheat fields under conventional and integrated management. *Agric. Ecosyst. Environ.* 51: 129-143.

Boekel, P., 1985. *Invloed van organische stof op bodemstructuur. Inst. Bodemvruchtbaarheid, Rap. 10-85*, Haren, The Netherlands (In Dutch).

Boels, D., J.B.H.M. Van Gils, G.J. Veerman and K.E. Wit, 1978. Theory and system of automatic determination of soil moisture characteristics and unsaturated hydraulic conductivity. *Soil Sci.* 126: 191-199.

Boersma, O.H. and M.J. Kooistra, 1994. Differences in soil structure of a silt loam soil Typic Fluvaquents under various agricultural management practices. *Agric. Ecosyst. Environ.* 51: 21-42.

Booltink, H.W.G., 1993. Morphometric methods for simulation of water flow. PhD-thesis Wageningen Agricultural University, The Netherlands.

Bouma, J., 1982. Measuring the hydraulic conductivity of soil horizons with continuous macropores. *Soil Sci. Soc. Am. J.* 46: 438-441.

Bouwman, L.A. and K.B. Zwart, 1994. The ecology of bacterivorous protozoans and nematodes in arable soil. *Agric. Ecosyst. Environ.*, 51: 145-160.

Bronswijk, J.J.B., 1988. Modelling of water balance, cracking and subsidence of clay soils. *J. Hydrol.* 97: 199-212.

Brussaard, L., 1994. An appraisal of the Dutch Programme on Soil Ecology of Arable Farming Systems (1985-1992). *Agric. Ecosyst. Environ.* 51: 1-6.

Brussaard, L., J.A. Van Veen, M.J. Kooistra and G. Lebbink, 1988. The Dutch Programme on Soil Ecology of Arable Farming Systems; I. Objectives, approach and some preliminary results. In: H. Eijssackers and A. Quispel (Eds.), *Ecological Implications of Contemporary Agriculture*. Proc. of the 4th European Ecology Symposium 7-12 September 1986, Wageningen. *Ecol. Bull.* 39, pp. 35-40.

References

Butters, G. L., W. A. Jury and F. F. Ernst, 1989. Field scale transport of bromide in an unsaturated soil. 1. Experimental methodology and results. *Water Resour. Res.* 25: 1575-1581.

Butters, G. L. and W. A. Jury, 1989. Field scale transport of bromide in an unsaturated soil. 2. Dispersion modelling. *Water Resour. Res.* 25: 1583-1589.

Cannell, R.Q., M.J. Goss, G.L. Harris, M.G. Jarvis, J.T. Douglas, K.R. Howse and S. Le Grice, 1984. A study of mole drainage with simplified cultivation for autumn-sown crops on a clay soil. 1. Background, experiment and site details, drainage systems, measurement of drain flow and summary of results 1978-80. *J. Agric. Sci.* 102: 539-559.

Celia, M.A., E.T. Bouloutas and R.L. Zarba, 1990. A general mass-conservative numerical solution for the unsaturated flow equation. *Water Resour. Res.* 26: 1483-1496.

Corré, W.J., 1995. Denitrificatie in poldergronden. AB-DLO rapport 41, AB-DLO, Wageningen/Haren, The Netherlands (in Dutch).

Dagan, G., 1989. Flow and transport in porous formations. Springer-Verlag, Berlin, Germany.

Dalton, F.N. and M. Th. Van Genuchten, 1986. The Time Domain Reflectometry method for measuring soil water content and salinity. *Geoderma* 38: 237-250.

Deal, J.W., J.W. Gilliam, R.W. Skaggs and K.D. Konyha, 1986. Prediction of nitrogen and phosphorous losses as related to agricultural drainage system design. *Agric. Ecosyst. Environ.* 18: 37-51.

De Bakker, H., 1979. Major soil and soil regions in The Netherlands. Pudoc, Wageningen, The Netherlands.

De Bakker, H. and J. Schelling, 1966. A system for soil classification for The Netherlands. The higher levels. Pudoc, Wageningen, The Netherlands.

De Bruin, H.A.R., 1987. From Penman to Makkink. In: J.C. Hooghart (Ed.), *Evaporation and Weather: Technical Meeting 44*, Ede, The Netherlands, 25 March 1987. Proceedings and Information / TNO Committee on Hydrological Research; No. 39, pp. 5-31.

De Loor, G.P., 1966. Dielectric properties of heterogeneous mixtures. *Appl. Sci. Res.* B3: 479-482.

De Loor, G.P., 1990. The dielectric properties of wet soils. BCRS (Netherlands Remote Sensing Board) Report no. 90-13. TNO Physics and Electronics Laboratory, The Hague, The Netherlands.

De Ruiter, P.C., J.C. Moore, K.B. Zwart, L.A. Bouwman, J. Hassink, J. Bloem, J.A. De Vos, J.C.Y. Marinissen, W.A.M. Didden, G. Lebbink and L. Brussaard, 1993. Simulation of nitrogen mineralisation in the belowground foodwebs of two winter wheat fields. *J. Appl. Ecol.*, 30: 95-106.

De Ruiter, P.C., J. Bloem, L.A. Bouwman, W.A.M. Didden, G.H.J. Hoenderboom, G. Lebbink, J.C.Y. Marinissen, J.A. De Vos, M.J. Vreeken-Buijs, K.B. Zwart and L. Brussaard, 1994. Simulation of dynamics in nitrogen mineralisation in the belowground foodwebs of two arable farming systems. *Agric. Ecosyst. Environ.*, 51: 199-208.

De Valk, C.F. and P.A.C. Raats, 1995. Lumped models for convective solute transport in heterogeneous soils. *Water Resour. Res.* 31: 883-892.

De Vos, J.A., 1991. A program for calculating time-depth curves from daily water balance data. *Inst. Bodemvruchtbaarheid*, Nota 239.

De Vos, J.A., M.S. Inckel and P.A.C. Raats, 1992. The water balance of the unsaturated zone, considered in the context of sustainable agriculture. In: M.Th. van Genuchten, F.J. Leij and L.J. Lund (Eds.), *Proc. Int. Workshop on Indirect Methods for Estimating Hydraulic Properties of Unsaturated Soils*. University of California, Riverside, CA; pp. 585-599.

De Vos, J.A., P.A.C. Raats and E.C. Vos, 1994. Macroscopic soil physical processes considered within an agronomical and a soil biological context. *Agric. Ecosys. Environ.* 51: 43-73.

De Willigen, P., 1990. Calculation of uptake of nutrients and water by a root system. *Inst. Bodemvruchtbaarheid*, Nota 210, Haren, The Netherlands.

De Zeeuw, J.W. and F. Hellinga, 1958. *Neerslag en afvoer*. Landbouwk. Tijdschrift 70: 405-422 (in Dutch).

Diels, J., 1994. A validation procedure accounting for model input uncertainty: methodology and application to the SWATRER model. PhD-thesis, Catholic Agricultural University of Leuven, Belgium.

Dienst Getijdewateren en Dienst Binnenwateren, 1990. *Jaarboek van afvoeren, waterstanden, golven en waterkwaliteit 1987*. 's Gravenhage (in Dutch).

References

Dirksen, C., 1991. Unsaturated hydraulic conductivity. In: K.A. Smith and C.E. Mullins (Eds.), *Soil Analysis, Physical Methods*, Dekker, New York.

Dirksen, C. and S. Dasberg, 1993. Effects of bound water and bulk density on calibration of soil water content measurements by Time Domain Reflectometry. *Soil Sci. Soc. Am. J.* 57: 660-667.

Dixon, J. B. and S. B. Weed (Eds.), 1989. Minerals in soil environments, 2nd ed, SSSA Book Series, no. 1, Soil Sci. Soc. Am., Madison, Wisconsin.

Dobson, M.C, F.T. Ulaby, M.T. Hallikainen and M.A. El-Rayes, 1985. Microwave dielectric behavior of wet soil. Part II: Dielectric mixing models. *IEEE Trans. Geoscience Remote Sensing GE23*, pp. 35-46.

Domingo, W.R., 1951. De physische rijping van de jongere Zuiderzee-afzettingen in de Noordoostpolder. *Van Zee tot Land*, nr. 2, Tjeenk Willink N.V., Zwolle, The Netherlands (In Dutch).

Doner, H. E. and W. C. Lynn, 1989. In: Dixon, J. B. and S. B. Weed (Eds.), Minerals in soil environments, 2nd ed, SSSA Book Series, no. 1, Soil Sci. Soc. Am., Madison, Wisconsin, pp. 279-330.

Dumm, L.D., 1954. Drain spacing formula. *Agric. Eng.* 35: 726-730.

Duynisveld, W.H.M., 1984. Entwicklung und Anwendung von Simulationsmodellen fur den Wasserhaushalt und den Transport von gelosten Stoffen in wasserungesattigten Boden. Ermittlung der Nitratauswaschungsgefahr unter Ackernutzung. Dissertation, Technische Universität Berlin.

Ernst, L.F., 1956. Calculation of the steady flow of groundwater in vertical cross-sections. *Neth. J. Agric. Sci.* 4: 126-131.

Ernst, L.F., 1962. Grondwaterstromingen in de verzadigde zone en hun berekening bij aanwezigheid van horizontale evenwijdige open leidingen. *Versl. Landbouwk. Onderz.* 67-15. Pudoc, Wageningen, The Netherlands (in Dutch).

EU, 1991. Richtlijn van de Raad van 12 december 1991 inzake de bescherming van wateren tegen verontreiniging door nitraten uit agrarische bronnen, Richtlijn nummer 91/676/EG. Brussels: European Union (in Dutch).

FAO-UNESCO, 1974. Soil map of the world. Volume I. FAO, Rome.

Feddes, R.A., 1987. Crop factors in relation to Makkink reference crop evaporation. In: J.C. Hooghart (Ed.), *Evaporation and Weather: Technical Meeting 44*, Ede, The Netherlands, 25 March 1987. Proceedings and Information / TNO Committee on Hydrological Research; No. 39, pp. 33-45.

Feddes, R.A., P.J. Kowalik and H. Zaradny, 1978. Simulation of field water use and crop yield. Wageningen, Pudoc.

Feyen, J. and P. Van Aelst, 1983. Test of a simple growth model simulating sugar beet yields. *Pedologie* 33: 281-293.

Fipps, G., R.W. Skaggs and J.L. Nieber, 1986. Drains as a boundary condition in finite-elements. *Water Resour. Res.* 22: 1613-1621.

Firestone, M.K., R.B. Firestone and J.M. Tiedje, 1980. Nitrous oxide from soil denitrification: Factors controlling its biological production. *Science* 208: 173-179.

Fletcher, P., K. M. Holtzclaw, C. Jouany, G. Sposito and C. S. LeVesque, 1984. Sodium-calcium-magnesium exchange reactions on a montmorillonitic soil: II. Ternary exchange reactions. *Soil Sci. Soc. Am. J.* 48: 1022-1025.

Fokkens, B., 1966. De landbouwwaterhuishouding in de Noordoostpolder, mede in vergelijking met die in andere zeekleipolders. *Van Zee tot Land*, nr. 44, Tjeenk Willink N.V., Zwolle, The Netherlands (In Dutch).

Fritschen, L.J. and L.W. Gay, 1979. Environmental instrumentation. Springer Verlag, New York.

Gaston, L. A., H. M. Selim and P. M. Walther, 1993. Predicting cation transport in smectitic soils. *Soil Sci. Soc. Am. J.* 57: 307-310.

Gee, G. W. and J. W. Bauder, 1986. Particle-size analysis. In: A. Klute (Ed.), *Methods of soil analysis. Part 1. 2nd ed.* ASA and SSSA, Madison, Wisconsin, pp. 383-411.

Groffman, P.M., 1991. Ecology of nitrification and denitrification in soil at scales relevant to atmospheric chemistry. In: J.E. Rogers and B.W. Whitman (Eds.), *Microbial production and consumption of greenhouse gases*. Am. Soc. Microbiology, pp. 201-218.

Gureghian, A.B. and E.G. Youngs, 1975. The calculation of steady-state water-table heights in drained soils by means of finite-element method. *J. Hydrol.*, 27: 15-32.

Harmsen, 1986. Optimalisatie van kolomkeus, eluentsamenstelling en detectie bij ionchromatografie van anorganische ionen. Nota 1699. Instituut voor Cultuurtechniek en Waterhuishouding, Wageningen, The Netherlands (in Dutch).

References

Harris, G.L., M.J. Goss, R.J. Dowdell, K.R. Howse and P. Morgan, 1984. A study of mole drainage with simplified cultivation for autumn-sown crops on a clay soil. 2. Soil water regimes, water balances and nutrient loss in drain water, 1978-80. *J. Agric. Sci.* 102: 561-581.

Hassink, J., 1992. Effects of soil texture and structure on carbon and nitrogen mineralisation in grassland soils. *Biol. and Fertil. Soils* 14: 126-134.

Heil, J.W., 1988. Pore size distributions from soil water retention characteristics for studying soil organisms. MSc-thesis, Colorado State University, Ford Collins, Colorado.

Heimovaara, T.J., 1993. Time Domain Reflectometry in soil science: Theoretical backgrounds, measurements and models. Ph. D. Thesis University of Amsterdam, The Netherlands.

Heimovaara, T.J., 1995. Design of triple-wire Time Domain Reflectometry probes in practice and theory. *Soil Sci. Soc. Am. J.* 57: 1410-1417.

Heimovaara, T.J. and W. Bouter, 1990. A computer controlled 36 channel TDR system for monitoring soil water contents. *Water Resour. Res.* 26: 2311-2316.

Heinen, 1997. Dynamics of water and nutrients in closed, recirculating cropping systems in glasshouse horticulture with special attention to lettuce grown in irrigated sand beds. PhD-thesis, Wageningen Agricultural University, Wageningen, The Netherlands.

Herkelrath, W.N., S.P. Hamburg and F. Murphy, 1991. Automatic, real-time monitoring of soil moisture in a remote field area with Time Domain Reflectometry. *Water Resour. Res.* 27: 857-864.

Hesterberg, D., J. Bril and P.A.C. Raats, 1994. Coupled chemical-equilibrium/transport model calculations of soil trace metal leaching as influenced by interactive effects of dissolved organic matter, pH, and electrolyte conditions. In: N. Senesi and T. M. Miano (Ed.) *Humic substances in the global environment and implications on human health*. Elsevier Publ. Co., Amsterdam, pp. 1131-1140.

Hiemenz, P. C., 1986. *Principles of colloid and surface chemistry*, 2d ed. Marcel Dekker, New York.

Hillel, D., 1980. *Fundamentals of soil physics*. Academic Press, New York.

Hillel, D. and W.R. Gardner, 1970. Measurement of unsaturated conductivity and diffusivity by infiltration through an impeding layer. *Soil Sci.* 109: 149:153.

Hofstee, C., 1993. The scaling-up of water flow models in unsaturated heterogeneous soils: from the pore scale to the field-scale. Inst. Bodemvruchtbaarheid, Nota 265, Haren, The Netherlands.

Hooghoudt, S.B., 1940. Bijdrage tot de kennis van eenige natuurkundige grootheden van den grond No. 7. Algemeene beschouwingen van het probleem van de detailontwatering en de infiltratie door middel van parallel loopende drains, greppels, slooten en kanalen. Departement van Landbouw en Visscherij, Directie van de Landbouw. Algemeene Staatsdrukkerij, The Hague, The Netherlands. Verslagen van Landbouwkundige Onderzoeken, No 46(14), pp. 515-707 (in Dutch).

Hopmans, J.W., 1987. Presentation and application of an analytical model to describe soil hydraulic properties. *J. Hydrol.*, 87: 135-143.

Houba, V.J.G. and J. Uittenbogaard, 1994. Chemical composition of various plant species. International Plant-Analytical Exchange (IPE), Dept. Soil Science and Plant Nutrition, Wageningen Agricultural University, The Netherlands.

Inskeep, W. P. and P. R. Bloom, 1986. Calcium carbonate supersaturation in soil solutions of Calciaquolls. *Soil Sci. Soc. Am. J.* 50: 1431-1437.

Jackson, M. L., C. H. Lim and L. W. Zelazny, 1986. Oxides, hydroxides, and aluminosilicates. In: A. Klute (Ed.) *Methods of soil analysis*, Part 1, 2nd ed. ASA and SSSA, Madison, Wisconsin, pp. 101-150.

Keeney, D.R., I.R. Fillery and G.P. Marx, 1979. Effect of temperature on the gaseous nitrogen products of denitrification in a silt loam soil. *Soil Sci. Soc. Am. J.* 43: 1124-1128.

Kirkham, D., 1949. Flow of ponded water into drain tubes in soil overlying an impervious layer. *Eos. Trans. AGU* 30: 369-385.

Klein Tank, A.M.G., 1996. Klimaat, neerslag en verdamping. In: Cramer, W., J. de Jong and J.A. Los (Eds.), *Waterbeheer, Handboek voor milieubeheer*. Samson H.D. Tjeenk Willink, Alphen aan den Rijn, The Netherlands (in Dutch).

Klute, A. (Ed.), 1986. *Methods of soil analysis*, Part 1. Physical and mineralogical methods, *Agronomy Monographs* no. 9 (2nd edition), Am. Soc. Agron., Madison, Wis., .

Knight, J., 1992. Sensitivity of Time Domain Reflectometry measurements to lateral variations in soil water content. *Water Resour. Res.* 28: 2345-2352.

References

Kooistra, M.J., G. Lebbink and L. Brussaard, 1989. The Dutch Programme on Soil Ecology Farming Systems. 2. Geogenesis, agricultural history, field site characteristics and present farming systems at the Lovinkhoeve experimental farm. *Agric. Ecosyst. Environ.* 27: 361-387.

Kuikman, P, 1990. Mineralization of nitrogen by protozoan activity in soil. Doctoral thesis, Wageningen Agricultural University, The Netherlands.

Kumada, K., 1987. Chemistry of soil organic matter. Japan Scientific Soc. Press and Elsevier Sci. Publ., Tokyo.

Lebbink, G., H.G. Van Faassen, C. Van Ouwerkerk and L. Brussaard, 1994. The Dutch Programme on Soil Ecology of Arable Farming Systems: Farm management monitoring programme and general results. *Agric. Ecosyst. Environ.* 51: 7-20.

Ledieu, J., P. De Ridder , P. De Clerck and S. Dautrebande, 1986. A method of measuring soil moisture by Time Domain Reflectometry. *J. Hydrol.* 88: 319-328.

Leffelaar, P.A., 1987. Dynamics of partial anaerobiosis, denitrification, and water in soil: experiments and simulation. Doctoral thesis, Wageningen Agricultural University, The Netherlands.

Leij, F.J., M.Th. van Genuchten, S.R. Yates, W.B. Russell and F. Kaveh, 1992. RETC: a computer program for analyzing soil water retention and hydraulic conductivity data. In: M.Th. van Genuchten, F.J. Leij and L.J. Lund (Eds.), *Proc. Int. Workshop on Indirect Methods for Estimating Hydraulic Properties of Unsaturated Soils*. University of California, Riverside, CA, pp. 263-272.

Linden, D. R., C. E. Clapp and W. E. Larson, 1984. Quality of percolate water after treatment of a municipal waste water effluent by a crop irrigation system. *J. Environ. Qual.* 13: 256-264.

Lindsay, W. L., 1979. Chemical equilibria in soils. John Wiley and Sons, New York.

Maasland, M., 1957. Soil anisotropy and land drainage. In: J.N. Luthin (Ed.), *Drainage of agricultural lands*. Americ. Soc. Agron., Madison, Wisconsin. *Agronomy* 7, pp. 216-285.

Makkink, G.F., 1957. Testing the Penman formula by means of lysimeters. *Journ. Inst. of Water Eng.* 11: 277-288.

Marinissen, J.C.Y., 1994. Earthworm populations and stability of soil structure in a silt loam of a recently reclaimed polder in The Netherlands. *Agric. Ecosyst. Environ.* 51: 75-87.

Marthaler, H.P., W. Vogelsanger, F. Richard and P.J. Wieringa, 1987. A pressure transducer for field tensiometers. *Soil Sci. Soc. Am. J.*, 47: 624-627.

Martinez Beltran, J., 1988. Drainage criteria for heavy soils with a shallow impervious layer. *Agric. Water Manag.* 14: 91-96.

Matus, F.J., 1994. Crop residue decomposition, residual soil organic matter and nitrogen mineralisation in arable soils with contrasting textures. PhD-thesis, Wageningen Agricultural University, The Netherlands.

Meadows, D.H., D.L. Meadows, J. Randers and W.W. Behrens, 1972. The limits to growth. A report for the Club of Rome's project on the predicament of mankind. Earth Island Limited, London.

Millington, R.J. and J.M. Quirk, 1961. Permeability of porous solids. *Trans. Faraday Soc.* 57: 1200-1207.

Moene, A., 1992. Flow of water in anisotropic unsaturated soils. Inst. Bodemvruchtbaarheid, Nota 257, Haren, The Netherlands.

Mualem, Y., 1976. A new model for predicting the hydraulic conductivity of unsaturated porous media. *Water Resour. Res.*, 12: 513-522.

Munster, C.L., R.W. Skaggs, J.E. Parsons, R.O. Evans, J.W. Gilliam and M.A. Breve, 1994. Simulating aldicarb transport in a drained field. *Trans. ASAE*, Vol. 37: 1817-1824.

NEN-5783, 1991. Bodem. Onverzadigde zone. Bepaling van de drukhoogte met behulp van een tensiometer. Nederlands Normalisatie Instituut, Delft, The Netherlands (in Dutch).

NEN-5785, 1991. Bodem. Onverzadigde zone. In-situ bepaling van de waterretentiekarakteristiek. Nederlands Normalisatie Instituut, Delft, The Netherlands (in Dutch).

NEN-5786, 1991. Bodem. Onverzadigde zone. Bepaling van de waterretentiekarakteristiek. Onderdrukmethode tot $h = -200$ cm. Bepaling met een poreuze plaat in combinatie met een buret. Nederlands Normalisatie Instituut, Delft, The Netherlands (in Dutch).

NEN-5789, 1991. Bodem. Bepaling van de verzadigde waterdoorlatendheid. Nederlands Normalisatie Instituut, Delft, The Netherlands (in Dutch).

NEN-5781, 1992. Bodem. Onverzadigde zone. Gravimetrische bepaling van het watergehalte en de droge volumieke massa van grond. Nederlands Normalisatie Instituut, Delft, The Netherlands (in Dutch).

References

NEN-5788, 1994. Bodem. Onverzadigde zone. Bepaling van de waterretentiekarakteristiek van $h = -500$ cm tot $h = -20000$ cm. Overdrukmethode. Gravimetrische laboratoriumbepaling met een pers. Nederlands Normalisatie Instituut, Delft, The Netherlands (in Dutch).

Nieber, J.L. and D. Misra, 1993. Modeling flow and transport in heterogeneous dual-porosity drained soils. 15th International Congress of ICID, The Hague, Workshop on subsurface drainage simulation models. ICID-CIID, Cemagref; 174-184.

NRLO, 1990. Meerjarenvisie Landbouwkundig onderzoek 1991-1994. Nationale Raad voor Landbouwkundig Onderzoek, 's Gravenhage, The Netherlands (in Dutch).

NRLO, 1994. Landbouwkundig onderzoek op weg naar de 21^e eeuw. Meerjarenvisie Landbouwkundig onderzoek 1995-1998. Nationale Raad voor Landbouwkundig Onderzoek, 's Gravenhage, The Netherlands (in Dutch).

NVN-5791, 1995. Bodem. Onverzadigde zone. Bepaling van de onverzadigde waterdoorlatendheidskarakteristiek en waterretentiekarakteristiek de verdampingsmethode volgens Wind. Normalisatie Instituut, Delft, The Netherlands (in Dutch).

NVN-5790, 1996. Bodem. Onverzadigde zone. Bepaling van de waterdoorlatendheidskarakteristiek met een infiltrometer. Nederlands Normalisatie Instituut, Delft, The Netherlands (in Dutch).

Oenema, O. and T.A. van Dijk (Eds.), 1994. Fosfaatverliezen en fosfaatoverschotten in de Nederlands landbouw. Projectgroep Verliesnormen, deelrapport I. Rapport van de technische projectgroep "P-deskstudie" (in Dutch).

Olsen, S. R. and L. E. Sommers, 1982. Phosphorus. In: A. L. Page (Ed.), Methods of Soil Analysis, part 2, ASA-SSSA, Madison, Wisconsin, pp. 403-430.

ORACLE, 1990. The relational database management system, version 6.0. Oracle Corporation, Redwood Shores, California.

Otten, W., 1994. Dynamics of water and nutrients for potted plants induced by flooded bench fertigation: experiments and simulation. PhD-thesis, Wageningen Agricultural University, Wageningen, The Netherlands.

Owens, L. B. and W. M. Edwards, 1992. Long-term groundwater quality changes from a one-time surface bromide application. J. Environ. Qual. 21: 406-410.

Parker, D., W. A. Norvell and R. L. Chaney, 1990. Usage notes for GEOCHEM-PC, version 2.0. Available from senior author, University of California, Riverside, California.

Payne, W. J., 1981. Denitrification. John Wiley and Sons, New York.

Postma, J., 1989. Distribution and population dynamics of *Rhizobium* sp. introduced into soil. Doctoral thesis, Wageningen Agricultural University, The Netherlands.

Raats, P.A.C., 1975. Distribution of salts in the root zone. *J. Hydrol.*, 27: 237-248.

Raats, P.A.C., 1981a. Transport in structured porous media. In: Verruijt, A. and F.B.J. Barends (Eds.), *Flow and transport in porous media*. Proc. Euromech. 143, September 2-4, Delft. Balkema, Rotterdam, The Netherlands, pp. 221-226.

Raats, P.A.C., 1981b. Residence times of water and solutes within and below the root zone. *Agric. Water Manage.* 4: 63-82.

Raats, P.A.C., 1992. A superclass of soils. In: M.Th. van Genuchten, F.J. Leij and L.J. Lund (Eds.), *Proc. Int. Workshop on Indirect Methods for Estimating Hydraulic Properties of Unsaturated Soils*. University of California, Riverside, California, pp. 45-51.

Rappoldt, C., 1992. Diffusion in aggregated soil. PhD thesis, Wageningen Agricultural University, The Netherlands.

Rappoldt, C., 1995. Experimental and theoretical contribution to the integrated grassland N₂O project. AB-DLO, Wageningen/Haren, The Netherlands.

Rappoldt, C., J.A. De Vos. and W.J. Corré, 1995. Anaerobiosis in the soil in relation to denitrification. Annual report AB-DLO, AB-DLO Wageningen/Haren, The Netherlands, pp. 38-41.

Rappoldt, C. and W.J. Corré, 1997. Spatial pattern in soil oxygen content and nitrous oxide emission from drained grassland. *Proceedings of IGER conference on Nitrogen emissions in grassland* (In press).

Rhoades, J. D., 1982. Soluble salts. In: A. L. Page, R. H. Miller, and D. R. Keeney (Eds.), *Methods of soil analysis*, Part 2, ASA-SSSA, Madison, Wisconsin, pp. 167-179.

Ridder, T.B., 1978. Over de chemie van de neerslag; Vergelijking meetresultaten. Scientific report W.R. 78-4. KNMI, De Bilt, The Netherlands (in Dutch).

Ritzema, H.P., 1994. Subsurface flow to drains. In: H.P. Ritzema (Ed.), *Drainage principles and applications*, ILRI Publication 16 (2nd ed), Wageningen, The Netherlands, pp. 263-304.

References

Roth, K., H. Fluhler, W.A. Jury and J.C. Parker (Eds.), 1990. Field-scale water and solute flux in soils. Monte Verita, Proceedings of the Centre Stefano Franscini, Ascona, Birkhauser Verlag, Basel, Switzerland.

Salama, R. B., P. Farrington, G. A. Bartle and G. D. Watson, 1993. The chemical evolution of groundwater in a first-order catchment and the process of salt accumulation in the soil profile. *J. Hydrol.* 143: 233-258.

Schoonderbeek, D. and J.F.Th. Schouten, 1994. Root and root-soil contact of winter wheat and sugar beet in a conventional and integrated cropping system. *Agric. Ecosyst. Environ.* 51: 89-98.

Schröder, J. en J. Vos, 1995. De stikstofkringloop: keten of vergiet? In A.J. Haverkort en P.A. Van der Werff (Eds.), *Hoe ecologisch kan de landbouw worden?* Themadag KLV, AB-DLO en PE op 21 november 1995 te Wageningen. AB-DLO Thema's 3, Wageningen, The Netherlands, pp. 37-63. (in Dutch).

Schweich, D., M. Sardin and M. Jauzein, 1993a. Properties of concentration waves in presence of nonlinear sorption, precipitation/dissolution, and homogeneous reactions 1. Fundamentals. *Water Resour. Res.* 29: 723-733.

Schweich, D., M. Sardin and M. Jauzein, 1993b. Properties of concentration waves in presence of nonlinear sorption, precipitation/dissolution, and homogeneous reactions 2. Illustrative examples. *Water Resour. Res.* 29: 735-741.

Sieben, W.H., 1951. *De ontwatering van zavelgronden in de Noordoostpolder.* Van Zee tot Land, nr. 3, Tjeenk Willink N.V., Zwolle, The Netherlands (in Dutch).

Simunek, J., T. Vogel and M. Th. Van Genuchten, 1994. The SWMS_2D code for simulating water flow and solute transport in two-dimensional variably saturated media. Version 1.2. Research Report no. 126, U.S. Salinity Laboratory, Riverside, California.

Simunek, J., M. Sejna and M. Th. Van Genuchten, 1996. The HYDRUS-2D software package for simulating water flow and solute transport in two-dimensional variably saturated media. Version 1.0. Research Report, U.S. Salinity Laboratory, Riverside, California.

Sisson, J.B. and M.Th. Van Genuchten, 1991. An improved analysis of gravity drainage experiments for estimating the unsaturated soil hydraulic functions. *Water Resour. Res.* 27: 569-575.

Skaggs, R.W. and J.W. Gilliam, 1981. Effect of drainage system design and operation on nitrate transport. *Trans. ASAE*, Vol. 24 (4): 929-934.

Smiles, D.E., 1988. Aspects of the physical environment of soil organisms. *Biol. Fertil. Soils* 6: 204-215.

Smits, H., A.J. Zuur, D.A. Schreven en W.A. Bosma, 1962. *De fysische, chemische en microbiologische rijping der gronden in de IJsselmeerpolders. Van Zee tot Land*, nr. 32, Tjeenk Willink N.V., Zwolle, The Netherlands (In Dutch).

Snedecor, G. W. and W. G. Cochran, 1967. *Statistical methods*, 6th ed., Iowa State Univ. Press, Ames, Iowa.

Snow, V. O., B. E. Clothier, D. R. Scotter and R. E. White, 1994. Solute transport in a layered field soil: experiments and modelling using the convection-dispersion approach. *J. Contam. Hydrol.* 16: 339-358.

Soil Survey Staff, 1975. *Soil Taxonomy. A basic system of soil classification for making and interpreting soil surveys*. U.S. Dept. Agric., Agricultural Handbook 436, U.S. Governmental Printing Office, Washington DC.

Spencer, D.S.C. and M.J. Swift, 1992. Sustainable agriculture: definition and measurement. In: K. Mulongoy, M. Gueye and D.C. Spencer (Eds.), *Biological Nitrogen Fixation and Sustainability of Tropical Agriculture*. Wiley, Chichester: pp. 15-24.

Sposito, G., 1989. *The chemistry of soils*. Oxford University Press, New York.

Sposito, G. and S. V. Mattigod, 1979. *GEOCHEM: a computer program for the calculation of chemical equilibria in soil solutions and other natural water systems*. Kearney Foundation of Soil Science, Univ. of California, Riverside, California.

Sposito, G. and R.J. Reginato (Eds.), 1992. *Opportunities in Basic Soil Science Research*. Soil Science Society of America, Inc., Madison, Wisconsin.

Stanford, G., R.A. Vander Pol and S. Dzienia, 1975. Denitrification rates in relation to total and extractable soil carbon. *Soil Sci. Soc. Am. Proc.* 39: 284-289.

Stolte, J., J.I. Freijer, W. Bouting, C. Dirksen, J.M. Halbertsma, J.C. Van Dam, J.A. Van den Berg, G.J. Veerman and J.H.M. Wosten, 1994. Comparison of six methods to determine unsaturated soil hydraulic conductivity. *Soil Sci. Am. J.* 58: 1596-1603.

Strelbel, O., W.H.M. Duynisveld and J. Bottcher, 1989. Nitrate pollution of groundwater in Western Europe. *Agric. Ecosyst. Environ.* 26: 189-214.

References

Stumm, W. and J. J. Morgan, 1981. *Aquatic chemistry*. Wiley, New York.

Stuyt, L.C.P.M., 1992. The water acceptance of wrapped subsurface drain. Doctoral thesis. Wageningen Agricultural University, Wageningen, The Netherlands.

Suarez, D. L., J. D. Wood and I. Ibrahim, 1992. Reevaluation of calcite supersaturation in soils. *Soil Sci. Soc. Am. J.* 56: 1776-1784.

Topp, G.C., J.L. Davis and A.P. Annan, 1980. Electromagnetic determination of soil water content in coaxial transmission lines. *Water Resour. Res.* 16: 574-582.

Towner, G.D., 1980. Theory of time response of tensiometers. *J. Soil Sci.* 31: 607-621.

Towner, G.D., 1984. The time response characteristics of tensiometers in heavy clay soils. *Proc. ISSS symposium on Water and Solute Movement in Heavy Clay Soils*. ILRI publication 37, Wageningen, The Netherlands, pp. 320-323.

Van der Gon, H.D. and R.J. Swart, 1990. *Emissies van distikstoxyde in Nederland*. Milieu 2: 33-37 (in Dutch).

Van der Molen, W.H., 1958. *Over de zouthuishouding in de Noordoostpolder*. Van Zee tot Land, nr. 23, Tjeenk Willink N.V., Zwolle, The Netherlands (in Dutch).

Van der Molen, W.H. and W.H. Sieben, 1955. *Over de landbouwkundige betekenis en de kartering van de kwel in de Noordoostpolder*. Van Zee tot Land, nr. 12, Tjeenk Willink N.V., Zwolle, The Netherlands (in Dutch).

Van Dieren, W., 1995. Taking nature in account - towards a sustainable national income. A report to the club of Rome. IMSA, Amsterdam.

Van Faassen, H.G. and G. Lebbink, 1990. Nitrogen cycling in high-input versus reduced input arable farming. *Neth. J. Agric. Sci.*, 38: 265-282.

Van Faassen, H.G. and G. Lebbink, 1994. Organic matter and nitrogen dynamics in conventional versus integrated farming. *Agric. Ecosyst. Environ.*, 51: 209-226.

Van Genuchten, M. Th., 1978. Calculating the unsaturated hydraulic conductivity with a new closed form analytical model. *Res. Rep. no.78-WR-08*. Princeton University, Princeton, New Jersey.

Van Genuchten, M.Th., 1980. A closed form equation for predicting the hydraulic conductivity of unsaturated soils. *Soil Sci. Soc. Am. J.* 44: 892-898.

Van Genuchten, M. Th., 1986. Program to analyse observed soil water retention and hydraulic conductivity data. U.S. Salinity Laboratory, Riverside, California, 34 pp.

Van Genuchten, M.Th., D.H. Tang and R. Guennelon, 1984. Some exact and approximate solutions for solute transport through large cylindrical macropores. *Water Resour. Res.* 20: 335-346.

Van Hoorn, J.W., 1981. Salt movement in unsaturated soil profiles. In Verruijt, A. and F.B.J. Barends (Eds.), *Flow and transport in porous media*. Proc. Euromech. 143, September 2-4, Delft. Balkema, Rotterdam, The Netherlands, pp. 227-232.

Van Kooten, J., 1996. Advective-dispersive contaminant transport towards a pumping well. PhD thesis, Wageningen Agriculture University, The Netherlands, 120 p.

Van Lanen, H.A.J., M.H. Bannink and J. Bouma, 1987. Use of simulation to asses the effects of different tillage practices on land qualities of a sandy loam soil. *Soil Tillage Res.*, 10: 347-361.

Van Loon, W.K.P., 1991. Heat and mass transfer in frozen porous media. PhD thesis, Wageningen Agricultural University, Wageningen, The Netherlands.

Van Noordwijk, M., G. Brouwer, H. Koning, F.W. Meijboom and W. Grzebisz, 1994. Production and decay of structural root material of winter wheat and sugar beet in conventional and integrated cropping systems. *Agric. Ecosys. Environ.* 51: 99-113.

Van Ommen, H.C., M. Th. Van Genuchten, W.H. Van der Molen, R. Dijksma, and J. Hulshof, 1989. Experimental and theoretical analysis of solute transport from a diffuse source of pollution. *J. Hydrol.* 105: 225-251.

Van Schilfgaarde, J. (Ed.), 1974. *Drainage for agriculture*. Agronomy 17, Amer. Soc. Agron., Madison, Wis.

Van Wijk, A.L.M., R.A. Feddes, J.G. Wesseling and J. Buitendijk, 1988. *Effecten van grondsoort en ontwatering op de opbrengst van akkerbouwgewassen*. Rapport 31, Instituut voor Cultuurtechniek en Waterhuishouding, Wageningen, The Netherlands (in Dutch).

Van Wijk, W.R. (Ed.), 1963. *Physics of plant environment*. North-Holland Publishing Company, Amsterdam, The Netherlands.

Vimoke, B.S., T.D. Yura, T.J. Thiel and G.S. Taylor, 1963. Improvements in construction and use of resistance networks for studying drainage problems. *Soil Sci. Soc. Am. J.*, 26: 203-207.

References

Vogel, T. and M. Cislerova, 1988. On the reliability of unsaturated hydraulic conductivity calculated from the moisture retention curve. *Transport in Porous Media* 3: 1-15.

Volker, A. and W.H. van der Molen, 1991. The influence of groundwater currents on diffusion processes in a lake bottom: an old report reviewed. *J. Hydrol.* 126: 159-169.

Vos, E.C. and M.J. Kooistra, 1994. The effect of soil structure differences in a silt loam under various farm management systems on soil physical properties and simulated land qualities. *Agric. Ecosyst. Environ.* 51: 89-98.

Walter, A. L., E. O. Frind, D. W. Blowes, C. J. Ptacek and J. W. Molson, 1994. Modeling of multicomponent reactive transport to groundwater 1. Model development and evaluation. *Water Resour. Res.* 30: 3137-3148.

Whittig, L. D. and W. R. Allardice, 1986. X-ray diffraction techniques. In: A. Klute (Ed.), *Methods of soil analysis*, Part 1, 2nd ed. ASA-SSSA, Madison, Wisconsin, pp. 331-362.

Wiggers, A.J., 1955. The genesis of the Noordoostpolder area. Tjeenk Willink, Zwolle, The Netherlands (in Dutch).

Willems, W.J. and B. Fraters, 1995. Naar afgestemde kwaliteitsdoelstellingen voor nutriënten in grondwater en oppervlaktewater. *Discussienotitie*. RIVM-rapport nr. 714901003, Bilthoven, The Netherlands (in Dutch).

WMO, 1983. World Meteorological Organization, Guide to meteorological instruments and methods of observation. WMO-8, Geneva, Switzerland.

Wobschall, D., 1977. A theory of the complex dielectric permittivity of soil containing water: The semi-disperse model. *IEEE Transactions on Geoscience Electronics*, Vol. GE-15, No. 1, pp. 49-58.

Wösten, J.H.M., 1990. Use of scaling techniques to quantify variability in hydraulic functions of soils in The Netherlands. In: Roth, K., H. Flühler, W.A. Jury and J.C. Parker (Eds.), *Field-scale water and solute flux in soils*. Monte Verita, Proceedings of the Centro Stefano Franscini Ascona, Birkhäuser Verlag Basel, Switzerland.

Wösten, J.H.M., M.H. Bannink and J. Beuving, 1987. *Waterretentie- en doorlatendheidskarakteristieken van boven- en ondergronden in Nederland: de Staringreeks*. Stiboka Rapport 2019, Wageningen, The Netherlands (in Dutch).

Water flow and nutrient transport in a layered silt loam soil

Wösten, J.H.M. and M.Th. Van Genuchten, 1988. Using texture and other soil properties to predict the unsaturated soil hydraulic functions. *Soil Sci. Soc. Am. J.* 52: 1762-1770.

Yeh, G.T., 1981. On the computation of Darcian velocity and mass balance in finite element modeling of groundwater flow. *Water Resour. Res.* 17: 1529-1534.

Zandt, P.A., 1995. Handleiding voor het programma Meteolog. Internal paper DLO Inst. Agrobiol. Soil Fert., Haren, The Netherlands (in Dutch).

Zaradny, H., 1993. Groundwater flow in saturated and unsaturated soil , edited by R.B. Zeidler. Balkema, Rotterdam, The Netherlands.

Zaradny, H. and R.A. Feddes, 1978. Calculation of non-steady flow towards a drain in a saturated-unsaturated soil by finite-elements. *Agric. Water Manag.* 2: 37-53.

Zegelin, S.J., I. White and D.R. Jenkins, 1989. Improved field probes for soil water content and electrical conductivity measurements using Time Domain Reflectometry. *Water Resour. Res.* 11: 2367-2376.

Zienkiewicz, O.C., 1977. The finite element method, 3rd edition. McGraw-Hill, London.

Zuur, A.J., 1951. Ontstaan en aard van bodem van de Noordoostpolder. *Van Zee tot Land*, nr. 1, Tjeenk Willink N.V., Zwolle, The Netherlands (in Dutch).

Zuur, A.J., 1952. Drainage and reclamation of lakes and of the Zuiderzee. *Soil Sci.* 75-89.

LIST OF MAIN SYMBOLS

LIST OF MAIN SYMBOLS

This list presents the main symbols that occur regularly throughout this thesis. Symbols that are only used locally are not listed. A **bold** notation is used for vectors. Values are usually in SI units. However, I felt free to use prefixes to be able to express the dimensions in the units which are commonly used. For example, for small distances or depths I mostly used centimetres (cm) and sometimes millimetres (mm). I also used units like hectare (ha) and year (yr), because this is common in agricultural research.

Symbol	Representation	Units
a_l	Longitudinal dispersivity	m
a_t	Transversal dispersivity	m
c	Solute concentration	mg m^{-3}
C	Solute concentration (Chapter 7)	mol m^{-3}
C	Differential water capacity	m^{-1}
c_{light}	Speed of light = $3 \cdot 10^8$	m s^{-1}
E	Soil evaporation per unit area	m
E_p	Potential evapotranspiration rate of a cropped surface	m d^{-1}
E_{ref}	Maximum possible evapotranspiration rate of a reference cropped surface	m d^{-1}
f	Crop factor	-
h	Pressure head	m
H	Hydraulic head	m
K	Hydraulic conductivity	m d^{-1}
K_k	Hydraulic conductivity at transition point $h = h_k$	m d^{-1}
K_s	Hydraulic conductivity at saturation	m d^{-1}
$K_{s,a}$	K_s above the drain depth	m d^{-1}
$K_{s,b}$	K_s below the drain depth	m d^{-1}
L_{probe}	Length of TDR probe	m
L	Empirical parameter in Mualem's Eq. 2.17	-

List of main symbols

<i>m</i>	Empirical parameter in Van Genuchten's Eq. 2.16	-
<i>M</i>	Mass of solute	kg
<i>n</i>	Empirical parameter in Van Genuchten's Eq. 2.16	-
<i>n_a</i>	Apparent refractive index	-
<i>P</i>	Precipitation per unit area	m
<i>q</i>	Volumetric water flux density vector	$m^3 m^{-2} d^{-1}$
<i>Q</i>	Amount of water per unit area	m
<i>S</i>	Volumetric density of water uptake by roots	$m^3 m^{-3} d^{-1}$
<i>S_e</i>	Degree of saturation	-
<i>t</i>	Time	d
<i>T</i>	Temperature	°C
<i>v</i>	Velocity of EM wave	$m s^{-1}$
<i>V</i>	Volume of water	m^3
<i>W</i>	Water storage in the soil profile per unit area	m
<i>X</i>	Charge fraction	-
<i>z</i>	Gravitational head; and also vertical coordinate, with the origin at the soil surface, directed positively upwards	m
<i>α</i>	Empirical parameter in Van Genuchten's Eq. 2.16	m^{-1}
$\gamma(h)$	Root water uptake reduction function	-
ε_r	Relative dielectric permittivity	-
ε_a	Apparent relative dielectric permittivity	-
ε_{air}	Relative dielectric permittivity of air	-
ε_w	Relative dielectric permittivity of water	-
ρ_b	(dry) Bulk density	$kg m^{-3}$
θ	Volumetric water content	$m^3 m^{-3}$
θ_k	Volumetric water content at transition point $h = h_k$	$m^3 m^{-3}$
θ_r	Residual volumetric water content	$m^3 m^{-3}$
θ_s	Volumetric water content at saturation	$m^3 m^{-3}$
τ	Tortuosity factor	-
τ_{aq}	Turnover time of an aquifer	d

CURRICULUM VITAE

CURRICULUM VITAE

Jan Abraham de Vos werd geboren op 14 december 1959 te Rotterdam. In 1978 behaalde hij het Atheneum-B diploma aan de Scholengemeenschap Prins Alexanderpolder te Rotterdam. Vervolgens begon hij de studie Technische Natuurkunde aan de Technische Hogeschool Delft. Het afstudeeronderzoek werd verricht in de sectie Warmtetransport van de vakgroep Fysische Transportverschijnselen. In 1983 werd het warmteverlies van een oven van een steenfabriek onderzocht, waarbij gebruik werd gemaakt van temperatuurmetingen in de oven en van numerieke modellen. Het afstudeerwerk in 1984 betrof het ontwerpen en bouwen van een schaalmodel van de verbrandingskamer van een glasoven. In de turbulente stroming van de straal van de modelbranders werden Laser-Doppler snelheidsmetingen uitgevoerd. Op 14 mei 1985 werd de ingenieurstitel behaald.

Vanaf februari 1986 werkt hij als bodemfysicus bij het DLO-Instituut voor Bodemvruchtbaarheid (IB-DLO), dat in 1993 met het DLO-Centrum voor Agrobiologisch Onderzoek (CABO-DLO) fuseerde tot het DLO-Instituut voor Agrobiologisch en Bodemvruchtbaarheidsonderzoek (AB-DLO). In de periode tot en met 1992 vond een groot gedeelte van het bodemfysisch onderzoek plaats op de Dr. H.J. Lovinkhoeve te Marknesse, in het kader van het "Bodemecosystemenproject". Na 1992 werd de Lovinkhoeve als veldlocatie gehandhaafd maar kwam het accent van het onderzoek meer te liggen op waterstroming en stoffentransport naar drains. In al het onderzoek werd getracht een balans te vinden tussen het gebruik van modellen en het verrichten van experimenteel werk.

Verder verrichtte hij onderzoek in de AB-DLO windtunnel naar de werkzaamheid van anti-stuifmiddelen ter bestrijding van winderosie, en werd een methode voor het meten van de sapstroom in stengels, stammen en wortels verder ontwikkeld. Deze sapstroommeter werd, samen met bodemfysische en meteorologische apparatuur, tijdens een tweetal werkbezoeken aan Mali operationeel gemaakt binnen het ontwikkelingssamenwerkingsproject "Production Soudano-Sahélienne". Vanaf 1997 verricht hij onderzoek naar de mogelijkheden van beregening in ecologische teelten, gericht op sturing van de stikstofmineralisatie, optimalisatie van de nutriëntenbenutting, en vermindering van stikstofverliezen.